# Inhibitors of the PD1/PD-L1 interaction: missteps, mechanisms and mysteries

by

Ronan Hanley
B.Sc., McGill University, 2011

A Dissertation Submitted in Partial Fulfillment
of the Requirements for the Degree of

DOCTOR OF PHILOSOPHY

in the Department of Chemistry

# Supervisory Committee

Inhibitors of the PD1/PD-L1 interaction: missteps, mechanisms and mysteries

by

Ronan Hanley
B.Sc., McGill University, 2011

**Supervisory Committee**

Dr. Jeremy E. Wulff, Department of Chemistry
**Supervisor**

Dr. Fraser Hof, Department of Chemistry
**Co-Supervisor**

Dr. Alexandre Brolo, Department of Chemistry
**Departmental Member**

Dr. Brad Nelson, Department of Biochemistry and Microbiology
**Outside Member**

# Abstract

**Supervisory Committee**
Dr. Jeremy E. Wulff, Department of Chemistry
**Supervisor**
Dr. Fraser Hof, Department of Chemistry
**Co-Supervisor**
Dr. Alexandre Brolo, Department of Chemistry
**Departmental Member**
Dr. Brad Nelson, Department of Biochemistry and Microbiology
**Outside Member**

The interactions of tumours with normal host tissue are key determinants of cancer growth and progression. The ability or inability of the patient's immune system to mount a response against the tumour is tightly correlated with prognosis. One of the ways tumours avoid detection and elimination by the immune system is by expressing programmed death ligand 1 (PD-L1). PD-L1 binds to its receptor programmed death 1 (PD1) on T cells, inhibiting T cell responsiveness to antigenic stimuli. Blockade of the PD1/PD-L1 pathway removes this negative signal and restores anti-tumour immunity. While this blockade of PD1/PD-L1 is well established through the use of antibodies, small molecule inhibitors of PD1/PD-L1 are relatively unknown.

We employed *in silico* docking in order to find small molecules capable of binding to either PD1 or PD-L1, and the highest-ranked compounds were tested in biophysical assays for their ability to inhibit PD1/PD-L1 binding. A thermal shift assay identified a pyrazole compound as a possible binding partner for PD-L1, but follow-up assays showed that it had no effect on the PD1/PD-L1 interaction and that its apparent binding was probably due to aggregation. An ELISA assay identified a tryptophan diamine compound as an apparent

*stabilizer* of the PD1/PD-L1 interaction. However this compound, too, was later identified to be inactive in orthogonal assays.

We identified a family of salicylic acid derivatives that interfered with TR-FRET measurements – an unusual observation, given that TR-FRET is touted as being insensitive to most mechanisms of compound interference. This discovery should help other fragment-screening groups identify false positives more easily.

We also probed the mechanism of inhibition of a recently disclosed family of small molecule PD1/PD-L1 inhibitors from Bristol-Myers Squibb. Concurrently with other groups, we used protein NMR, size exclusion chromatography, and SPR to determine that the compounds were inducing homodimerization through the PD1-binding face of PD-L1. Furthermore, using cellular crosslinking and live cell imaging, we showed that these first generation inhibitors are fairly ineffective at inhibiting this interaction on the cell surface. More potent compounds will be needed to see any cellular effect from this mechanism of action.

# Table of Contents

# List of Figures

# List of Schemes

# List of Tables

# List of Abbreviations

| Abbreviation | Meaning |
|---|---|
| ∂ | chemical shift |
| $^{13}$C NMR | Carbon Nuclear Magnetic Resonance |
| $^{1}$H NMR | Proton Nuclear Magnetic Resonance |
| Å | angstrom |
| Ac | acetyl |
| AIDS | acquired immune deficiency syndrome |
| Ala | alanine |
| APC | antigen-presenting cell |
| Arg | arginine |
| Asn | asparagine |
| Asp | aspartic acid |
| BMS | Bristol-Myers Squibb |
| Bn | benzyl |
| Boc | *tert*-butoxycarbonyl |
| $Boc_2O$ | di-*tert*-butyldicarbonate |
| br | broad |
| $B_{reg}$ | regulatory B cell |
| $BS^3$ | bis(sulfosuccinimidyl)suberate |
| BSA | bovine serum albumin |
| calcd | calculated |

| | |
|---|---|
| Cbz | carboxybenzoyl |
| CD | cluster of differentiation |
| CFP | cyan fluorescent protein |
| CHO | Chinese hamster ovary |
| $cm^{-1}$ | wavenumbers |
| CTLA-4 | cytotoxic T-lymphocyte associated protein 4 |
| Cys | cysteine |
| d | doublet |
| Da | Dalton |
| DCM | dichloromethane |
| DEAD | diethyl azodicarboxylate |
| DELFIA | dissociation-enhanced lanthanide fluorescence immunoassay |
| DMAP | N,N-dimethylaminopyridine |
| DMF | N,N-dimethylformamide |
| DMSO | dimethylsulfoxide |
| DNA | deoxyribonucleic acid |
| dppf | 1,1'-Bis(diphenylphosphino)ferrocene |
| DTSSP | 3,3'-dithiobis(sulfosuccinimidyl propionate) |
| E. coli | Escherichia coli |
| EDC | 1-Ethyl-3-(3-dimethylaminopropyl)carbodiimide |
| EGS | ethylene glycol bis(succinimidyl succinate) |
| ELISA | enzyme-linked immunosorbent assay |
| ERK | extracellular signal-regulated kinase |

| | |
|---|---|
| Et | ethyl |
| FDA | U.S. Food and Drug Administration |
| FITC | fluorescein isothiocyanate |
| FRET | Förster resonance energy transfer |
| GFP | green fluorescent protein |
| Gln | glutamine |
| Glu | glutamic acid |
| Gly | glycine |
| Grb2 | growth factor receptor-bound protein 2 |
| GSK3ß | glycogen synthase kinase 3 beta |
| GuaCl | guanidinium chloride |
| HAS | human serum albumin |
| HEK | human embryonic kidney |
| His | histidine |
| HIV | human immunodeficiency virus |
| HNSCC | head and neck squamous cell cancer |
| HOBt | hydroxybenzotriazole |
| hPD1 | human PD1 |
| hPD-L1 | human PD-L1 |
| HPLC | high-performance liquid chromatography |
| HRMS | high resolution mass spectrometry |
| HRP | horseradish peroxidase |
| HSQC | heteronuclear single quantum correlation |

| | |
|---|---|
| IBX | 2-iodoxybenzoic acid |
| $IC_{50}$ | half maximal inhibitory concentration |
| ICOS | inducible T-cell costimulator |
| IFNγ | interferon gamma |
| Ig | immunoglobulin |
| IgC | immunoglobulin constant domain |
| IgV | immunoglobulin variable domain |
| Ile | isoleucine |
| iPr | *iso*-propyl |
| irAE | immune-related adverse event |
| ITIM | immunoreceptor tyrosine-based inhibitory motif |
| ITSM | immunoreceptor tyrosine-based switch motif |
| J | coupling constant |
| kDa | kiloDalton |
| LAG3 | lymphocyte-activation gene 3 |
| LAT | linker of activation for T cells |
| LC-MS | liquid chromatography-mass spectrometry |
| Lck | lymphocyte-specific protein tyrosine kinase |
| Leu | leucine |
| logP | logarithm of the partition coefficient |
| Lys | lysine |
| M | molarity |
| M+ | molecular ion |

| | |
|---|---|
| MAPK | mitogen-activated protein kinase |
| Me | methyl |
| Met | methionine |
| MHC I | major histocompatibility complex I |
| MHC II | major histocompatibility complex II |
| mTOR | mammalian target of rapamycin |
| NCI | National Cancer Institute |
| NIH | National Institute of Health |
| NMR | nuclear magnetic resonance |
| NSAID | non-steroidal antiinflammatory drug |
| NSCLC | non-small cell lung cancer |
| p | pentet |
| PAINs | pan assay interference compounds |
| PD1 | programmed cell death protein 1 |
| PDB | Protein Data Bank |
| PD-L1 | programmed death ligand 1 |
| PD-L2 | programmed death ligand 2 |
| PE | phycoerythrin |
| Ph | phenyl |
| PH | pleckstrin homology |
| Phe | phenylalanine |
| PI3K | phosphatidylinositol-4,5-bisphosphate 3-kinase |
| PIP3 | phosphatidylinositol (3,4,5)-trisphosphate |

| | |
|---|---|
| PKC | protein kinase C |
| PLCγ | phospholipase C gamma |
| Pro | proline |
| q | quartet |
| qPCR | quantitative polymerase chain reaction |
| R | generalized substituent |
| RCC | renal cell carcinoma |
| SA | streptavidin |
| Ser | serine |
| SHP2 | Src homology region 2 domain-containing phosphatase 2 |
| SIV | simian immunodeficiency virus |
| SOS | Son of sevenless homolog 1 |
| sPD1 | soluble PD1 |
| sPD-L1 | soluble PD-L1 |
| SPR | surface plasmon resonance |
| STD | saturation transfer difference |
| t | triplet |
| t or tert | tertiary |
| TAM | tumour-associated macrophage |
| TBS | *tert*-butyldimethylsilyl |
| $T_c$ | cytotoxic T cell |
| TCR | T-cell receptor |
| TCT | cyanuric chloride |

| | |
|---|---|
| TEMPO | (2,2,6,6-tetramethylpiperidin-1-yl)oxidanyl |
| Tf | trifluoromethanesulfonyl |
| TGFB | transforming growth factor beta |
| $T_h$ | helper T cell |
| THF | tetrahydrofuran |
| Thr | threonine |
| TIL | tumour-infiltrating lymphocyte |
| TIM3 | T-cell immunoglobulin and mucin-domain containing-3 |
| $T_m$ | melting temperature |
| TME | tumour microenvironment |
| TR-FRET | time-resolved Förster resonance energy transfer |
| $T_{reg}$ | regulatory T cell |
| Trp | tryptophan |
| Ts | p-toluenesulfonyl |
| Tyr | tyrosine |
| UC | urothelial cancer |
| Val | valine |
| VISTA | V-domain Ig suppressor of T cell activation |
| wt | wild type |
| YFP | yellow fluorescent protein |
| Zap70 | zeta-chain-associated protein kinase 70 |
| ZINC | ZINC is not commercial |

# Acknowledgments

*"Results! Why, man, I have gotten a lot of results. I know several thousand things that won't work." –Thomas A. Edison*

I am first and foremost indebted to my supervisors, Dr. Jeremy Wulff and Dr. Fraser Hof. I knew barely anything about chemical biology or synthetic chemistry when I applied to their groups (some might say I still don't), but they took me in anyway. I've had a bumpy ride where projects are concerned, but I've learned a lot by struggling through. It's been character-building and character-destroying all at once.

I also need to thank Abby Carter right off the bat (it's a baseball reference!). Meeting her has been the turning point in my life, and for that reason I'll never have any regrets about doing grad school in Victoria. She's put up with insane hours, she's got me through the darkest times of thesis writing, and she's made the whole thing worthwhile. I otter be so grateful I found her (or that she found me).

I was fortunate to join UVic just in time to overlap with the "old guard" of grad students, and I learned so much just by being around them and listening to their discussions. That they became my good friends was an added bonus. Dr. Jason Davy, Dr. Mike Brant, Dr. Emma Davy, and Dr. Natasha O'Rourke have been excellent mentors and even better friends to me. I have also been very fortunate to have joined UVic in the same cohort as a bunch of other really talented chemists. Together with the soon-to-be Drs. Jun Chen, Natasha Milosevich, and Alok Shaurya (with an honourable mentions to Meagan Beatty and old man Mike Gignac), being part of the "Dream Team" (now "Broken Dream Team")

has been a blast; even if grad school has stolen my 20s, it's at least given me some of the best friends I've ever had.

I've also been fortunate to have some great undergraduate colleagues over the years, particularly Shanti Horvath. Chapter 2 is basically 50% her work, with my name slapped on the cover. Likewise, our collaborators in the UK, Dr. Mark Carr and Kayleigh Walker, really drove the second half of this project. I'm indebted to them for their intellectual and material contributions to the project (I won't send my thanks through the mail, though).

I would like to acknowledge my committee for their support and guidance: Dr. Brad Nelson and Dr. Brolo have pushed me to learn about aspects of my project that I would've been content to leave as black boxes. The staff at UVic has been so helpful: Chris Barr makes sure the NMRs always run on time, and I'm convinced that Andrew MacDonald can fix pretty much anything. I must also acknowledge Dr. Ori Granot's for high-res mass spec data as well as his management of the mass spec facility. It's a tough job, and he makes it look effortless. Meanwhile, TAing for Kelli Fawkes and Dr. Peter Marrs almost convinced me that chemical education was the career for me. … almost.

Finally, I wouldn't be here without my family. Thanks to my parents and my brothers, I've been saturated with science since before I could even spell the word. There's no substitute for growing up in that kind of intellectual, critical environment, and I'm eternally grateful that my family are all a bunch of nerds.

# Dedication

*For Mom and Dad, who got me here*

*And for Abby, who got me through*

# Chapter 1

## 1.1 Cancer as an immune disease

### 1.1.1 Two sides to every tumour

Cancer is often simplistically defined as uncontrolled cell growth and division[1-2]. The growing masses of cells consume unnecessary amounts of nutrients, secrete toxic molecules, and invade other organs or tissues, thus impairing their ability to function and eventually leading to the death of the host. The uncontrolled growth of these tumours is often attributed to deficiencies within the malignant cells themselves: loss of tumour suppressor activities combined with activation of oncogenic processes[3].

The best-known models, theories, and hallmarks of cancer growth that have informed our understanding of this complex disease reinforce the tumour-centric paradigm. Boveri postulated that chromosome damage could lead to cells possessing unlimited growth potential that could be passed on to their daughter cells[4]. Knudson's two-hit hypothesis posits that cancers arise from repeated and accumulated mutations in a cell's DNA, and that additional lesions make the cell more susceptible to malignant transformation[5]. The famous Warburg effect describes the increased reliance of cancer cells on glycolysis[6]. The third most highly cited article in oncology, in its initial version, lays out six "hallmarks of cancer"[7]— of which five (growth signal self-sufficiency, growth restriction insensitivity, resistance to apoptosis, immortality, and tissue invasion) are focused on the characteristics and behaviours of the tumour itself (angiogenesis being the only nod towards tumour-host interactions).

Treatment modalities for cancer have similarly focused on the molecular and cellular features of the tumours themselves. Radiation therapy is designed to damage tumours directly, inducing apoptosis and introducing double-strand DNA breaks and crosslinks that cause cell death upon attempted replication[8]. Most first-line chemotherapies are cytotoxic drugs that target the accelerated rate of metabolism or cell division in tumours. Genotoxic therapies exploit the typically abrogated DNA-repair mechanisms in tumours. More sophisticated approaches include the targeting of specific genes and proteins that drive tumour growth and survival. The heterogeneity and genomic instability of cancers, meanwhile, is a large contributor to the development of resistance towards these drugs[9-11]. The more mutations a cell acquires at some point in its life, the greater the likelihood that one of those mutations confers resistance to a given treatment regimen.

The definition given above tells only half the story, though. The growth and invasiveness of cancers depend greatly on their interactions with the host. Tumour-extrinsic growth factors can drive early tumour growth, while tumour-extrinsic cytokines can slow it. Cell-cell contacts between malignant and benign cells can inhibit, stimulate, or direct growth[12]. Immune cells can recognize tumour cells and either eliminate them or tolerate them, and communicate that decision to other immune cells[13]. Up to 50% of the tumour mass can be composed of non-malignant cells, all of them aiding, abetting, or antagonizing tumour growth in some way[14]. In short, no tumour is an island.

As cancers grow, they intrude on nearby tissues, actively remodeling the architecture and composition of the surrounding areas. The host response to the damage inflicted by tumour invasion is analogous, though not identical, to wound healing[15-16]. The host response promotes cell survival, cell growth, blood vessel growth (angiogenesis), immunosuppression, and remodeling of the extracellular matrix[12]. Contrary to wound healing, in which the response ends upon wound closure, the response to tumour invasion is not self-limiting, creating a structure that is chronically pro-tumorigenic. This area surrounding and within the tumour is termed the tumour microenvironment (TME), and it can serve as an incubator and a protector for the tumour itself[13-14, 16]. The composition of the TME can be a powerful predictor of the patient's prognosis. Immunosuppression and the pro-inflammatory TME have been added to the famous "hallmarks of cancer", reflecting a growing awareness of their importance[17].

### 1.1.2 Immune cells in the tumour microenvironment

The immune cells that infiltrate or reside in the TME are key determinants of the host response to cancer. The unique conditions of the TME attract immune cells of various lineages, which secrete factors that either promote or inhibit tumour growth and survival. $T_{reg}$ lymphocytes secrete transforming growth factor beta (TGF-ß), which induces dedifferentiation of the tumour itself to a more pluripotent phenotype; neutrophils can inhibit the action of TGF-ß, leading to increased immune activity[15]. Moreover, the various cell types regulate each other's proliferation and activity – from $T_{reg}$ and $B_{reg}$ cells that produce immunosuppressive interleukin-10 to the neutrophils that inhibit TGF-ß-mediated

immunosuppression[16]. The composition of this immune population determines whether the overall immune response is to eliminate the tumour or to tolerate it[15, 17].

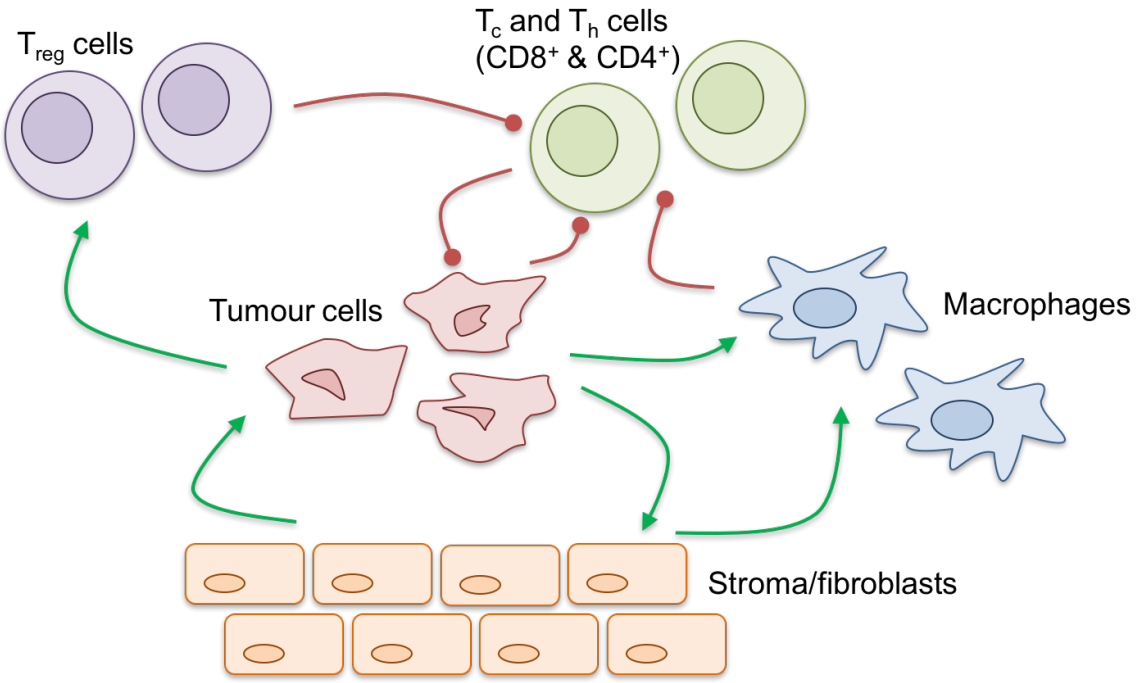


**Figure 1: The immunosuppressive, pro-tumorigenic microenvironment. Cancerous cells stimulate fibroblast migration and angiogenesis, while stromal cells release mitogens that promote tumour growth and survival. Macrophages establish an inflammatory environment. Both the tumour itself and associated $T_{reg}$ cells inhibit tumour-specific T cell responses. Green arrows indicate positive stimuli, red circles represent negative stimuli.**

Tumour sites are generally well-populated with macrophages (called tumour-associated macrophages or TAMs), neutrophils, and dendritic cells. These cells are attracted to the hypoxic, necrotic conditions of densely populated tumours, and attempt to rectify these conditions by promoting angiogenesis and remodeling of the extracellular matrix[15]. Moreover, while these cells are professional antigen-presenting cells, the neutrophils and

dendritic cells found in tumours often exhibit impaired antigen presentation, and exert immunosuppressive effects on the T cell population[13-14, 16, 18-21]. The presence of TAMs in the TME is thus often a poor prognostic indicator – a counterintuitive observation, given that macrophages are tasked with defending the host from infection.

The most numerous immune cells in the TME are lymphocytes, consisting of T cells and B cells. The combined activation of T cells and B cells leads to antigen clearing by one of two pathways: cell-mediated immunity and antibody-mediated (or humoral) immunity. Antibody-mediated immunity is largely carried out by B cells and T helper ($T_h$) cells, which work together to produce antibodies that bind to antigens on pathogen surfaces. These antibodies can either induce direct toxicity through the activation of the complement cascade, or indirect toxicity by tagging cells for destruction by natural killer cells. Cell-mediated immunity relies on direct binding and destruction of infected cells by cytotoxic T cells ($T_c$), whose activity is enabled and enhanced mostly by T helper 1 ($T_{h1}$) cells[22].

In addition to the pro-immune T cells and B cells, each lineage has types that serve to inhibit immune responses; these cells are called regulatory T cells and B cells ($T_{reg}$ and $B_{reg}$, respectively). These cells function to promote self-tolerance and rein in uncontrolled immune responses by damping the activity and proliferation of their pro-immunogenic peers.

The exact composition of tumour-infiltrating lymphocytes (TILs), then, determines the immune response towards the tumour. Cell-dependent immunity seems to be the

predominant antitumour activity; higher proportions of $T_c$ cells in the TME are therefore usually correlated with better prognoses[23]. In most cases, increased numbers of $T_{reg}$ cells are associated with reduced antitumour immune responses and poorer outcomes[15-16].

### 1.1.3 Neoantigens, immunosurveillance, and immunoediting

The immunosuppressive TME described above is representative of mature tumours that have grown large enough to reshape their surroundings. How do cancers progress to that stage without the protection of the TME? And if the immune system can be so easily defeated, why do we not develop cancer more often?

Transformation of normal cells into malignant ones is often the result of damage to the cell's chromosomes. Mutations in the DNA are manifested as mutations in the proteins for which those genes code; the mutant proteins suffer either a gain or loss of function that promotes the unchecked growth of the malignant cell and its descendents[7]. Meanwhile, damage to the chromosome structure itself, either from direct cleavage or from errors during replication, can lead to translocations and the creation of aberrant fusion genes that are not subject to the same regulation as the native genes. The acquisition of one of these tumour-driving mutations is facilitated if the DNA repair mechanisms of the cell are compromised or damaged in some way, and dysfunctional DNA repair leads to high overall genomic instability. The mutational load of many aggressive cancers therefore tends to be very high[24-27].

A fraction of these mutated proteins, although derived from human genes, are nevertheless different enough from their "normal" homologs to be recognized as foreign by immune cells. The immune system undergoes a negative selection process very early in life, whereby self-reactive lymphocyte clones are permanently destroyed in a process called "central tolerance"[28-29]. However, despite being derived from these "tolerated" antigens, the mutated proteins are different enough that they appear "new" to the immune system, and are thus coined "neoantigens". These neoantigenic proteins are subject to the same proteolytic turnover as normal proteins, and the peptides resulting from degradation are displayed on the cell surface, bound to the Major Histocompatibility Complex (MHC) I. The antigen–MHC complex is recognized by the specific T cell receptor (TCR) of $CD8^+$ T cells that survived central tolerance, and that clone rapidly replicates and activates to mount an immune response to destroy the transformed cell. In parallel, transformed cells are phagocytosed by macrophages, which then present neoantigens bound to MHC II. This antigen–MHC II complex is recognized by the TCR of CD4+ T cells, which (in general) replicate and activate to activate B cell and CD8+ T cell responses through the release of various cytokines. This constant monitoring of neoantigen-bearing cells is widely thought to be an important piece of the immune system's attempts to control tumour initiation, growth, and spread (immunosurveillance)[30-31].

For a cancer, then, the propensity for mutation is a double-edged sword. On one hand, the tumour must activate enough oncogenes and inactivate enough tumour suppressor genes to achieve self-sufficient survival and growth. On the other hand, the more mutations it accumulates, the greater the chances that one or more of those mutations will generate a

neoantigen that will lead to recognition and destruction by the immune system. There is therefore an evolutionary selective pressure toward tumours that can acquire the minimum number of oncogenic mutations while avoiding immunosurveillance.

As a result of this selection pressure, malignant cells that become numerous enough to form tumours have already acquired mechanisms to escape immunosurveillance. The early detection and elimination of more immunogenic cancer cells allows the less immunogenic populations of cells to become dominant. This is one of the main reasons why the immune response to established tumours is generally so poor. The mechanisms by which immune escape occurs are diverse, from selection for tumours bearing few neoantigens, to some tumours reducing their expression of MHC I, but many rely on inhibiting T cell function. Tumours release immunosuppressive and inflammatory cytokines, or express ligands for immunoinhibitory receptors on immune cells. The end result is that the tumours fight the immune system to a stalemate, buying time for the cancer to establish an immunosuppressive microenvironment and develop additional mutations that will allow it to escape from immune surveillance completely[30-33]. Cancer is therefore in large part a disease (or a failing) of the immune system[19].

In contrast to central tolerance, the immunosuppression induced by the TME does not result in total clonal deletion. Many T and B cells that recognize tumour antigens are still alive and present, but are trapped either in the dormant state called *anergy*[29, 34-35] or in an "exhausted" state. Anergy arises from insufficient co-stimulation during the initial phase of antigen presentation to the T cell ("priming" – see section 1.2.1 Cellular actors and their

roles in the adaptive immune response), and is a largely cell-intrinsic process that does not require the continued presence of the antigen. T cell exhaustion, meanwhile, arises from chronic antigenic stimulation of the T cell without destruction of the infectious agent, resulting in a feedback loop that downregulates effector functions and growth potential. Cells of both these dormant phenotypes can still bind to antigens, albeit weakly due to reduced antigen receptor expression, but are unable to proliferate or mount an immune response as a result of that stimulus. This inhibition is an active process, however – removal of the immune blockade can reactivate dormant cells, and neoantigen-rich tumours can still be killed by the action of these revitalized cells. This strategy of reactivating ineffectual immune cells forms the basis of several forms of cancer immunotherapy, and has become a very active area of research in recent years[36]. This approach has the advantages that immune responses are exquisitely selective, limiting systemic toxicity. It uses the immune system as the toxic agent, limiting the effect of intrinsic resistance mechanisms in the tumour. It can reactivate T cells targeting many different neoantigens, making resistance due to mutation or loss of target expression less likely. It can also be synergistic with traditional radiation or chemotherapy, due to alteration of the TME and release of tumour antigens during tumour destruction[37-40]. However, designing the right agent to reactivate tumour-specific T cells selectively, with minimal reactivity towards healthy tissue, requires careful consideration of both the cellular and biochemical players involved.

## 1.2 Cell-mediated immune response: activation and deactivation

### 1.2.1 Cellular actors and their roles in the adaptive immune response

The adaptive immune response is primarily carried out by two types of cells: B cells, which develop and mature in the bone marrow, and T cells, which migrate from the bone marrow to the thymus to develop and mature. Both sets of cells undergo central selection in order to weed out self-reactive clones. Both cells rely on antigen recognition by their B and T cell receptors, respectively. B cells mediate humoral immunity, while T cells mostly mediate cell-dependent immunity, although there is crosstalk between the two pathways. The regulatory pathways studied in this work are mostly involved in T cell regulation, so B cell activation will not be discussed further.

The activation of the adaptive immune system starts with antigen presentation. Antigenic proteins within normal cells are cleaved by the proteasome into short peptides. These short peptides are then bound by MHC I, which is found on nearly every cell type (including cancerous cells). Meanwhile, dendritic cells, macrophages, and other immune cells take up antigenic proteins, cleave them to peptides, and display these antigenic peptides bound to MHC II. Only select immune cells express MHC II, so these cells are referred to as professional antigen-presenting cells (APC).

The antigen-MHC complex is then recognized by the T cell receptor (TCR) on naïve T cells. Each T cell, regardless of activation status, has a unique TCR that binds a specific

antigen. This remarkable diversity is generated by the somatic recombination of DNA exons coding for various segments of the TCR[41]. This binding event ensures that only those T cell clones specific for that antigen are affected[42]. The co-receptor expressed by the T cell determines the specificity of the response. The CD8 co-receptor binds to MHC I, while the CD4 co-receptor binds to MHC II. Most mature T cells express only one of these two co-receptors.

The antigen presentation event is necessary, but not sufficient for T cell clonal expansion and activation. It must also be accompanied by a second activation signal, most commonly through the CD28 co-receptor that is constitutively expressed on both naïve and activated T cells. The binding of CD28 on the T cell by CD80 or CD86 (also known as B7-1 and B7-2) on the APC lowers the threshold for TCR-induced activation of the T cell, and initiates the production of pro-effector cytokines. The most notable of these cytokines is interleukin-2 (IL-2), which is induced through CD28-dependent mRNA stabilization and transcriptional activation. IL-2 is critical for T cell effector function, and TCR signaling in the absence of the secondary activation signal leads to anergy of that clone and, in some cases, apoptosis. The combination of specific TCR activation and CD28 activation is called T cell priming[43].

The dual stimulation of TCR signaling and CD28 co-receptor signaling induces growth, division, and activation of that clone of T cells. For $CD8^+$ lymphocytes, this involves differentiation into "cytotoxic T cells" ($T_c$) that travel to the site of infection. Infected cells display antigens in a complex with MHC I (which is expressed by all nucleated cells).

$CD8^+$ lymphocytes bind to the antigen-MHC I complex through the TCR and form an immune synapse, leading to release of perforins, granzymes, and other factors that lyse the infected cell[22, 44].

$CD4^+$ lymphocytes also require two stimulatory signals from the TCR and CD28 for activation, although the mature "T helper" cells ($T_h$) are less involved in direct pathogen destruction. Rather, $T_h$ cells are so called because they facilitate and direct the activities of $CD8^+$ T cells and B cells. The type and intensity of immune response is largely controlled by the subtype of $CD4^+$ cells mediating that response. Naïve $CD4^+$ cells can differentiate into many $T_h$ subtypes that are named either based on the order of their discovery ($T_{h1}$ and $T_{h2}$ were the first subtypes identified), their cytokine expression profile (e.g. $T_{h19}$ cells produce IL-19), or their biological role. The $T_h$ subtypes are characterized by differences in their cytokine production profiles[22, 45].

If the infection is resolved through destruction of the pathogen, most of the activated T cells die off while a subset enter a dormant state as memory T cells. These memory cells can be activated again if needed. This reactivation does not seem to require a full priming event, although emerging evidence points to the need for secondary signaling from CD28 for full immune reengagement[46-47].

### 1.2.2 Primary and secondary immune signaling and immune checkpoints

Binding of the TCR to MHC-bound antigen alongside CD28 is the basic requirement for immune stimulation, but full T cell activation is controlled by the amplitude of various signal transduction pathways. These signals can be enhanced or suppressed by other co-activators and co-inhibitors, and the final decision of activation–vs–anergy depends on the sum of all these signals.

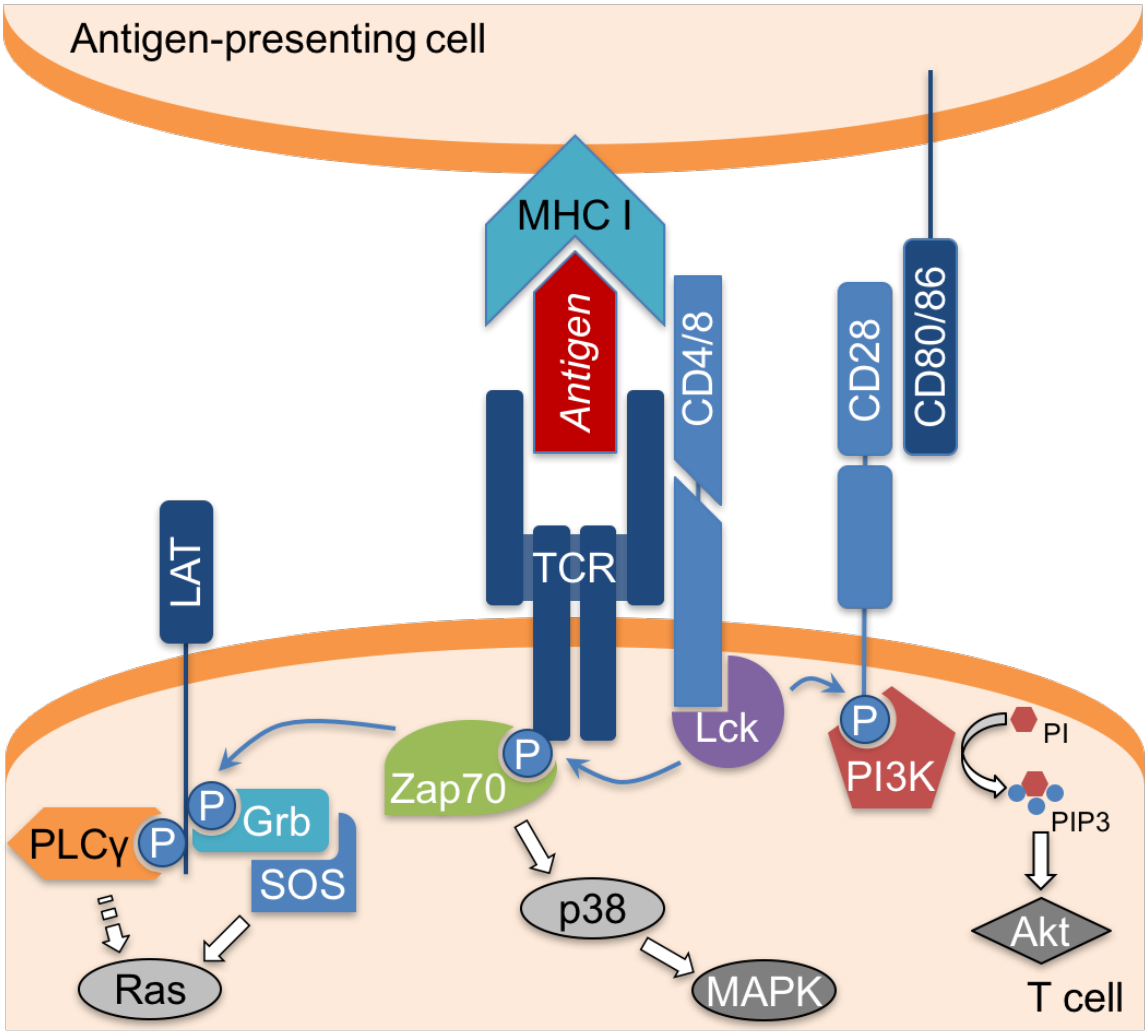


**Figure 2: Signaling pathways involved in T cell priming.**

The primary signal produced by TCR binding is activation of Zap70. When antigen-loaded MHC I is bound by the TCR, it also binds either CD4 or CD8 in the immunological synapse. This brings the TCR and CD4/8 into close proximity, while the inhibitory phosphatase CD45 is excluded from the synapse. The lymphocyte-specific protein tyrosine kinase (Lck) and Fyn kinases associated with CD4/8 can phosphorylate the cytoplasmic tails of the TCR unimpeded. These phosphorylated sites recruit Zap70, which is then itself phosphorylated and thereby activated by Lck. Zap70 is itself a kinase, and it phosphorylates p38, triggering activation of the p38-family mitogen activated protein kinase (MAPK) pathway[44, 48].

Zap70 also phosphorylates the aptly named scaffold protein linker of activated T cells (LAT), opening binding sites for a variety of signalling molecules. LAT activates the Grb2/SOS pathway, leading to activation of the ERK pathway through Ras. Association with phosphorylated LAT also activates phospholipase C (PLCγ1), eventually leading to protein kinase C (PKC) activation, ERK activation once again through Ras, as well as calcium influx.

The secondary signal produced by CD28 binding is activation of the PI3K pathway. The formation of the immune synapse leads to phosphorylation of CD28 by Lck. Phosphorylated CD28 recruits phosphatidylinositide-3-kinase (PI3K) to the plasma membrane, where it generates phosphatidylinositol-3,4,5-triphosphate (PIP3) from membrane-bound phosphatidylinositol. Production of PIP3 activates AKT, which

transmits pro-survival signals through mTOR and cytokine-production signals through PKC[44, 48-50].

The activation of the T cell can be enhanced or inhibited either by direct binding of the TCR or CD4/8, or by activation/inhibition of their downstream effectors. The receptors that carry out these activities are called *immune checkpoint proteins*, in that they are expressed at precise times on specific cell types in order to turn the immune response on and off. Most immune checkpoints were discovered relatively recently, and their characterization constitutes an active area of research[51-55].

One of the best-known immunoinhibitory checkpoint proteins is the cytotoxic T lymphocyte associated protein 4 (CTLA-4). CTLA-4 is a homolog of CD28, and has an even greater affinity for CD80 and CD86 than does the stimulatory receptor CD28. Thus, when CTLA-4 is expressed at the T cell surface, it outcompetes CD28 for ligand binding[56-58]. The unligated CD28 cannot transmit the necessary secondary stimulus, and the T cell becomes anergic. CTLA-4 has also been shown to mediate endocytosis and degradation of APC-bound CD80 and CD86, preventing that APC from stimulating other T cells[59].

A second mechanism for CTLA-4 inhibition of T cell responses, which is somewhat more controversial, is through recruitment of SHP2 phosphatase[60]. CTLA-4 binds to the TCR and recruits SHP2 to the immune synapse. SHP2 then inhibits phosphorylation of the TCR, either by directly dephosphorylating it, or by deactivating Lck. Thus, CTLA-4 interferes

with both direct cell-cell signal transduction as well as the intracellular signal cascade that leads to T cell activation.

CTLA-4 expression is induced on T cells within a few hours of activation[61-62]; this rapid response is due to mobilization of intracellular stores of the protein[57, 62-64]. The levels of CTLA-4 are maintained for 24-48 hours in naïve T cells, and even longer in anergic T cells. CTLA-4 thus mediates both long-term tolerance as well as the short-term kinetics of T cell activation[63].

CTLA-4 was the first immune checkpoint to be targeted pharmacologically, and has seen use in both pro- and anti-immune indications. Fusion proteins of CTLA-4 with human immunoglobulins have been used to inhibit autoimmune responses. Two such drugs, Abatacept and Belatacept, were developed by Bristol-Myers Squibb and have been approved for use in rheumatoid arthritis (Abatacept) and tissue graft rejection (Belatacept)[65].

Blocking antibodies for CTLA-4, meanwhile, were the first such agents used for cancer immunotherapy. Ipilimumab is currently approved for melanoma treatment, but its use carries a significant risk of autoimmune-related side-effects[66-67]. This is likely due to CTLA-4's central role in self-tolerance and regulation of very early T cell expansion. CTLA-4 targeting provided proof of concept that modulating immune activation through immune checkpoint proteins could be a disease-altering therapy[51, 68].

**Table 1: Selected immune checkpoints of therapeutic interest.**

| Receptor | Ligand | Effect on immunity | Therapeutic target? | Notes |
|---|---|---|---|---|
| ICOS (CD278) | ICOSL | + | Yes[69] | |
| OX40 (CD137) | OX40L (CD252) | + | Yes[70-71] | |
| CD27 | CD70 | + | Yes[72] | |
| CD40 | CD40L/CD154 | + | Yes[73] | |
| 4-1BB (CD137) | 4-1BBL | + | Yes[74-75] | |
| GITR | GITRL | + | Yes[76-77] | |
| CTLA-4 | CD80/CD86 | – | Yes – see above | |
| TIM3 | Galectin-9 | – | Yes[78] | |
| LAG3 | MHC II | – | Yes[78] | |
| HVEM | BTLA | – or + | No | |
| *unknown* | B7-H3 (CD276) | – | Yes[78] | |
| *unknown* | B7-H4 | – | Yes[78] | |
| VISTA | *Unknown* | – | Yes – see below | VISTA acts as both a ligand and a receptor |
| *unknown* | VISTA | | | |
| PD1 | PD-L1 and PD-L2 | – | Yes – see below | PD-L1 can also bind CD80[79-80]; the functional outcome of this is debatable |

While CTLA-4 was the first immune checkpoint to be studied in-depth, many others have come to the fore, and others have yet to be discovered. Among co-stimulatory receptors, ICOS/CD278 and OX40 are perhaps the best-known; ICOS shares homology with CD28 and is important in activation and proliferation of $T_h$ (especially $T_{h2}$) cells[81], while OX40

is important for long-term maintenance of immune activation[82-84]. Among inhibitory receptors on T cells, LAG3, B7-H3, VISTA, and TIM3 are perhaps the best-known; B7-H3 and VISTA are part of the CTLA-4 family, while LAG3 is in the Ig superfamily and TIM3 contains both Ig and mucin domains. However, the most studied immune checkpoint, if not necessarily the best-understood, is programmed death 1 (PD1).

### 1.2.3 Programmed cell death 1 and its signaling pathway

Programmed cell death 1 (PD1) is another immune inhibitory receptor, in the same family of proteins as CD28 and CTLA-4. It is expressed at low levels on naïve T and B cells, and expression is induced by T or B cell activation[35, 85]. The lag time between T cell activation and PD1 expression is longer than for CTLA-4, with expression taking between 24 and 48 hours[86-87].

PD1 has two known ligands: programmed death ligand 1 (PD-L1) and programmed death ligand 2 (PD-L2). PD-L1 is constitutively expressed on many tissues[88], particularly those that are "immune-privileged" like the heart, eye, and placenta[89]. Its role in these tissues is to maintain peripheral tolerance in these sensitive locations. PD-L1 is also inducibly expressed by many immune effector cells (macrophages, dendritic cells, T cells, B cells) upon activation, providing a feedback loop to control the duration of immune responses. PD-L2 expression is largely restricted to immune cells, particularly APCs like dendritic cells, though it is expressed at a low level on many tissues[35, 42].

On a physiological level, PD1 plays an important role in induction and maintenance of peripheral tolerance, especially in the restraint of self-reactive T cells[90-91]. PD1 expression is induced by TCR signaling, and the lag time between T cell activation and PD1 signaling opens a window for T cells to carry out their effector functions. The increasing PD1 signaling then starts to limit both TCR expression and cytokine secretion (limiting effector functions), and promotes a senescent phenotype characterized by cell cycle arrest and a switch from a glycolytic metabolism to a lipolytic one[89, 92]. Moreover, in addition to its direct role in inhibiting $T_h$ and $T_c$ activation, PD1/PD-L1 signaling is critical in inducing and maintaining activation of $T_{reg}$ cells[93].

Thus, in contrast to CTLA-4, which is responsible for the amplitude of initial immune responses and breaking of self-tolerance, PD1 plays a more subtle and specialized role. It sets the threshold for TCR activation by counteracting the signaling pathways involved and by downregulation of TCR expression[91], acts to rein in peripheral immune responses after an appropriate amount of time, and then maintains those clones in a dormant state[42]. While CTLA-4 blockade typically results in activation and proliferation of many new T cell clones in lymphoid tissue, blockade of PD1 reactivates a much smaller subset of cells, and affects primarily their effector function rather than their proliferation. Defects in either PD1 or PD-L1 typically lead to eventual uncontrolled self-reactive immunity, and genetic defects in PD1 are associated with various autoimmune disorders[94].

On a biochemical level, TCR-associated PD1 is activated by binding to either of its two ligands. The bound PD1 is then phosphorylated by Lck (or Fyn, in B cells), creating a

binding site for the recruitment of SHP1 and/or SHP2 phosphatases. SHP1/2 act to dephosphorylate TCR-bound Zap70 as well as effectors downstream of CD28[49, 86]. PD1 thus inhibits both the primary TCR-mediated and secondary CD28-mediated signals for immune activation, though it is proposed to affect the secondary signal to a greater degree[42].

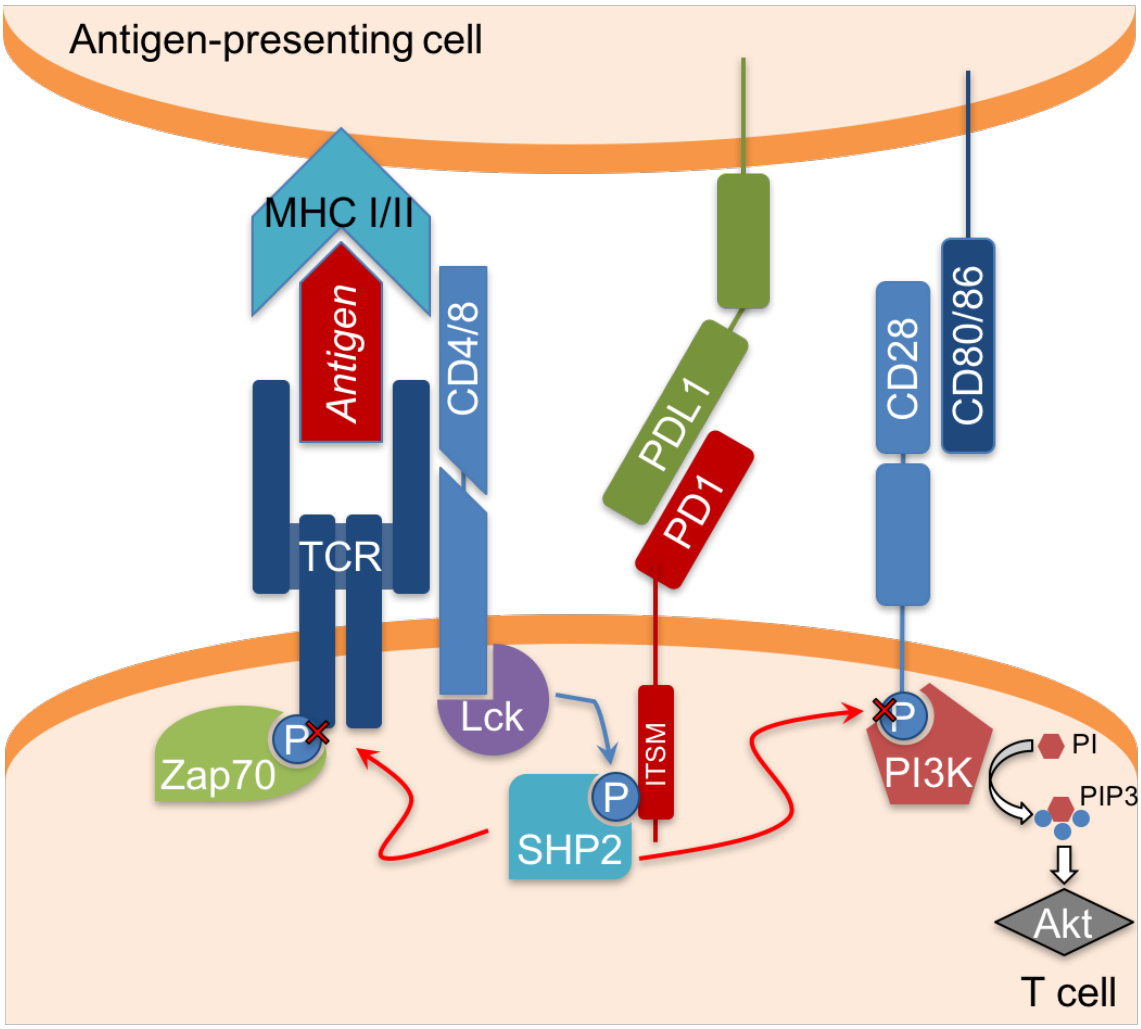


**Figure 3: Signal transduction pathway of PD1. Note that PD1 acts only indirectly on T cell activation pathways.**

The SHP2-mediated signaling of PD1 also has downstream effects on T cell behaviour beyond TCR/CD28 signaling. Ligation of PD1 leads to cell cycle arrest of the affected lymphocytes, a key event in T cell anergy[34]. Moreover, PD1 signaling leads to a switch from highly active glycolytic metabolism to a lower-activity metabolic state. PD1 signaling also increases the rate of TCR internalization and degradation through upregulation of E3 ubiquitin ligases. These pathways have the combined effect of reducing the number of T cell receptors for antigen binding, reducing the sensitivity of the T cell to antigenic signals, and interfering with the T cell's ability to respond to antigenic signals[35, 44, 95].

## 1.3 Structure and interactions of PD1 and PD-L1

### 1.3.1 Structure of PD1

PD1 is a 288-amino acid type 1 protein, of which the first 20 amino acids constitute a signal peptide that is cleaved upon membrane insertion. PD1 consists of a large extracellular portion with a single IgV-like domain perched atop a short stalk, a transmembrane domain, and a cytoplasmic domain containing both an immunoreceptor tyrosine-based inhibitory motif (ITIM) and an immunoreceptor tyrosine-based switch motif (ITSM)[35, 49].

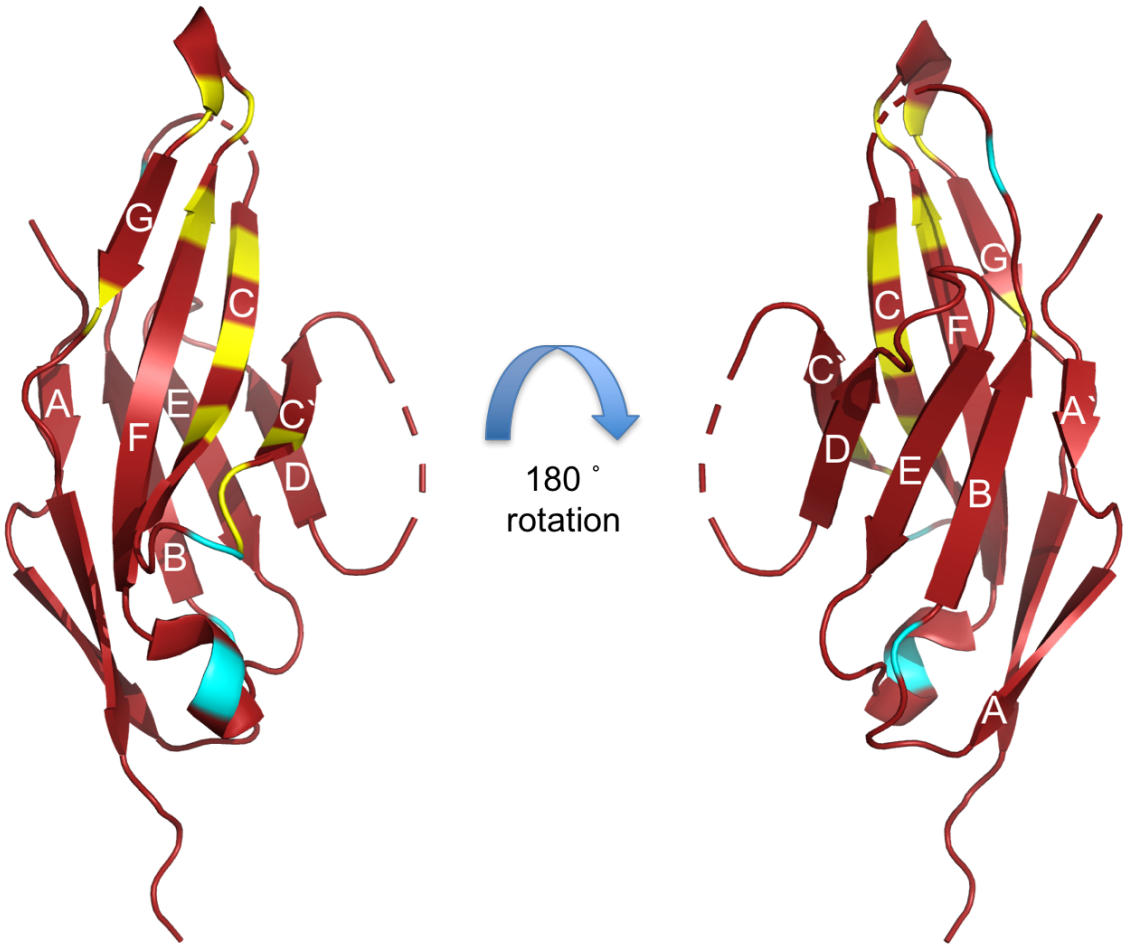


**Figure 4: Crystal structure of human apo-PD1 (PDB: 3RRQ). The C terminus (bottom) connects to the transmembrane domain. Yellow: PD-L1-binding surface; cyan: glycosylation sites.**

The IgV domain of PD1 adopts a ß-sandwich topology, similar to other members of the B7 family. Two beta sheets of four strands each lay flat, one atop the other, and are stabilized by an intramolecular cross-sheet disulfide bridge between Cys54 and Cys123. The front face, comprising the GFCC` beta-sheet, contains most of the ligand binding site[96-97].

In contrast to other B7 family receptors like CD28, PD1 does not form covalent homodimers through a membrane-proximal cysteine. Moreover, PD1 has been shown to be rigorously monomeric, both in solution[98-99] and on the cell surface[96].

PD1 is extensively glycosylated on its extracellular domain, although what effects these have, if any, on its biological function remain unknown. The sites of glycosylation are distal to the PD-L1-binding surface, and there is no indication that the sugar chains are involved in ligand binding. The glycan was originally implicated in binding to a PD1-blocking antibody, but it was later found that it was the N-terminal loop, not the sugars, that was responsible for binding[100]. Rather, glycosylation of PD1, especially fucosylation, is important for protecting the protein from targeted proteasomal degradation[101].

The intracellular domain of PD1 mediates its signal transduction, though little is known about its secondary and tertiary structure. The central tyrosine of both the ITIM and the ITSM can be phosphorylated, resulting in recruitment of SHP1 and SHP2 phosphatases. Of the two recruitment sites, only ITSM seems to be essential for the inhibitory effects of PD1 ligation, and phosphorylation of that tyrosine is required for downstream signaling[49, 86]. Mutation of the ITSM tyrosine results in a protein incapable of inhibiting immune responses, while mutation of the ITIM tyrosine is tolerated. Likewise, only SHP2 has been conclusively shown to be necessary for immunosuppression. The exact role of both the ITIM sequence and SHP1 in PD1 signaling are unclear.

### 1.3.2 Structure of PD-L1

PD-L1 is a 290 amino acid type 1 protein, of which the first 18 amino acids constitute a signal peptide that is cleaved upon membrane insertion. PD-L1 consists of a large extracellular portion with a membrane-distal IgV-like and a membrane-proximal IgC-like domain, a transmembrane domain, and a very short cytoplasmic tail. Like PD1, PD-L1 differs from its B7 family members by not forming disulfide-linked homodimers. This has led to the assumption that it is monomeric at the cell surface, although this assumption accounts only for covalent linkages – whether PD-L1 forms oligomers through weak interactions is unknown. The Gao group has reported that PD-L1 forms noncovalent dimers based on a crystal structure and solution-phase covalent crosslinking[102]. The two protein units of this symmetric homodimer line up parallel to one another, with the dimer interface consisting of large hydrophobic patches between the back faces of the two IgV domains (buried surface area of 859 Å) and between the back faces of the two IgC domains (buried surface area of 1292 Å). Gao made no mention of PD-L1's oligomeric behaviour by gel filtration or any other dynamic methods.

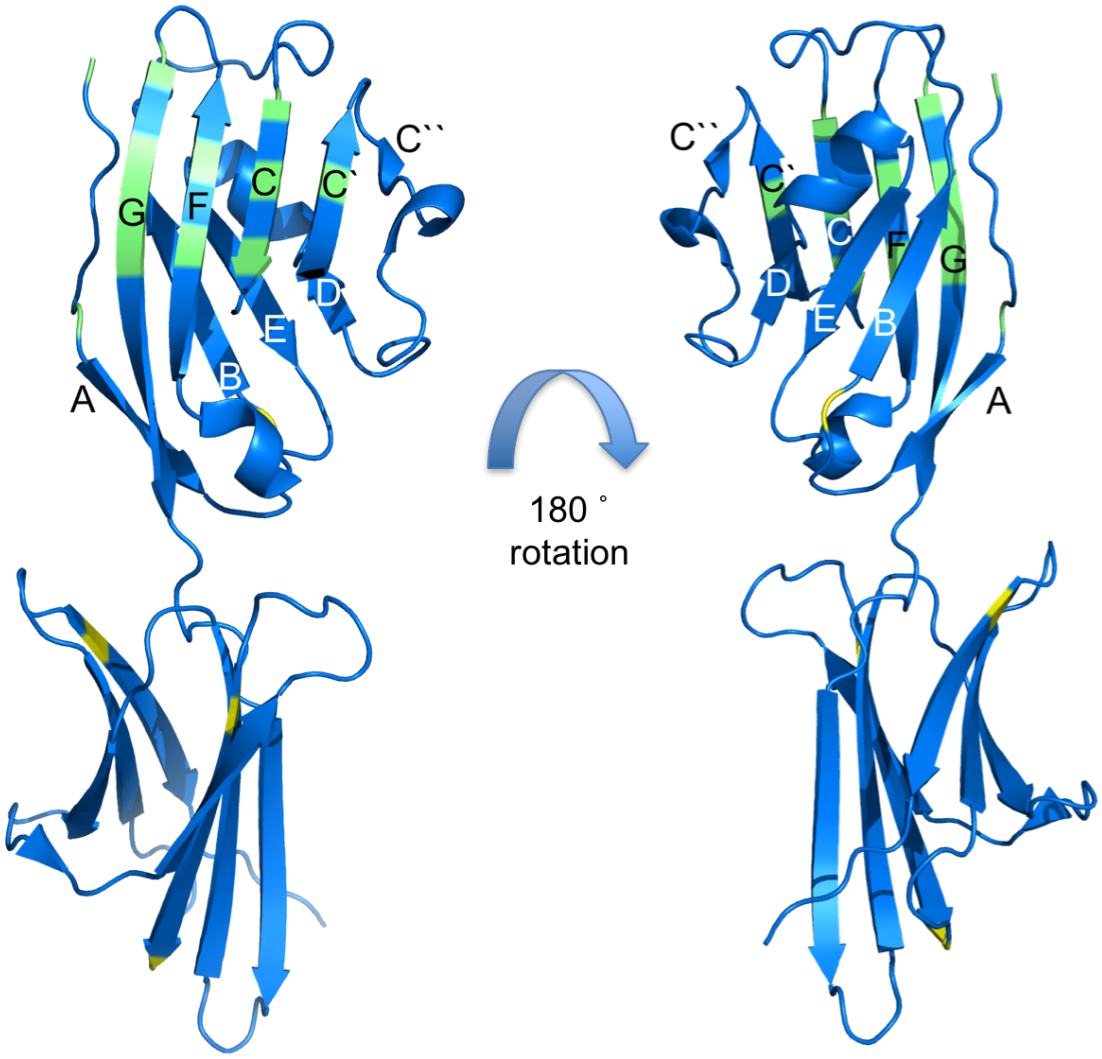


**Figure 5: Crystal structure of human apo-PD-L1 (PDB: 3BIS). The C terminus (bottom) connects to the transmembrane domain. Green: PD1-binding surface; yellow: glycosylation sites.**

The IgV domain of PD-L1 is arguably its most important feature, as it contains the entirety of the PD1 binding site. This region adopts the characteristic ß-sandwich typical of immunoglobulin domains, with one sheet of 5 strands linked to the other sheet of 3 strands by a central disulfide between Cys40 and Cys114. The front face of the PD-L1 IgV domain contains the binding site for PD1[97, 102-103].

The IgV domain is heavily *N*-glycosylated, although like PD1 this glycosylation does not interfere with the binding face. Rather, the extent of glycosylation is important for PD-L1 stability. Glycogen synthase kinase 3ß (GSK3ß) phosphorylates PD-L1, and this phosphorylation targets PD-L1 for ubiquitination and proteasomal degradation. Glycosylation of PD-L1 inhibits GSK3ß binding, thereby preventing phosphorylation and subsequent ubiquitination[104].

The IgC domain of PD-L1 is also a ß-sandwich, with sheets of 4 and 3 ß-strands rigidified by a central disulfide bond between Cys155 and Cys209. The residues closest to the hinge region between the two Ig domains are conserved across both murine and human PD-L1, and seem to interact with one another in some way[102]. The physiological relevance of this interaction will be discussed below, as well as in Chapter 2.

### 1.3.3 Structure of the PD1/PD-L1 complex

PD1 and PD-L1 bind to one another in a 1:1 stoichiometry, although 2:1 and 2:2 units in crystal structures are not uncommon as the result of crystallization artefacts or packing forces[97, 103, 105]. Both proteins bind to one another through large hydrophobic patches on their front faces; the interaction largely takes place between the ß-sheets, and the inter-strand loops are not involved. The measured affinity of the interaction varies in the literature between 0.77-8 μM[80, 98, 103, 106].

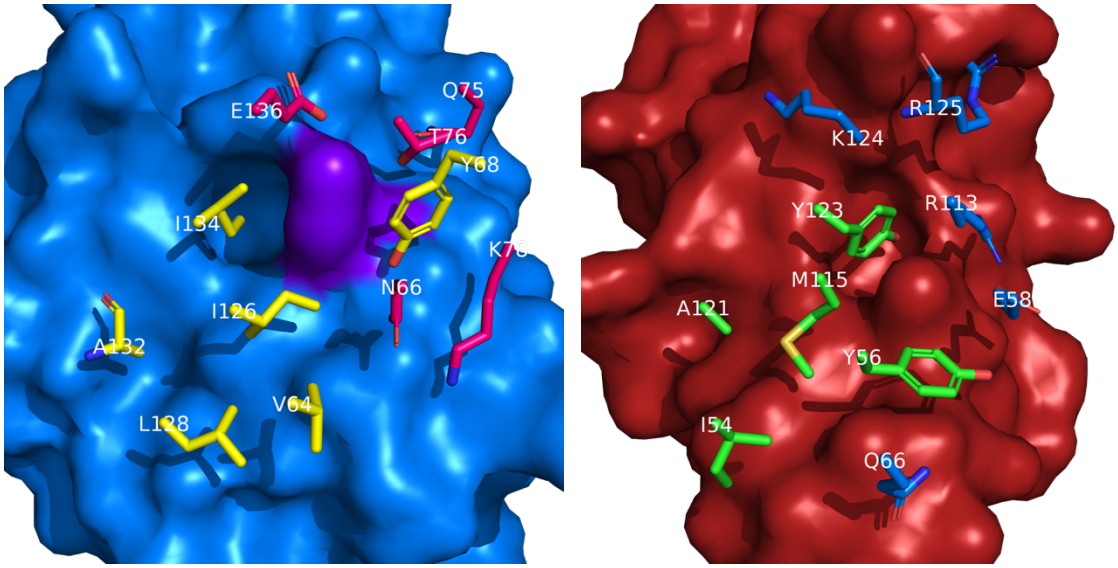


**Figure 6: Simplified view of the PD1/PD-L1 interaction surfaces. Left: hPD-L1 (blue) with the sidechains of the most important hPD1 residues for binding (yellow: hydrophobic; red: hydrophilic). Right: hPD1 (red) with the sidechains of the most important hPD1 residues for binding (green: hydrophobic; blue: hydrophilic).**

The primary interaction between the two proteins is a hydrophobic surface of 1,970 Å$^2$. This core is bordered by polar interactions on all sides other than the BC and FG loops. One can thus envision the interaction surface as a hydrophobic "palm" stabilized and protected by solvent-accessible polar residues[97-98, 103].

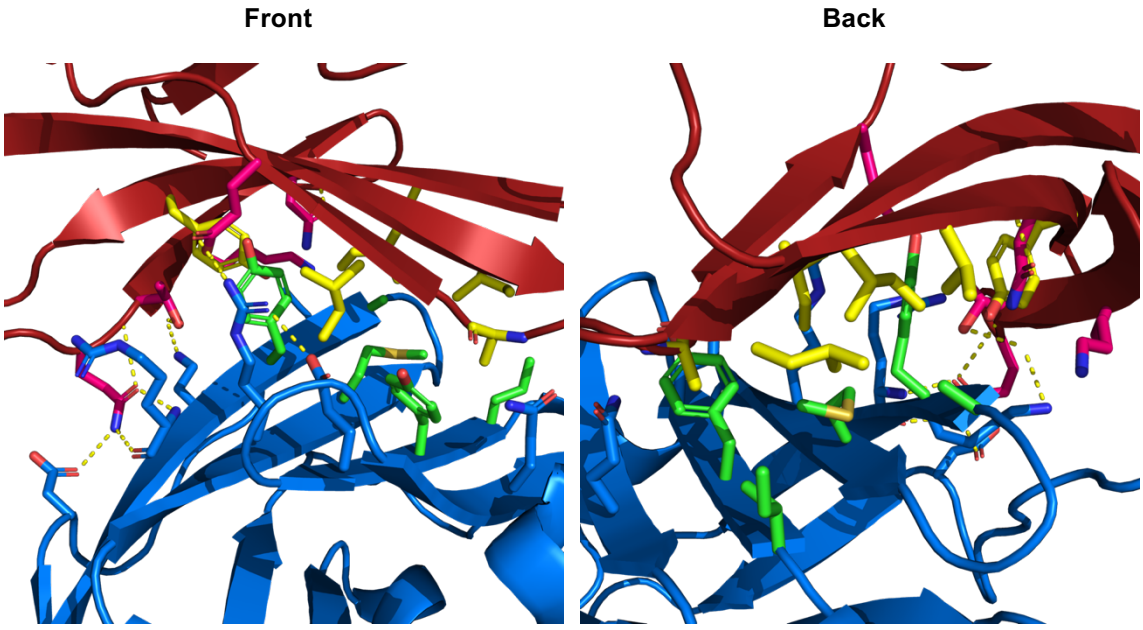


**Figure 7: Interaction surface of hPD1 and hPD-L1 in a co-crystal structure (PDB: 4ZQK). hPD1 in red, hPD-L1 in blue. Hydrophobic residues are coloured in yellow (hPD1) and green (hPD-L1), while polar residues are coloured the same as the main chains.**

PD1 undergoes significant rearrangement upon PD-L1 binding. The relatively flexible CC` loop of apo-PD1 clamps down around PD-L1, forming four hydrogen bonds (through the side chains and backbones of Gln75 and Thr76) in the process.

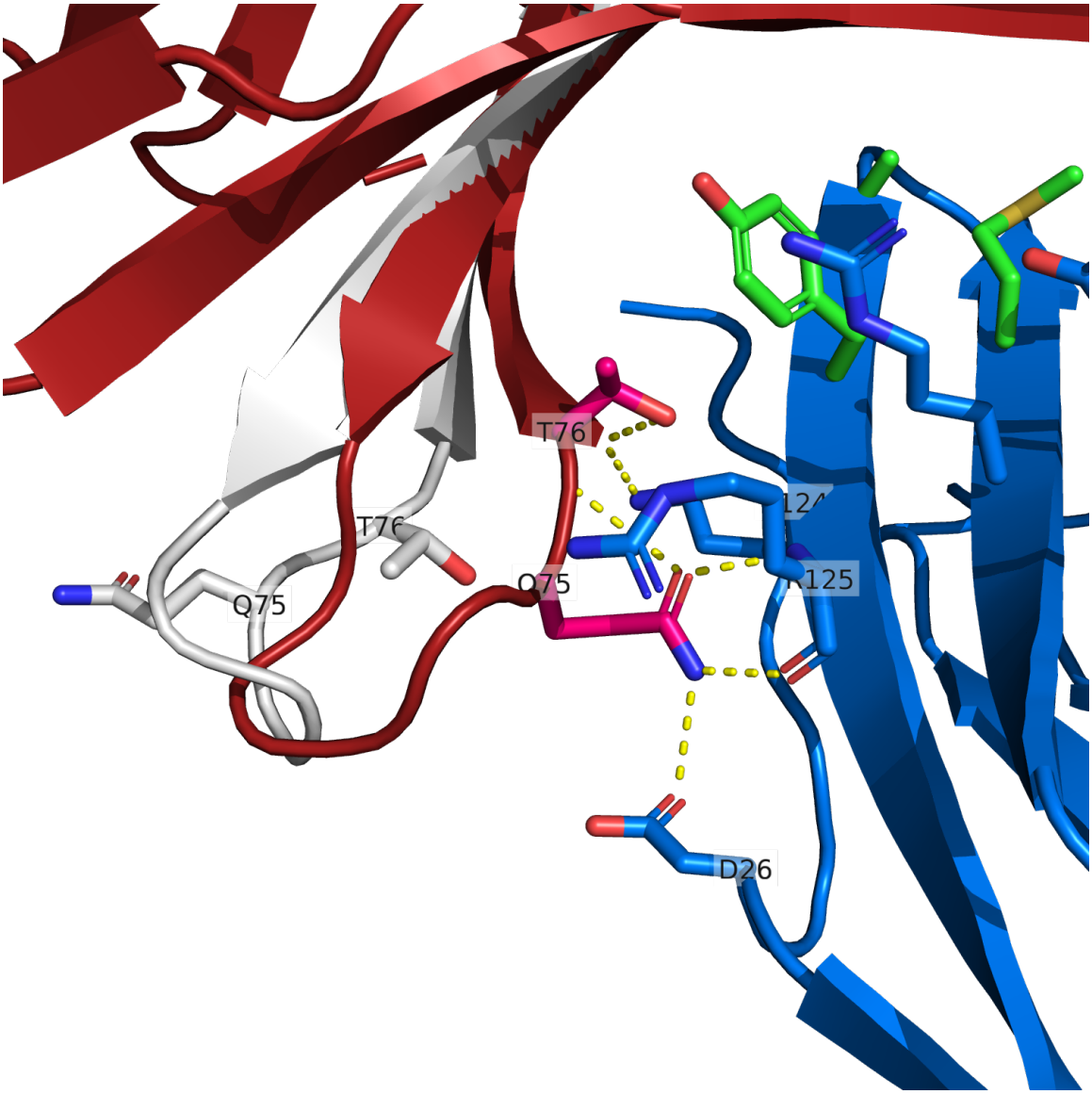


**Figure 8: Conformational change in CC` loop of hPD1 on binding. Compared to the apo structure (white, PDB: 3RR1), the CC` loop of PD-L1-bound hPD1 (red) moves in towards the interaction surface, with Q75 and T76 forming new hydrogen bonds with D26, K124, and R125 of PD-L1.**

PD-L1, meanwhile, does not undergo much change to the backbone structure or even to the conformation of individual sidechains. Glu58, Met115, and Tyr123 come together to form a hydrophobic pocket for Ile134 of PD1, and Ile54 and Ala121 move slightly, but most changes in position are less than 3 Å. The exception is Arg113, whose sidechain

moves to form a salt bridge with Glu136 of PD1 and an intramolecular hydrogen bond with Glu58.

The structure of the protein-protein interface suggests that specific residues will have a disproportionate influence on the strength of binding; these are known as hotspots. Hotspots are important in drug discovery for protein-protein interactions, as they provide the greatest gains in inhibitory activity relative to the area or volume they occupy[97]. The main feature of hPD1 is the deep cleft formed to accommodate Tyr123 of hPD-L1 (see Figure 6), which could be targeted with similar phenolic compounds. Meanwhile, hPD-L1 is somewhat more shallow, with a hydrophobic groove extending around Tyr123.

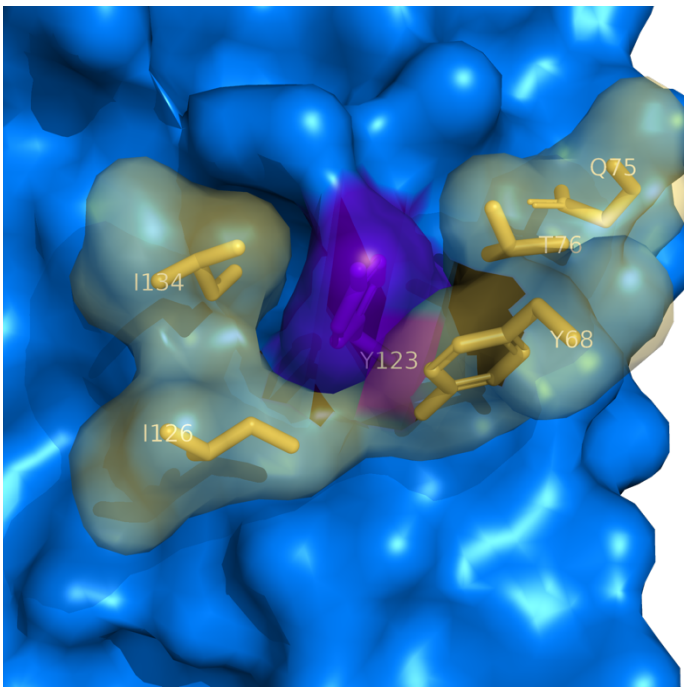


**Figure 9: Hydrophobic groove surrounding Tyr123 of hPD-L1 (blue). Space filled with interacting sidechains from hPD1 (yellow).**

While the fine structure of PD-L1 does not change very much upon ligand binding, its gross structure changes quite considerably. Apo-PD-L1 bends by about 30˚ at the hinge region between the two domains, whereas PD1-bound PD-L1 adopts a straight, elongated conformation, with concomitant loss of inter-domain interactions[102]. It is possible that the elongation event is necessary for PD1; it is also possible that it is entirely irrelevant to the function of the protein. Chapters 2 and 3 expand on the relevance of PD-L1 hinge interactions.

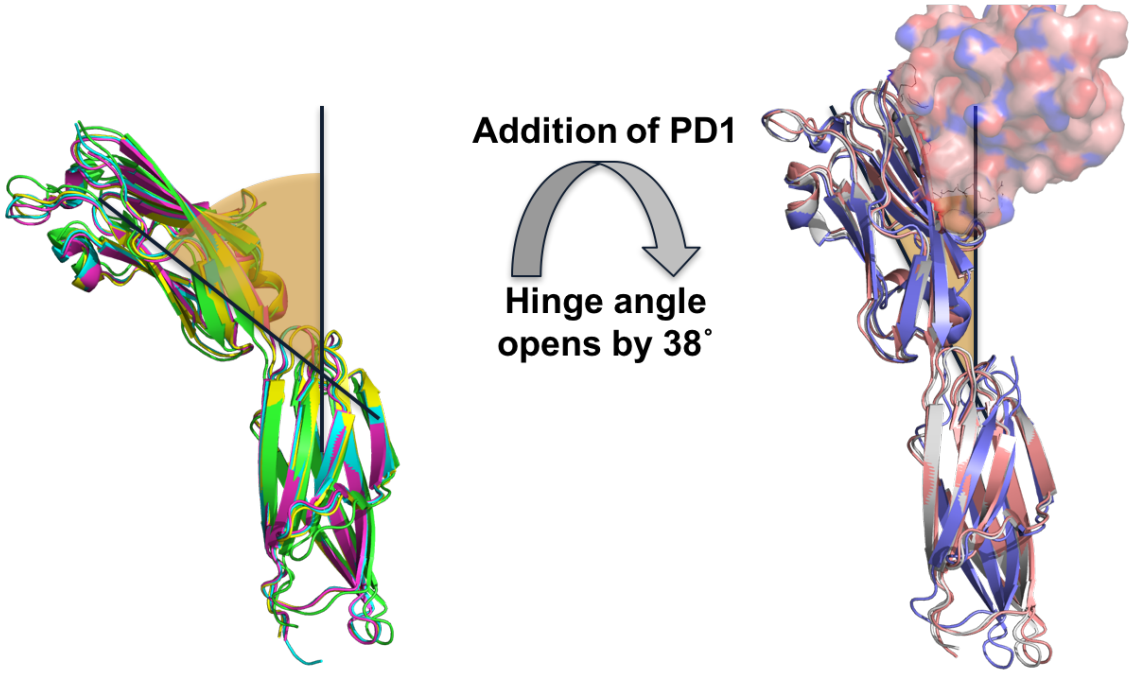


**Figure 10: Structural rearrangement of PD-L1 on ligand binding. Left: multiple apo-PD-L1 structures aligned (PDB: 3BIS, 3FN3, 4Z18, 5JDR). Right: multiple PD1-bound PD-L1 molecules, aligned by binding domain (PD1 as a space-filling model; PDB: 3BIK, 3SBW).**

### 1.3.4 Soluble PD-L1

While membrane-bound PD1 and PD-L1 have been investigated mostly for their role in direct cell-cell communication, recent studies have found that the extracellular domains of both PD1 and PD-L1 exist as soluble proteins in the plasma. This discovery is relatively recent, and most of the work on elucidating the provenance and roles of these proteins is still in early stages[107].

Soluble PD1 (sPD1) seems to be produced solely as the result of alternative splicing, with one of the five known splice variants (Δex3) lacking the exon coding for the transmembrane domain of PD1[107-112]. sPD1 is found in normal human serum, but is significantly elevated in various cancers, autoimmune disorders, and chronic viral infection[108-110, 113-115]. sPD1 retains PD-L1 binding, however, and as a result should function as a "decoy" receptor for PD-L1, inhibiting binding to T cell-bound PD1. In theory, this should result in increased immune function, the same way a PD-L1 blocking antibody would. In practice, the results are mixed. In some cases, sPD1 plasma levels correlate with better response to immunotherapy[109, 116-117] or aberrant autoimmune responses[108, 110-111, 115], while in others they correlate with poor immune function[118-119]; in some cases, sPD1 levels appear to be irrelevant[114]. sPD1 may be a causative agent of autoimmunity, a host response to immunosuppression, or merely a coincidental biomarker. It is too early to say definitively which explanation best reflects the reality.

The origins and probable role of soluble PD-L1 (sPD-L1) are very different from sPD1. sPD-L1 is almost certainly the product of proteolysis of membrane-bound PD-L1[120], with the extracellular domain being shed into the extracellular space[121]. The source of sPD-L1 seems to be both the cancers themselves[122] as well as non-cancerous immune and stromal cells[123], highlighting the importance of non-malignant cells and the tumour microenvironment in immunosuppression. The biological role of sPD-L1 seems clear: elevated sPD-L1 correlates with poor prognosis and poor response to both chemotherapy and immunotherapy[122, 124-131], in keeping with its role as a ligand for an immunoinhibitory receptor.

## 1.4 PD1/PD-L1 in disease states

### 1.4.1 The PD1/PD-L1 axis in virology

The clinical importance of aberrant PD1/PD-L1 function was first realized in the context of virology. It was observed that PD1 was highly expressed on $T_c$ cells upon chronic viral infection, as in SIV/HIV[132-133] or hepatitis C[134]; these T cells were unable to replicate even in the presence of antigens, and were therefore termed "exhausted" – as though their state of chronic activation had eroded their ability to respond to further challenges[35, 135-138]. Since T cell exhaustion led to chronic infection and disease progression, and PD1 appeared to be a key mediator of T cell exhaustion, PD1 blockade should rejuvenate these exhausted T cells. Indeed, blocking of either PD1 or PD-L1 with antibodies results in restoration of virus-specific T cell activity in lymphocytes isolated from patients with HIV[133-134, 137]. This

model provided proof of concept that PD1 inhibition could be a viable therapeutic target for increasing T cell function[53].

However, targeting PD1 in an HIV setting was fraught with safety and efficacy issues. One of the primary causes of death in patients with HIV is opportunistic bacterial or viral infection[139-140]. Although blocking the PD1 pathway results in increased T-type anti-HIV immunity, it can also throw off the delicate balance between innate and adaptive immune responses. Knockdown of PD1 has been shown to actually *increase* susceptibility to *M. tuberculosis* infection[141-142] – certainly not a desirable effect in immunocompromised patients with AIDS.

Moreover, AIDS is a systemic and chronic disease. HIV-infected lymphocytes are ubiquitous, and the inflammation they induce is delocalized and long-lived. Thus, while PD1 is a good marker of exhausted virus-specific T cells[132-133, 137], it is only one of many inhibitory co-receptors responsible for maintenance of T cell exhaustion. Moreover, it has been suggested that exhaustion of the human immune system results from many more inhibitory events (checkpoint receptors, loss of CD28) than the murine immune system, and therefore interventions in humans might require multiple checkpoint inhibitors to achieve the same effects seen with PD1 blockade in mice[138, 143-144]. Nevertheless, the benefits of PD1 blockade in HIV settings are still under study.

### 1.4.2 The PD1/PD-L1 axis in cancer – importance and status as a therapeutic target

Following the elucidation of PD1/PD-L1 misregulation in viral infection, a key discovery was made that PD1 ligands are upregulated in a variety of human cancers[145-150]. PD-L1 is overexpressed in urothelial cancer[151-152], liver cancer[153-155], lung cancers[156-162], ovarian cancer[163-165], gastric cancer[166], leukemias and lymphomas[167-176], breast cancer[148, 177-178], esophageal and oral cancers[149, 179-181], melanoma[182-183], and renal cell carcinoma[184-186]. Moreover, while PD-L1 is not universally expressed in all cases of a given cancer (as few as 10-20% of patient samples may test positive), PD-L1 expression is also correlated with tumour stage[148, 150-152, 158, 178, 180-182, 185-186] and most commonly with poor survival outcomes[147-151, 153-154, 157-158, 163, 166, 168, 176, 178, 180, 182, 185], making it a strong prognostic marker.

Critically, multiple groups showed that experimental ablation of PD1 or PD-L1 could reverse exhaustion of tumour-specific T cells, and that such a blockade led to improved tumor clearance and survival in immunocompetent animals[187-190]. On a genomic level, Honjo and coworkers[189] showed that PD1 knockout mice were more resistant to liver metastasis than wildtype and PD1-expressing transgenic mice. Moreover, transgenic PD1-expressing mice showed accelerated rates of primary tumour growth. The same study by Honjo found that antibody blockade of PD1 achieved similar resistance to liver cancer metastasis as PD1 genomic knockout. Kline and coworkers[191] showed that immunocompetent C57BL/6 mice rapidly develop tumours when injected with a syngeneic myeloid leukemia cell line, but that PD1 knockout mice resisted the tumour challenge due

to improved antitumour immunity. Pharmacological interventions showed similarly encouraging results. In a seminal report, Blank *et al.*[187] showed that an anti-PD-L1 antibody enhanced $T_c$ and $T_h$ effector activity after *in vitro* priming by either antigen-loaded beads or PD-L1-expressing cancer cell lines. Nomi *et al.*[154] have shown that blockade of either PD1 or PD-L1 results in delayed tumour growth in a murine model of liver cancer. In one study, co-administration of an anti-PD-L1 or anti-PD1 antibody with gemcitabine resulted in complete tumour destruction in a murine model of pancreatic cancer[154]. In short, PD-L1 expression is not just a tumour marker – it is a therapeutic target.

### 1.4.3 Antibody therapeutics for the treatment of cancer

Early research validating PD1 and PD-L1 as cancer targets has led to the development of therapeutic antibodies that block their interaction. Some of these are now FDA approved for various indications, while others still are in clinical trials. The results of PD1 and PD-L1 inhibition by antibodies have been extremely successful in some contexts; as a result, the individual antibodies, as well as their utility in various indications, have been thoroughly and repeatedly reviewed[68, 78, 190, 192-195]. What follows is merely a summary of their features and drawbacks.

Antibodies targeting PD1 were the first therapeutics to see clinical trials and FDA approval. Pembrolizumab/Keytruda™ by Merck and nivolumab/Opdivo™ by Bristol-Myers Squibb were the first PD1-targeting agents to gain FDA approval for cancer therapy, and are now approved for melanoma, non-small cell lung cancer, Hodgkin's lymphoma, head and neck

squamous cell carcinoma, and bladder cancer. Opdivo is additionally approved for renal cell carcinoma; Keytruda is additionally approved for treatment of urothelial carcinoma and gastric junction adenocarcinoma. Keytruda has also received the first ever approval for treatment of cancers defined by their genomic features, not their original location[196]. These therapies are particularly attractive in that they target cancers that are highly resistant to traditional chemotherapy.

Keytruda and Opdivo are both humanized IgG4 monoclonal antibody targeted to the PD-L1-binding face of PD1[100, 197-199]. Because their targets reside on the T cells that clinicians hope to activate, both antibodies have been designed so that they do not trigger antibody-dependent cellular toxicity[194]. Nivolumab and pembrolizumab show very similar profiles in the types of cancers that respond, as well as their quantitative efficacy[194]. Synergistic effects have also been seen in trials of nivolumab/ipilimumab (anti-CTLA-4) combinations, with response rate jumping from 11% for ipilimumab alone to 60% for ipilimumab plus nivolumab. This suggests that combinations of immune checkpoint inhibitors may be a viable strategy for boosting therapeutic effects in the future[200].

An important determinant of the success of immune checkpoint blockade appears to be the level and location of checkpoint expression. Nivolumab recently failed to show efficacy as a first-line treatment in non-small cell lung cancer, while pembrolizumab met its endpoints for a trial of a similar indication. The two therapeutic agents are mostly interchangeable; the difference lies in the patients selected for inclusion. The pembrolizumab trial had strict criteria requiring >50% of cells to stain positive for PD-L1 in a recent biopsy. On the other

hand, the nivolumab trial required only >5% staining for inclusion, and these biopsies were performed up to 6 months prior to treatment. Moreover, the staining agents used by each company are different, as are the criteria for which cells to count (all cells vs. malignant vs. TILs). Despite encouraging results from difficult disease areas, checkpoint inhibition is clearly not a cure-all, and care must be taken to ensure that the checkpoint being inhibited is actually relevant in a particular patient[201-203].

Among antibodies targeting PD-L1, three are currently approved for use: avelumab/Bavencio™ by Merck and Pfizer, atezolizumab/Tecentriq™ by Genentech and Roche, and durvalumab/Imfinzi™ by MedImmune and AstraZeneca. These agents have arrived somewhat more recently than the PD1 inhibitors, although the first PD1/PD-L1-targeting therapy to make it to clinical trials was actually a PD-L1 blocking antibody (BMS-936559)[194]. So far, atezolizumab is approved for urothelial carcinoma and lung cancer, while avelumab is only approved for Merkel cell carcinoma[204], and durvalumab is only approved for urothelial carcinoma[205].

Many other PD1- and PD-L1-targeting antibodies are at various stages of development, and are being tested in various indications. The list presented in Table 2 is not exhaustive, nor will it be current for very long. The progress of each of these agents is reviewed frequently, however[190, 195, 206-208].

**Table 2: Summary of anti-PD1 and anti-PD-L1 agents in clinical trials[190, 206]**

| Inhibitor | Type | Company | Target | Phase | Approved for |
|---|---|---|---|---|---|
| **Nivolumab** | IgG4 | Bristol-Myers Squibb | PD1 | Approved | Melanoma, NSCLC, Hodgkin's lymphoma, HNSCC, RCC |
| **Pembrolizumab** | IgG4 | Merck | PD1 | Approved | Melanoma, NSCLC, Hodgkin's lymphoma, HNSCC, UC, any solid cancer with microsatellite instability or DNA mismatch repair deficiencies |
| **Durvalumab** | IgG1 | AstraZeneca | PD-L1 | Approved | UC |
| **Avelumab** | IgG1 | Merck/Pfizer | PD-L1 | Approved | Merkel cell carcinoma |
| **Atezolizumab** | IgG1 | Roche | PD-L1 | Approved | UC, NSCLC |
| | | *in development* | | | |
| **AMP-224** | PD-L2 fusion | GlaxoSmithKline | PD1 | 1 | |
| **AMP-514** | IgG4 | GlaxoSmithKline | PD1 | 1 | |
| **Pidilizumab** | IgG1 | Cure Tech | PD1 | 1/2 | |
| **BMS-936559** | IgG4 | Bristol-Myers Squibb | PD-L1 | *Inactive* | |
| **PDR001** | IgG4 | Novartis | PD1 | 1/2 | |

While PD1/PD-L1 inhibition has shown remarkable efficacy in some disease settings, preclinical validation has not always matched up with results in humans. In particular, pancreatic cancer has proven particularly resistant to anti-PD1 therapy[209-211] (as it has to most other treatments), likely as a result of its relative non-immunogenicity. Moreover, pancreatic tumours typically have extremely dense stroma; this results in both poor tumour penetration of the antibody, as well as inhibited infiltration by T cells[212]. Furthermore, response to PD1/PD-L1-targeting immunotherapy is highly variable and closely tied to expression of various biomarkers[213-214]. However, PD-L1 expression itself does not guarantee response[215-218], and many patients whose tumours test as PD-L1-negative can still derive benefits from PD1-targeting antibodies[219-220]. Immunotherapy is therefore best

directly at T cell-accessible tumours that are immunogenic[221] and bear the appropriate biomarkers for susceptibility to checkpoint inhibition. The identification and detection of those biomarkers is crucial to the effective use of immunotherapy, but has lagged behind the development of these antibodies themselves.

Moreover, while checkpoint inhibitors do not have the direct host toxicity of traditional cytotoxic chemotherapies, they do have adverse effects. The pattern of adverse effects caused by these checkpoint inhibitors is unique, and these events have been termed immune-related adverse events (irAEs)[222-224]. These consist of gastrointestinal, pulmonary, hematologic, ocular, cardiac, and neurologic toxicities brought about by autoimmune activation, and their occurrence is very common. The irAEs seen in anti-CTLA-4 therapy are both more common (~60% vs 40% for anti-PD1) and more likely to be serious (40% vs 5%). These results are consistent with CTLA-4 being a central regulator of *de novo* immunity, while PD1 controls peripheral tolerance to existing antigens.

The irAEs due to anti-PD1 therapy can nevertheless limit their tolerability and usefulness, and there is some indication that the antibody nature of PD1 blockers is at least partly responsible for these effects. The antibodies used in anti-PD1 therapy have long half-lives (18-28 days for both pembrolizumab and nivolumab, depending on dosage[225-227]), meaning therapy cannot be effectively withdrawn in the case of an autoimmune response, and the toxic response must be treated with additional drugs and the patient monitored during this time[228]. These immunotoxic effects, combined with poor tissue penetration of

antibodies[229-231], and high cost of production[202, 232] make antibodies a less-than-ideal platform for broad-use therapy.

### 1.4.4 Peptides, proteins, and related compounds

Over the years, several groups have attempted to use high-affinity mutants of PD1 as PD-L1-blocking agents. These proteins have the advantages that they are smaller (14 kDa vs 150 kDa) and less immunogenic than antibodies, their binding sites are definitively known and tunable through rational mutation, and they can be produced in robust, high-capacity CHO or bacterial cells rather than capricious hybridomas.

Maute and Gordon applied systematic mutations to PD1 using a targeted yeast display system, and selected for mutants with higher PD-L1 binding affinity[231]. They focused on randomizing 22 residues at the PD-L1 binding surface of PD1, then on applying mutations to the positions that converged on a residue other than the natural one (i.e. the positions at which there was a systematic preference for mutation). The consensus mutants had affinities for PD-L1 up to 40,000 times stronger than native PD1, and slowed growth of syngeneic tumours in mice. Labelled mutants were also used as proof-of-concept PET tracers for delineating PD-L1-expressing tumours. Pascolutti *et al* later showed that the mutations introduced additional rigidity into the PD1 structure, while providing additional salt bridges and hydrogen bonds between the mutant PD1 and PD-L1[105].

In a similar manner, Lázár-Molnár et al discovered that a singly mutated PD1 construct bound PD-L1 45 times more strongly than the wild-type[106]. While the residues chosen for mutation were similar to those of Maute and Gordon, the scope of this work was much narrower. Mutants were rationally designed based on analysis of the PD1/PD-L1 cocrystal structure and generated by traditional PCR-based mutagenesis; only singly mutated proteins were produced. In contrast to the Maute work, the best mutation resulted in extended hydrophobic contacts between PD1 and PD-L1. Ig fusions of this construct were then used in mouse tumour models. The authors mention that Ig domains tend to noncovalently dimerize; the Ig fusions thus generated benefit from increased avidity as well as affinity, though at the expense of increased molecular weight.

**Table 3: Reported peptidic, peptidomimetic, and small-molecule inhibitors of PD1 or PD-L1.**

| | Example compound | Type | Origin |
|---|---|---|---|
| A | 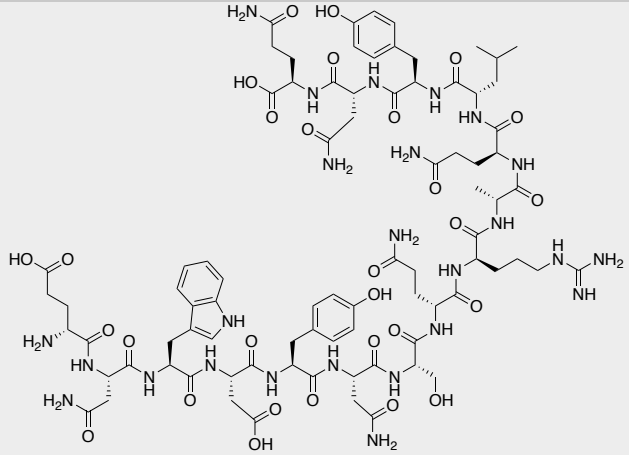 | Peptide | Li *et al.*[233] |
| B | 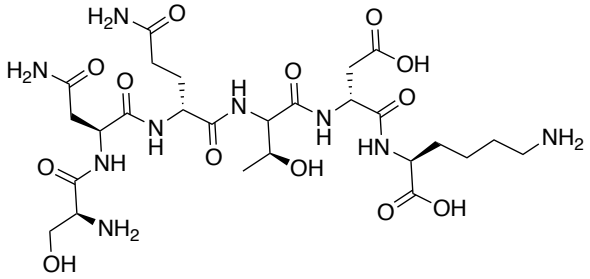 | Peptide | Wang *et al.*[234] |

| | | | |
|---|---|---|---|
| C | 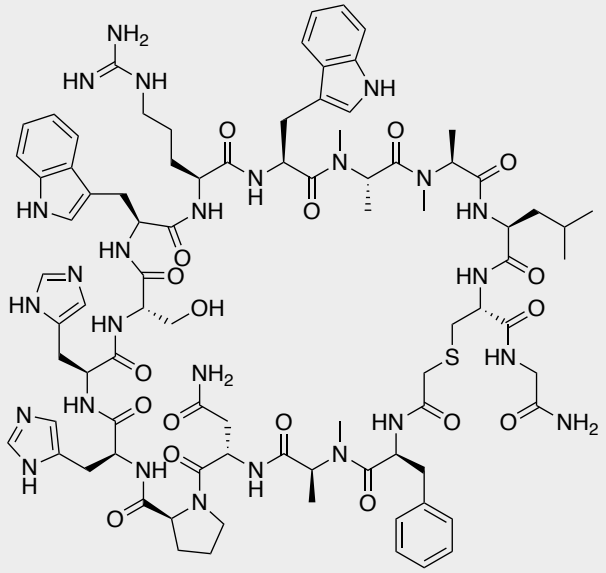 | Peptide | Bristol-Myers Squibb [235] |
| D | 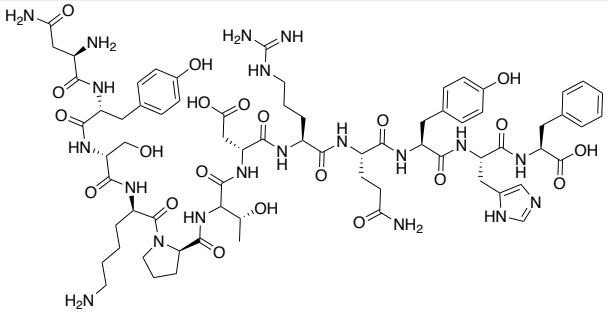 | Peptide | Gao *et al.*[236] |
| E | 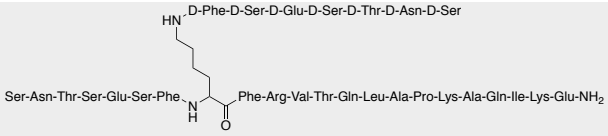  | Peptide | Aurigene[237] |
| F | 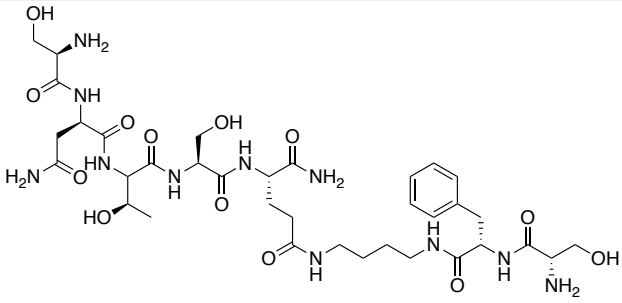 | Peptide | Aurigene[238] |

| | | | |
|---|---|---|---|
| G | 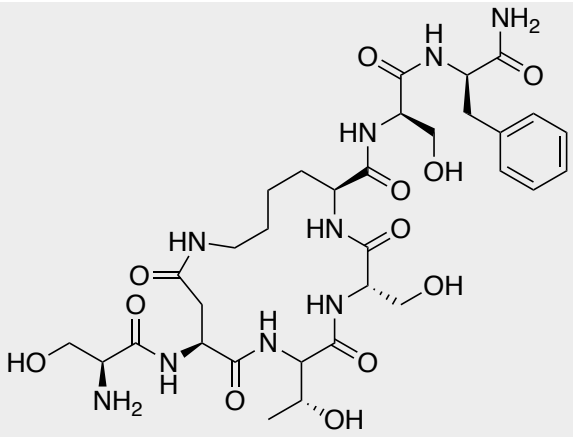 | Peptide | Aurigene[239] |
| H | 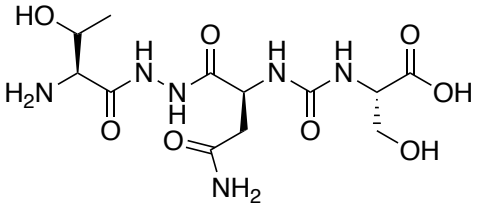 | Peptido-mimetic | Aurigene[240] |
| I | 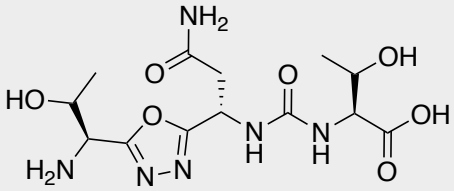 | Peptido-mimetic | Aurigene (Curis)[241] |
| J | 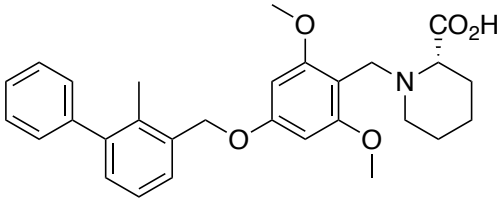 | Small molecule | Bristol-Myers Squibb[242-243] |
| K | 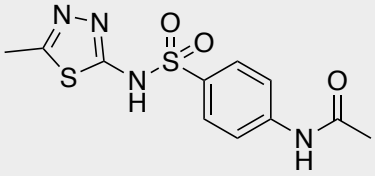 | Small molecule | Sharpe *et al.*[244] |
| L | 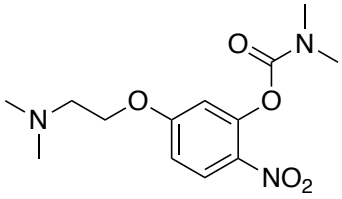 | Small molecule | Liu *et al.*[245] |

Peptides blocking PD1 have received relatively little attention over the years; for whatever reason, most programs have aimed to inhibit PD-L1 (*vide infra*). However, the Li group

combined computational methods and the "hot spot" theory of protein-protein interactions—that certain residues represent privileged binding sites and contribute disproportionately to binding energy[246]—to design PD1-binding peptides. The authors used modeling software to connect the Tyr56, Arg113, Ala121, Asp122, and Tyr123 residues of PD-L1 within various peptidic scaffolds, ranked these *in silico*, and synthesized the four highest-ranked peptides (Table 3, entry A). These exhibited modest affinity for PD1 ($K_D$ = 1.38-3.39 μM), and were able to inhibit PD1/PD-L1 binding and restore cytokine production in Jurkat cells.

The first proper peptidic inhibitor of PD-L1 was discovered by Wang and coworkers at the Zhejiang School of Medicine in Hangzhou, China[234]. Their lead compound (Table 3, entry B) is the result of a straightforward truncation of the FG strand of PD1, yielding a hexameric peptide comprised entirely of natural amino acids. The compound showed binding to PD-L1-expressing cells, but was mostly used as a tool compound to investigate the effects of PD1 inhibition on cancer cell lines.

Bristol-Myers Squibb has made their own series of peptidic PD-L1 inhibitors, opting for macrocyclic peptides (Table 3, entry C) in order to achieve conformational control[235]. While no details are given about how these compounds were chosen or even which protein they target, later work by the Holak group has shown that they target the PD1-binding face of PD-L1[247]. These peptides are not based on the native PD1 sequence, however, and various example compounds of different ring sizes bind to PD-L1 in drastically different conformations. The commonality between these peptides is their amphiphilic binding

mode. Most of the peptide consists of hydrophobic, mostly aromatic, residues held inside or below the macrocycle. These residues interact with the hydrophobic "palm" of the PD1-binding surface. Meanwhile, a small cluster of hydrophilic residues at one edge make polar contacts with the protein near D61. The cyclic nature of the peptide enforces the clustering of aromatic residues to cover the majority of the PD-L1-binding surface.

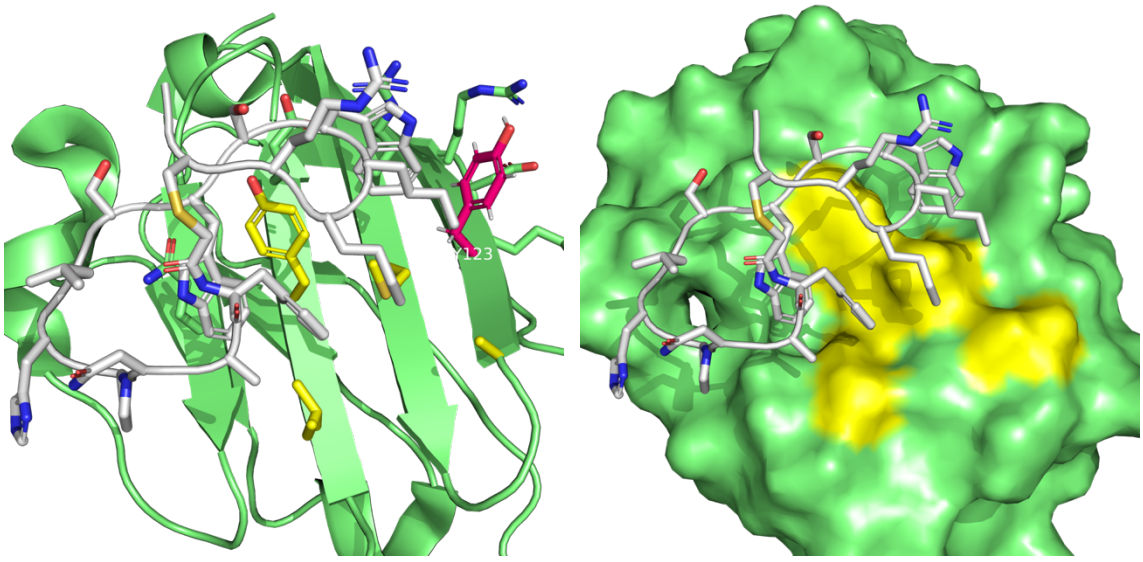

**Figure 11: Binding mode of cyclic peptides from Bristol-Myers Squibb to PD-L1. White: peptide. Green ribbon/surface: PD-L1. Green sticks: polar residues. Yellow sticks: nonpolar residues. Magenta: tyrosine 123.**

One of the main disadvantages of peptidic inhibitors is their vulnerability to proteolytic cleavage; the most straightforward way of protecting peptides against proteolysis is incorporation of non-natural amino acids, often D-amino acids, that are not recognized by endogenous proteases. While this approach often leads to metabolically robust compounds, the peptides in question must be made by chemical synthesis—diversity-oriented strategies that use living organisms as the synthetic machinery (phage display, bacterial surface display, aptamer selection, etc) are limited to natural amino acids and nucleotides. Gao et

al have applied an elegant solution to this problem: to find a D-peptide that binds to the natural L PD-L1, they used the unnatural D-protein to select from a library of natural L-peptides generated by standard phage display[236]. The IgV domain of PD-L1 is only 124 amino acids, and was synthesized through a combination of peptide synthesis and native chemical ligation. This mirrored PD-L1 was then chemically refolded, and used for biopanning with an M13 phage library. The binding clones were resynthesized as their D-peptide isomers (Table 3, entry D), and tested for their ability to bind to PD-L1 and to inhibit the PD1/PD-L1 interaction *in vitro* and on cells. The binding affinity of these peptides was modest, topping out at 510 nM, but they were resistant to proteolysis in human serum, and apparently nontoxic to cells. Administration of the compound to tumour-bearing mice led to delayed tumour growth and accumulation of the compounds at the tumour site.

Aurigene Discovery Technologies, a biotechnology company based in Bangalore, India, has disclosed a number of peptidic inhibitors for the PD1/PD-L1 axis[237-239]. The first generation of peptides were little more than truncated sequences from native PD1 ligated together (Table 3, entry E), although they nevertheless showed promise in both functional assays of immune function (lymphocyte proliferation and IFN-γ release) and reduction of tumour volume in syngeneic mouse models. The more complicated examples include branched structures, derived from symmetric or asymmetric acylation of the ß- and γ-amines of lysine residues. Also included were a handful of olefin-stapled macrocyclic peptides, although the company later appears to have eschewed these in favour of more fruitful endeavors.

A follow-up patent narrowed its focus to the BC loop of PD1 as the key fragment for the design of PD-L1 inhibitors[238]. This patent describes the synthesis of peptides containing a Ser-Asn-Thr tripeptide attached by various linkers to a Ser-Phe dipeptide, along with permutations in the order and attachment point of the dipeptide (Table 3, entry F). These choices are curious in light of the fact that the BC loop faces *away* from PD-L1, and is not involved in binding whatsoever.

Aurigene applied for yet another patent in 2013[239], doubling down on the BC loop analogues while incorporating cyclic motifs from their first publication (Table 3, entry G). The peptides are cyclized by amide formation between the sidechains of glutamic acid and lysine, and the Ser-Asn-Thr motif is variably included in the endocyclic and exocyclic portions of the macrocycle. The macrocyclization presumably restrains the peptides in a favourable conformation while simultaneously providing some metabolic stability and improved membrane permeability, though these are not explicitly addressed in the patent.

2011: typical compound is two copies of BC loop conjugated to PD-L1-binding motif

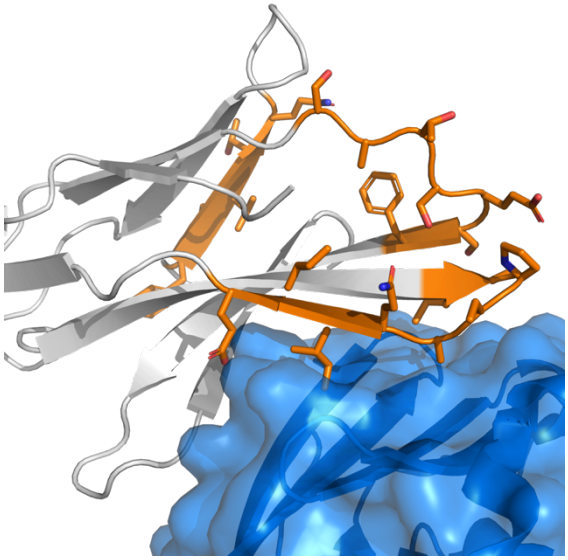

2012: fragments shortened to BC loop only

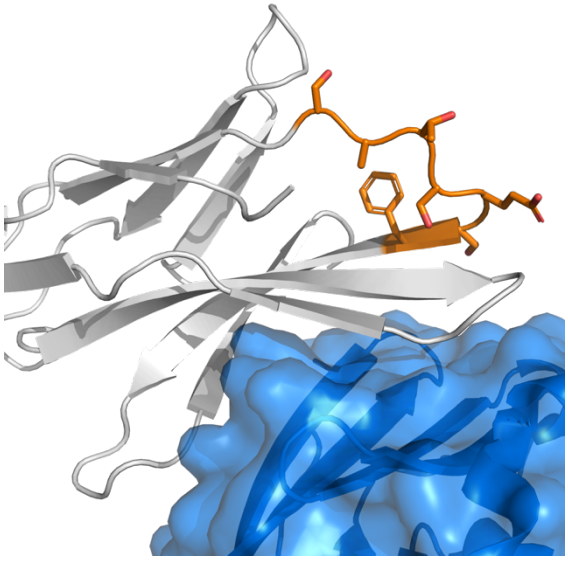

2013–present: peptides and peptidomimetics comprising a short section of the BC loop

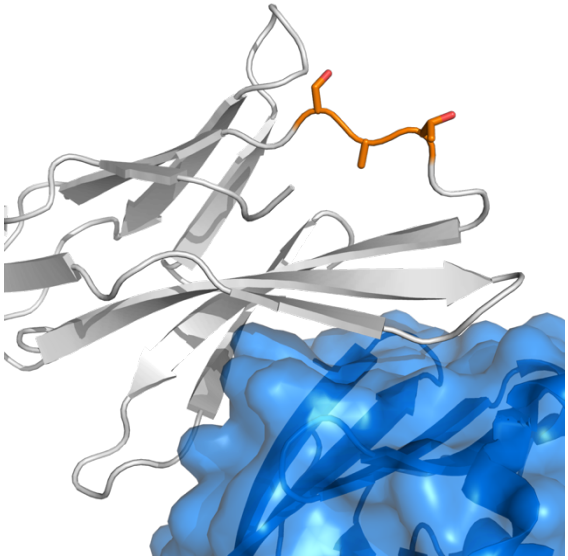

**Figure 12: Progression of hPD1 truncation in Aurigene peptides and peptidomimetics. The sequence in orange corresponds to the fragment of PD1 used for generation of analogues. Blue: hPD-L1. White: hPD1. Based on crystal structure of hPD1/hPD-L1 complex (PDB: 4ZQK).**

The continued emphasis on the BC loop of PD1 raises an interesting question about the mechanism of action of these compounds. Since the BC loop is not part of the PD-L1 binding surface[97], it is unlikely that these compounds work by competitive displacement of PD-L1. It is also unlikely that the BC peptides bind to PD1 in place of the native BC loop and cause a rearrangement of the nearby FG sheet. Lin and Freeman, however, raise a tantalizing possibility: the outwardly directed BC, C'C", and FG loops of PD1 and PD-L1 together map onto the antigen-binding loops of antigen receptors like antibodies and the TCR. It is possible, then, that PD1 and PD-L1 form a ternary complex with an as-yet unknown protein through these loops[103, 248]. If this were the case, the surprising potency of the Aurigene peptides could be explained, although it raises yet more questions about the identity, druggability, and clinical relevance of this mysterious third binding partner.

### 1.4.5 Industrial reports of small-molecule PD-L1 inhibitors

While nearly every major pharmaceutical company has developed at least one antibody- or peptide-based inhibitor for the PD1/PD-L1 axis, their small-molecule programs, if they exist, have not been as fruitful. Reports of small molecule inhibitors of PD1 or PD-L1 are scarce. Reports of small molecule inhibitors with both biophysical and functional data are all but nonexistent.

The paucity of small-molecule PD1/PD-L1 inhibitors is likely due to the lack of obvious small-molecule binding sites on either protein. Neither protein has any (known) endogenous small-molecule or peptide binding sites, so neither protein has a deep binding pocket to accommodate a small molecule. Meanwhile, the protein-protein interaction surface of both PD1 and PD-L1, as is typical for protein-protein interaction surfaces, is extremely large, hydrophobic, and shallow. Such a surface is unlikely to accommodate any small molecule selectively[193, 199]. The structural work by Holak *et al.* pointed out potential hotspots on each protein for a small molecule to bind to, but the pockets were very shallow, and the preliminary screen for hotspot binders did not yield any useful compounds[97].

One particular challenge in inhibiting the PD1/PD-L1 interaction is that, in contrast to classical drug targets like enzymes that function as individual units, the pharmacological target is the ensemble of all PD1/PD-L1 binding events on the cell surface, not just one single protein complex. While the individual PD1/PD-L1 binding event is relatively weak ($K_d$ = 1-8 μM), there are many copies of PD1 and PD-L1 at the cell surface. Any useful

inhibitor therefore has to counteract the cumulative affinity (avidity) of those interactions[249], and must have an affinity for the target many orders of magnitude stronger than that of the endogenous ligand. The situation becomes grimmer when considering that PD1/PD-L1 binding is not necessarily stochastic, but often occurs in the constrained area of the immune synapse, further increasing effective receptor concentration[250-251]. This may explain the apparent prevalence of antibody therapeutics for inhibiting cell surface receptors, as antibodies are inherently multivalent and typically have very strong (nM or pM) affinities for their epitopes[252].

The first report of any small-molecule inhibitor came from the Indian pharmaceutical company Aurigene, describing peptidomimetic compounds (Table 3, entry H) that are clearly extensions of their PD1-derived peptides[240]. The key motif in these molecules appears to be the Ser-Asn-Thr sequence from their earlier work; the peptide backbone is replaced with an N,N'-dialkylurea and N,N'-diacylhydrazine, presumably conferring some measure of resistance towards proteolysis as well as conformational restraint about the N-N bond[253]. These compounds are also drastically truncated compared to the peptides reported earlier, though no head-to-head comparisons of binding affinity are made. It is assumed that they have the same binding site as the earlier peptides, although this is not addressed. These compounds are able to rescue mouse splenocytes cultured in the presence of PD-L1 (as soluble fusion proteins or constitutively expressed on MDA-MB-231 cells) as well as increase their production of IFN-γ (as a proxy for immune activation). While not far removed from their peptide forebears, these compounds are the first small molecules reported to inhibit the PD1/PD-L1 interaction.

Aurigene later replaced the diacylhydrazine linker with various azoles to generate a series of example compounds (Table 3, entry I) including their clinical candidate AUPM-170 (the exact structure is unknown)[241]. This compound was then licenced to Curis, who renamed it CA-170 and demonstrated that it can induce T cell proliferation and IFN-γ production in cellular models. Moreover, CA-170 slows tumour growth, inhibits metastases, and increases markers of peripheral immune activation in syngeneic murine tumour models. CA-170 is bioavailable when given orally, and well-tolerated at high doses (1000 mg/kg in both mice and macaques). These preclinical data led Curis to initiate a Phase I clinical trial of the compound in 2016[254]; this trial is still ongoing.

Intriguingly, CA-170 is proposed to be an antagonist of not only PD-L1 and PD-L2, but also the immune receptor/ligand VISTA. This is not unexpected, as VISTA shares significant sequence similarity to PD-L1, but PD1 is not a known binding partner of VISTA. Curis has licensed another—presumably similar—molecule from Aurigene, dubbed CA-327, that is proposed to inhibit both PD-L1 and TIM3. CA-327 is still in preclinical development, but initial results are promising, showing antagonism of PD-L1 and TIM3, activation of tumour-infiltrating lymphocytes, and reduced tumour growth in syngeneic mouse models. This approach of exploiting immune checkpoint homology to develop antagonists for multiple targets, as opposed to combinations of single-target antibodies, is an intriguing way of activating immune function in controlled ways. These multi-targeted compounds could be useful to avoid checkpoint-specific resistance mechanisms, a goal that would be significantly more difficult to achieve using antibodies.

The only other pharmaceutical company to report a non-peptidic PD1 or PD-L1 inhibitor is Bristol-Myers Squibb, whose strong immunooncology program claimed a series of biaryl benzyl ethers (Table 3, entry J) in late 2014[242], with more compounds added in 2015[243]. The compounds were discovered using a homogeneous TR-FRET assay as the primary screen; the compounds were tested for inhibition of PD1/PD-L1, PD1/PD-L2, PD-L1/CD80, and CD80/CTLA-4, although only PD1/PD-L1 inhibition values are reported. While physical compound binding to one of the two proteins is evident, no indication is given of which of those two proteins it is. Moreover, the patents contain no information about the compounds' cellular activity, if any; no academic publications by Bristol-Myers Squibb accompanied or followed the patent filings. The patents, and the compounds described therein, are discussed further in Chapter 3.

### 1.4.6 Miscellaneous small-molecule PD-L1 inhibitors

The primary academic disclosure of small-molecule PD1 inhibitors comes from the group of Dr. Arlene Sharpe, at Harvard University. The compounds reported by the Sharpe group are bi(hetero)aryl sulfonamide derivatives of the FDA-approved antibiotic sulfamethizole[244]. A number of derivatives of these compounds have been patented (Table 3, entry K), although no follow-up publications or patent updates have been published.

These compounds were discovered using a PD1-specific phenotypic assay for immune activation. T cells that either constitutively express PD1 ($PD1^c$) or that are deficient in PD1

($PD1^{-/-}$) are stimulated with an anti-TCR antibody along with either a PD-L2 fusion protein or a control Ig fusion protein in the presence or absence of compounds. T cell activation is then assessed by measuring the amount of IFN-γ produced using a bead-based ELISA assay. Compounds were determined to be PD1-specific if they enhanced or inhibited IFN-γ production only on PDc cells and only in the presence of PD-L2–Ig.

Despite their clear effects on PD1- and PD-L2-specific T cell inactivation, Sharpe's sulfonamides cannot yet be called PD1 inhibitors. The patent does not describe any biophysical assay showing direct binding of the compounds to either of the two proteins. Since the readout of the assays (T cell proliferation, IFN-γ production) are downstream consequences of PD1 activity, these compounds could be inhibiting PD-L2, PD1, or *any of the other signaling molecules that they affect*. This includes any of the kinases and phosphatases that transduce PD1 signaling within the cell. Moreover, since the assays are performed over a long period of time (typically 96 hours), molecules that specifically affect PD1 expression levels or stability would be indistinguishable from direct activators and inhibitors. Both our group and the Dömling group have tested sulfamethizole in various biophysical assays for PD1 or PD-L1 binding and inhibition, and found it to be inactive[97].

The hypothesis that sulfamethizole inhibits PD1 directly is especially tenuous in light of the fact that sulfamethizole is a known—if weak—inhibitor of various intracellular kinases. Sulfamethizole and sulfamethoxazole were predicted to inhibit mTOR based on *in silico* screening, and indeed both had *in vitro* inhibitory activity at 10 μM[255]. Sulfamethizole derivatives also inhibit Aurora kinase A[256]. More damningly, sulfamethoxazole and

derivatives thereof are known inhibitors of the pleckstrin homology (PH) domain of AKT[257-260], a *direct downstream target of PD1 activity*[49]. While both PD1 and sulfamethizole act as inhibitors of this pathway, suggesting they should have complementary rather than conflicting effects on T cell activity, the implication of aryl sulfonamide compounds in this pathway at all suggests that they could be affecting any number of downstream signaling molecules, rather than PD1.

Only one other purported PD1/PD-L1 inhibitor has surfaced in the academic literature, although compared with sulfamethizole the data behind it are much more sparse. The Liu group at Jilin University in China attempted to find a new scaffold for PD1/PD-L1 inhibitors by combining binding information from the sulfonamides described by Sharpe et al and the biaryl ethers disclosed by Bristol-Myers Squibb with structural insights from crystal structures of the PD1/PD-L1 complexes[245].

The Liu group carried out molecular docking in order to determine the binding site and mode of binding of sulfamethizole and sulfamethoxypyridazine to PD1. They propose that these compounds bind to the C and C' strands that form part of the interface with PD-L1. They then designed compounds to bind in this proposed pocket based on the "V-type" motif embodied by the Bristol-Myers Squibb compounds described above. This "V" refers to the projection of two sidechains at 120˚ angles from a central meta-substituted aromatic ring (Table 3, entry L). After some optimizing of the compound structures, they report compounds that inhibit the PD1/PD-L1 interaction by 43% at 500 μM.

While the scarcity of any small-molecule PD1/PD-L1 inhibitors makes any report of such chemical matter noteworthy, the results reported by Liu fall short of proving PD1 binding or inhibition. Much of the work in their paper is built on the Sharpe sulfonamides as guide compounds for *in silico* modeling and positive controls for their assays. However, the Sharpe compounds have not been confirmed to bind either PD1 or PD-L1 in any kind of biophysical assay to date, making them poor choices for docking experiments and assay validation.

Moreover, the compounds in the Liu study were tested in only a single assay for PD1/PD-L1 inhibition—a TR-FRET assay, which can be vulnerable to compound interference (see Section 2.4.4 PAINs and suffering: suspicion, confirmation, and mechanism of TR-FRET interference by salicylates)—and at only a single concentration for each compound. Since the positive control compounds (sulfamethizole and sulfamethoxypyridazine) showed only modest inhibition at very high concentrations, the dynamic range for their assay is limited. In addition, although they claim to have tested each compound in triplicate, no standard errors are provided for the inhibition data. Given that no dose-response relationship is established for the test compounds, it is difficult to distinguish real inhibition from experimental noise.

Finally, the authors support their claim of physical compound-protein binding by simple proton NMR, pointing to a minuscule change in chemical shift (0.007 ppm) of a single resonance upon PD1 addition. Rigorous methods for detecting weak protein–small molecule interactions by ligand-observed NMR, such as saturation-transfer difference

NMR[261], do not appear to have been done. The results of this paper should therefore be viewed with considerable scepticism, though it may be possible that the compounds described therein are real inhibitors of the PD1/PD-L1 interaction, if weak and poorly characterized.

## 1.5 Opportunities for novel small-molecule PD1/PD-L1 inhibitors

While traditional therapies for cancer have aimed to block the tumour's mechanisms of growth or kill it through direct cytotoxic mechanisms, immunotherapy has emerged as a viable alternative. Current strategies have focused on blocking immunoinhibitory receptors, with the CTLA-4 and PD1/PD-L1 axes being the first and most successful targets to date. While CTLA-4 blockade is associated with therapy-limiting adverse effects, PD1 blockade is well-tolerated enough to have seen use in many indications. Both approaches have demonstrated impressive objective responses and extensions of survival in patients with otherwise bleak prognoses.

The antibody treatments that have so far dominated immunotherapy, and the PD1/PD-L1 axis in particular, are not without their drawbacks. Antibodies are expensive to produce, store, and administer. The long $k_{off}$ and plasma half-life of antibodies means that treatment cannot be withdrawn rapidly in the event of a dangerous reaction to the medication. And as large proteins, antibodies have difficulty accessing poorly vascularized tumours.

The solution to the problems above is a small, nonpeptidic inhibitor of PD1 or PD-L1 that can be dosed orally, is non-immunogenic, hepatically or renally eliminated, and would be inexpensive to produce, store, and formulate. However, the molecular features of the PD1/PD-L1 interaction, as well as the structures of the proteins themselves, make them inherently hard to target with small molecules. As a result, very few such molecules have been reported to date. The discovery of such a molecule, or even the discovery of a binding site for such a compound, would be of great value to the field and to patients bearing immunogenic tumours, and was therefore our goal at the outset of this research.

# Chapter 2

This chapter describes the identification of possible small molecule binding sites on the PD1 and PD-L1 protein surfaces, computational docking of compounds to those sites, and the screening assays employed to validate the *in silico* results. New compounds were synthesized in order to improve solubility and test structural requirements for activity. New mechanisms of assay interference were discovered. The work on salicylate interference in TR-FRET assays produced one first-author publication.

Computational work was done by Dr. Jianghong An, a staff scientist in computational biology at the Michael Smith Genome Sciences Centre. Thermal shift and denaturation assays were performed by the author. ELISA assays were carried out by Henry Gong and Shanti Horvath, who were both undergraduate students in the Wulff group at the University of Victoria. The TR-FRET experiments were performed almost exclusively by Shanti Horvath. Biacore experiments were performed by the author. Compound synthesis was also performed by the author, although JW-VI-13 was synthesized by the author's supervisor Dr. Jeremy Wulff for this project, and the TBS-protected ethylene glycol used in Scheme 7 was generously donated by Jun Chen, a fellow PhD candidate in Dr. Wulff's research group.

## 2.1 Rationale for targeting allosteric PD1/PD-L1 inhibitors

### 2.1.1 Structural biology basis of compound selection

As mentioned in chapter 1, while PD1 and PD-L1 have been actively targeted with antibodies and peptides, very few genuine small molecules have been found that inhibit this protein-protein interaction. Of the small molecules that have been reported, very few of them have been validated in biophysical binding assays. Given the keen interest in pharmacological disruption of the PD1/PD-L1 pathway, it is likely that many pharmaceutical companies have already conducted high-throughput screens of their compound libraries against these targets and come up empty.

Small molecules capable of inhibiting this interaction are challenging to find due to the large, flat nature of the protein–protein interface[262]. The binding face of the two proteins buries about 1900 $Å^2$ of surface area[97, 103] – much larger than the majority of small molecules. Moreover, the protein-protein interaction itself relies on preorganization of the two partners into flat ß-sheets, and even that results in a low binding affinity ($K_D$ >1 μM).

Moreover, the success rate of unbiased high-throughput screens is generally low, even for highly druggable proteins. Most estimates put the hit rate for high-throughput screens at 0.1% or less[263], and most of those screens target proteins that have native binding sites for small molecules. Hit rates for protein-protein interactions are often far lower, at <0.01%[264-265]. Moreover, these preliminary hit rates do not account for false positives. In short, the key to finding a genuine small molecule protein-protein interaction inhibitor in an unbiased high-throughput screen is to screen many, many compounds. We had neither the financial

resources to acquire such a large library, nor the automation required to screen such a large library in a reasonable timeframe.

One way to alleviate the need for thousands of compounds, as well as avoid the difficulties of targeting a protein-protein interface, was to search for allosteric inhibitors based on information from the available crystal structures. A concave pocket or groove on either protein would likely accommodate a small molecule better than the binding interface would[266]. Moreover, starting from a cavity of known size, shape, and polarity would allow us to prescreen *in silico*, resulting in a higher hit rate during actual compound screening[265, 267].

The use of *in silico* docking to increase hit rates in high-throughput screens is increasingly popular in medicinal chemistry programs. In these experiments, millions of compounds are modelled into protein binding sites by a supercomputer. The compounds can then be scored based on their shape and physicochemical complementarity to the binding site, and ranked relative to one another in terms of which compounds are most likely to bind. While docking does require a solved protein structure (or at least a homology model), it is resource economical in that no physical reagents or consumables are expended. This can reduce both the storage space needed for the millions of compounds as well as the need for expensive robotic screening equipment and large quantities of assay reagents and protein (which may be limited). This strategy is not without its drawbacks, however. A persistent challenge in this field is the inability to accurately model solvents (both bulk solvent and active-site solvent molecules), metal ions, protonation state, and tautomers, which can drastically

affect the predicted binding mode[268-270]. Moreover, protein targets are often set as static (or nearly static) objects during docking, which ignores the dynamic, flexible behaviour of proteins in solution. When using a crystal structure for docking studies, there is also the intrinsic assumption that the solid state structure is representative of the protein's structure in solution. On a quantitative note, there are many different systems for scoring docked compounds, and no one system is best at predicting binding accurately. These scores are also relative, and rarely predict binding energy/affinity with any accuracy[268-270].

In particular, we hypothesized that the observed bending of the PD-L1 interdomain hinge is important for PD1 binding (see Figure 13). While the individual residues of the PD1 binding face of PD-L1 stay remarkably constant between the bound and free forms ([103], the angle between the IgC and IgV domains opens by > 30˚ upon PD1 binding. This suggests a conformational preference for the elongated structure when bound to PD1. These conformational preferences are observed in multiple crystal structures[102-103, 271] (see also PDB: 3SBW), so crystallization artefacts are unlikely to be the source of this difference. The implication of the hinge angle in PD1 binding is supported by mutagenesis experiments. Mutation of E31, a residue on the opposite face from the PD1 binding site involved in a key hydrogen bond stabilizing the bent apo structure, results in a protein with diminished PD1 binding affinity[272].

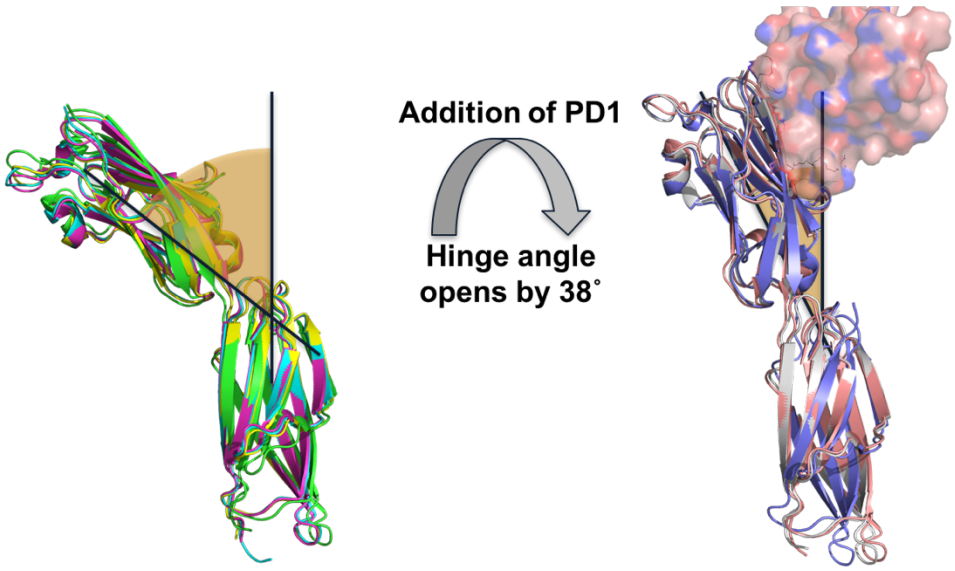


**Figure 13: Change in PD-L1 hinge angle upon PD1 binding. See Chapter 1.**

Stabilizing this apo conformation would prevent PD-L1 flexion, thereby inhibiting PD1 binding. Even if hinge stabilization on its own does not inhibit PD-L1 activity, it provides an anchor point on the protein proximal to the interaction surface; it would then be possible to design a small molecule that could reach up and block or disrupt the binding interface, and favourable hinge binding at one end of the molecule would make up for the unfavourable energetics of disrupting the ß-sheet[266].

While we focused mostly on the interdomain hinge region of PD-L1, we also attempted to find allosteric sites on PD1, as well as at the interface of the PD1/PD-L1 complex (in order to find molecules capable of stabilizing the interaction). For PD1, we focused on areas close to the interacting surface, on the hypothesis that because PD1 undergoes more significant rearrangement upon ligand binding, those flexible regions should be susceptible to subtle perturbations in their conformational preferences. As for the interface, our

hypothesis was straightforward – filling unoccupied hydrophobic space between the two proteins would likely lead to stabilization of the interaction (such a compound would therefore be an agonist of the interaction).

### 2.1.2 Pocket finding and docking

Our collaborator, Dr. Jianghong An, scanned the existing crystal structures of human PD1 and PD-L1 for potential small molecule binding pockets. Using the program he developed (PocketFinder)[273], our collaborator evaluated the geometric and electronic constraints of the areas of interest, in order to find cavities that could accommodate a small molecule. This program works by computing the van der Waals potential across a grid of the protein crystal structure, then filtering for contiguous envelopes with a given volume and dimensions.

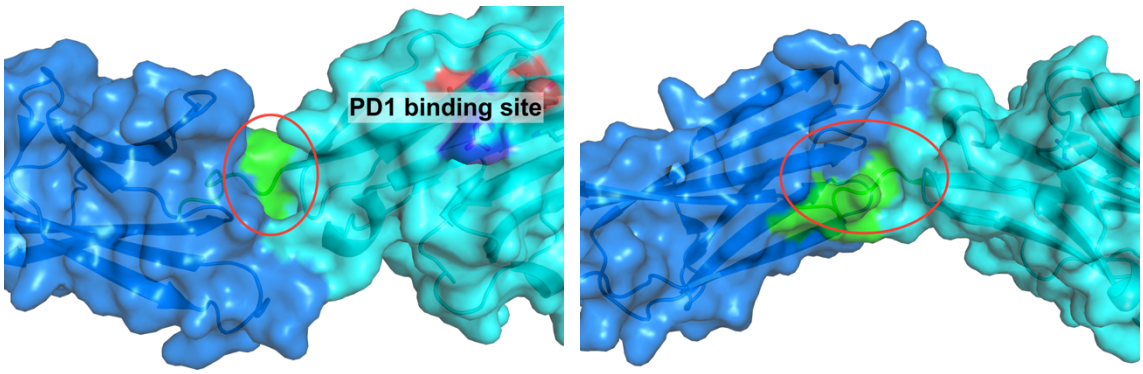


a) b)

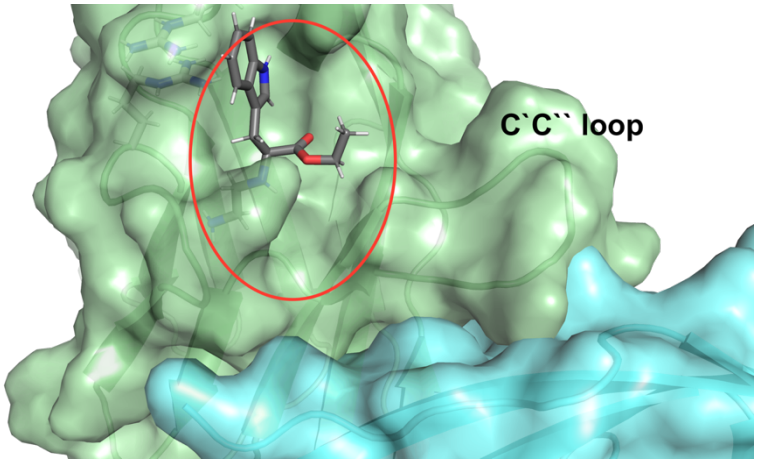


c)

**Figure 14: Computationally predicted allosteric sites on PD-L1 and PD1. a) Front face of PD-L1. b) Back face of PD-L1. c) PD1, with docked small molecule to illustrate the proposed binding pocket.**

This experiment resulted in the discovery of two putative pockets on PD-L1 at the hinge region and one putative pocket on PD1 near the binding face. In PD-L1, this supported our hypothesis that the hinge region is probably the optimal site for small molecule binding. For PD1, we discovered a pocket that opens upon PD-L1 binding; this pocket is proximal to the CC` loop that clamps down on PD-L1 upon binding, as well as the instrinsically disordered C`C`` region that stabilizes into a short ß-sheet upon PD-L1 binding. The flexibility of this region in the apo protein gave us reason to believe that small molecule binding would be favoured, and its proximity to the important CC` and its many PD-L1 contacts made it an obvious choice for modulating the interaction.

In order to increase our chances of finding a molecule that would bind in one of these pockets, our collaborator Dr. An carried out in silico docking studies on compounds from three compound collections. Our collaborator used the Internal Coordinates Mechanics

program[274], which docks small molecules in a variety of poses and placements in order to minimize its free energy, taking into account both intramolecular and intermolecular van der Waals, electrostatic, polar, and steric interactions. Hundreds of thousands of compounds were screened *in silico* from three databases: the National Cancer Institute's compound collection, the ZINC database of commercially available druglike small molecules[275], and a small database of orally bioavailable, marketed drugs[276].

### 2.1.3 Assay choice

With a potential binding site and a compound collection in hand, we required an experimental method to determine if any of those compounds bound to PD1 or PD-L1. We were primarily constrained by our lack of ready access to large amounts of protein, owing to the difficulty of refolding bacterially produced PD1 and PD-L1 (both proteins are trapped in inclusion bodies when expressed in *E. coli*[277-278]); our own PD-L1 protein was produced in insect cells by our collaborators. We tried to choose label-free methods whenever possible, in order to minimize protein losses due to incomplete reaction or additional purification as well as to prevent possible interactions between test compounds and the labels.

Moreover, we were forced to use complete domains of each protein rather than more easily produced peptide sequences. A truncated peptide from either protein's interaction surface would naturally not have allosteric sites, so they could not be used as the compound binding partner. We were also not confident that a peptide corresponding to the interacting surface

of the non-compound-binding protein would respond the same way to allosteric regulation; the binding sites of both proteins span multiple strands, so any reasonably sized contiguous sequence would not contain all of the interacting residues.

Many of the usual methods for measuring ligand-receptor binding were therefore not amenable to our screening efforts. Fluorescence polarization is a common method of measuring ligand-protein binding[264], wherein the decrease in rotation and diffusion of a dye-labelled ligand upon protein binding is reflected in an increase in fluorescence polarization. In this assay, the change in fluorescence polarization is proportional to the change in complex size. A small peptide binding to a large protein will therefore exhibit a large change in polarization, whereas two similarly sized proteins binding to one another will exhibit a much smaller change in polarization, resulting in an insensitive assay. AlphaScreen and related bead-based technologies require labelling of at least binding partner, if not both[279]. Isothermal titration calorimetry is label-free and provides binding constants as well as the thermodynamic information, but is slow, laborious, and consumes large amounts of protein based on our group's previous experience.

### 2.1.4 The spectre of false positives

Although the compounds we tested were predicted to bind strongly to the proteins, we did not expect to find potent inhibitors at this early stage. These protein targets have doubtless been subject to numerous small molecule screens at pharmaceutical companies and large research institutions – if a potent inhibitor existed in these commercial libraries, it would

likely have been found by now. Furthermore, the pockets we were targeting had not been previously validated, so we had no idea how strongly any given molecule *could* realistically bind to them. Moreover, allosteric inhibition differs from competitive inhibition in that complete binding does not always result in complete protein inhibition, since a given protein perturbation may only result in a slightly less active conformer. This could make detection of inhibitors even more difficult, as weak binders with a weak maximum effect size would appear only at very high concentrations. We therefore decided to treat this campaign like a fragment screen despite the relative complexity of our compound collection, and to test each molecule at a fairly high concentration (500 to 1000 μM)[280].

We were cognizant that screening test compounds at high concentration against a target with no known ligands would likely result in many more false positives than genuine hits. While some of these false positives are random errors, an inactive compound that reproducibly shows up as a hit in any given assay could lead to lots of wasted effort optimizing an unoptimizable scaffold. We were therefore rigorous in validating any apparently active compounds.

Many of the compounds selected for *in vitro* testing are highly conjugated, electrophilic, or redox-active, raising the possibility that they might react with the assay components and distort the signal measurement. Whenever a compound with a suspicious structure showed activity, we tested it with each of the assay components in order to rule out endogenous fluorescence, inhibition of reporter enzymes, or other mechanisms of assay interference. Moreover, we tried to test hit compounds at a broad range of concentrations and to screen

structurally related compounds, as assay interferants tend to have poor structure-activity relationships and unpredictable dose-response relationships[281].

We were also aware that many of the compounds tested could aggregate nonspecifically with the protein components. Many of the compounds in the sample set are highly lipophilic, and while not every lipophilic compound aggregates, most aggregators are lipophilic[282]. We therefore tried to include or carrier proteins like bovine serum albumin (BSA) in each assay.

Finally, we did not perform any kind of quality control on externally supplied compounds. While in theory we could have run HPLC analysis on every compound received to determine purity, this would have been costly and time-consuming. Moreover, not all interferants are UV-active or even organic[283]. We therefore chose to account for this by resynthesizing apparently active compounds and comparing the activity to the externally sourced material.

## 2.2 Thermal shift assay for PD-L1 binding and pyrazole-based lead compounds

### 2.2.1 Theory and optimization of a thermal shift assay for PD-L1 stabilization

Thermal shift measurements are based on the premise that proteins are stabilized upon ligand binding, such that the protein-ligand complex has a higher melting temperature. When a protein binds to a ligand, the new complex is more stable than the apo complex,

which manifests as an increased resistance to denaturation. The energy required for denaturation is an intrinsic property of the protein, and can be estimated by finding the temperature at which 50% of the proteins are denatured (the "melting temperature" or $T_m$). If the $T_m$ of a given protein changes upon addition of a compound, it is inferred that the compound binds to the protein[284-286].

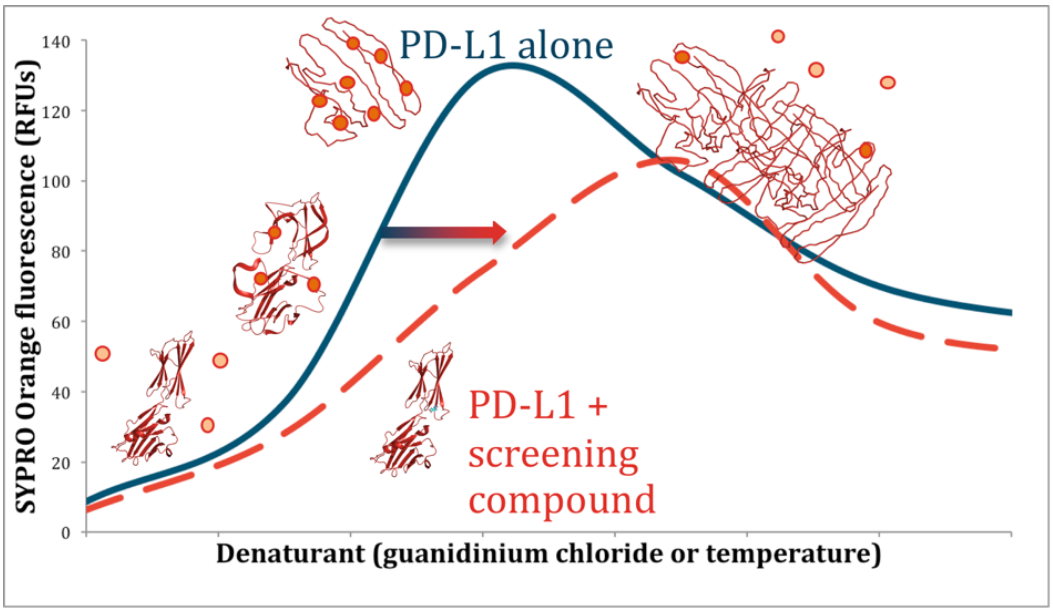


**Figure 15: Schematic of a thermal shift assay. Progressive protein denaturation opens hydrophobic sites for dye binding; bound dye becomes fluorescent. Compound-stabilized protein would exhibit resistance to denaturation.**

We chose the environmentally sensitive dye SYPRO Orange as the reporter for protein denaturation. As proteins denature, the hydrophobic effect that drives protein folding is overcome, and more hydrophobic regions of the protein are exposed to solvent. This increase in hydrophobic surface area is measured using a fluorescent dye that is quenched in aqueous medium. Binding to a hydrophobic surface shields it from water, releases it

from quenching, and restores fluorescence. An increase in measured fluorescence therefore indicates an increase in hydrophobic surface area, which in turn indicates protein denaturation[284, 286].

Access to a tandem thermocycler/fluorimeter enabled single-well analysis of melting temperature, allowing us to reduce our protein consumption while providing a more complete dataset for each compound. In the early stages, we optimized this assay using varying concentrations of guanidinium chloride (GuaCl) to effect protein denaturation. While guanidinium chloride denatured PD-L1 in a dose-dependent manner and did not interfere with fluorescence measurements, each assay well provided only one individual data point, forcing us to choose between more rigorous denaturation curves or protein conservation. Moreover, we were unsure how the guanidinium chloride would affect the activity of the test compounds, either by decreasing their solubility or by disrupting their interactions with the protein. We later switched to using a qPCR fluorimeter/thermocycler, which allowed us to track the full course of denaturation with increasing temperature all from one assay well[286].

### 2.2.2 Screening of compounds for PD-L1 binding by thermal shift

The parameters for high-throughput screening were first established (see Figure 16). The concentrations of guanidinium chloride required to achieve 50% denaturation (the pseudo-$T_m$) was ~0.7 M, so the assays were run at 0.5 M and 0.75 M guanidinium chloride in order to achieve maximal sensitivity. The concentration of PD-L1 was then optimized to provide a usable signal-to-noise ratio with minimal protein usage. The optimum dye concentration

was then determined by titrating SYPRO Orange into PD-L1 and gradually denaturing the protein. The lowest concentration that produced a measurable fluorescence response upon protein denaturation was then used in the screening experiments.

a)

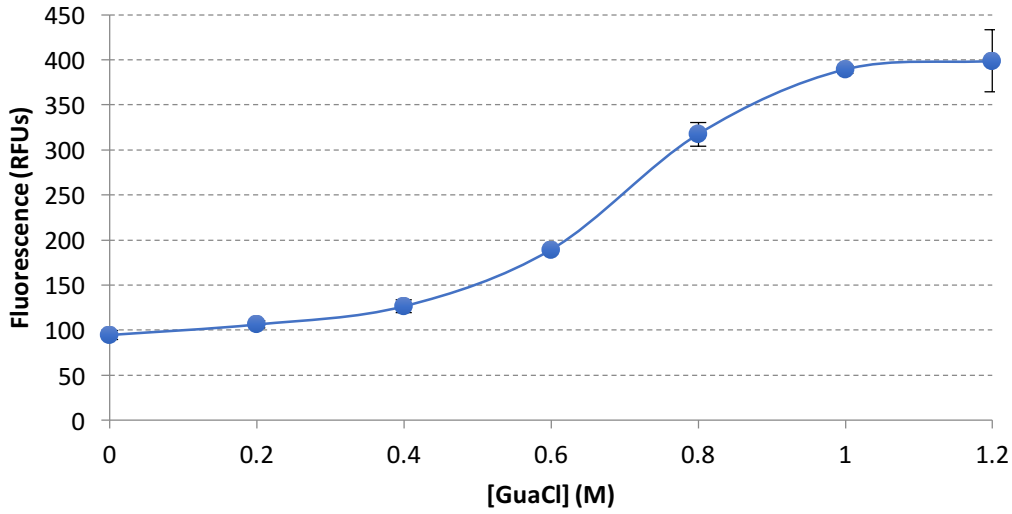


b)

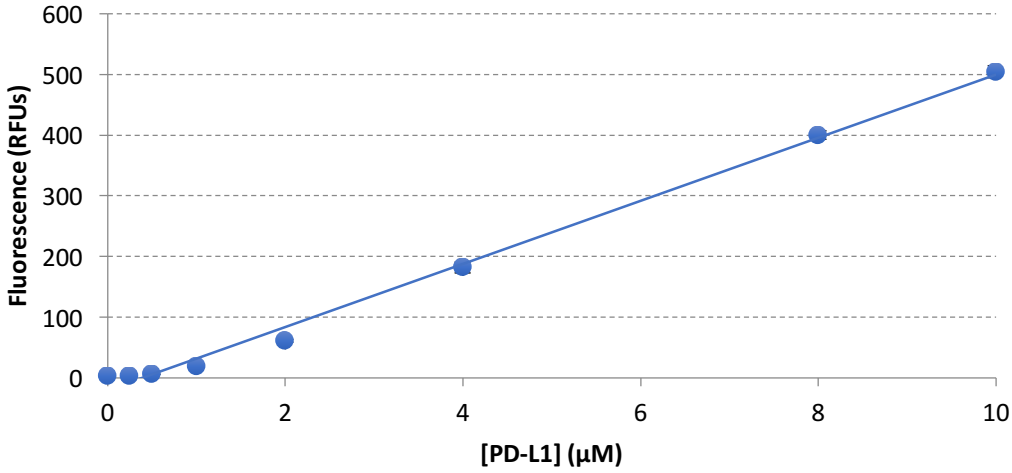

c)

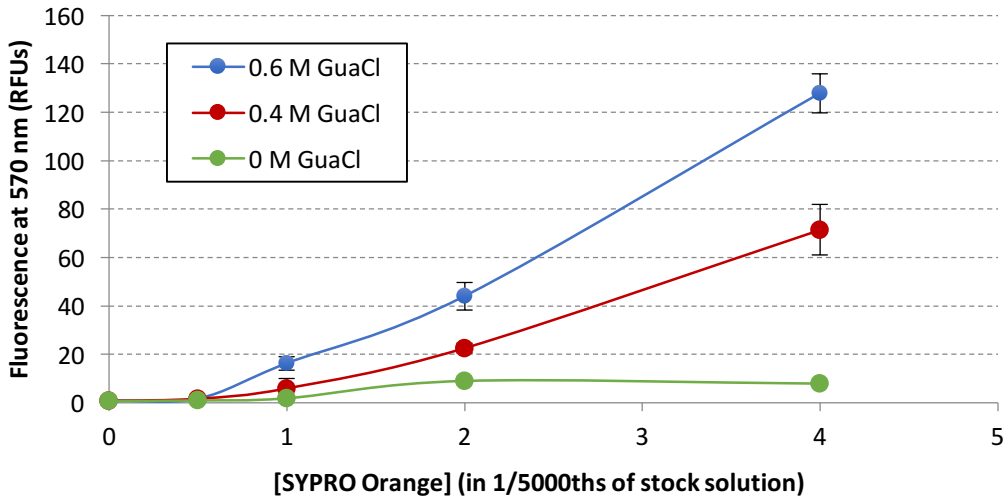


**Figure 16: Optimization of dye, protein, and denaturant concentrations for the thermal shift assay. a) Fluorescence response of SYPRO Orange in the presence of PD-L1 at varying concentrations of guanidinium chloride. b) Fluorescence response of SYPRO Orange with varying concentrations of PD-L1 (no denaturant). c) Fluorescence response of varying concentrations of SYPRO Orange in the presence of PD-L1 at various concentrations.**

We screened 23 proposed PD-L1 hinge-binding compounds in the guanidinium chloride denaturation assay, and several compounds showed apparent inhibitory activity based on the decrease in dye activity. Most of the other apparent "hits" were later found to quench the dye fluorescence without shifting the denaturation curve (the curve moves down but not to the right), but Z289983522 did not have this effect. This compound showed the largest shift in $T_m$ of any of the compounds we tested, and this activity was retained in a thermal denaturation assay. This compound also lacks obvious reactive functional groups, and bears similarity to approved drugs.

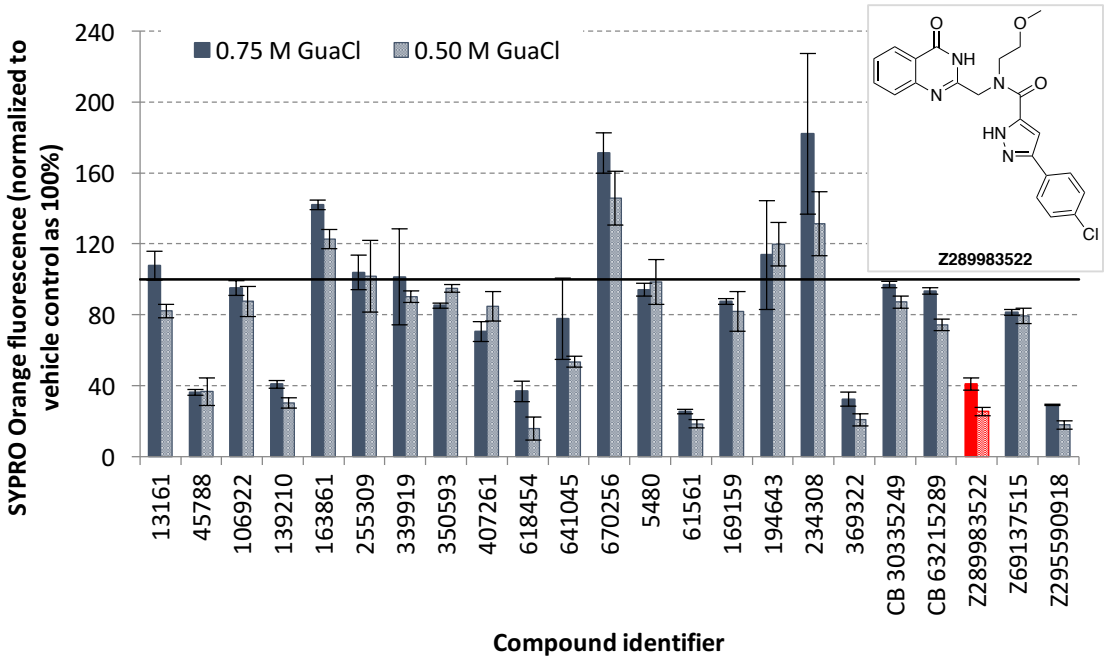


**Figure 17: Summary of compound screening by guanidinium chloride denaturation assay. All compounds were screened at 1 mM.**

Unfortunately, Z289984522 also seemed to interact with the dye; we postulated that this effect was due to poor solubility and possible aggregation. A concentration series of this compound (see Figure 18) revealed that the $T_m$ of PD-L1 is shifted only at high concentrations (>100 µM) of compound, and that the fluorescence intensity is also increased. Moreover, a thermal shift assay with lysozyme in the place of PD-L1 revealed a large signal interference at compound concentrations greater than 100 µM, while addition of compound to the dye alone also results in high, spurious signals. As Z289983522 is only sparingly soluble in buffer and contains many lipophilic aromatic and heteroaromatic groups, compound aggregation and/or insolubility seemed like a likely culprit.

a)

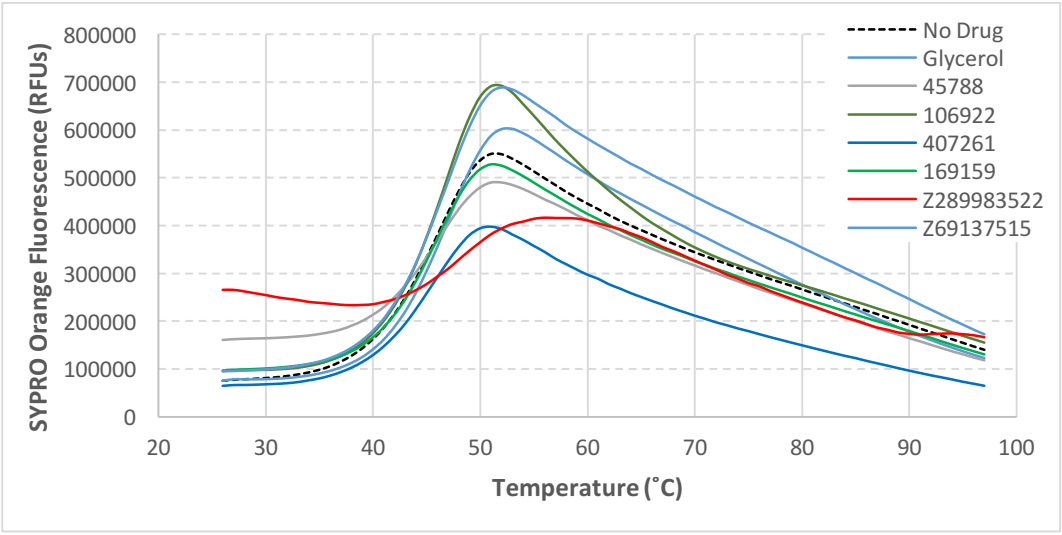
SYPRO Orange Fluorescence (RFUs)
800000
700000
600000
500000
400000
300000
200000
100000
0
20
30
40
50
60
70
80
90
100
Temperature (˚C)
No Drug
Glycerol
45788
106922
407261
169159
Z289983522
Z69137515

b)

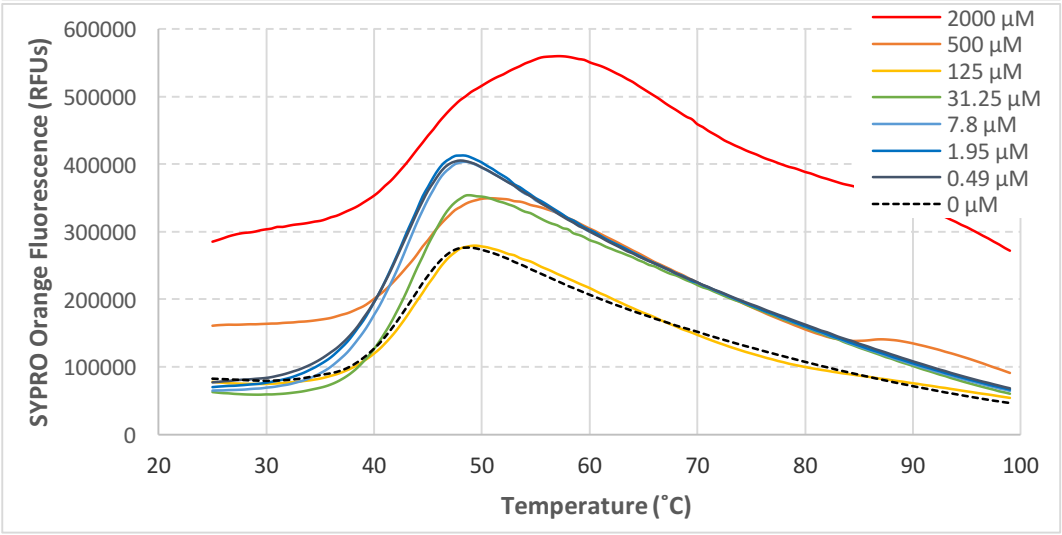
SYPRO Orange Fluorescence (RFUs)
600000
500000
400000
300000
200000
100000
0
20
30
40
50
60
70
80
90
100
Temperature (˚C)
2000 µM
500 µM
125 µM
31.25 µM
7.8 µM
1.95 µM
0.49 µM
0 µM

c)

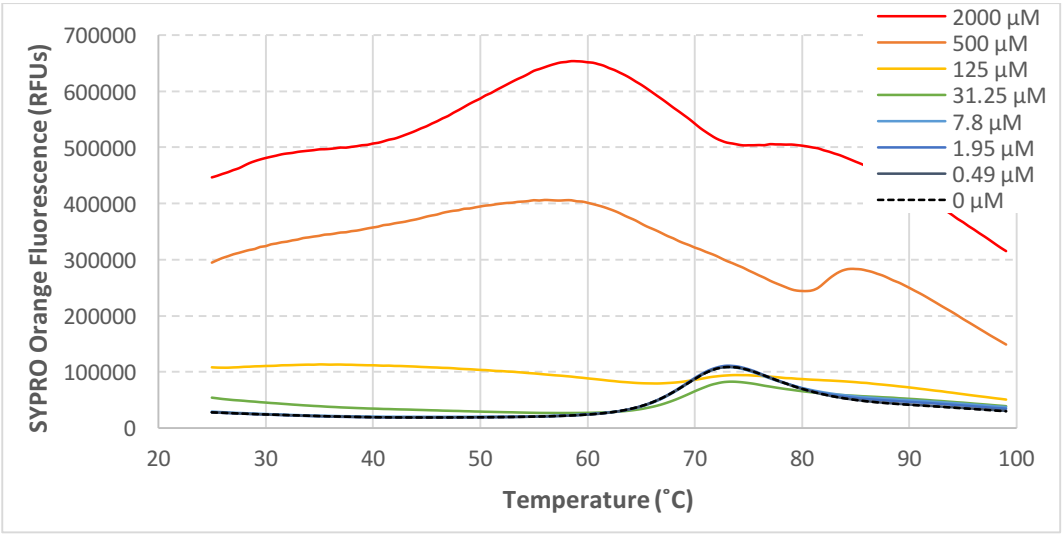
SYPRO Orange Fluorescence (RFUs)
700000
600000
500000
400000
300000
200000
100000
0
20
30
40
50
60
70
80
90
100
Temperature (˚C)
2000 µM
500 µM
125 µM
31.25 µM
7.8 µM
1.95 µM
0.49 µM
0 µM

d)

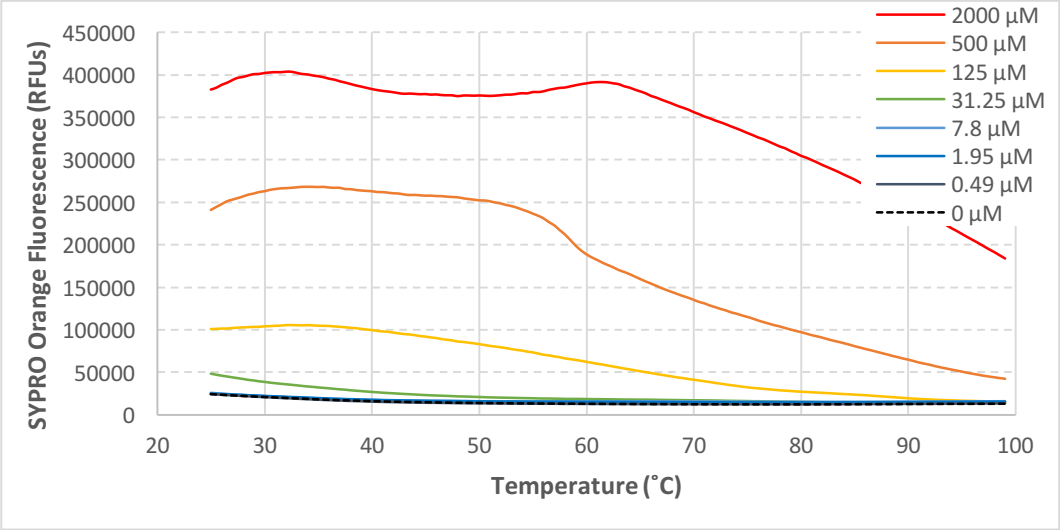


**Figure 18: Thermal shift screening and hit validation. a) PD-L1 thermal shift assay carried out in the presence of various screening compounds at 1 mM (hit compound in red). b) PD-L1 thermal shift assay carried out in the presence of varying concentrations of Z289983522. c) Lysozyme thermal shift assay carried out in the presence of varying concentrations of Z289983522. d) Change in SYPRO Orange baseline fluorescence with varying concentrations of Z289983522.**

To address poor solubility and establish a structure-activity relationship, we synthesized a handful of analogues. We hoped that improved aqueous solubility would overcome the apparent interaction with SYPRO Orange and allow us to evaluate whether this class of compounds actually bound to PD-L1.

### 2.2.3 Synthesis of Z289983522 derivatives

We hypothesized that at least one of the termini of the compound was likely solvent-exposed; as such, we focused our structural modifications on these positions. Specifically,

we aimed to replace the lipophilic para-chloro substituent on the phenyl ring with a methyl ether and a free phenol, in order to increase the polarity and number of hydrogen bonding sites. We also targeted a para-bromo compound, to facilitate further functionalization at this position through cross-coupling chemistry. At the other end of the molecule, one arm of the amide terminates in a methyl ether; we proposed to replace this with a simple alcohol, again to increase hydrogen bonding capability. We also aimed to resynthesize the Z289983522 hit itself, in order to validate it as the active molecule in the sample we received.

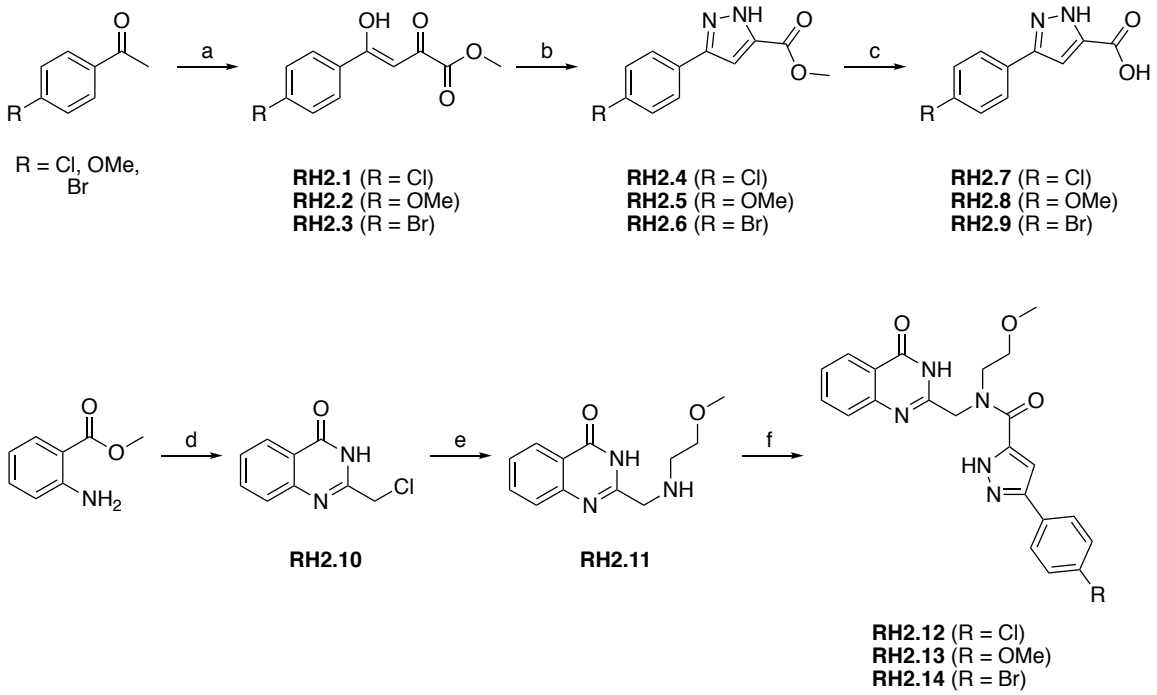


**Scheme 1: Synthesis of Z289983522 analogues. a) NaOMe, dimethyl oxalate, 63-89%. b) $NH_2NH_2•H_2O$, AcOH/iPrOH, 79%-94%. c) NaOH/$H_2O$, Δ, 88-98%. d) anhydr. $HCl_{(g)}$, chloroacetonitrile, dioxane, 94-97%. e) 2-methoxyethylamine, $K_2CO_3$, KI, MeCN, 60 ˚C, 47-61%. f) EDC•HCl, HOBt, $Et_3N$, DMF, 70%.**

The synthesis of the arylpyrazole carboxylate was accomplished uneventfully through adapted literature procedures. Briefly, acetophenone derivatives were subjected to Claisen condensation with dimethyl oxalate using either sodium methoxide (generated in situ from sodium metal and methanol) or potassium *tert*-butoxide as base. The diketoester thus produced was observed only as its enol tautomer, due to the high level of conjugation accessible. This diketoester was then condensed with hydrazine under mildly acidic conditions to form the pyrazole ring. Ester hydrolysis with potassium hydroxide provided the corresponding carboxylic acids **RH2.7-RH2.9** in high overall yield, with minimal chromatographic purification.

The synthesis of the quinazolinone heterocycle, as well as amination thereof, was slightly more technically challenging. The methyl quinazolinone ring was accessed by a modified Niementowski reaction of acetonitriles with methyl anthranilate. Chlorination of the unsubstituted methyl quinazolinone proved to be inefficient, and use of inexpensive chloroacetonitrile provided the desired product in one step. Nucleophilic displacement of the chloride with 2-methoxyethylamine provided the desired intermediate **RH2.11**.

The use of anhydrous hydrogen chloride in the quinazolinone synthesis was technically challenging. The gas was prepared by slow addition of 98% sulfuric acid to sodium chloride, which was then passed through a drying tube of calcium chloride and bubbled into the reaction mixture. Gassing a solution of the acetonitrile and anthranilate often resulted in precipitation and blockage of the dispersion tube, leading to overpressure of HCl in the HCl generator. This setup was also prone to suckback of the reaction mixture

into the generator, presenting a serious safety hazard. Saturation of dioxane with HCl before substrate addition solved both of these problems, and the reaction could be performed safely and on large (15 gram) scale with excellent (94-97%) yield.

Alkylation of 2-methoxyethylamine required a fair amount of optimization. The dialkylated amine often comprised a significant proportion of the product, despite the 1:1 molar ratio of starting materials used and the reduced nucleophilicity of the secondary amine due to the electron-withdrawing quinazolinone. This poor selectivity is likely due to the much higher solubility of the monoalkylated product compared to the aryl chloride, which forms a suspension with most solvents. Increased dilution and moderate heat solved these problems somewhat, though the final conditions are far from ideal.

Amide formation between the two halves of the molecule proved difficult due to poor nucleophilicity of the amine, and product isolation was difficult due to poor solubility. Several harsh amide-forming reactions were attempted, but did not result in isolable product. Direct aminolysis of the methyl ester **RH2.8** also failed; in this case, the N-methylated pyrazole ester was formed as the result of Krapcho-like nucleophilic demethylation of another equivalent of **RH2.8**. Finally, it was found that milder amide-forming conditions (EDC, HOBt) provided the desired products in good (~70%) yield.

### 2.2.4 Validation of Z22 derivatives and Thermal shift drawbacks

While the thermal shift assay led us to the putative hit Z22, we were reluctant to use it as a long-term screening strategy. Our initial experiments had shown that many of the aromatic compounds in our screening library interfered with the reporter dye's fluorescence output, complicating any assessment of their activity. Moreover, we were eager to test if these proposed hinge-binding compounds could affect PD1/PD-L1 binding in any way.

## 2.3 ELISA assay for PD1/PD-L1 inhibition and tryptophan-based lead compounds

To find out if our screening collection could inhibit the PD1/PD-L1 interaction, we required an assay that was robust, label-free or minimally labeled, dye-free, and amenable to the microplate format. For this application we chose an Enzyme-linked immunosorbent assay (ELISA). ELISA does not require any fluorescent or luminescent labels or reporters during the compound binding step, and only one (or even none) of the protein binding partners need affinity tags.

### 2.3.1 Theory and optimization of a commercial ELISA assay for PD1/PD-L1 inhibition

ELISA are used to detect protein-protein binding events based on adsorption of one binding partner to a surface and physical separation. A buffered solution of one binding partner is

added to a plastic microplate and allowed to adsorb to the bottom of the well, immobilizing it. The remaining solution is decanted or pipetted off, and the remaining surface area of the well is coated with an excess of a non-reactive "blocking" protein (often bovine serum albumin, milk casein, or even commercial skim milk). The analyte is then added to the well, and ligands for the immobilized protein are bound and retained; the excess solution is removed, and the wells washed to remove unbound non-specifically bound. The bound ligand is then detected using a ligand-specific binder (an antibody, for untagged proteins; streptavidin, for biotinylated proteins) conjugated to an enzyme that catalyzes a colour- or light-producing reaction. The colour or light produced is proportional to the amount of enzyme bound, which is in turn proportional to the amount of analyte bound.

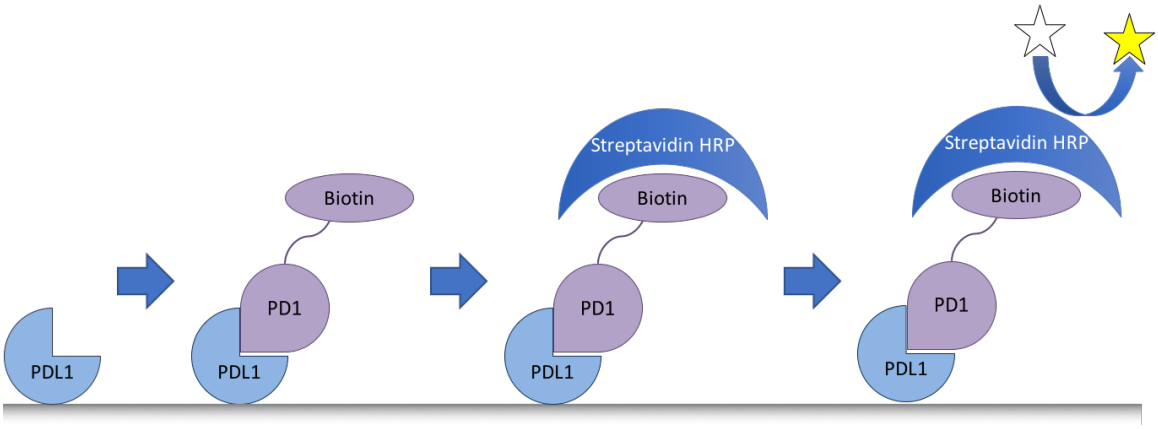


**Figure 19: Schematic of an ELISA assay for PD1/PD-L1 binding.**

In order to get useful binding information quickly, we chose a commercially available ELISA kit from BPS Bioscience. We attempted to develop our own ELISA in-house, but the signal-to-noise ratio could not be improved to give a sufficient dynamic range between negative and positive controls. We therefore chose to purchase a validated, commercial kit

that had only just become available from BPS Bioscience (the first commercial PD1/PD-L1 assay kit, as far as we were aware)[287]. Briefly, the assay kit calls for the adsorption of untagged PD-L1 to an assay plate, blocking, binding of PD-L1 to PD1 tagged at the C terminus with a single biotin moiety, followed by binding of the biotinylated PD1 to a streptavidin-horseradish peroxidase (HRP) conjugate, and finally addition of chemiluminescent substrate and detection of the luminescent enzyme output.

### 2.3.2 Screening of compounds for PD1/PD-L1 inhibition by ELISA

We began our investigation by testing the Z22 analogues we had made; unfortunately, these were ineffective at inhibiting the PD1/PD-L1 interaction in the ELISA assay (see Figure 20). The compounds were tested at very high concentration (1 mM), but could not inhibit PD1/PD-L1 binding by even 30%. These results, combined with the suspicious dye interactions observed in the thermal shift assay, led us to abandon this series of compounds and conclude that there were probable assay artifacts (i.e. assay interference due to aggregation with reporter dye).

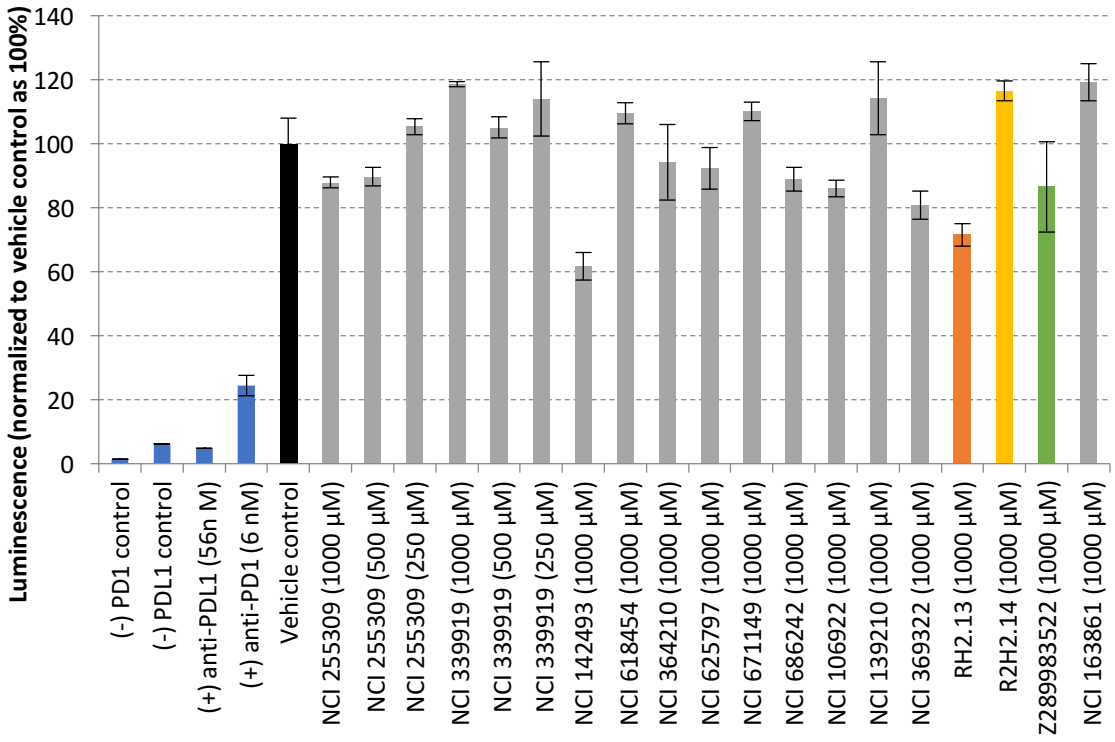


**Figure 20: PD1/PD-L1 ELISA assay results, with Z289983522 and analogues highlighted.**

Screening the remainder of our initial set of compounds, as well as new compounds generated from ongoing docking experiments and sourced from the NIH, led to a handful of apparent hits, although few of them were reproducible in subsequent assays. NCI compound 339919 showed apparent inhibition of the PD1/PD-L1 interaction of 65% and 83% at 1 mM in two different assays, but when the compound was run in a series of concentrations to determine the dose-response relationship, all concentrations (1 mM, 500 µM, 250 µM) were indistinguishable from the vehicle control (data not shown). We therefore attributed the single-concentration results to experimenter errors.

However, in one of the early assays we ran using this ELISA kit, we discovered NCI 280784 to be a strong apparent agonist of the PD1/PD-L1 interaction (see Figure 21a, other

test compounds removed for clarity). Addition of 1 mM compound increased the ELISA signal output by almost six times, indicating *stronger* binding of PD1 to PD-L1. As mentioned, the PD1/PD-L1 interaction is extremely difficult to modulate with small molecules; any compound that can do so is worth pursuing. We therefore decided to characterize this molecule more fully, and determine the mechanism and specificity of this apparent PD1/PD-L1 agonism.

a)

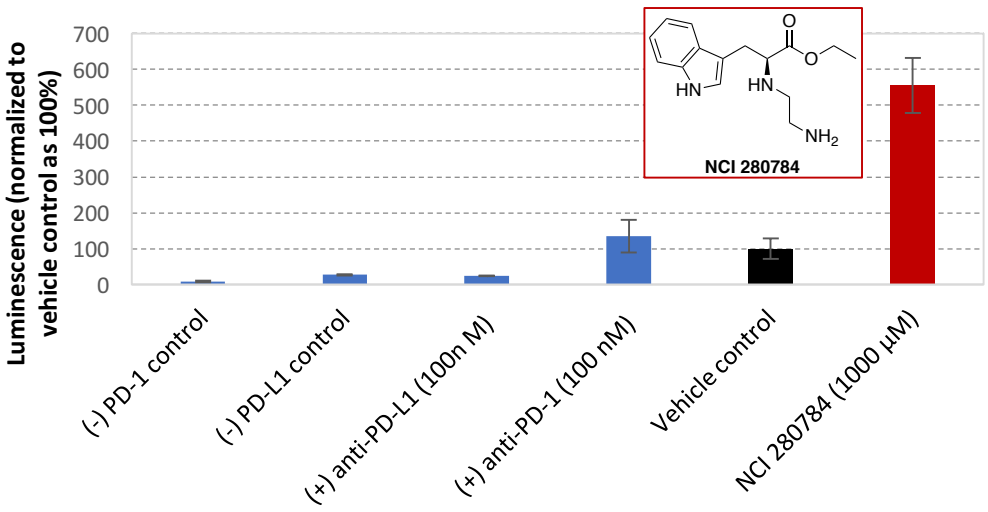

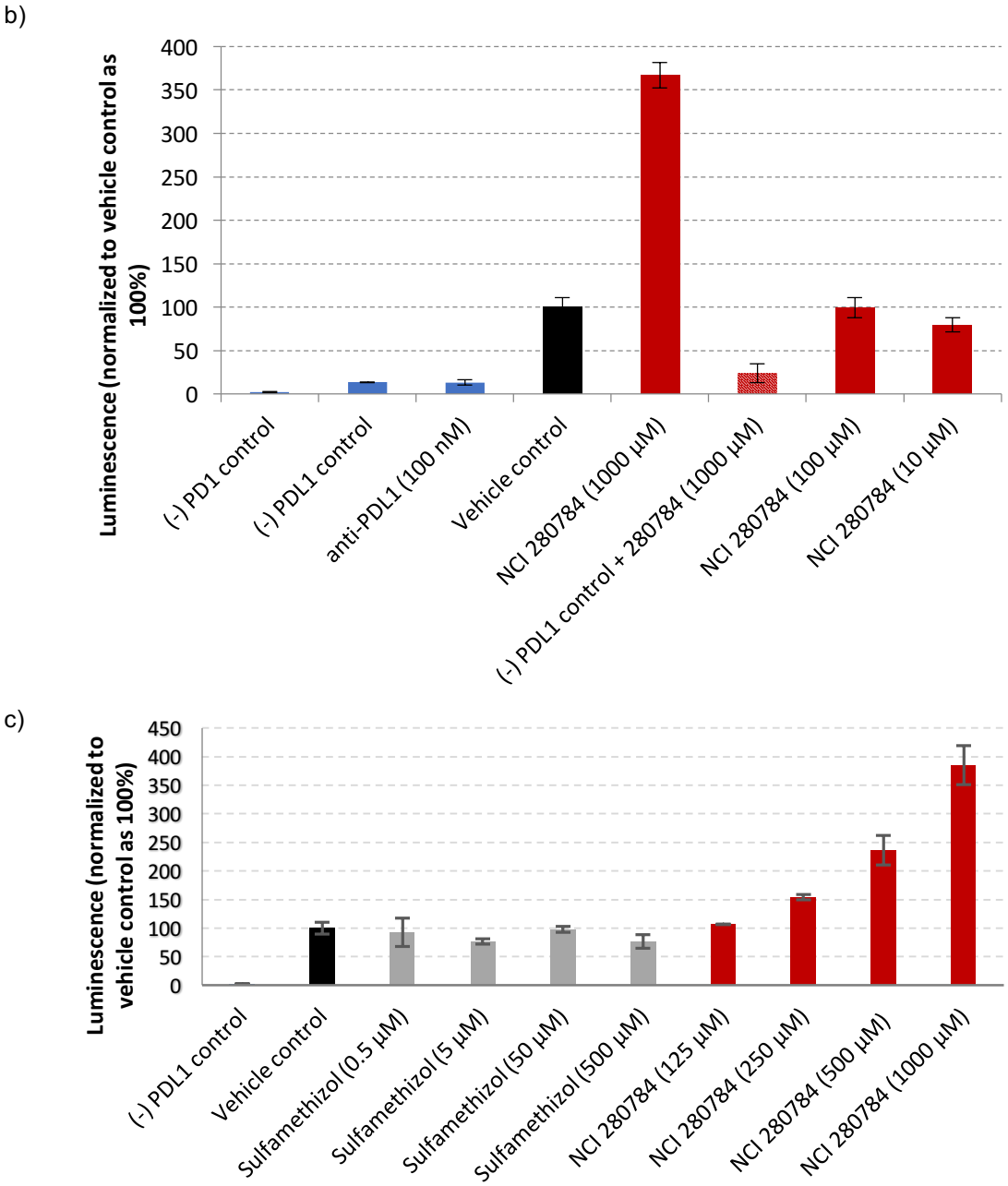


**Figure 21: Discovery and validation of NCI 280784 as a lead from ELISA. a) Signal enhancement due to NCI 280784. b) Replication of initial result and counter-screen for nonspecific activity. c) Dose-response curve for NCI 280784.**

Our attempts to invalidate this molecule's activity were not successful; every indication was that PD1/PD-L1 agonism was both real and specific. NCI 280784 reliably increased

signal output in almost every ELISA we ran, although the absolute value of signal amplification varied. While this was concerning, as it meant our assay was not completely stable, we established a dose-response relationship with this compound (see Figure 21c), and found that its signal enhancement decreased proportionally with concentration. Moreover, a counter-screen with this compound in the absence of immobilized PD-L1 (see Figure 21b) gave similar results to the control with no compound and no PD-L1 (24% vs 14%). This indicated that the PD1/PD-L1 interaction was required for the compound's activity.

Furthermore, there was nothing about the molecule's structure or physical and chemical characteristics that gave us reason to doubt its activity. The compound contains no electrophilic functional groups, and appeared to be fully soluble in the assay buffer used, ruling out protein alkylation or precipitation as a possible mechanism of assay interference. Furthermore, we thought that because tryptophan has previously been shown to affect the refolding of spent HRP as well as function as a substrate for HRP, perhaps the tryptophan-derived NCI 280784 could be enhancing luminescence in this way. However, incubation of the compound with the chemiluminescent substrate produced no luminescence, while addition of the compound to a mixture of the substrate and HRP did not significantly enhance the luminescent output of the reaction. These data indicate that NCI 280784 does not react with the luminescent substrate in the absence of the enzyme, and probably does not affect the rate of reaction in the presence of HRP.

Despite our intention to find antagonists of the PD1/PD-L1 interaction, an agonist would have interesting applications in autoimmune settings. CTLA-4 agonists are used in the treatment of rheumatoid arthritis (see Chapter 1), and defects in PD1 function have been implicated in various autoimmune disorders, particular lupus[288-289]. As opposed to blocking an interaction, though, stabilizing an interaction is a much more difficult activity to build into an antibody. A small molecule capable of stabilizing this interaction would therefore have a relatively open field as compared to PD1/PD-L1 inhibitors, which would have to show clear benefits over the multitude of antibodies available.

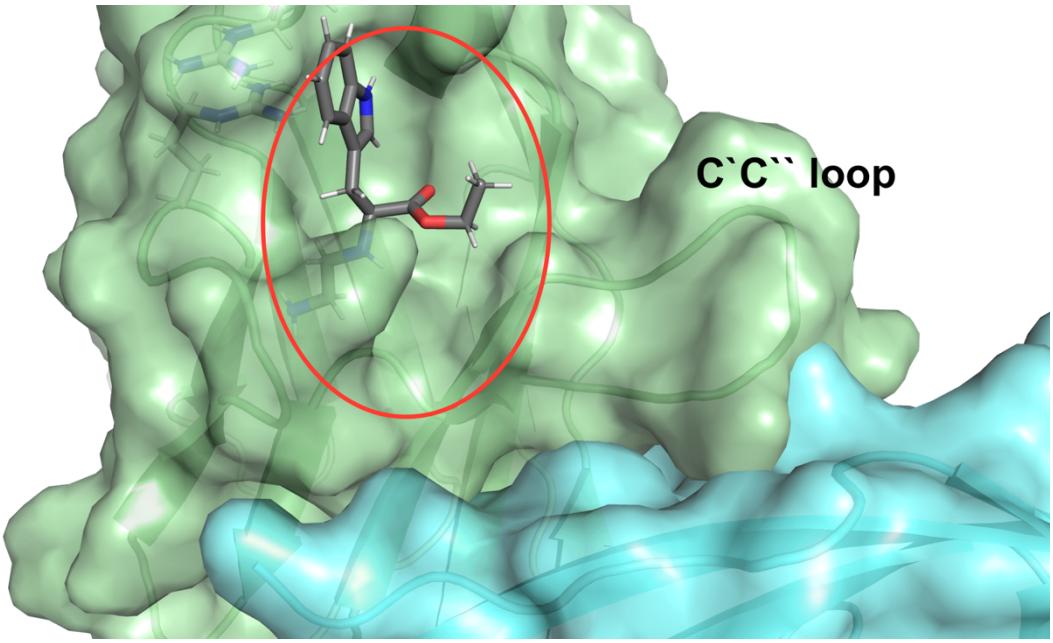


**Figure 22: NCI 280784 docked into the loop-proximal binding pocket of PD1. (PDB: 4ZQK)**

Moreover, this molecule was predicted to bind proximal to the C`C`` loop of PD1 (see Figure 22). This loop clamps down on PD-L1 during binding, but is disordered and flexible in the apo state. This indicated to us that compound binding could disrupt or control the

conformation of this loop considerably, and that we could either enhance or inhibit the PD1/PD-L1 interaction by tuning the compound to pull in or push out the loop. This compound, while identified as an agonist in our screen, could therefore serve as a scaffold for the synthesis of inhibitors, too.

### 2.3.3 Synthesis and screening of tryptophan derivatives

We synthesized or purchased a number of simple unsubstituted, N-alkylated, and N-amidated tryptophan esters in order to generate a structure-activity relationship for this lead compound. We focused our efforts on determining the steric and electronic requirements of three areas: the indole ring, the ethyl ester, and the ethylenediamine unit. For the indole, we were interested in whether an even more electron-rich ring, like a hydroxylated or methoxylated indole, would improve binding. For the ethyl ester, we were interested in the size and lipophilicity requirements of the ester (methyl vs. ethyl vs. isopropyl), as well as whether amides would be tolerated (amides are more hydrolytically stable and offer two points of diversification vs. one for esters). Finally, for the diamine unit, we wanted to explore the length, size, and charge requirements by extending the chain length (propylenediamine vs. ethylenediamine), swapping the basic terminal amine for a polar yet neutral alcohol, forming an amide at the α-amine, and removing the extra heteroatom entirely.

Most of the desired indoles and esters could be purchased or synthesized in one step based on literature procedures. The methyl and isopropyl esters of tryptophan were

synthesized by acid-catalyzed Fischer esterification. Indole-modified tryptophan and tryptamine derivatives were purchased and used as-is.

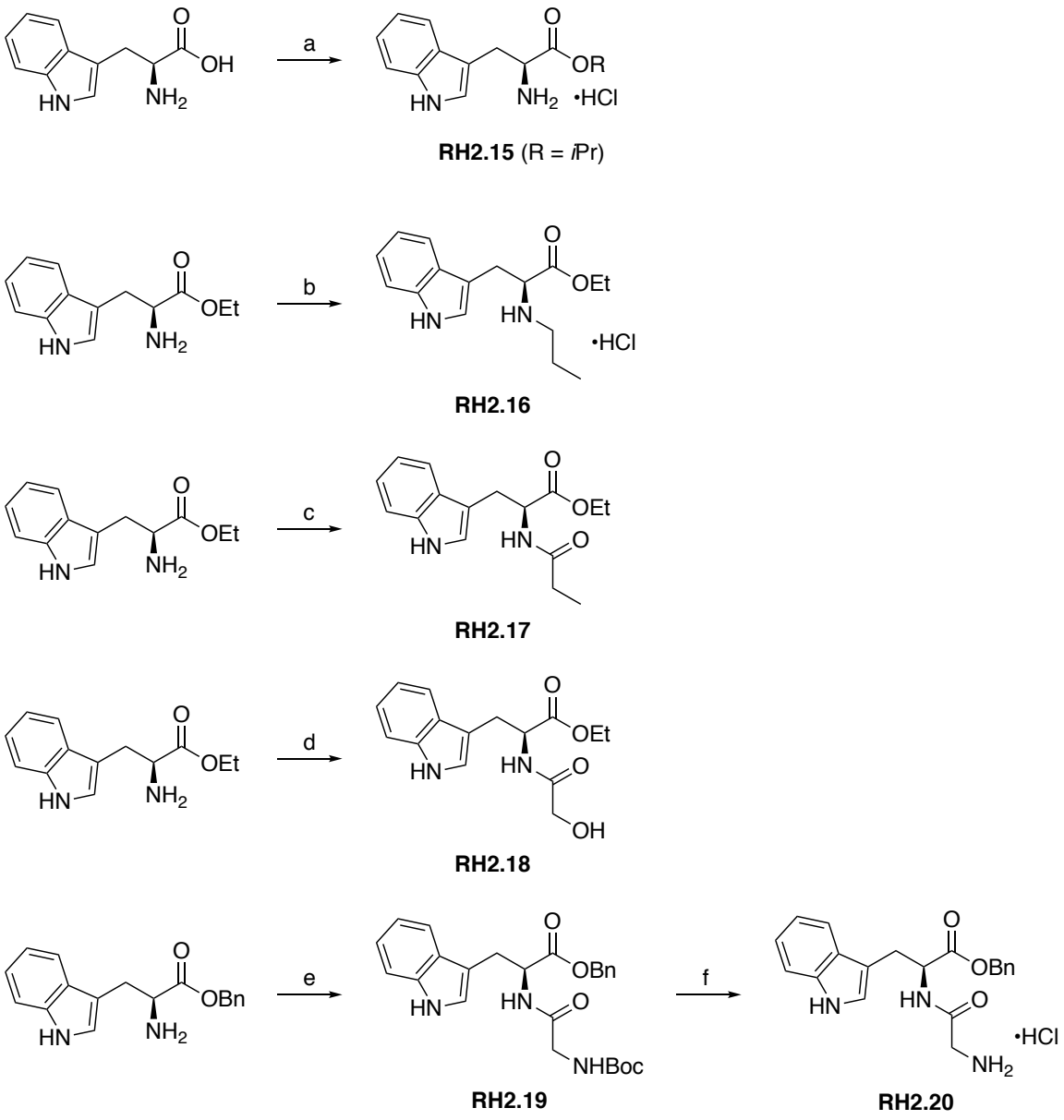


**Scheme 2: Synthesis of simple tryptophan analogues. a) $SOCl_2$, MeOH or *i*PrOH, Δ, quantitative. b) Propionaldehyde, $NaBH_3CN$, 29%. c) Propionic anhydride, pyridine, 81%. d) Glycolic acid, EDC•HCl, HOBt, Hünig's base, 35%. e) N-Boc glycine, EDC•HCl, HOBt, 38%. f) HCl, MeOH, quantitative.**

The synthesis of simple N-amido and N-alkyl derivatives was similarly uncomplicated. Reductive amination of tryptophan ethyl ester with propanal was straightforward, although the yield was low due to overalkylation. Propionamide formation was easily accomplished by addition of propionic anhydride, while N-Boc glycine and glycolic acid were coupled using standard conditions (EDC, HOBt). The N terminus of the Boc-Gly-Trp-OEt dipeptide **RH2.19** was then deprotected with acid. Tryptophan amides were similarly prepared by EDC/HOBt coupling.

The synthesis of the ethylenediamines was considerably more challenging, owing to the instability of glycinal and its N-protected derivatives. Reductive amination seemed like the obvious choice to alkylate the amine of tryptophan, so we set about preparing the requisite aldehyde. N-protection of ethanolamine with phthalic anhydride in the melt proceeded uneventfully, but oxidation of the alcohol to the aldehyde was challenging. Reaction under Swern conditions produced an intractable black sludge, although the NMR indicated the presence of the desired product. Substituting cyanuric chloride for the more reactive oxalyl chloride, as well as use of the Albright-Onodera modification using phosphorous pentoxide[290-291], gave similar results. Variations of the biphasic, TEMPO-catalyzed Anelli oxidation using aqueous hypochlorite[292], Oxone™[293], or iodine[294] as terminal oxidants were similarly low-yielding and produced complex mixtures. In all cases, any attempts to purify the aldehyde resulted in its degradation, and the compound degraded upon storage, even at -20 ˚C.

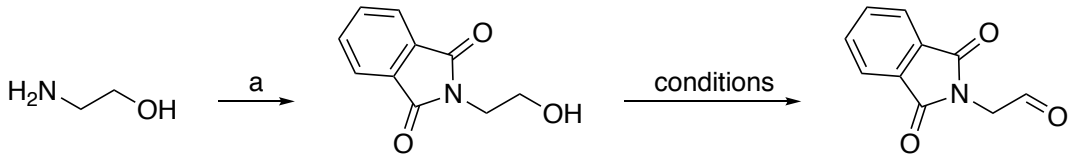


**RH2.21** **RH2.22**

| Condition | Result |
|---|---|
| DMSO, oxalyl chloride, $Et_3N$, DCM -78 ˚C | 100% conversion, 41% yield thick black sludge |
| DMSO, TCT, $Et_3N$, DCM -20 ˚C | 100% conversion, thick black sludge |
| DMSO, $P_4O_{10}$, $Et_3N$, DCM, 0 ˚C | 100% conversion, thick black sludge |
| TEMPO, $NaOCl_{aq}$, KBr, $NaHCO_3$, DCM/$H_2O$ | ~40% conversion |
| TEMPO, Oxone™, $Bu_4NBr$, DCM/$H_2O$ | Compound degradation |
| TEMPO, $I_2$, $NaHCO_3$, DCM/$H_2O$ | Compound degradation |

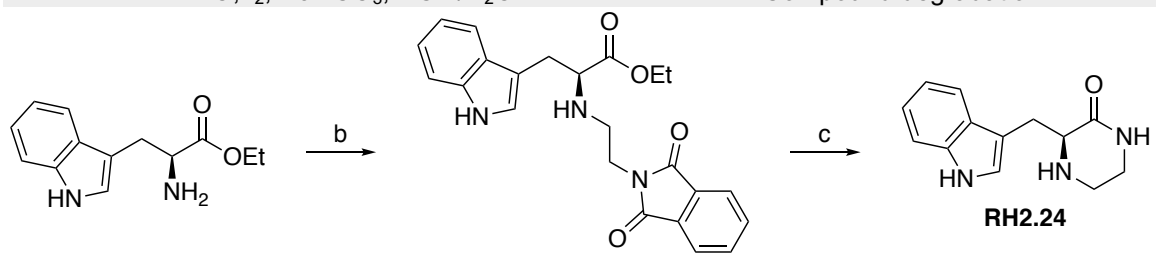


**RH2.23** **RH2.24**

**Scheme 3: Attempted synthesis of tryptophan ethylenediamine using the phthalimide protecting group. a) Phthalic anhydride, neat, 175 ˚C, 92%. b) RH2.22, $NaBH_3CN$, AcOH, MeOH, 25%. c) $NH_2NH_2$•$H_2O$, EtOH, 70 ˚C.**

Nevertheless, the crude phthalimido acetaldehyde was subjected to reductive amination, producing the protected diamine **RH2.23**. The hydrazinolysis of the phthalimide also cleaved the ethyl ester, and the product was originally misidentified as the hydrazide. This proposed structure was corrected to the ketopiperazine **RH2.24** following analysis by mass spectrometry. This result suggested to us that intramolecular cyclization of the diamine onto the ester would be relatively facile, and that the nucleophilicity of the amine would need to be abrogated. We thus chose to replace the phthalimide with the acid-cleavable Boc group.

The Boc-protected glycinal **RH2.26** exhibited the same instability as its phthalimide analogue. N-Boc protection of ethylenediamine was clean and high-yielding, but Anelli oxidation resulted in hemiacetal formation and overoxidation to the corresponding ester. Eventually, it was found that oxidation with IBX in refluxing ethyl acetate or acetonitrile furnished the desired aldehyde in reasonable yield and purity. However, extended reaction times decreased the yield significantly, as did attempted storage in the freezer, so the aldehyde had to be made fresh each time and the effective concentration of aldehyde determined by NMR. While this aldehyde is apparently commercially available, its instability and difficulty of isolation have been noted before[295].

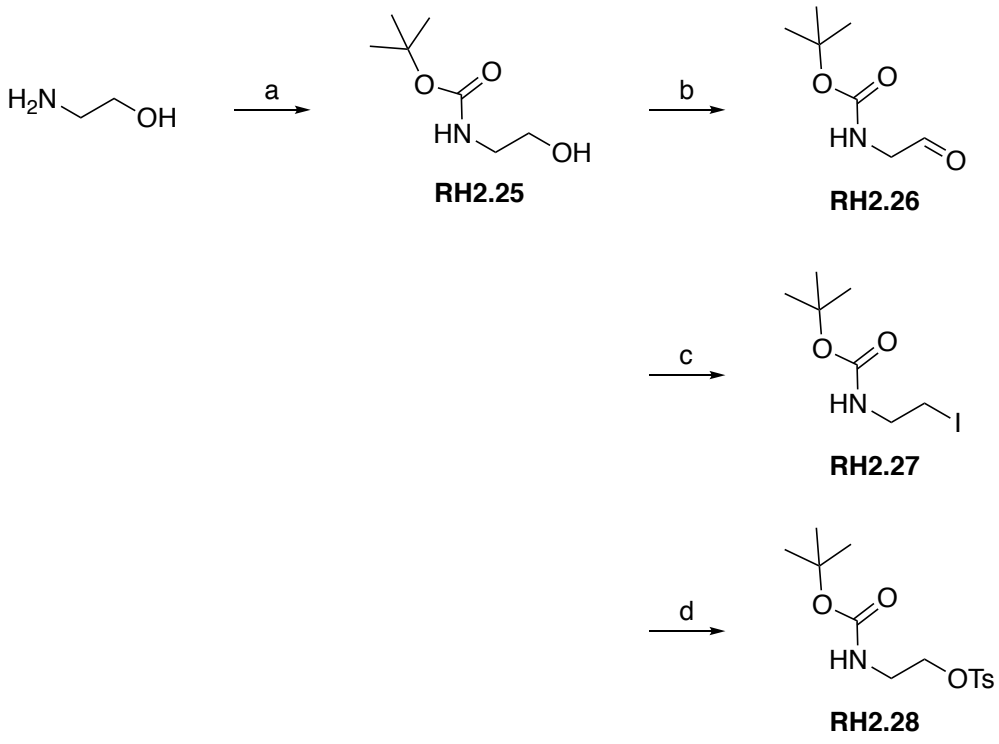


**Scheme 4: Synthesis of *N*-protected ethylenediamine electrophiles. a) $Boc_2O$, $Et_3N$, DCM, 72%. b) IBX, EtOAc, Δ 2 hours, 54-61% (crude). c) $PPh_3$, $I_2$, imidazole, 68%. d) TsCl, $Et_3N$, DCM, 63%.**

Reductive amination using the aldehyde obtained above was similarly non-trivial. Yields were generally low, and the products were accompanied by many co-eluting side products that complicated purification. **RH2.26**'s propensity for amine-catalyzed self-aldol reaction precluded preformation of the imine with tryptophan derivatives. The aldehyde and reducing agent therefore had to be added all at once, which in turn increased the degree of polyalkylation. This problem was further exacerbated by the difficulty in accurately measuring the concentration of aldehyde to begin with. Attempts to control the concentration and equivalents of aldehyde by hydrolyzing the acetal of N-Boc aminoacetaldehyde dimethyl acetal were not fruitful.

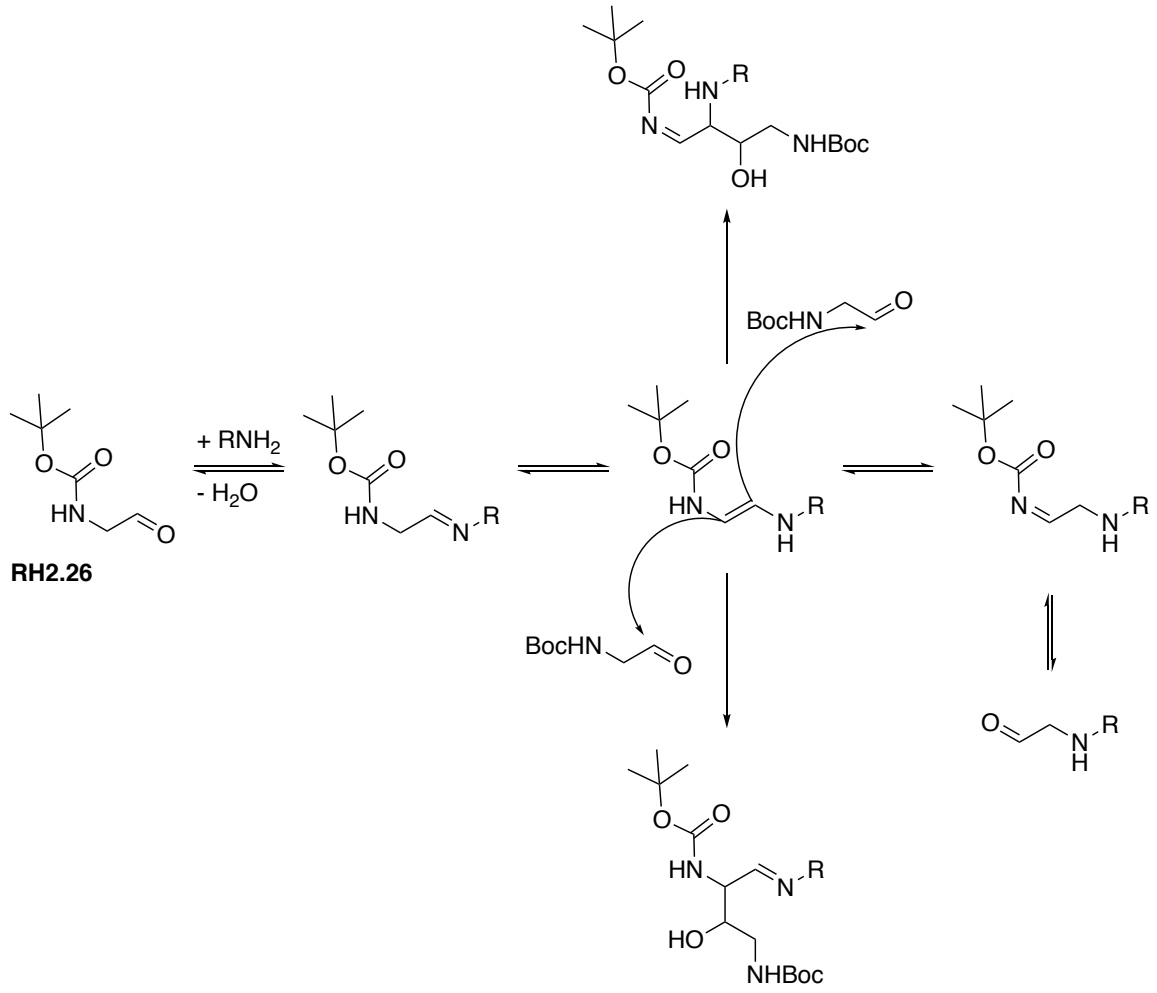


**Scheme 5: Putative mechanism for Boc-glycinal degradation and byproduct formation.**

As reductive amination had proven difficult, N-alkylation of tryptophan esters was attempted. N-Boc ethanolamine was converted to the corresponding iodide and tosylate (**RH2.27** and **RH2.28**), as well as to N-Boc aziridine. Both the tosylate and iodide gave low yields of the desired product under various conditions, presumably because of the low nucleophilicity of the amine. Meanwhile, attempted ring-opening of the protected aziridine with tryptophan esters was largely unproductive. Nevertheless, each analogue was synthesized and deprotected in sufficient quantities to provide enough final product for biological testing.

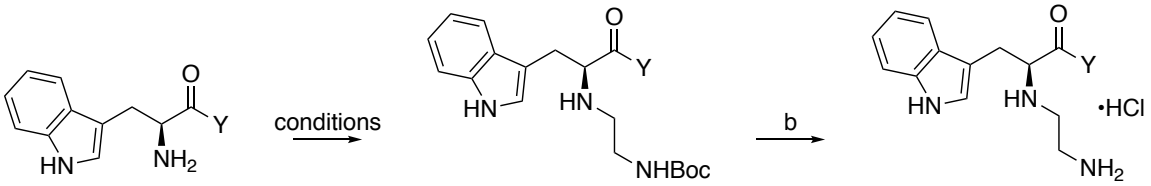


**RH2.29** (Y = OEt)
**RH2.30** (Y = OBn)
**RH2.31** (Y = NHBn)

**RH2.32** (Y = OEt)
**RH2.33** (Y = OBn)
**RH2.34** (Y = NHBn)

| Amine | Reagent & conditions | Yield |
|---|---|---|
| Tryptophan ethyl ester | **RH2.26**, $NaBH_3CN$, MeOH | 20-75%* |
| Tryptophan benzyl ester | **RH2.26**, $NaBH_3CN$, MeOH | 19-37% |
| Tryptophan benzamide | **RH2.26**, $NaBH_3CN$, MeOH | 16% |
| Tryptophan ethyl ester | **RH2.27**, $K_2CO_3$, DMF, 70 ˚C | Trace |
| Tryptophan ethyl ester | **RH2.27**, $K_2CO_3$, MeCN, 70 ˚C | Trace |
| Tryptophan ethyl ester | **RH2.27**, $K_2CO_3$, THF, 70 ˚C | Trace |
| Tryptophan ethyl ester | **RH2.27**, $K_2CO_3$, 1,4-dioxane, 70 ˚C | Trace |
| Tryptophan ethyl ester | **RH2.27**, $Cs_2CO_3$, DMF | Trace |
| Tryptophan ethyl ester | **RH2.28**, Hünig's base, MeCN, 60 ˚C | 26% |
| Tryptophan ethyl ester | **RH2.28**, $K_2CO_3$, DMF, 60 ˚C | 6% |
| Tryptophan ethyl ester | **RH2.28**, Hünig's base, DMF, 60 ˚C | 3% |
| Tryptophan ethyl ester | **RH2.28**, Hünig's base, 0.1 eq KI, MeCN, 60 ˚C | 25% |
| Tryptophan ethyl ester | **RH2.28**, Hünig's base, 1 eq KI, MeCN, 60 ˚C | 26% |
| Tryptophan ethyl ester | **RH2.28**, $K_2CO_3$, 0.1 eq NaI, 1,4-dioxane, 82 ˚C | 27% |
| Tryptophan ethyl ester | **RH2.28**, $Cs_2CO_3$, 0.1 eq NaI, 1,4-dioxane, 82 ˚C | 30% |
| Tryptophan ethyl ester | 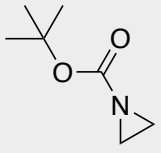 , Hünig's base, Lewis acids: LiCl, LiBr, $CeCl_3$•$7H_2O$, or $Yb(OTf)_3$ | Trace |

**Scheme 6: Synthesis of ethylenediamine-substituted tryptophan analogues. b) HCl, MeOH, quantitative. * = highly variable, not reproducible.**

The aminoalcohol derivative **RH2.37** was also prepared by reductive amination. The aldehyde **RH2.35** produced by IBX oxidation of a monosilylated ethyleneglycol was, again, unstable. Nevertheless, reductive amination and acid-mediated desilylation provided enough of the product **RH2.37** for biological testing.

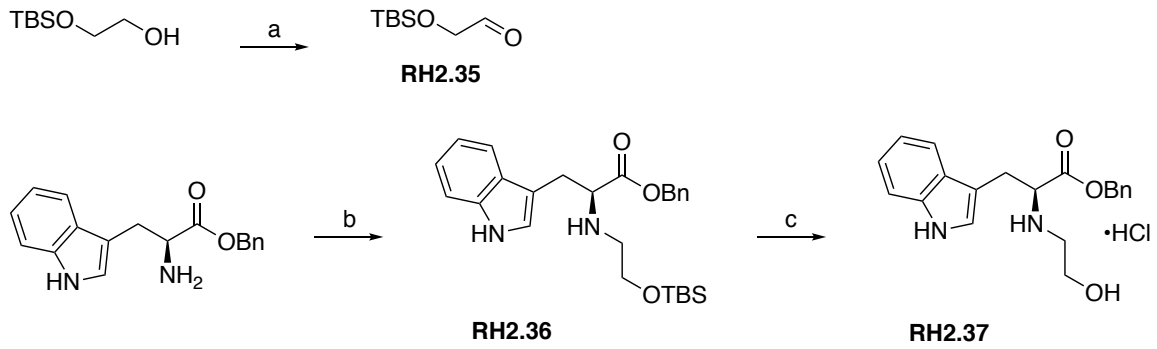


**Scheme 7: Synthesis of an aminoalcohol tryptophan derivative. a) IBX, EtOAc, Δ 2 hours, crude product used. b) RH2.35, $NaBH_3CN$, MeOH, 27%. c) HCl, MeOH, 84%.**

Extension of the diamine or aminoalcohol unit to 3 carbons was comparatively straightforward. N-boc aminopropanal suffered no issues with stability, and was produced in quantitative yield by Anelli oxidation. Reductive amination using this aldehyde gave compounds **RH2.40** and **RH2.41**, which were deprotected with acid.

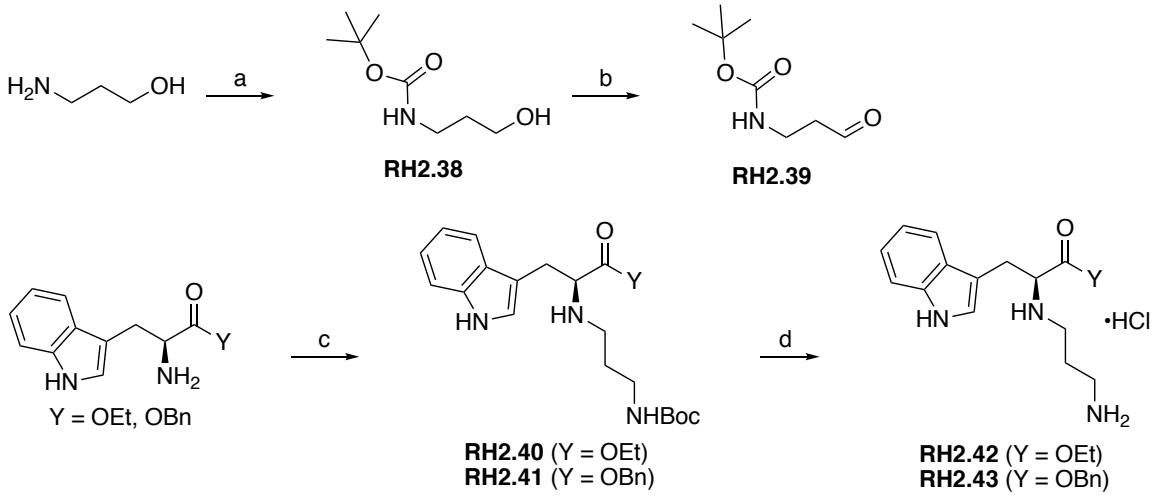


**Scheme 8: Synthesis of chain-extended tryptophan diamines. a) $Boc_2O$, $Et_3N$, THF, quantitative. b) *N*-chlorosuccinimide, TEMPO, $Bu_4NCl$, $NaHCO_3$, $CHCl_3/H_2O$, 98%. c) RH2.39, $NaBH_3CN$, MeOH, 29-45%. d) HCl, MeOH, quantitative.**

### 2.3.4 Assay instability

We were able to perform a preliminary assay with some of the early compounds, and determine a basic structure-activity relationship (see Figure 23). First, we found that the chirality of the compound matters, as L-tryptophan was twice as active as D-tryptophan – a good sign that the effect is specific, since L- and D-tryptophan have identical physical properties. The benzyl ester of tryptophan was more active than the ethyl ester, indicating that large aromatic sidechains at the C terminus were favoured; the isopropyl ester was comparable to the ethyl. 5-Hydroxytryptophan was similarly more active than tryptophan itself, indicating that the more electron-rich indole was preferred. The ketopiperazine **RH2.24** that was produced accidentally seemed to behave as a weak inhibitor, though the results would need reproduction before any conclusions could be drawn. The N,O-dicyanomethyl compound JW-VI-13 was only a moderate agonist, while NCI 280784 continued to be the strongest agonist by far, highlighting the importance of its ethylenediamine to its activity. Unfortunately, the resynthesized **RH2.32** was not ready in time to run a head-to-head comparison with externally sourced NCI 280784 at this time.

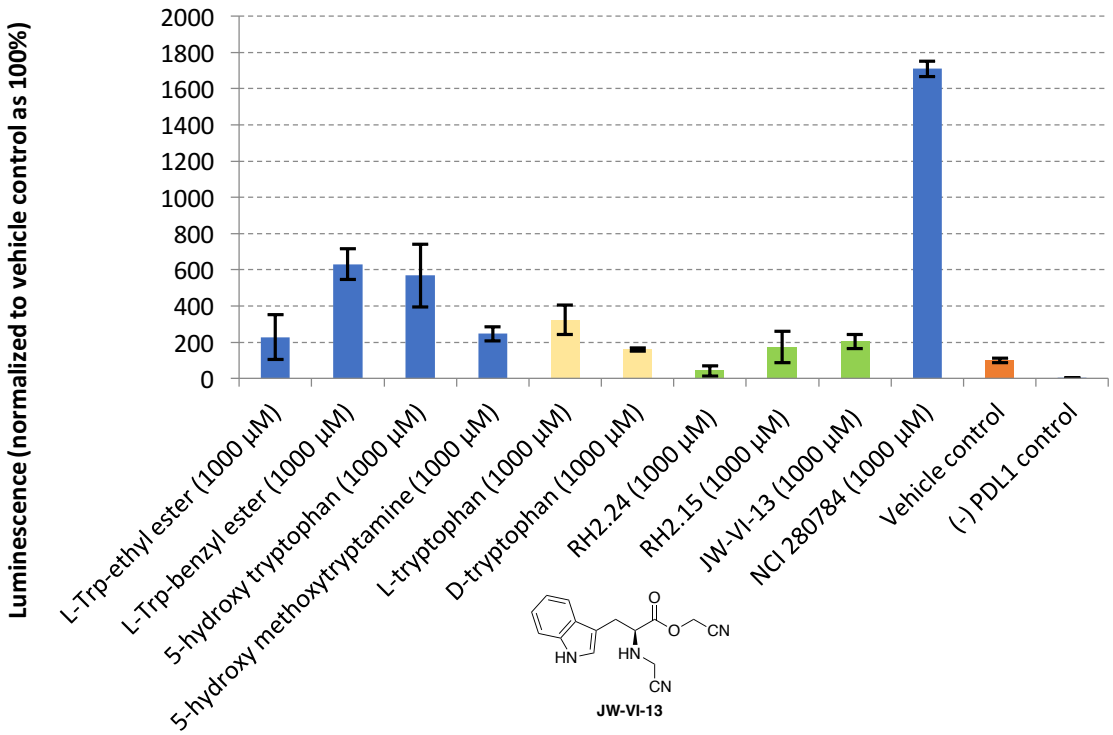


**Figure 23: ELISA results from simple tryptophan analogues.**

While the synthesis of the more complex tryptophan derivatives was in progress, we began to observe significant and apparently systematic irreproducibility within and across assay plates (see Figure 24 for an example dataset – no replicates omitted). After December of 2014, the error between replicates in any given plate ballooned. NCI 280784, which had been demonstrated to have a robust dose-response relationship, produced erratic responses. Of more concern, the readings from the vehicle control wells also began to vary by up to 100%. Clearly, this was not a compound issue – it was an assay issue.

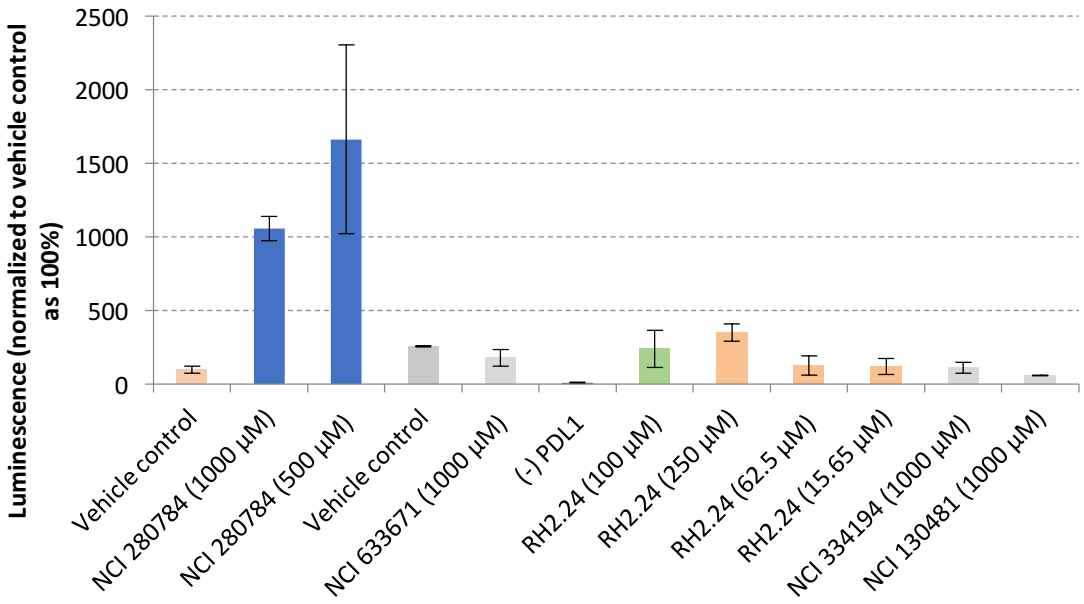


**Figure 24: Example of an unstable ELISA. Note the large error bars, reversal of previously observed dose-response for NCI 280784, and the two-fold difference between the two sets of vehicle controls in the first and fourth columns.**

Moreover, we occasionally observed a periodicity to the assay instability, although this was difficult to ascertain due to the different contents of each well and the fact that triplicates were run in adjacent wells.

We extensively investigated possible mechanical, procedural, and user problems, but could not find any issues that would explain the variability in results. The same student was performing these assays throughout. Nevertheless, she tested her pipetting skills and found both the average variation as well as the average error to be less than 1% – a validation of both the user's and the pipette's precision and accuracy. To rule out plate reader errors, the assay plates were routinely read both in the normal configuration and with the plate rotated

180˚. The assay was also run with X-ray film overtop the assay plate to capture the luminescent output, and the intensity of the images in the developed film matched up with the plate reader values – again, confirming that measurement error was not to blame[296].

We also investigated possible variations in kit components or their storage, though this likewise proved fruitless. The first few assay runs that showed this high variability were from the same lot as earlier, successful assays. Although we stored the kits according to manufacturer specifications, we tested components that had been stored in our freezer and compared them with newly arrived kits, with no detectable difference. We also ran a different kit type (where PD1 was immobilized on the plate, and biotinylated PD-L1 was the soluble analyte[297]), and again observed inter- and intra-plate variability.

Finally, we observed that assay variability was related to apparent defects in the assay plates. The student performing the assays noted that some well bottoms appeared to be "speckled" – performing the assay then revealed that the speckled wells had significantly lower luminescence output than others. Moreover, when buffer was applied to these "speckled" wells, it appeared to bead up, indicating that the surfaces had significant hydrophobic character compared to normal wells. One could speculate, then, that whatever surface treatment the plates receive had been applied unevenly. Unfortunately, ordering a new set of plates did not solve the issue.

Ultimately, we were unable to resolve the reproducibility issues in a satisfactory manner. With an apparent hit compound in hand, analogues to test, and no idea whether other groups

had discovered the same compound we had, time was of the essence, and we could not waste more time troubleshooting a bad assay.

## 2.4 TR-FRET assay for PD1/PD-L2 inhibition and salicylate-based lead compounds

Due to the instability of ELISA results, coupled with the assay's high cost and labour-intensive nature, we needed a new method to screen compounds for PD1/PD-L1 activity. To minimize any inconsistencies in user technique, we sought a method that would not require any kind of washing or separation steps. We had also been limited by the high cost and low throughput of the 96-well ELISA, and so miniaturization was high on our list of priorities. Despite our hesitance to use another BPS Bioscience product, we chose to employ their 384-well TR-FRET assay for PD1/PD-L2 inhibitor screening[298], due to its simple nature and robustness towards assay interference.

### 2.4.1 Theory and optimization of a commercial TR-FRET assay for PD1/PD-L2 inhibition

Förster resonance energy transfer (FRET) is a biophysical method of assessing solution-phase binding based on proximity; time-resolved FRET (TR-FRET) refers to an improved assay setup designed to reduce interference. In this assay, PD1 is covalently linked to a cryptand chelate binding europium, while PD-L2 is biotinylated, rendering it capable of binding to a dye-labelled streptavidin. The FRET donor (europium) absorbs light at 320

nm and enters an excited state; in the absence of an appropriate FRET acceptor, it emits 620 nm light. However, in the presence of an acceptor dye whose absorption spectrum overlaps with the lanthanide emission spectrum, a non-radiative energy transfer occurs between the donor and the acceptor, the acceptor enters an excited state, and then emits at its characteristic emission wavelength (665 nm). This non-radiative event is highly distance-dependent (decays according to $r^{-6}$), and is only efficient when the FRET donor and acceptor are brought into close physical proximity (typically 1-10 nm) by protein-protein binding. If the donor and acceptor are far apart, no energy transfer takes place, and the dye does not emit[299]. Thus, the emission at 665 nm stimulated by absorption at 320 nm is indicative of proximity between the donor and acceptor and, by extension, indicative of a binding event between PD1 and PD-L2. To control for pipetting errors or variable sample absorbance, the FRET signal is normalized to the emission of the donor (620 nm), and this 665 nm/620 nm **FRET ratio** is the measurement used to compare samples[298].

The time-resolved (TR) part of TR-FRET refers to the delay period introduced between excitation and measurement of emission. Lanthanides like europium have a very long excited state lifetime (several milliseconds) relative to organic chromophores (nanoseconds). Thus, while irradiation with 320 nm light will excite any and all chromophores that absorb at that wavelength, the organic chromophores will decay back to the ground state much faster compared to the lanthanides. Introducing a delay period between excitation and emission measurement ensures that all background fluorescence due to organic molecules has subsided, and that any signal measured *must* be coming from

the lanthanide. This extra feature renders TR-FRET mostly insensitive to interference from coloured or fluorescent compounds[299].

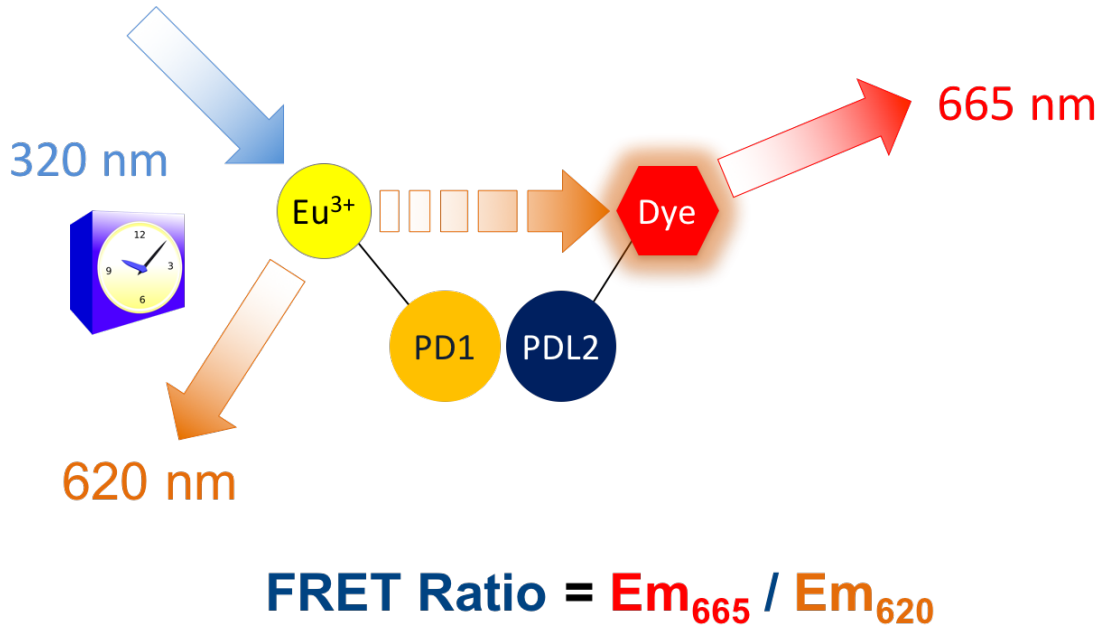


**Figure 25: Schematic of TR-FRET signal generation.**

Even though our primary interest was the PD1/PD-L1 interaction, the PD1/PD-L2 assay kit was the best product that met our needs at that time. At the time, there were simply no other commercial biophysical assay kits for the PD1 pathway. While the binding of PD1 to PD-L2 is somewhat different from PD1 to PD-L1 (PD-L2 binds 3 times more strongly, and with a greater enthalpic component[98]), PD-L2 shares sequence similarity to PD-L1 and binds to the same site on PD1 as PD-L1. Moreover, the kit we chose contained europium-labelled PD1 as one binding partner and biotinylated PD-L2 as the other. This left open the possibility of swapping out the PD-L2–biotin conjugate for a commercially available PD-L1-biotin conjugate.

### 2.4.2 Screening of compounds for PD1/PD-L2 inhibition by TR-FRET

We began by screening the hit compounds from our previous assays, and found that none of them reproducibly inhibited or activated the PD1/PD-L2 interaction. Neither the ketopiperazine **RH2.24** nor the hit compound **RH2.32** had a drastic effect on the FRET ratio (see Figure 26), despite both compounds having been modeled to bind *PD1*, not PD-L1.

Moreover, despite the huge variations in absolute ELISA signal output, the NCI 280784 received from the NIH always showed the highest luminescence of any test well in that assay. The resynthesized **RH2.32**, on the other hand, did not show dramatic signal enhancements, although those data were only acquired after the assay had become unstable. This indicated that an impurity in the original batch of NCI 280784 may have been responsible for its apparent activity.

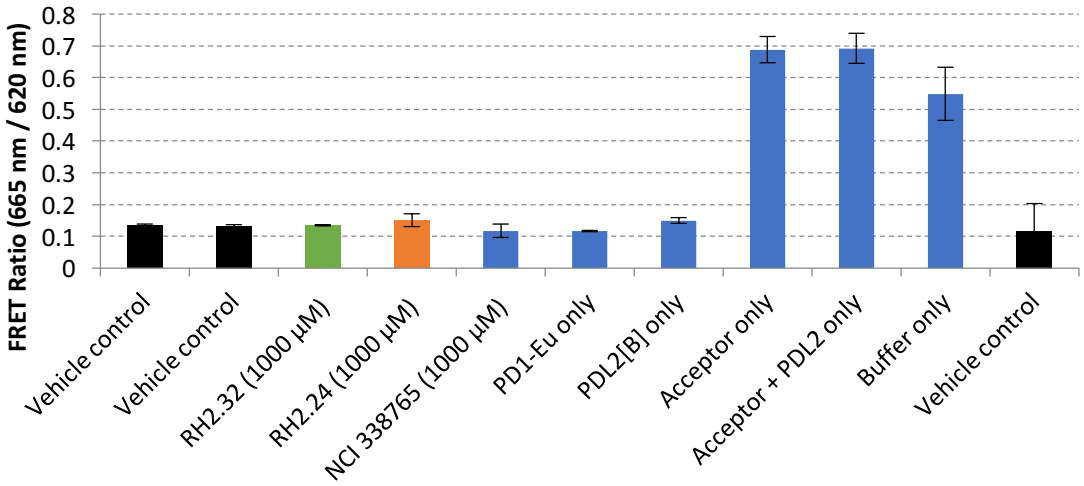


**Figure 26: PD1/PD-L2 TR-FRET assay including tryptophan compounds. Both appear to be inactive.**

We screened the remainder of the compounds from our collection, but most of the compounds that affected the TR-FRET ratio also seemed to be interfering in the assay. Alongside each measured FRET ratio, we collected full emission spectra; many compounds that have drastically different FRET ratios also quenched the fluorescence entirely, so that the ratio was meaningless.

However, an apparent agonist of the PD1/PD-L2, NCI 211845 (see Figure 27), piqued our interest despite its electrophilic nature. This compound contains an electrophilic iodoacetamide, a highly reactive functional group for thiol alkylation. Nevertheless, we were curious to see how this compound could affect FRET ratios, and even if it were covalently modifying one of the two proteins, it could still provide information about possible small molecule binding sites. Running a concentration series provided a

respectable dose-response curve, and the collected spectral data displayed no obvious quenching or peak shifts.

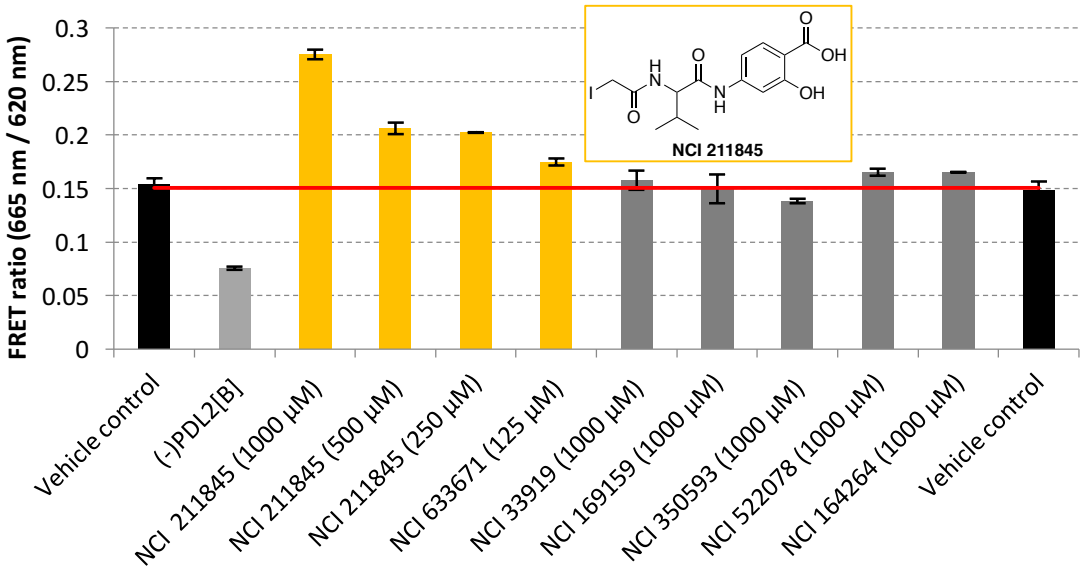


**Figure 27: Dose-dependent response of NCI 211845 in PD1/PD-L2 TR-FRET assay.**

Our fears about compound 211845 were allayed by the discovery that closely related salicylate NCI 211717 lacking the iodoacetamide was just as active, if not more so (see Figure 28). Not only did this confirm to us that the activity seen in the first compound was real, it established the molecular requirements for further screening and compound optimization. *N*-aminoacyl salicylic acids seemed to be the key functionality required for PD1/PD-L2 stabilization.

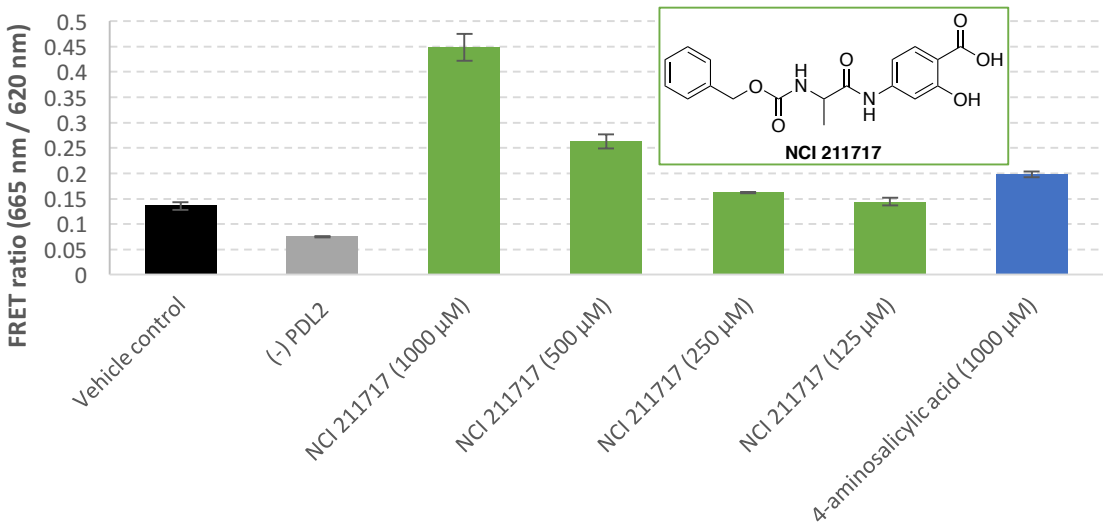


**Figure 28: Dose-dependent response of the non-electrophilic salicylate NCI 211717 in PD1/PD-L2 TR-FRET assay.**

### 2.4.3 Synthesis and screening of salicylate derivatives

We procured a number of substituted salicylate compounds, and found all of them to be apparent agonists, though varying in potency (see Table 4 for details). Analogous compounds from the NCI were tested in order to determine whether substitution at the amino acid could increase potency. However, the Cbz-protected alanine derivative remained the best agonist, and there was no immediately obvious pattern to the activity.

**Table 4: Enhancement of FRET ratio over vehicle control by salicylic acid derivatives.**

| Compound | Fold change | Compound | Fold change |
|---|---|---|---|
| 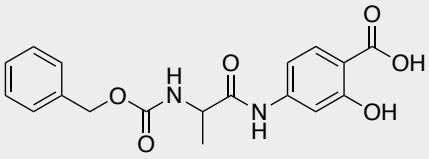 **NCI 211717** | 8X | 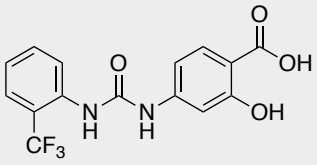 **NCI 216137** | 2.5X |
| 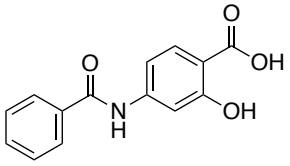 **RH2.45** | 7X | 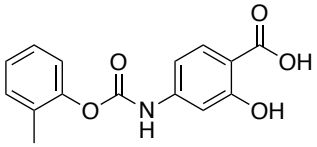 **NCI 161061** | 2X |
| 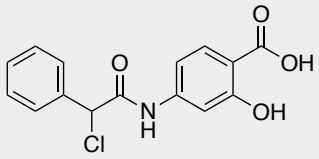 **NCI 59402** | 4X | 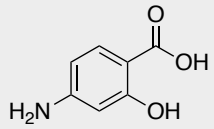 **4-aminosalicylic acid** | 2X |
| 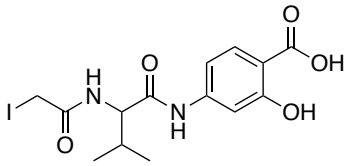 **NCI 211845** | 3X | 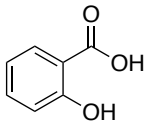 **Salicylic acid** | 1.8X |
| 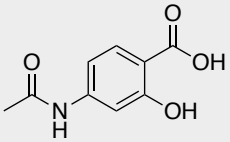 **RH2.44** | 3X | 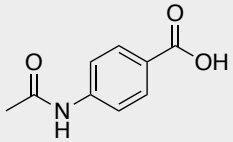 **RH2.46** | *No change* |

In order to determine the minimal pharmacophore for PD1/PD-L2 agonism, we truncated the lead compound to the smallest possible fragments: acetamidosalicylic acid, aminosalicylic acid, salicylic acid itself, and acetamidobenzoic acid. If adding more functional groups had not added potency, we hypothesized that removing functional groups would allow us to determine which substitutions had the greatest effect on compound activity. Simple amides of aminosalicylic acid were synthesized, and we found that while

the N-benzoyl derivative **RH2.45** had activity nearly equal to that of NCI 211717, even N-acetyl aminosalicylic acid **RH2.44**, aminosalicylic acid, and salicylic acid itself enhanced the FRET ratio by 2- to 3-fold. However, removing the phenolic hydroxyl group of N-acetyl aminosalicylic acid resulted in a compound with no detectable activity whatsoever (**RH2.46**).

### 2.4.4 PAINs and suffering: suspicion, confirmation, and mechanism of TR-FRET interference by salicylates

The failure of acetamidobenzoic acid **RH2.46** to elicit any response in the TR-FRET assay could have been rationalized as part of the structure-activity profile, but our suspicions were aroused by the results of our truncation screen. It seemed unlikely that a molecule as small and unfunctionalized as salicylic acid could appreciably influence the PD1/PD-L2 interaction. Moreover, while one could argue that removal of the phenol might eliminate binding to some part of the protein (see the main text and supporting information from the paper by the Holak group[97]), we saw it as a change from a chelating group to a non-chelating group. One of the many mechanisms of assay interference is metal binding – we questioned whether that might be the case here, in an assay built around the fluorescent properties of a bound metal.

While some false positives are due to random error, there are whole families of compounds that can reproducibly show activity in an assay, without interacting with the biological targets in any meaningful way. These compounds are not usually amenable to development

into useful chemical probes or drugs, and have earned the derogatory moniker of pan-assay interference compounds (PAINs)[281].

There are many subtypes of assay interference compounds, and they can interact nonspecifically or promiscuously with the biomolecules under study or they can interact with the assay components. The mechanisms of assay interference vary wildly. Compounds containing highly electrophilic groups like Michael acceptors or iodoacetamides can alkylate protein cysteine residues non-selectively, leading to apparent tight binding[300]. Tertiary amines can quench the singlet oxygen generated in AlphaScreen experiments, leading to the appearance of binding inhibition[301]. Other families of compounds do not have a chemical mechanism of assay interference, but are known for their strong and promiscuous protein binding; optimizing these scaffolds into a tight binder with a defined binding site is often a lost cause[302].

However, the results we had obtained thus far did not indicate that a classical PAINs mechanism was at play. The spectra obtained alongside the FRET ratios were well in line with the vehicle control wells, in terms of peak shape, position, and intensity. While it seemed that the majority of the change in FRET ratio seemed to be coming from diminished donor emission, variation in 620 nm emission was not uncommon, so it was difficult to compare across samples. Moreover, the signal enhancement was robust in the presence of detergent (Tween-20), and different salicylates enhanced the FRET signal by vastly different degrees, suggesting structure-dependent activity.

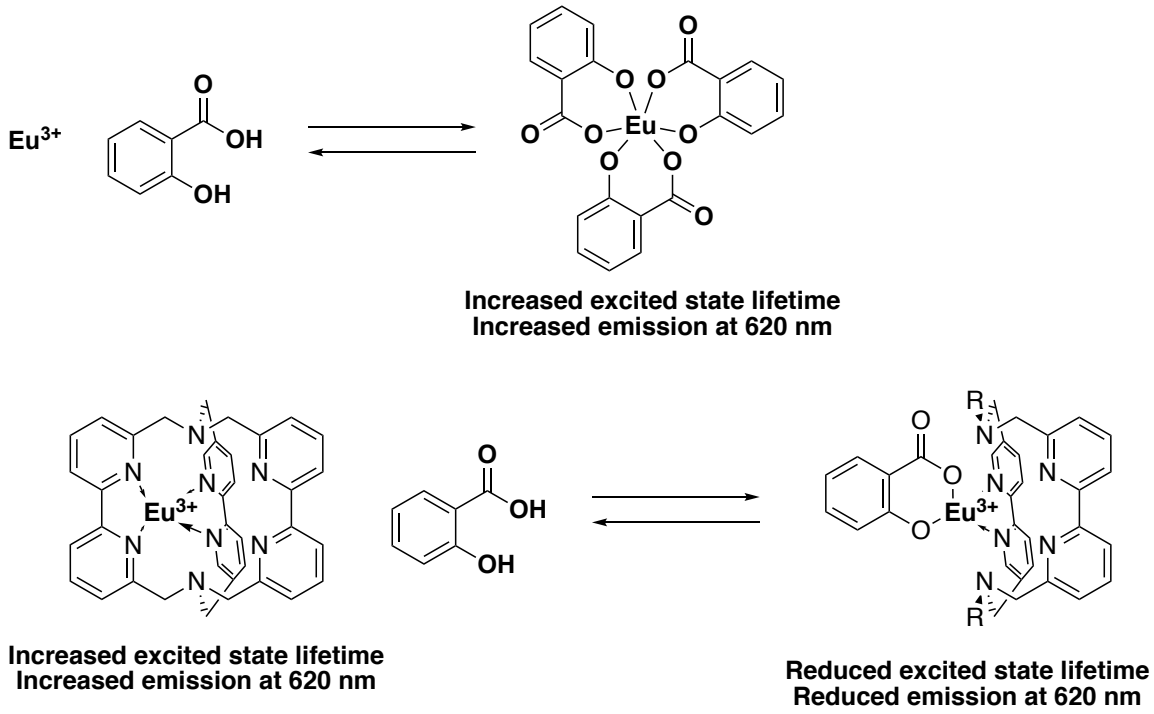


**Figure 29: Formation of europium-salicylate complexes as described in the literature, and proposed mechanism of FRET interference. Unconjugated Lumi4 cryptand is shown for illustrative purposes.**

A search of the literature allowed us to rationalize the suspicious SAR of the salicylates with their seemingly innocuous assay readouts. We found that salicylic acid is a *known ligand* for free europium chloride, and that salicylic acid is capable of binding to $Eu^{3+}$ in neat water[303-304]. Moreover, the formation of europium-salicylate chelates does not change the wavelength of any of the europium excitation or emission peaks, but specifically increases both the lifetime and the intensity of emission at 620 nm *only*[303-304]. These features would be indistinguishable from a change in FRET signal, even with examination of the emission spectrum.

The observations above have one small problem: an increase in 620 nm emission would lead to *decreased* FRET ratios, but we observed the opposite. While the addition of salicylates to "naked" europium increases their lifetime and emission, we hypothesized that the cryptands used in TR-FRET applications would be designed to optimize the emission properties of the lanthanide. Changing from a highly protected cryptand to a simple salicylate would therefore decrease the effective emission, and thus increase the FRET ratio.

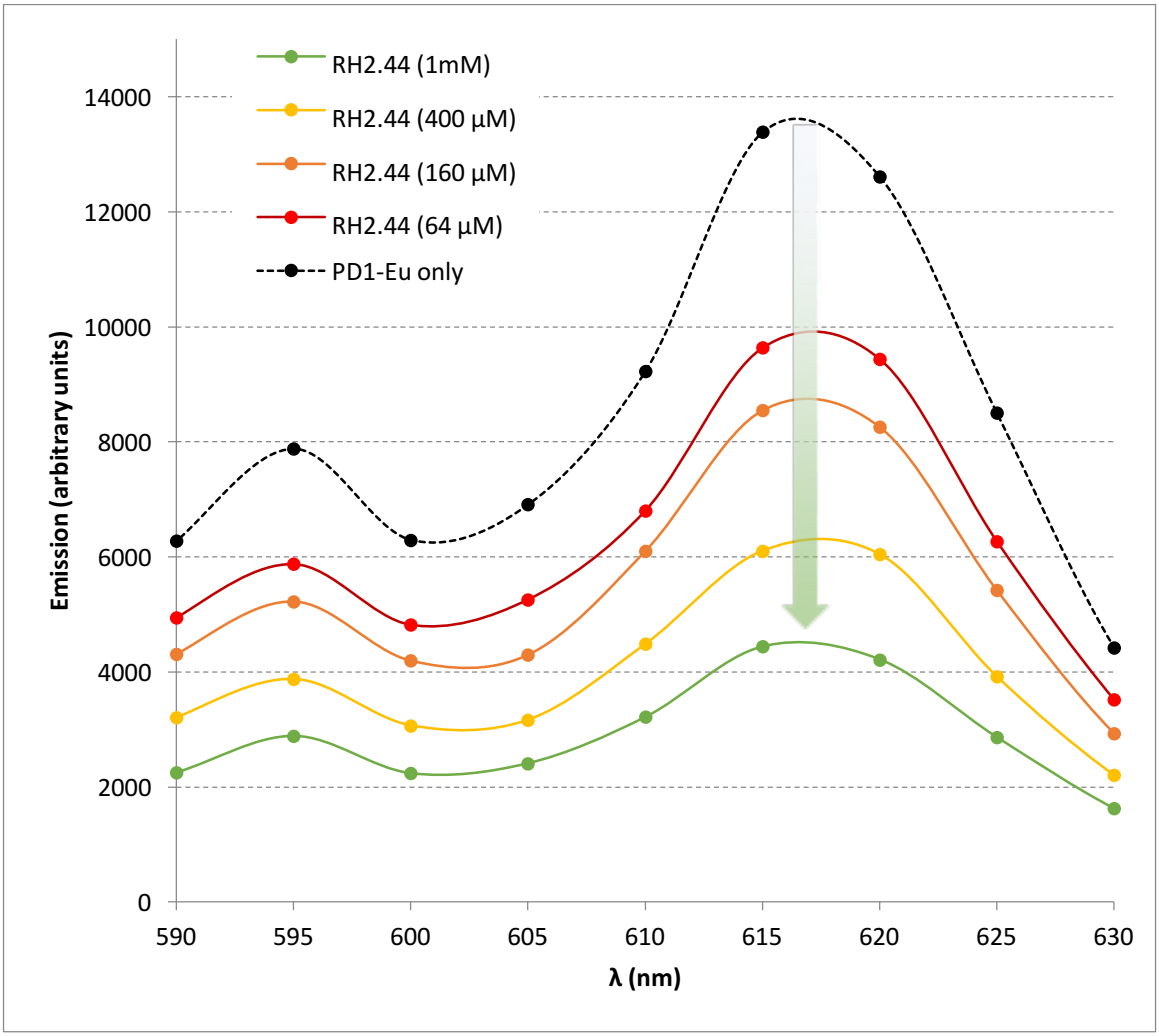


**Figure 30: Emission spectra of PD1-Eu complex with increasing concentrations of acetamidosalicylic acid RH2.44.**

We were sceptical that a weak, bidentate ligand like salicylic acid could displace the larger, multivalent chelating cryptands used in the assay kit (structure unknown). We therefore titrated increasing concentrations of acetamidosalicylic acid **RH2.44** into a solution of the PD1-Eu complex, and observed a dose-dependent decrease in lanthanide emission (see Figure 30). This provided an impetus to investigate the salicylate-europium interference more closely.

We confirmed our hypothesis that salicylate compounds were interfering with our TR-FRET assay by chelation of the europium FRET donor by running a counter-screen. If the salicylates were indeed binding to the protein, then an assay run without PD-L2 should have the same result as the vehicle control, as there is no affinity binding to bring the FRET donor and acceptor into proximity. In the event, however, we found that even without PD-L2 present, the salicylate compounds all increased the FRET ratio significantly, and that this increase was proportional to the increase seen in the PD-L2-containing experiment (see Figure 31). These results proved unequivocally that the salicylates were interfering with the assay readout.

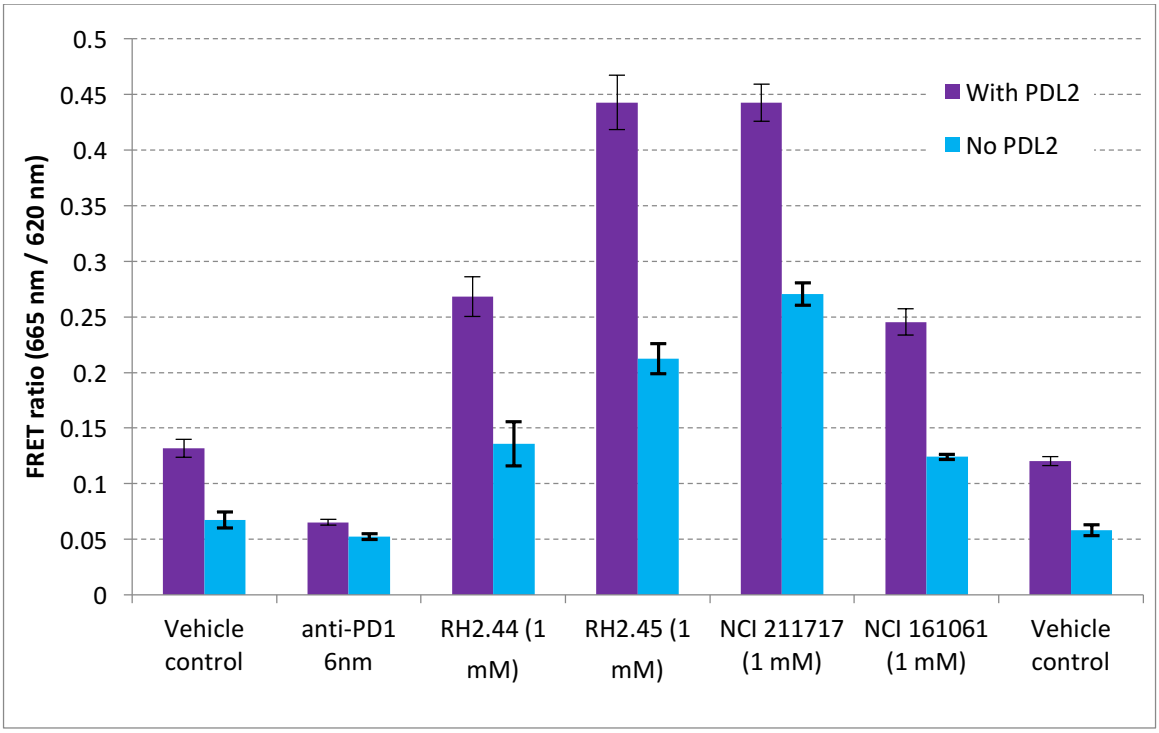


**Figure 31: Counter-screen for TR-FRET interference by salicylates. The "No PD-L2" conditions should all be identical, as there is no interaction to stabilize.**

Chelation of europium FRET donors by salicylates therefore seems to decrease only the single fluorescence emission peak at 620 nm without shifting the peak position. This change in the emissive properties of the lanthanide results in an artificially inflated FRET ratio due to the decrease in the denominator.

We observed this effect for a single TR-FRET assay kit using a europium chelate, but we expect that this interference may be operative in other assays using different chelates and different lanthanides. The biology of the assay system is irrelevant when it comes to assay interference; the assay components are the true targets. While we cannot make any predictions about how this interference may affect other chelating groups, it is worth nothing that the enhancement of terbium luminescence by salicylic acid forms the basis for many analytical techniques like DELFIA, salicylate quantification, and terbium quantification. It is therefore likely that terbium would be equally susceptible to salicylate coordination (and artificial signal enhancement) in a TR-FRET setting as well.

The discovery that salicylates can interfere with TR-FRET measurements is an important contribution to the scientific literature. Compound screening is increasingly performed by academic groups that may not have institutional knowledge of frequent hitters and assay interference compounds[305-306], and with that comes a slowly growing awareness that test compounds are not always as innocuous as they may seem. While many mechanisms of assay interference may be intuitive to chemists (Michael acceptors can react with thiols; quinones can act as oxidizing agents), many are not; this mechanism certainly wasn't

obvious to us. Given how well-represented salicylates are in screening libraries (the ChEMBL database of bioactive druglike molecules contains over 2100 salicylic acids, or 0.1% of all the compounds in the database[307]; the ZINC database contains over 4200 salicylic acids[275]), they are very likely to be included in HTS campaigns. Moreover, they are familiar and comforting structures to any chemist who has ever taken an aspirin, and might be accepted as bioactive lead compounds without serious scrutiny. To find out later that they interfere with a widely used screening assay that is lauded for its resistance to interference would be a bitter pill to swallow indeed.

## 2.5 Surface plasmon resonance – getting to the (Bia)core of the matter

Over the course of our studies, we used three different assays to evaluate the compounds in our collection for PD1/PD-L1 binding or inhibition; all three assays suffered from fairly extensive assay interference or instability. The thermal shift assay was prone to fluorescence quenching as well as aggregation with the test compounds. The ELISA assay suffered from extreme unreliability, apparently the result of plate manufacturing defects. The TR-FRET assay was revealed to be vulnerable to chelating agents like salicylates. The main problems were therefore the inability to characterize binding surfaces rigorously, and the fact that optical measurements were being taken from the test solution itself.

We finally turned to surface plasmon resonance (SPR) when a Biacore instrument became available; SPR is insensitive to sample absorbance, fluorescence, quenching, turbidity, chelation, aggregation, and most other mechanisms of assay interference. Surface plasmon

resonance is the phenomenon that light reflecting off a metallic surface (often gold) at a specific angle can induce an evanescent electromagnetic wave to travel along the metal surface (surface plasmon). The energy absorbed to induce this wave decreases the intensity of the reflected light. The reflection minimum is therefore the angle at which there is maximal surface plasmon resonance. This angle is dependent on the refractive index on *both* sides of the gold surface[308-309].

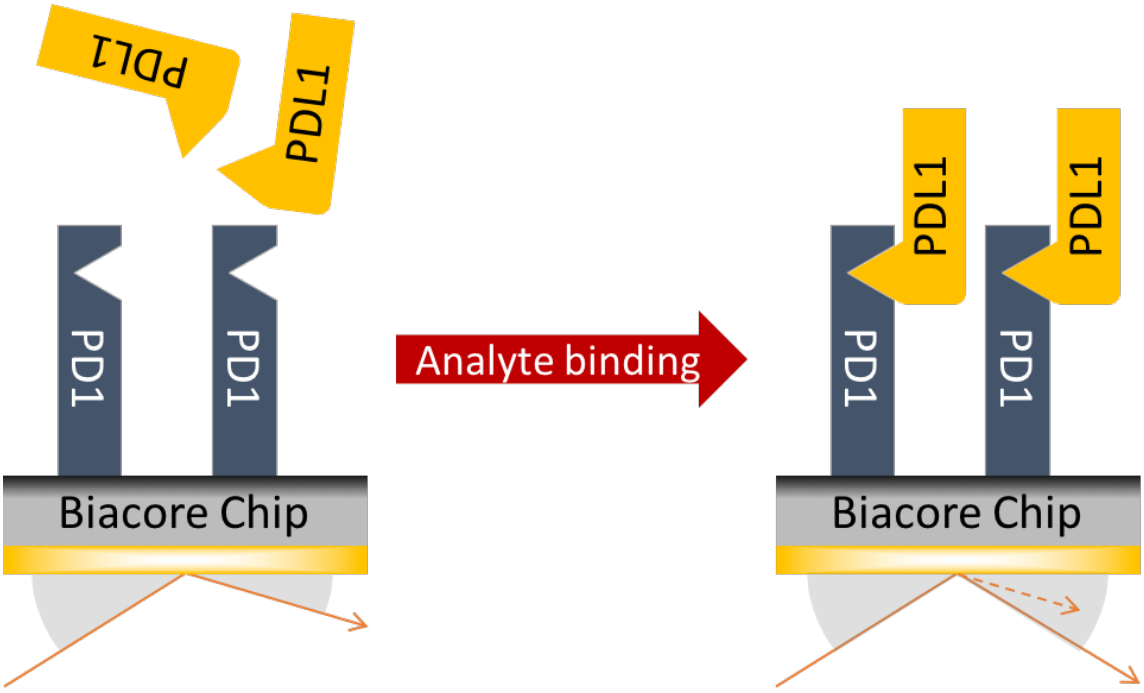


**Figure 32: Schematic of a Biacore assay. Note the measurable change in SPR angle upon ligand binding.**

In a Biacore instrument, one side of a gold sensor chip is coated with the biomolecule of interest, either by biotin capture, amide formation, or some other method. The other side of the sensor chip is fixed to a prism and optical sensor. When an analyte binds to the

immobilized biomolecule on *one side* of the sensor chip, this increase in bound mass (and therefore refractive index) is reflected in a change in SPR angle on the *other side* of the sensor chip. This change in angle can be measured either as a change in the position of the reflection intensity minimum or as a change in reflection intensity at a fixed angle. In this way, binding events can be detected without actually measuring any light going into or coming out of the test solution – the biology occurs on one face of the chip, and the measurement is isolated to the other side of the chip.

Moreover, because the Biacore system uses an integrated flow cell system, all immobilization, sample application, and washing steps are both automated and easily monitored, which limits the influence of the user's technique or defects in the materials. The sensor chips are standardized, and the degree of immobilization can be quantified exactly in the same way that binding interactions are – in contrast to the adsorption step of an ELISA. Moreover, application of the sample to the sensor chip is precisely controlled by microfluidics, meaning that "washing" steps are reproducible and automated. The tight control of sample injection and continuous monitoring of binding also means that kinetic parameters for the interaction can be extracted. In short, surface plasmon resonance takes many of the idiosyncrasies out of biophysical assays.

We therefore validated all previous "hits" for PD1/PD-L1 agonism or inhibition using SPR, with PD1 immobilized on the sensor chip and PD-L1 as the soluble analyte. Biotinylated PD1 was purchased from BPS Bioscience, and was identical to the PD1 used in the ELISA and TR-FRET assays. This was irreversibly immobilized onto a streptavidin-coated sensor

chip. The PD-L1 used was also from BPS Bioscience, as we attempted to replicate the conditions from our previous assays as much as possible.

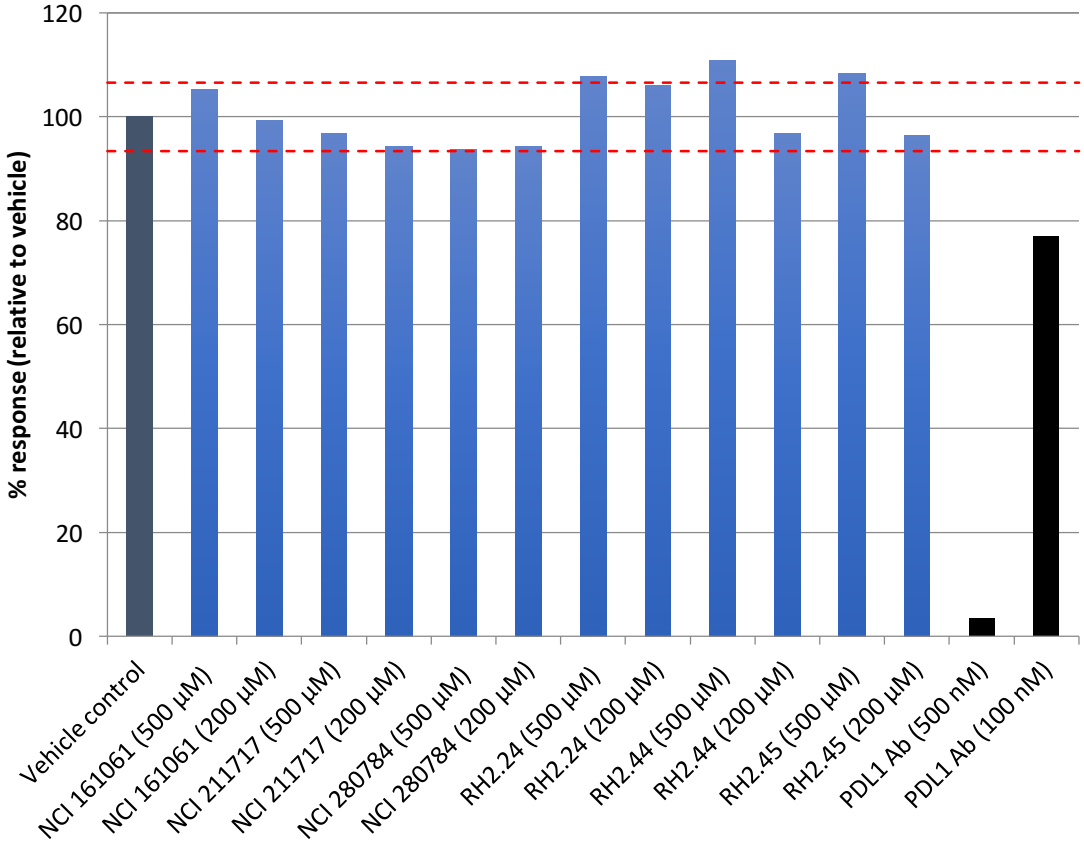


**Figure 33: Biacore measurement of PD1/PD-L1 inhibition by tryptophan compounds and salicylates. No inhibition is apparent. The red dashed line indicates the standard deviation of the vehicle control runs.**

Our results from the Biacore experiment showed that every single compound that had been proposed to affect the PD1/PD-L1 interaction was unable to do so (see Figure 33). Binding of PD-L1 to the sensor chip was unambiguous and highly reproducible. Samples where compounds had been added to the PD-L1 solution were indistinguishable from the vehicle

control, within a small degree of error. In an assay that is insensitive to interference, their true identities as PAINs were unmasked. It seems that finding a PD1/PD-L1 inhibitor in our screening deck just wasn't in the cards for us.

# Chapter 3

This chapter describes the characterization of a series of small molecule PD1/PD-L1 inhibitors disclosed by Bristol-Myers Squibb. A manuscript is currently in preparation based on these results.

The initial syntheses of compounds BMS-1, BMS-2, and BMS-3 were carried out by Dr. David Powell, a research scientist at the pharmaceutical company Inception Sciences. These stocks were used for preliminary ELISA, TR-FRET, Biacore, and NMR experiments. The re-synthesis of compounds BMS-2 and BMS-3 were done by the author with some assistance from Shanti Horvath (see Chapter 2), and these stocks were used in most of the Biacore, gel filtration, NMR, and cellular assays (BMS-1 had the most complex NMR spectrum and was the least active of the series, and was therefore not used in follow-up experiments). All analogue synthesis was carried out by the author, with some assistance on the phthalimide-bearing substrates from Max Thompson, an undergraduate student in the Wulff group at the University of Victoria.

The TR-FRET experiments were primarily performed by Shanti Horvath, and the data analyzed jointly by Shanti Horvath, Dr. Jeremy Wulff, and the author. Biacore experiments were performed by the author, with some assistance from Jaylene Sandhu, an undergraduate student in the Wulff group at the University of Victoria. ELISA and dendritic cell assays were performed by Dr. Davorka Messmer, a staff scientist at Inception Sciences. Protein production, circular dichroism, all protein NMR, and gel filtration were

performed by Kayleigh Walker, a graduate student, and analyzed by Kayleigh Walker and Dr. Mark Carr, a faculty member, at the University of Leicester.

## 3.1 Disclosure of small molecule inhibitors

In March of 2015, the pharmaceutical company Bristol-Myers Squibb filed a patent claiming a series of non-peptidic small molecules that inhibited the interaction of PD1 with PD-L1[243]. These compounds, whose core structure is shown in Figure 34, constitute the first non-peptidic, non-peptidomimetic small molecules to directly inhibit the PD1/PD-L1 interaction.

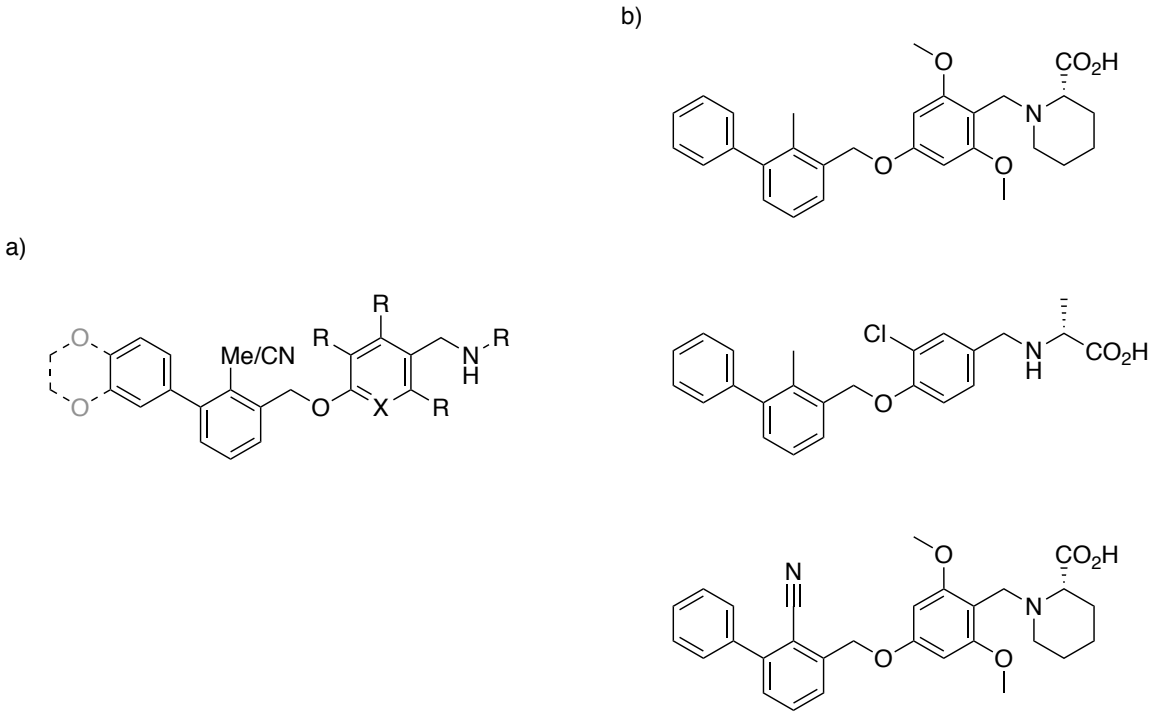


**Figure 34: Structures claimed by Bristol-Myers Squibb in a 2015 patent. a) General formula for PD1/PD-L1 inhibitors claimed by Bristol-Myers Squibb. b) Example compounds claimed, demonstrating the basic chemotype.**

Despite containing numerous example compounds and ample synthetic details for their preparation, the patent's characterization of these small molecules was scant. The patent describes the use of only a single assay—a TR-FRET assay similar to the one described in Chapter 2—as the basis for their evaluation of compound activity. Moreover, no structural details are given as to the binding site or mechanism of action of the compounds. Even the identity of the protein binding—PD1 or PD-L1—is left unaddressed.

Due to the dearth of validated small molecule inhibitors for this pathway, and coloured by our own experiences with assay interference (see Chapter 2), we were skeptical about the validity of the patent claims. The patent describes a single assay, with no indication that a counter-screen has been conducted to weed out assay interference compounds. Furthermore, while the assay was conducted in the presence of a mild surfactant, there is still the possibility that the compounds could aggregate and act in a nonspecific manner. No data was provided about their activity against PD1/PD-L2 or PD-L1/CD80, despite the inclusion of assays for such in the patent description. The compound structures, while containing no obvious electrophilic centres or coordinating groups, are relatively hydrophobic, containing multiple aromatic rings in series. While aggregation cannot be predicted with absolute certainty, the majority of compounds that aggregate are fairly hydrophobic ($\log P > 3$)[282].

If, however, the claims in the patent proved true, this series of molecules could serve as a useful guide for the validation of our own screening studies. While anti-PD1 and anti-PD-L1 blocking antibodies can be very useful positive controls for absolute inhibition of the

PD1/PD-L1 interaction, they do not indicate how small organic molecules will behave in any given assay system. Furthermore, available antibodies generally have very high affinity for their protein targets. Optimization using these agents may lead to binding assays that lack the dynamic range to detect weak inhibitors with different binding kinetic profiles.

Moreover, the ability of these molecules to inhibit the PD1/PD-L1 interaction despite their simple structures and low molecular weight could offer clues as to the most effective strategy to approach our own inhibitor design studies. Existing antibody and peptide inhibitors of the interaction primarily target the binding face of either PD1 or PD-L1, which is believed to be too large and flat to accommodate a small molecule inhibitor (*vide infra*). Mutational and structural analysis of PD-L1 has led to the identification of "hot spots" that are particularly important for PD1 binding, but even efforts targeting these sites have not proved fruitful.[97] Our own efforts at targeting the PD-L1 hinge region notwithstanding, there are no known allosteric binding sites on either PD1 or PD-L1. Any insights that could be gleaned from the mechanism of action of these compounds, regardless of their druglikeness or physicochemical properties, would be beneficial.

With these goals in mind, we chose to bring these molecules into our own lab to validate whether they indeed inhibit the PD1/PD-L1 interaction and to investigate their mode of binding.

## 3.2 Synthesis and preliminary characterization of BMS-X inhibitors

### 3.2.1 Choice of compounds and procurement

The original filing by Bristol-Myers Squibb contained over 300 compounds, with their potencies unhelpfully binned into three ranges. An effort was made to choose varied examples of the most potent compounds from the list, that would nevertheless be straightforward to synthesize. The basic chemotype is an aryl biarylbenzyl ether, functionalized at the para position of the C ring with various polar benzylamine sidechains.

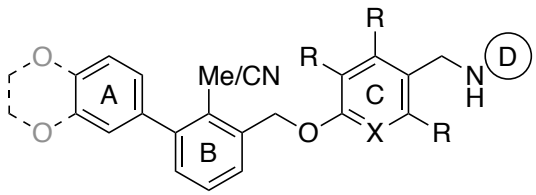


**Figure 35: General formula of BMS compounds and ring system nomenclature.**

The three comounds that were chosen had the same A, B, and C rings, enabling divergent synthesis of all three from a single precursor. Moreover, C ring of these analogues is C2 symmetric and contains strongly electron-donating methoxy groups, which simplifies the NMR and makes the C ring aromatic protons distinct from the rest of the molecule. The amine sidechains were chosen to maximize polarity (and therefore water solubility), and to be commercially available or easily prepared. The first synthesis of the three BMS compounds was carried out by David Powell at Inception Sciences, following the exact procedures outlined in the patent[243]. These initial syntheses produced approximately 10 mg of each compound—arbitrarily labelled BMS-1, BMS-2, and BMS-3—for testing. This proved to be an inadequate amount of compound for all the necessary experiments.

Moreover, impurities were later found in the BMS-2 thusly produced. Where necessary, the batch used will be indicated.

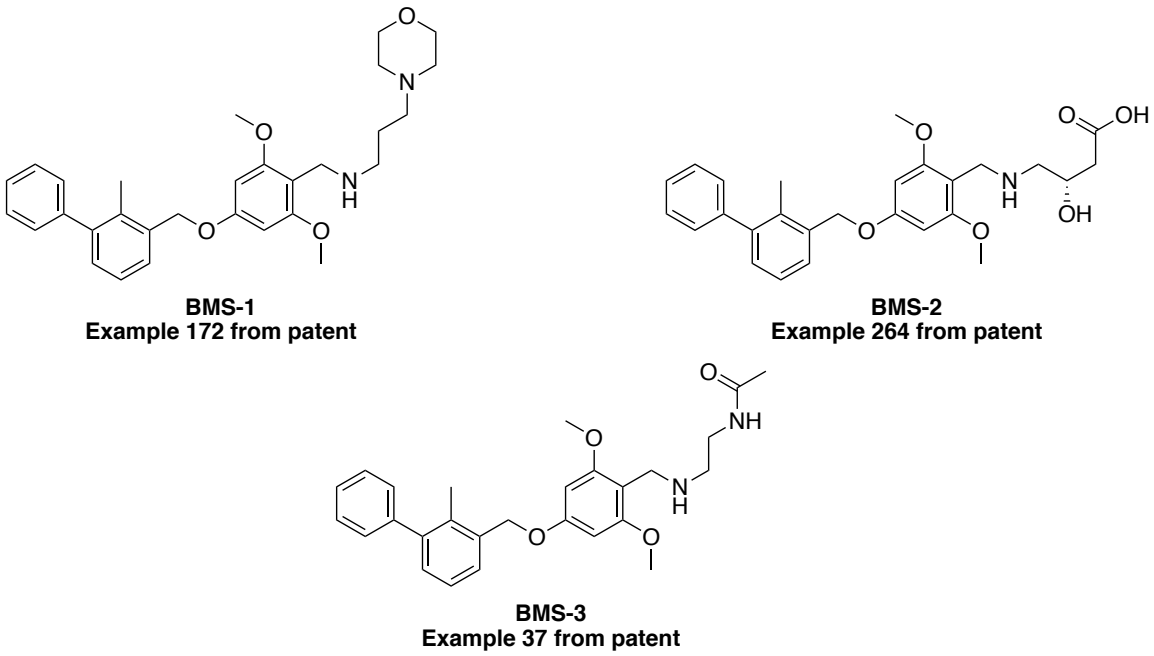


**Figure 36: Example compounds chosen from patent for in-house evaluation.**

BMS-2 and BMS-3 were later prepared at the University of Victoria by a modified route, summarized in Scheme 9. This route was optimized to require minimal chromatographic purification, as well as to promote speed, modularity, and the use of inexpensive reagents (palladium acetate vs. palladium phosphine complexes, $PBr_3$ vs. DEAD).

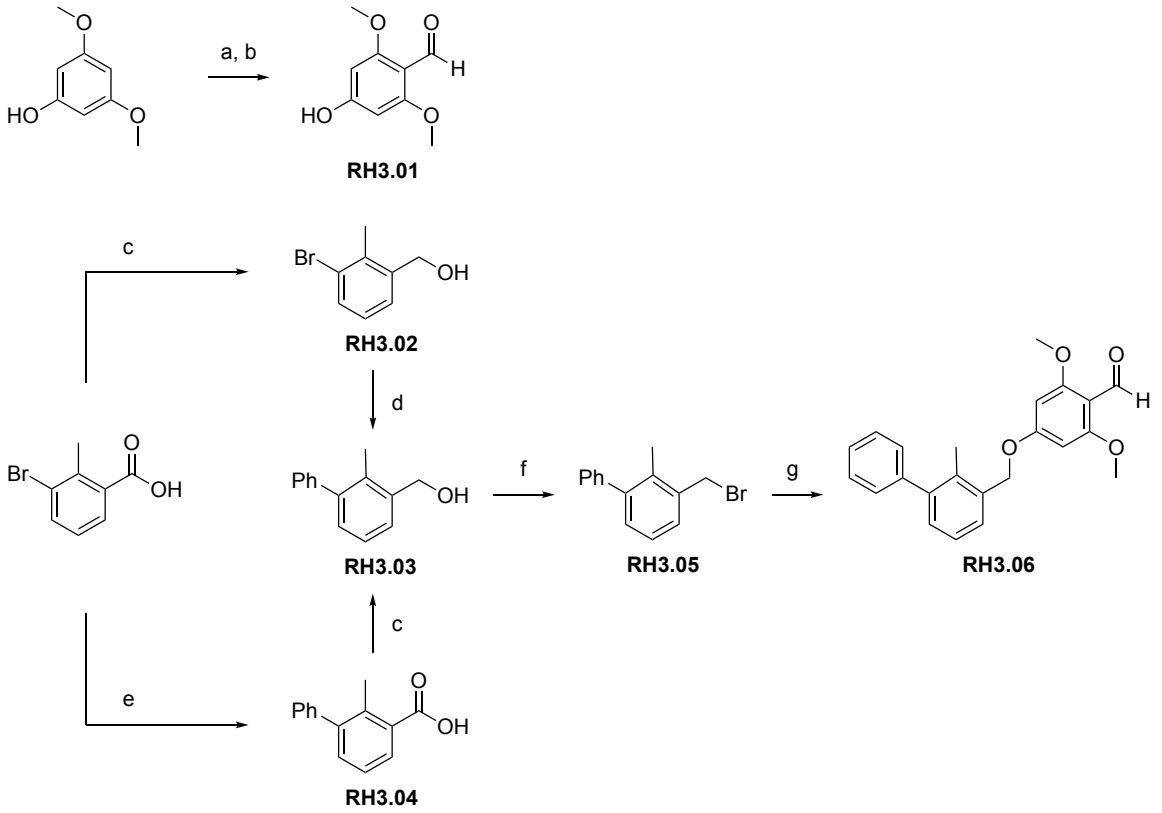


**Scheme 9: Synthesis of BMS precursor aldehyde. a) TIPS-Cl, imidazole, quantitative. b) (i) *n*BuLi (ii) DMF (iii) HCl/EtOH, 47-71%. c) $PhB(OH)_2$, $K_2CO_3$, $Pd(OAc)_2$, $H_2O$ 150 ˚C µW, 88-93%. d) $BH_3$•$Me_2S$, 79-86%. e) $PhB(OH)_2$, $K_2CO_3$, $Bu_4NBr$, $Pd(OAc)_2$, $H_2O$ 150 ˚C µW, 90-95% f) $PBr_3$, 78%. g) RH3.01, $Cs_2CO_3$, DMF, 63-88%.**

Briefly, the commercially available precursor 3-bromo-2-methylbenzoic acid was coupled with phenylboronic acid *via* microwave-assisted Suzuki reaction, then reduced to the benzylic alcohol **RH3.03** by $BH_3$•$Me_2S$ in THF. In the patent, the acid is reduced first, and the Suzuki is performed using expensive precatalysts like $Pd(dppf)Cl_2$ and 2nd generation XPhos precatalyst, necessitating both rigorous degassing before the reaction and HPLC purification afterwards. The microwave-assisted aqueous synthesis we adapted[310] is fast (10 minutes), does not require any degassing, and uses cheap palladium (II) acetate without

additional ligands – the only organic material should therefore be the product. We first followed the same order of reactions as the patent, where the acid is reduced first and the benzyl alcohol is used in the Suzuki. However, the relative insolubility of **RH3.02** in water necessitated the use of stoichiometric phase-transfer catalyst as well as careful presolubilization for efficient Suzuki coupling. Inadequate presolubilization led to diminished conversion as well as the production of unidentified byproducts that complicated purification. Conversely, the carboxylic acid **RH3.04** dissolves easily in the basic aqueous medium without the need for phase transfer catalyst, leading to efficient coupling, no detectable byproducts, and easy isolation by acidification of the reaction medium and filtration. This crude product is contaminated by traces of palladium, but the subsequent reaction with borane reduces these to insoluble palladium black, which is easily filtered out, providing compound **RH3.03** as a clean white powder.

The aldehyde **RH3.06** was prepared by conversion of compound **RH3.02** to the benzyl bromide **RH3.05**, followed by alkylation of the phenolic hydroxyl group of **RH3.01**. In the patent, the alkylation of the phenol is accomplished directly by Mitsunobu reaction. However, we found that separation of the product from triphenylphosphine oxide and DEAD/DIAD hydrazine byproducts was difficult. **RH3.06** coelutes with reduced DEAD on silica gel and is relatively insoluble in mixtures of hexanes/ethyl acetate. We therefore adopted a two-step process in order to avoid organic byproducts that would require chromatographic separation. The conversion of **RH3.03** to the benzyl bromide was easily accomplished using phosphorous tribromide, necessitating no purification beyond an aqueous wash to remove inorganic phosphite salts. The formylated phenol **RH3.01** was

prepared by a known route, whereby 3,5-dimethoxyphenol is subjected to O-protection, directed lithiation, quenching with DMF, and acid-mediated desilylation and imine hydrolysis. Coupling of the formylated phenol with the benzyl bromide proceeded smoothly in the presence of cesium carbonate to provide **RH3.06**, requiring no purification beyond an optional recrystallization.

Compound BMS-3 was prepared by reductive amination of precursor **RH3.06** with *N*-acetylethylenediamine **RH3.07**, itself synthesized by the slow reaction of excess ethylenediamine with ethyl acetate in methanol. The free amine compound is a tractable solid and can be purified by recrystallization.

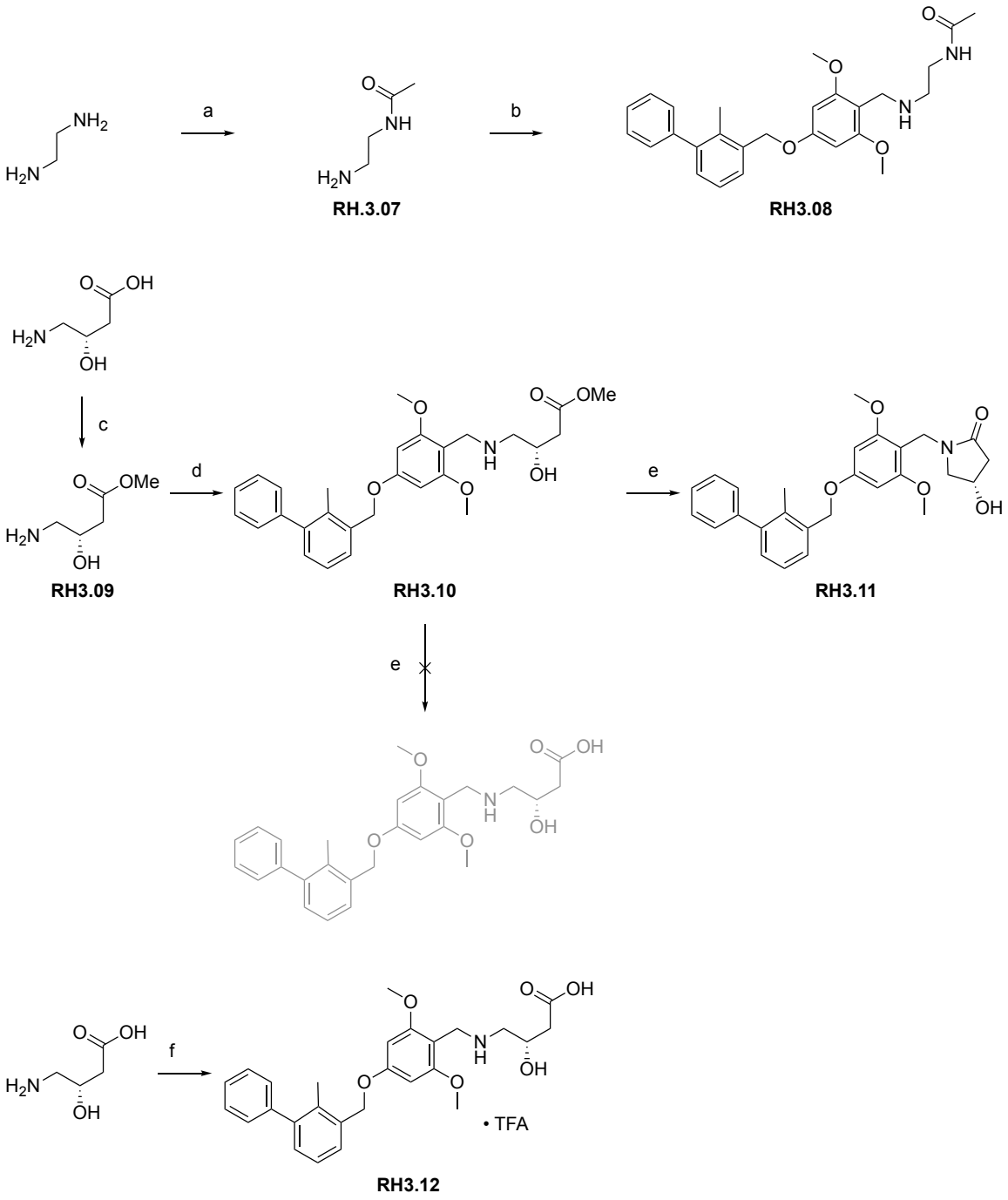


**Scheme 10: Synthesis of BMS analogues at UVic. a) EtOAc, 4 days, 85%. b) RH3.06, $NaBH_4$, 78% c) MeOH, AcCl, quantitative d) RH3.06, $NaBH_3CN$, 45%. e) LiOH, $H_2O$/MeOH, 73%. f) LiOH, RH3.06, $NaBH_4$, 16%.**

The synthesis of BMS-2 was not as smooth, but perhaps more informative. The direct reaction of aldehyde **RH3.06** with unprotected (S)-4-amino-3-hydroxybutyric acid in DMF with sodium cyanoborohydride under acidic conditions as reported in the patent led to low yields of BMS-2, both in the patent and as reported by Inception. Aldehyde **RH3.06** was therefore subjected to reductive amination with the corresponding methyl ester **RH3.09**, which proceeded smoothly in high yield. However, attempted basic hydrolysis of the ester **RH3.10** led to the exclusive formation of lactone **RH3.11**, likely by base-catalyzed intramolecular cyclization. This lactone was later found as an impurity in the material produced by Inception Sciences. The lactamization can presumably occur under neutral conditions in solution. This problem was averted by direct reductive amination of the lithium salt of (S)-4-amino-3-hydroxybutyric acid with **RH3.06**, followed by conversion to the TFA salt and HPLC purification under acidic conditions to negate the nucleophilicity of the benzylic amine.

Despite the chiral centre present in BMS-2/**RH3.12**, its $^{1}$H peaks are relatively sharp and well-dispersed. The same is true of BMS-3/**RH3.08**. However, the spectrum of BMS-1 displayed significant conformational isomerism, making it more complex than anticipated and therefore less attractive for any kind of NMR-based studies.

### 3.2.2 Synthesis of functionalized analogues for chemical biology applications

In addition to the example compounds pulled directly from the patent, we foresaw the need for compounds with reactive handles for chemical biology applications. Specifically,

compounds containing solvent-exposed azide and amine groups would enable conjugation to solid phase for affinity pulldown or direct binding experiments, fluorophore attachment for fluorescence polarization assays or cellular imaging, and click chemistry for making protein or polymer conjugates.

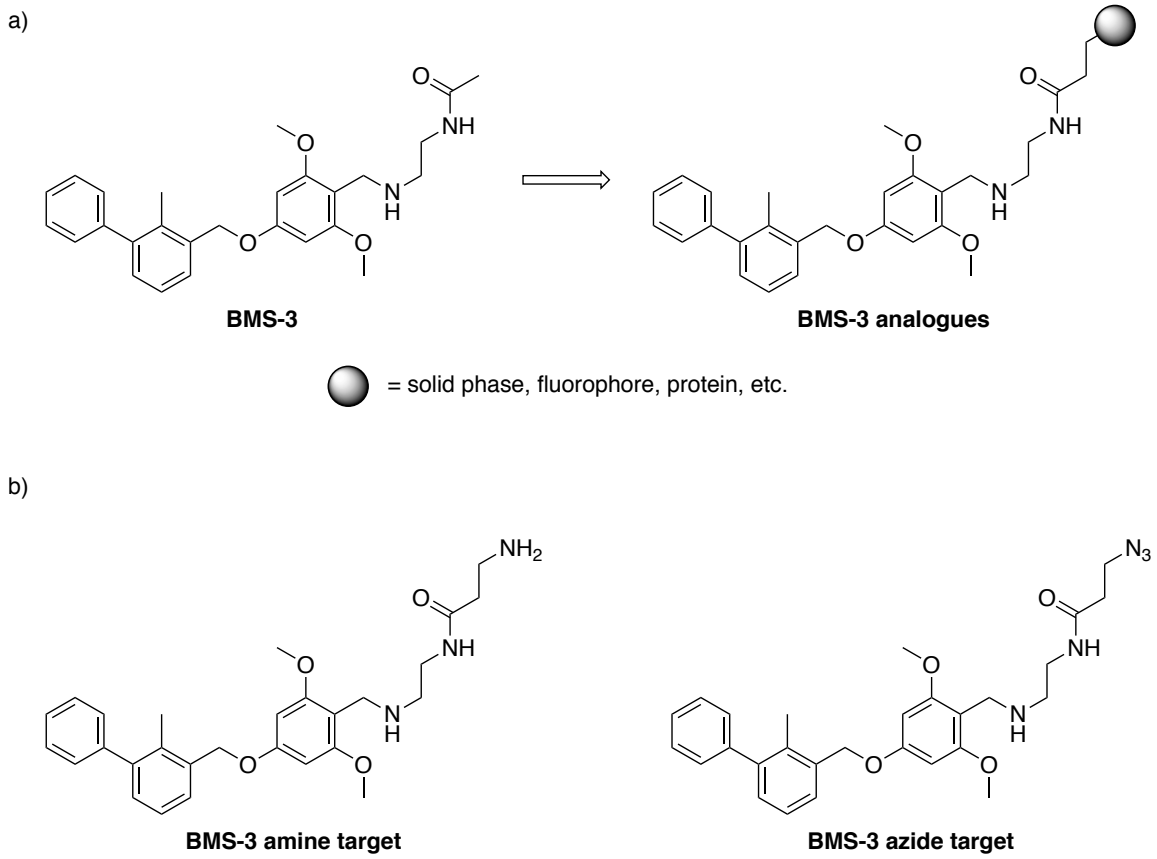


**Figure 37: Chemically reactive analogues of BMS-3 for chemical biology applications. a) Proposed site and length of linker. b) Target molecules with reactive handles.**

Analysis of structure-function data within the BMS patent, validated by the later structural studies (*vide infra*), suggested that the hydrophilic arms of the BMS compounds are solvent-exposed, and should therefore be the sites of conjugation. Using BMS-3 as a

model, we envisioned that the synthetic handles of interest could be linked to the acetamide of through a short one-carbon linker. This linker would be polar enough to provide comparable water solubility to BMS-3 without extraneous functional groups that would require protection and deprotection. As a control for the specific activity of the compound, we also planned to synthesize an analogue lacking the biphenyl moiety that seems to be required for PD1/PD-L1 inhibition.

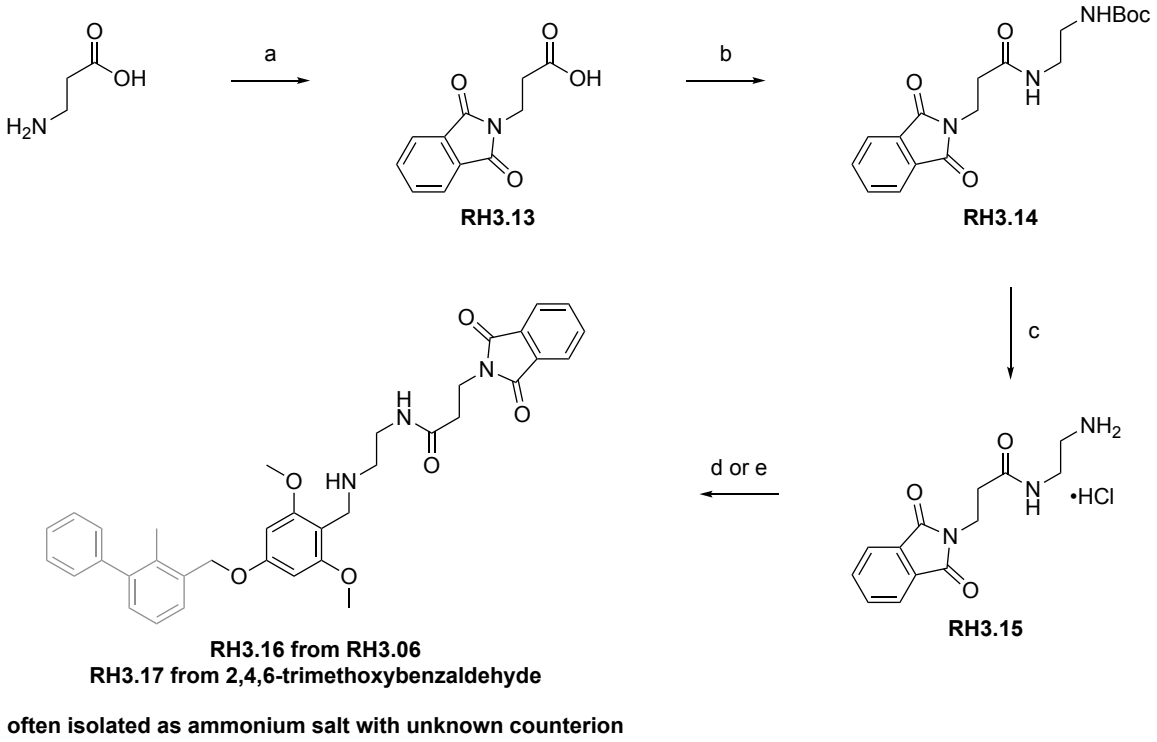


**Scheme 11: Attempted synthesis of functionalized BMS-3 analogues. a) Phthalic anhydride, neat, 175 ˚C, 91%. b) *N*-Boc-ethylenediamine, EDC•HCl, DMAP, 78%. c) MeOH, AcCl, 74-96%. d) RH3.06, $NaBH_3CN$, 38%. e) 2,4,6-trimethoxybenzaldehyde, $NaBH_3CN$, 22%.**

Our initial approach started by protection of ß-alanine with phthalic anhydride, followed by amide coupling with Boc-protected ethylenediamine and acidic deprotection to reveal

one of the terminal amine groups. This compound was then subjected to reductive alkylation with either 2,4,6-trimethoxybenzaldehyde or the universal BMS precursor **RH3.06**. While the conversions of these reactions were high, purification by silica gel chromatography was very difficult and often led to poor yields. The products decomposed within minutes on silica gel, to the point where the $R_f$ of individual spots on the TLC plate shifted based on the order in which the spots were applied. We determined that this streaking was due to the high basicity of the amine, and ammonium salts of the phthalimide-protected amines were often isolated. Addition of triethylamine to the eluent, or chromatography over Florisil (a less acidic solid phase) slightly increased the yields of free amine, but neither was ideal. The ambiguity of the ammonium salt counterion also made determination of yield difficult. The crude reductive amination product was occasionally pure enough to carry on to hydrazinolysis and FITC labeling directly, but this was a poor solution.

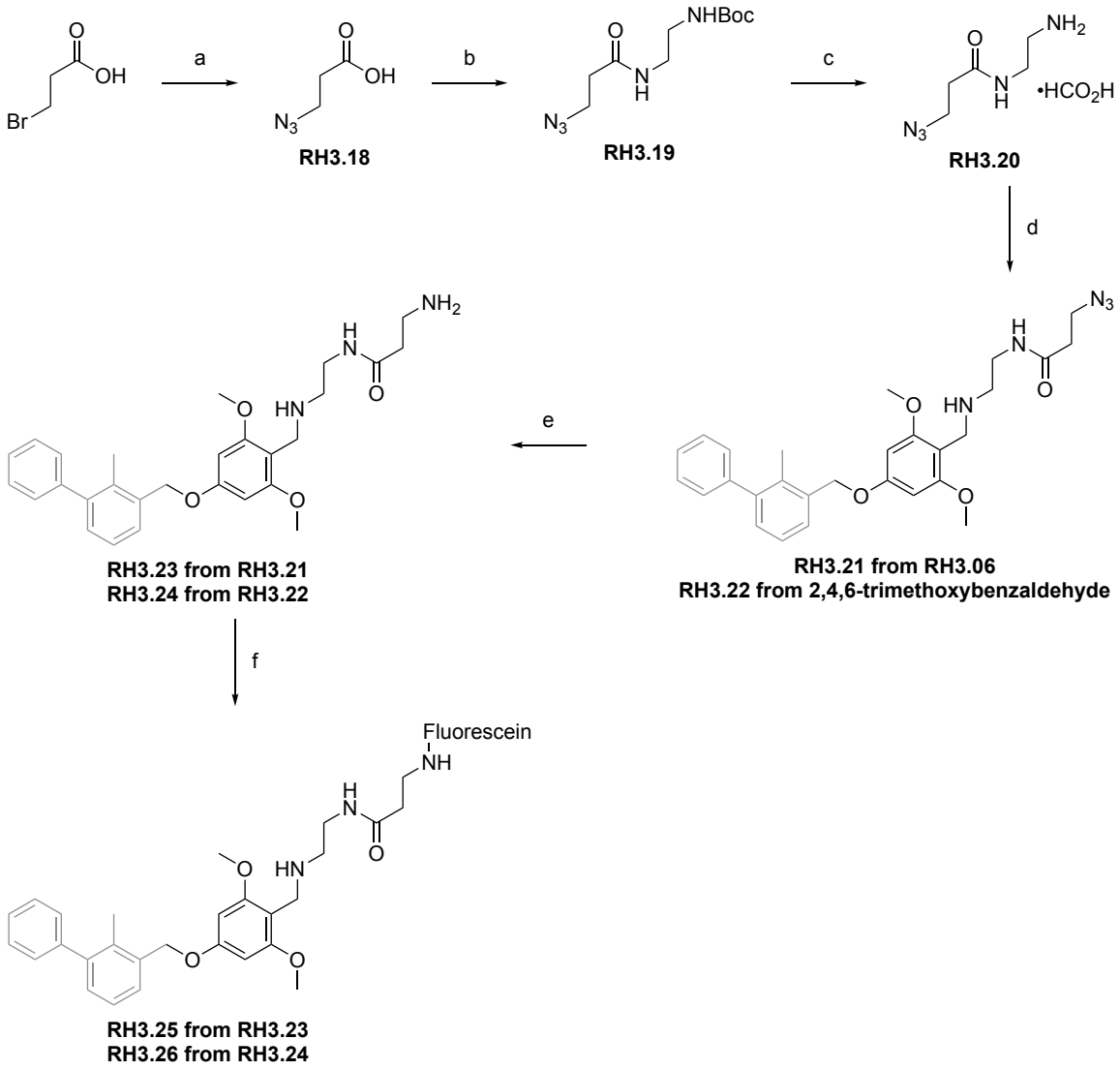


**Scheme 12: Improved synthesis of BMS-3-azide, BMS-3-amine, and BMS-3-FITC. a) $NaN_3$, $NaHCO_3$, $H_2O$, 120 ˚C µW, 74%. b) Boc-ethylenediamine, EDC, DMAP, 47%. c) $HCO_2H$, quantitative. d) RH3.06, $NaBH_3CN$, 64% e) 2,4,6-trimethoxybenzaldehyde, $NaBH_3CN$, 42%. f) $PtO_2$, $H_2$ (1 atm), quantitative. g) FITC, EtOH, $Et_3N$.**

Using an azide as the amine synthon led to more reproducible results and easier handling, while also providing access to "click" chemistry. Nucleophilic substitution of 3-bromopropionic acid with sodium azide in buffered water provided the azidopropionate in

excellent yield, with only trace amounts of elimination. Amide coupling with mono-Boc protected ethylenediamine proceeded smoothly, although deprotection of the Boc group with various acids led in all cases to salts that were oils rather than filterable solids. Nevertheless, the salts underwent facile reductive alkylation with the BMS precursor aldehyde **RH3.06** or 2,4,6-trimethoxybenzaldehyde in good yield, and purification of these intermediates was straightforward and uncomplicated. The azide was then hydrogenated using platinum on carbon to yield the terminal amine after filtration. A fluorescein-tagged inhibitor was synthesized by reaction of this amine-terminated compound with fluorescein isothiocyanate (FITC) in ethanol under basic conditions. We thought we might be able to use this compound in competitive fluorescence polarization assays to test the binding of new compounds, as well as to image compound binding directly on cells. Unfortunately, this analogue was not soluble in aqueous buffers, so these plans were abandoned.

### 3.2.3 Characterization by biophysical methods

The three BMS examples were initially subjected to an ELISA assay for disruption of PD1/PD-L1 binding. This assay, run at Inception Sciences, is virtually identical to that described in Section 0. It is unclear why their assay did not suffer from the reproducibility problems we observed, although they were using different lots of the kit that were presumably produced and shipped at different times. While not as potent as the clinically used antibody pembrolizumab/Keytruda, the compounds nevertheless show good inhibition of the PD1/PD-L1 interaction, with $IC_{50}$s in the mid-nanomolar range (see Figure 38).

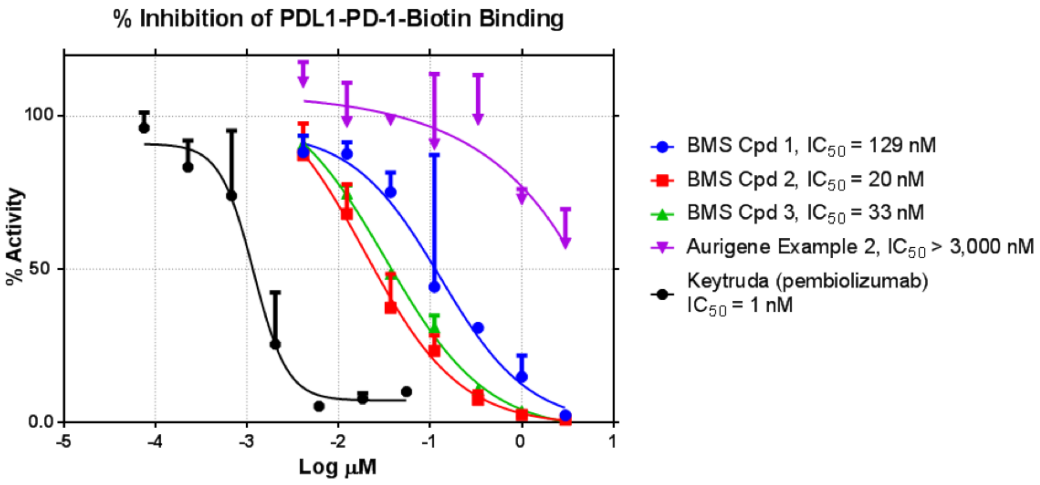


| | BMS Cpd 1 | BMS Cpd 2 | BMS Cpd 3 | Aurigene Example 2 | Keytruda (pembiolizumab) |
|---|---|---|---|---|---|
| IC50 | 0.1288 | 0.01954 | 0.03280 | ~ 94973 | 0.001183 |

**Figure 38: ELISA assay for disruption of PD1/PD-L1 binding. PD-L1 is adsorbed onto a 96-well plate; PD1-biotin is added as a soluble binding partner, followed by Streptavidin-HRP. Binding is measured using the chemiluminescent output of HRP enzyme activity.**

We confirmed Inception's observed inhibitory effects of the BMS series on the PD1/PD-L1 interaction using an orthogonal assay: surface plasmon resonance (SPR). With PD1 immobilized onto a streptavidin-coated Biacore chip, flow-through of soluble PD-L1 resulted in a signal attributable to the protein–protein interaction. Addition of BMS compounds to the PD-L1 analyte led to a measurable and dose-dependent decrease in binding (see Figure 39 and Table 5). Strangely, the degree of inhibition decreased with decreasing protein concentration, with no detectable inhibition at 100 nM PD-L1. This is in marked contrast to the antibody control, which naturally inhibited the signal more at lower protein concentrations (assuming very tight bivalent binding, the $IC_{50}$ should equal [PD-L1]/4).

Later experiments covering wider concentration ranges gave sigmoidal dose-response curves with 50% inhibition ($IC_{50}$) at roughly half the concentration of PD-L1, indicating tight binding. However, an assay run at 360 nM PD-L1 resulted in a calculated IC50 of 7 µM – weaker than the higher-protein $IC_{50}$s. We speculated that PD-L1 inhibition might be concentration-dependent, possibly as a result of dimer or oligomer formation.

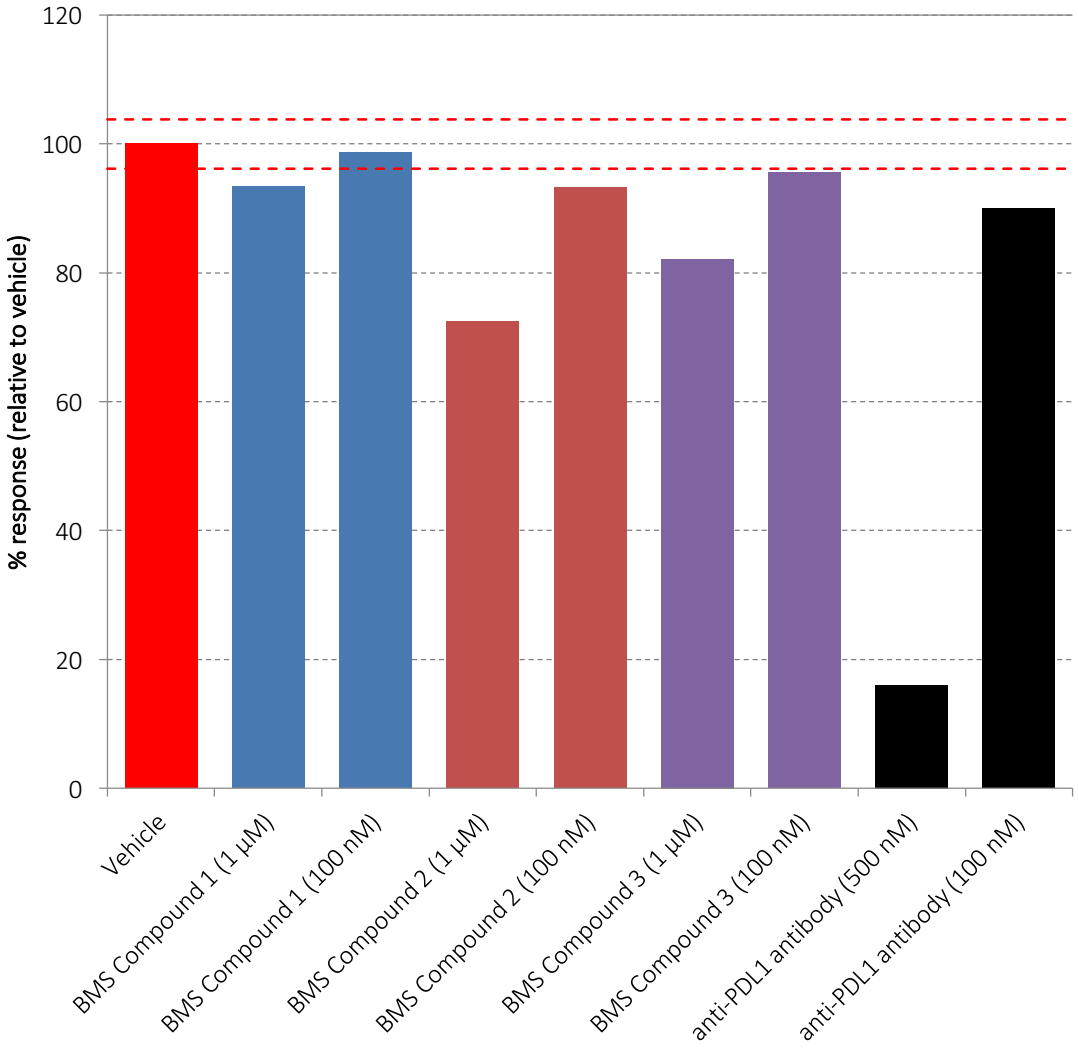


**Figure 39: Biacore assay for disruption of PD1/PD-L1 binding. PD1-biotin was immobilized on a streptavidin-coated chip (SA) to 2000 response units, and PD-L1 (1 µM, FLAG tag, full extracellular domain, expressed in HEK cells) flowed overtop. The red dashed line represents the standard deviation of the vehicle control.**

**Table 5: Dose-dependent inhibition of PD1/PD-L1 by BMS-2 (RH3.12) at various PD-L1 concentrations. Measured by Biacore.**

| [PD-L1] | $IC_{50}$ | Dose-response curve |
|---|---|---|
| 0.36 μM | 7.4 μM | 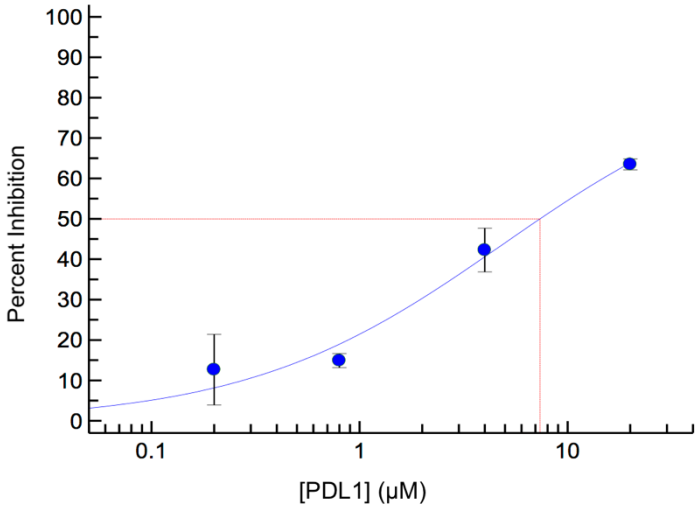 |
| 1.43 μM | 1.8 μM | 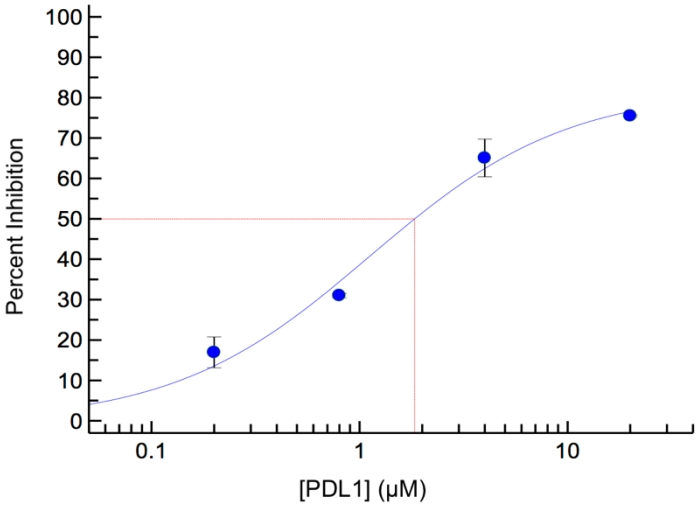 |

5.75 μM 2.2 μM

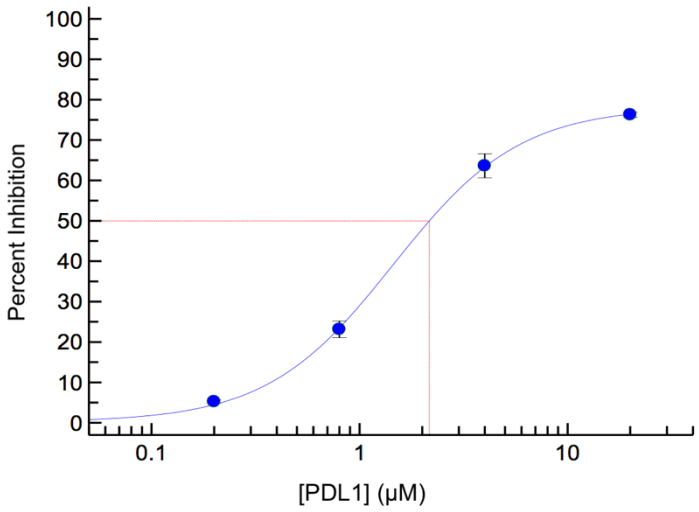


23 μM 15 μM

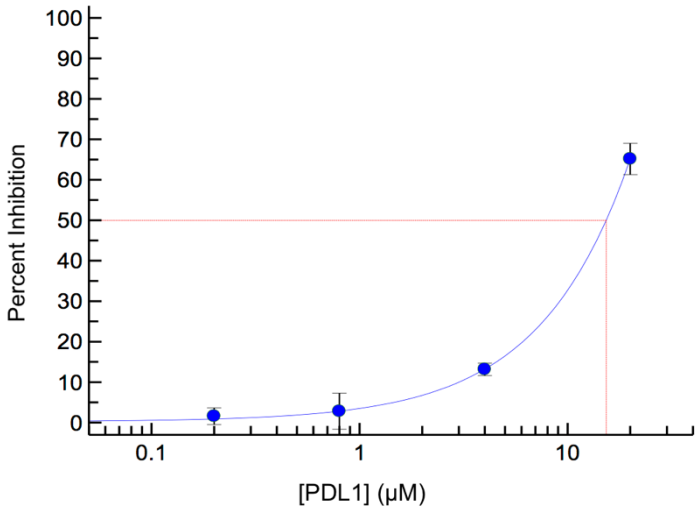


With a PD1/PD-L*2* TR-FRET assay already in-house (see Chapter 2), we were curious as to whether the BMS series could disrupt the binding of PD-L1's homolog. With PD-L1 and PD-L2 sharing 40% sequence identity, any difference in potency for either protein would point to high specificity and selectivity by the BMS compound series. Moreover, significant differences in inhibition between the two homologs would indicate that PD-L1 is the direct binding target of the BMS series, since PD-L1 and PD-L2 share similar binding sites on PD1.

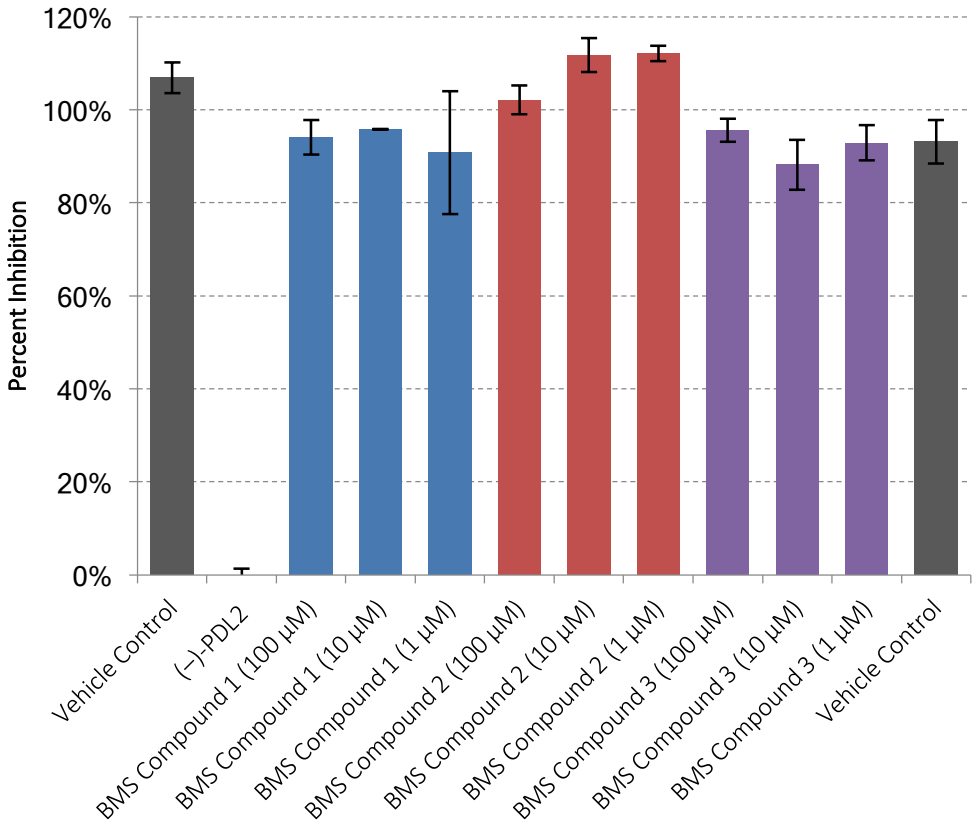


**Figure 40: TR-FRET assay for disruption of PD1/PD-L2 binding.**

The results from the PD1/PD-L2 TR-FRET assay (see Figure 40) stand in stark contrast to the other binding assays. The BMS compounds had absolutely no inhibitory effect on protein binding, even up to high micromolar concentrations.

Taken together, these orthogonal biophysical measurements validate the claims made by Bristol-Myers Squibb in their patent. Inhibition of PD1/PD-L1 binding was confirmed in multiple orthogonal assays, with IC50s consistently in the low micromolar to high nanomolar range. This variation is probably due to differences in the protein concentrations

used for each assay. The relative lack of activity in PD1/PD-L2 assays indicates, if not selectivity, at the very least some degree of specificity for this family of proteins.

These results also provide clues as to the identity of the protein binding partner for the BMS compounds. Since PD-L1 and PD-L2 share a common binding site on PD1, an inhibitor that binds to PD1 and disrupts its binding interface would be expected to have at least some inhibitory effect on the PD1/PD-L2 interaction. The absence of any such effect is a strong indicator that PD-L1 is the binding partner for these compounds, and that whatever site they occupy does not exist on PD-L2.

The exact binding site of these compounds, however, remained unknown.

### 3.2.3 Determination of the binding partner, binding site, and mechanism of action of the BMS series with single-domain PD-L1

In order to acquire direct information about the protein-compound binding event in solution, we chose to employ protein NMR as our primary structural analysis technique. While we had previously been able to grow single crystals of apo-PD-L1 and acquire X-ray data, there was no guarantee that we would be able to grow adequate quality inhibitor-bound crystals. Furthermore, while soaking of existing crystals can sometimes yield inhibitor-bound structures, gross conformational changes in the protein on ligand binding might be precluded in the solid state.

Our laboratory did not have the requisite facilities at the time to perform protein NMR, so we engaged in a collaboration with the group of Dr. Mark Carr at the University of Leicester. The Carr group had previously used NMR to determine the structure of human PD1 in solution, so they were well acquainted with the specific challenges posed by this family of proteins[98].

The Carr group first validated their ability to produce folded, functional PD-L1 protein. Expression in bacteria, followed by solubilisation and refolding, resulted in a soluble, folded protein capable of binding PD1. The folding was validated by circular dichroism and NMR, while binding competence was verified by titration into isotopically labelled PD1. With the conditions for unlabelled PD-L1 production optimized, the protein was then produced with enrichment of $^{15}N$ and $^{13}C$.

The addition of ligand to isotopically labelled PD-L1 gives rise to changes in the chemical shift of the protein, indicating a binding event. As seen in Figure 41, the HSQC spectrum for fully labelled PD-L1 changes significantly upon addition of ligand. These data confirm PD-L1 as the direct binding target of the BMS inhibitor family.

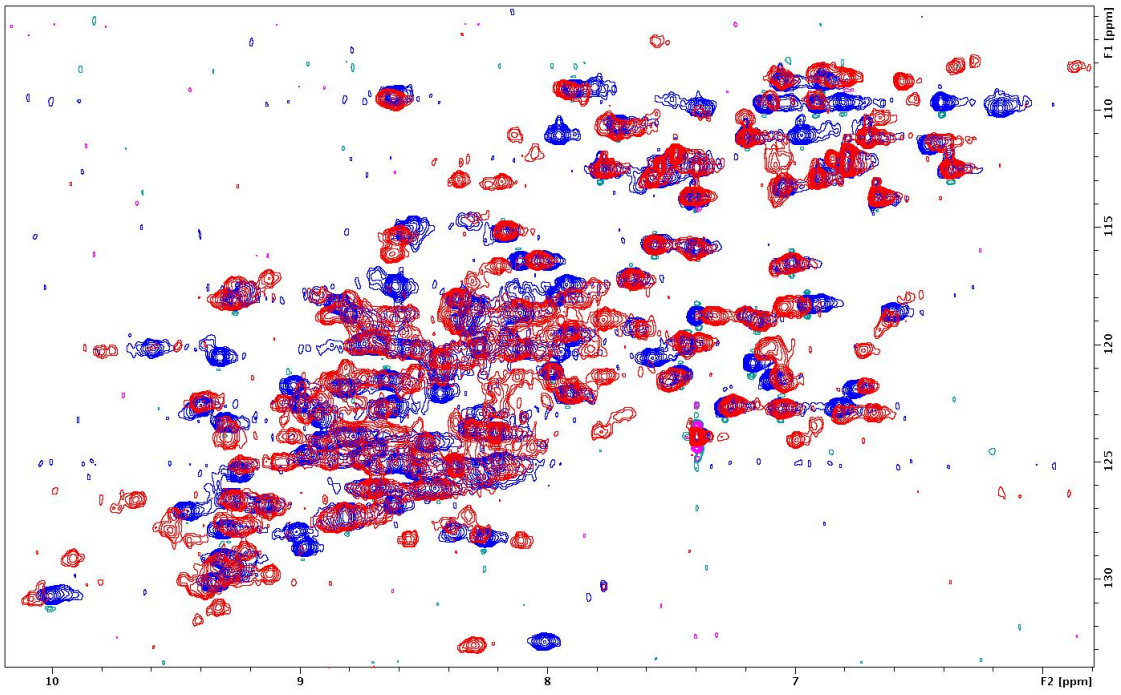


**Figure 41: $^{1}$H-$^{15}$N HSQC spectrum of single IgV domain of PD-L1 in the presence (red) or absence (blue) of BMS-2.**

Intriguingly, the ligand-bound protein seems to exist as two distinct species. The protein peaks that underwent changes to their chemical shift also split into two sets of peaks, indicating that inhibitor-bound PD-L1, but not free PD-L1, exists in two different conformations. These conformations could arise from the protein binding to two different conformations of the BMS ligands. This distribution could also be explained by an asymmetric oligomerization event, in which case two (or more) equivalents of PD-L1 assemble with one (or more) equivalents of the ligand to create a single complex.

Around this time, we observed an unexpected lactamization product from the attempted resynthesis of BMS-2, which we also identified in our DMSO stock solutions of BMS-2. While the conversion of the amino ester **RH3.07** to the lactam **RH3.08** is apparently

promoted by base and/or heat, the cyclization of the amino acid was found to occur in neutral DMSO. We hypothesized that perhaps this cyclized compound was also capable of binding PD-L1, and that mixed solutions of BMS-2 and the lactam would then bind PD-L1 in two different conformations.

We deliberately synthesized the lactam and tested its ability to disrupt PD1/PD-L1 binding by SPR, finding it to be inactive at even high micromolar concentrations. This result highlights the importance of the secondary benzylic amine for PD-L1 inhibition, and encouraged us to be more rigorous in our test compound quality control and storage. The lactam was a red herring in our search for the BMS series' mechanism of action, and one that cost us valuable time and effort, as other groups that had chosen more stable compounds were able to publish their results without this type of distraction.

At this time, the Holak and Dömling groups published a putative mechanism for PD-L1 inhibition by the BMS compounds.[311] Using protein NMR experiments very similar to our own, as well as X-ray crystallography, DSC, and gel filtration analysis, they determined that the BMS compounds induce homodimerization of PD-L1 at the IgV domain. The interface of this dimer, which is formed by the PD1-interacting faces of each PD-L1 monomer, creates a deep hydrophobic pocket that accommodates the relatively hydrophobic BMS benzyl biaryl moieties. With both PD1-binding faces occluded in the dimerization interface, neither molecule of PD-L1 is capable of binding to PD1. The induced PD-L1 dimers are asymmetric, which explains the split population of signals in the protein NMR.

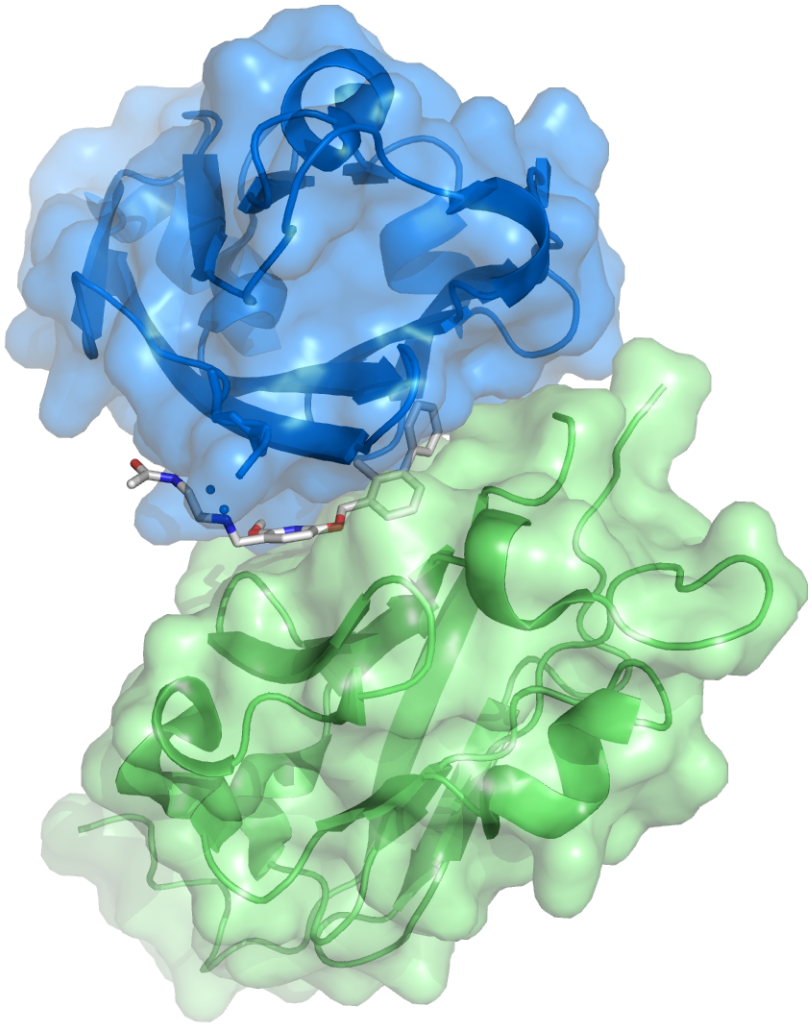

**Figure 42: Crystal structure of small molecule inhibitor with two equivalents of PD-L1.**

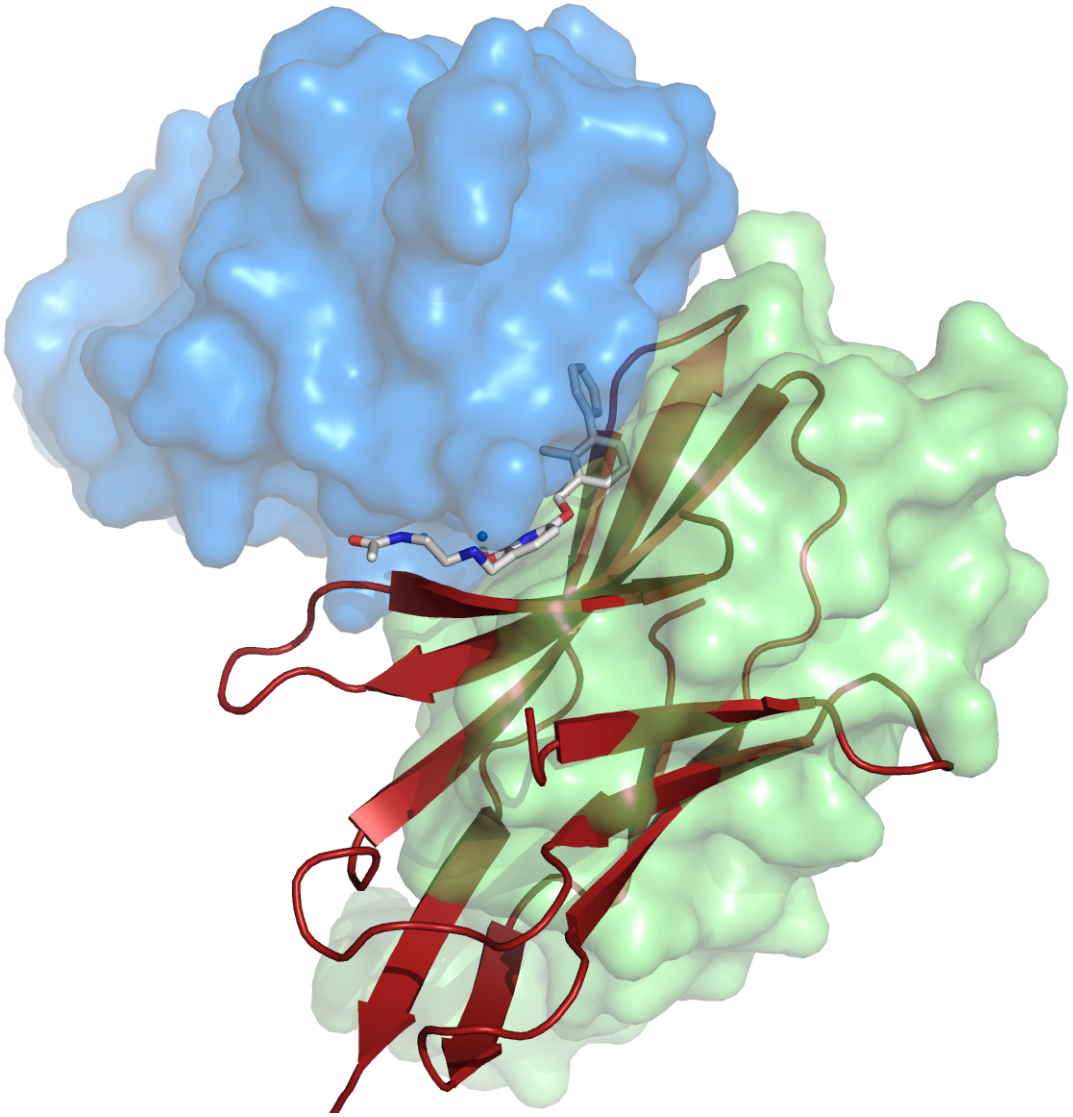

**Figure 43: Mechanism of PD1/PD-L1 inhibition by BMS compounds. The protein in blue is an overlay of PD-L1 from the complex with PD1 (red) and the complex with inhibitor and another molecule of PD-L1 (green). Note that both PD1 and the PD-L1-inhibitor complex occupy the same binding site.**

We independently confirmed that the BMS compound series induces PD-L1 dimerization by gel filtration and NMR.

NMR titration of PD-L1 with carefully measured aliquots of BMS-2 and BMS-3 revealed a 2:1 stoichiometry of binding, consistent with the induced-dimer model. Addition of more than 0.5 equivalents of either compound to isotopically labeled PD-L1 produced no change in the NMR spectrum, suggesting saturation at a 2:1 stoichiometry of protein to ligand. Moreover, addition of BMS-2 or BMS-3 in ratios of 1:1 or less did not result in new peaks or line broadening relative to free PD-L1 or dimerized PD-L1. We interpret these data to mean that the BMS series has a very low affinity for monomeric PD-L1 relative to PD-L1 dimers, as we are never able to observe the 1:1 compound-to-protein complex.

Mapping of the changes in chemical shift of the protein upon compound binding also supports the induced dimer model of inhibition proposed by Holak *et al*. Assigning the amino acid identities of each peak allowed us to calculate the change in chemical shift of individual residues upon ligand binding. The greatest changes in backbone chemical shift lie directly along the PD-L1-PD-L1 dimer interface seen in the Holak group's crystal structure, lending credence to that species' existence in solution. Moreover, the resonances that split into two distinct signals, or in other words the residues with the most asymmetry between the two dimer halves, make up the ligand-binding channel, as seen in Figure 44.

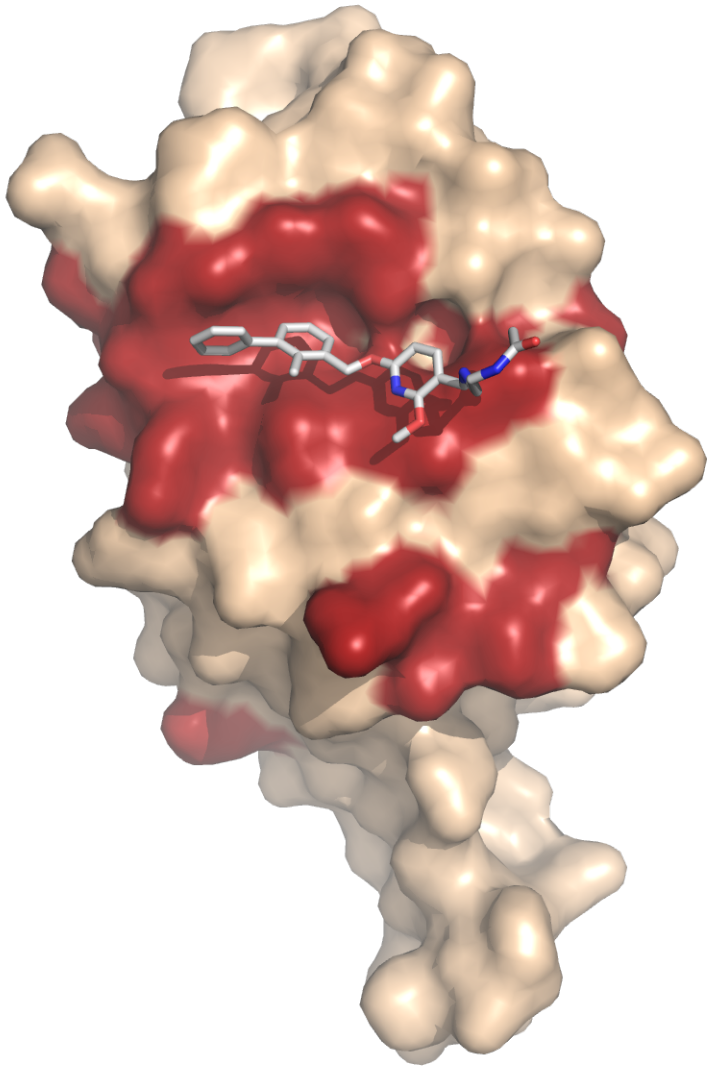

**Figure 44: Peak splitting due to compound-induced homodimerization. Red: peaks that split into two distinct signals upon ligand addition.**

The dimerization of PD-L1 was further supported by gel filtration analysis in the presence of BMS compounds. As seen in Figure 45, free PD-L1 IgV elutes as two distinct peaks from a gel filtration column, with the earlier peak corresponding to twice the molecular weight of PD-L1 and the later peak corresponding to the exact molecular weight of PD-

L1. We infer from these data that free PD-L1 forms apo dimers in solution that must have a relatively slow $k_{off}$. Addition of BMS compound to the protein prior to gel filtration results in a shift in peak distribution, with more PD-L1 eluting at the retention time of the dimer.

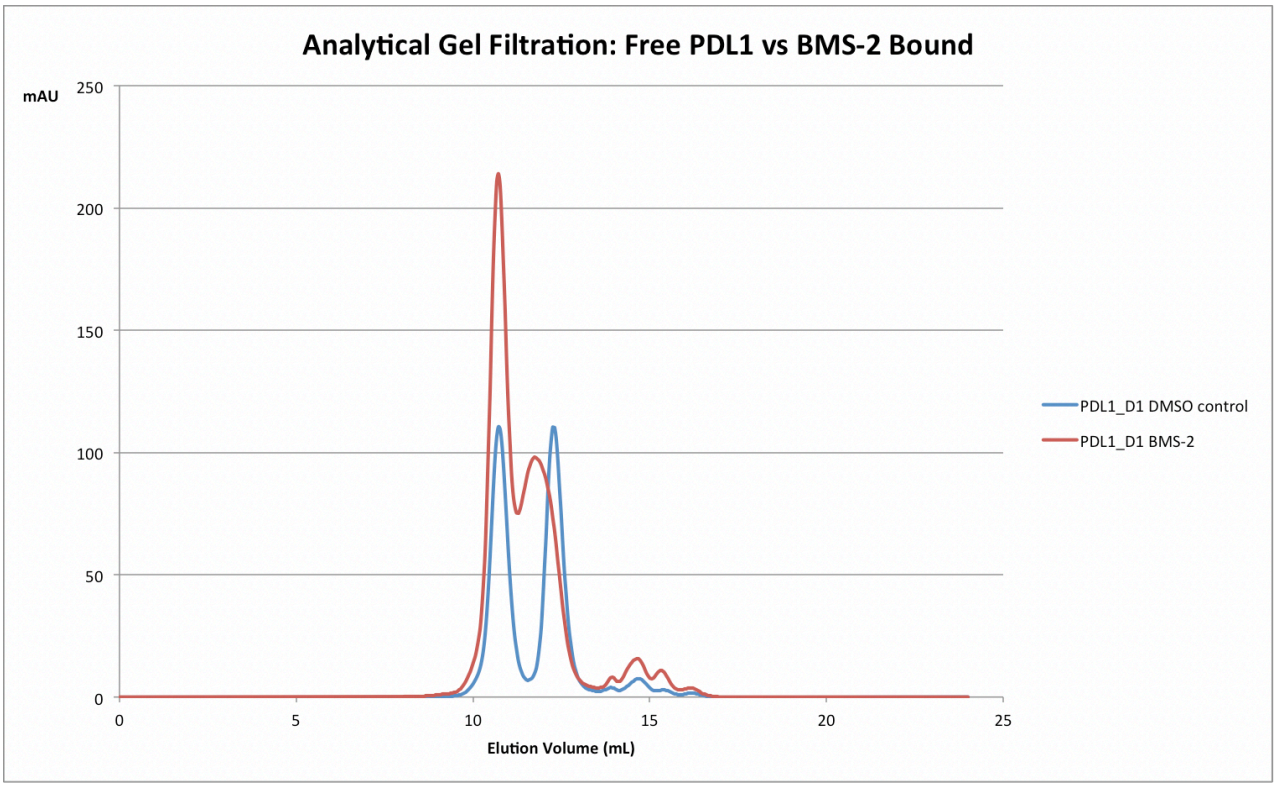


**Figure 45: Gel filtration trace of single-domain PD-L1 IgV with and without BMS-2.**

While we did not address the issue of glycosylation systematically, we believe that the glycosylation state of PD-L1 does not affect the potency or mode of action of these compounds. We and others have observed that glycosylation of PD-L1 does not affect its ability to bind PD1[98]; the known and predicted glycosylation sites for PD-L1 are all distal to the PD1 binding site[103]. We have used PD-L1 produced in both bacterial and mammalian

cells for Biacore and ELISA assays, and the BMS compounds inhibit PD-L1 from these expression systems with approximately equal potency. The data in Figure 39 were acquired using PD-L1 expressed in mammalian cells, while the data in Table 5 were acquired using bacterially expressed PD-L1. In both cases, BMS-2 at a concentration of ~1 μM inhibits ~1 μM PD-L1 by 30%.

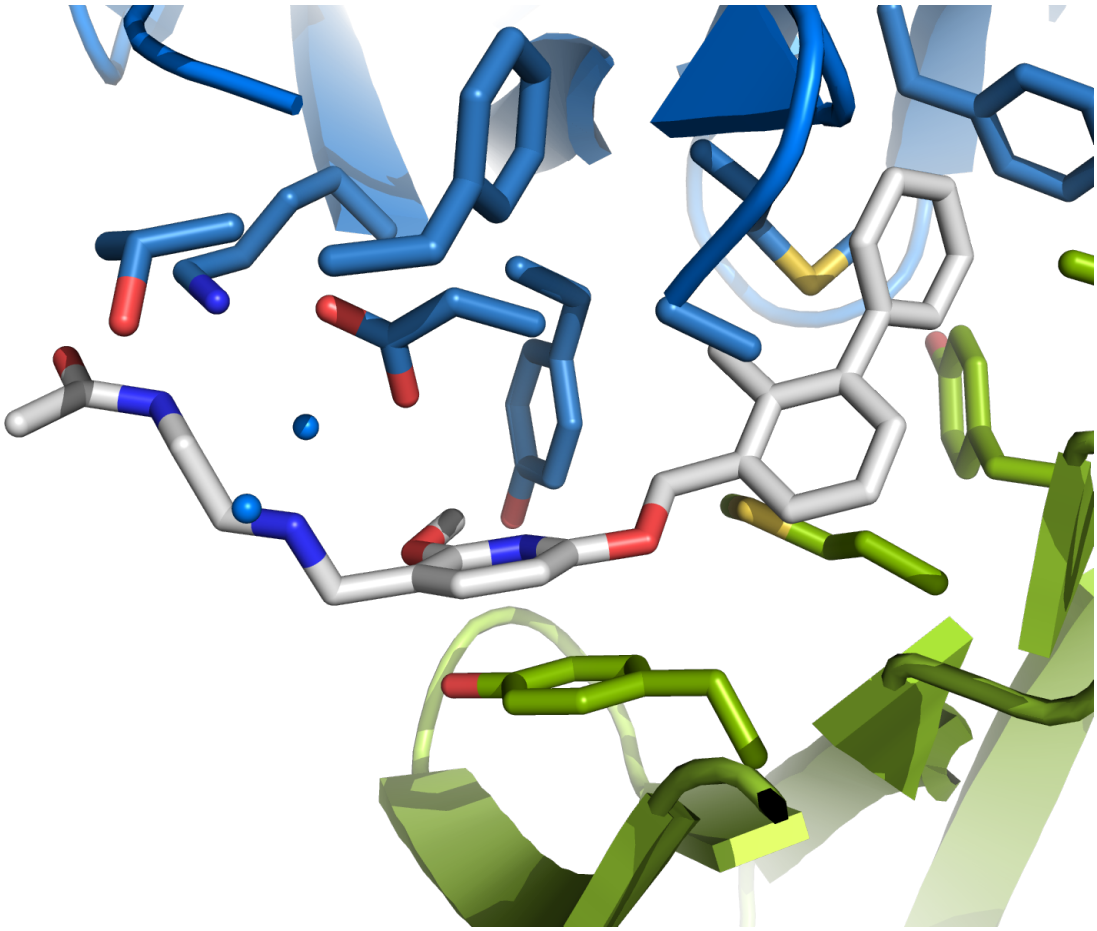

**Figure 46: Crystal structure of a BMS compound with two molecules of PD-L1. The A, B, and C rings of the inhibitor fit in a deep hydrophobic pocket that forms between the two protein surfaces, while the hydrophilic tail makes contact with the solvent as well as with charged residues at the entrance of the channel.**

Our studies on the interaction of the IgV domain of PD-L1 with the BMS compounds are in full agreement with the model of inhibition proposed by the Holak group. The BMS compounds induce dimerization of PD-L1, fitting into a narrow hydrophobic channel extending into the interface between the two molecules of PD-L1. This interface includes the binding site for PD1, occluding it and preventing PD1–PD-L1 interaction.

### 3.2.4 Differences in behaviour and mechanism with the full extracellular domain of PD-L1

While our data fully support the Holak model for BMS binding to PD-L1, the Holak model may not be representative of the situation in a real cellular environment. The Holak studies exclusively use the distal extracellular domain of PD-L1, the IgV domain. While the IgV domain contains the entirety of the PD1-binding region, and is therefore expected to interact with PD1 in an identical manner to full-length PD-L1, its oligomerization state, stability, and interactions with non-PD1 ligands may not be so similar. In particular, the ability of PD-L1 to dimerize around a ligand may be significantly abrogated by doubling the size of the protein, and the IgC domain could interact with either the compound or the IgV domain in ways that would change the binding mode or impede it altogether. Zak *et al* emphasize the importance of using physiologically relevant structures in their review of PD-L1 inhibitor development[312], yet they disregard the IgC domain, which constitutes half of the extracellular region of PD-L1, based on the assumption that it is a biologically inert "spacer".

Our Biacore and ELISA experiments with double-domain PD-L1 constructs have so far shown that the BMS series inhibit it to an equivalent degree as the single-domain construct. However, this in itself is not conclusive proof that the mechanism of action is unchanged when moving from one construct to another.

One striking difference between the single-domain PD-L1 and double-domain PD-L1 is the latter's propensity to form strong homodimers in the *absence* of compound. These dimers have been previously observed in both the crystal state and in solution by trapping with a crosslinking agent[102]. Our gel filtration data show that the full extracellular domain of PD-L1 elutes as a homodimer, and that this dimerization event is quite strong, as the elution profile does not change with increasing dilution.

Using paramagnetic NMR techniques, our collaborators sought to determine if the dimer formed by the double-domain construct of PD-L1 is the same as that described by the Gao group (see Section 1.3.2 Structure of PD-L1). Addition of a water-soluble paramagnetic agent to a protein solution enhances the relaxation rate of water-exposed protons[313]. This allows a rough estimate of which residues are protected from the solvent, and to what degree. The NMR of double-domain PD-L1 on addition of gadolinium chelates shows that the inner surface of the Gao-type dimer, *not* the PD1-binding face, is shielded from the solvent. This supports the existence of Gao-type dimers in solution (see Figure 47 and Section 1.3.2 Structure of PD-L1).

**Figure 47: Solvent-protected residues as determined by paramagnetic NMR. The structure by Gao is shown, with backbone residues shown as either solvent-exposed/not determined (green), moderately protected (yellow), or highly protected (red).**

In addition to forming stable dimers, double-domain PD-L1 differs from the single-domain construct in that addition of BMS-2 or BMS-3 results not in a change in chemical shift of

distinct peaks, but in an overall broadening and loss of signal. This could be the result of intermediate exchange, indicating that the kinetics of ddPD-L1 binding to the BMS compounds are different from those of the single domain—which may be detrimental to its pharmacokinetic properties, should the compounds be developed into drugs. This peak broadening could also be the result of oligomerization of the protein. Since the Gao dimer face and the BMS-binding face of the protein are on opposite sides of the protein, it is conceivable that both binding events could occur concurrently, resulting in an oligomer. The Carr group is now conducting gel filtration experiments in the presence of saturating amounts of BMS-3 in order to determine if oligomerization is the cause of this line broadening.

The Carr group has also assigned the backbone amides for the IgV domain of ddPD-L1 in order to compare it to sdPD-L1. While most of the domain matches up, there are a handful of residues near the interdomain region that shift significantly in the double-domain construct that appear to interact with the IgC domain in the crystal structure. Whether there is actually an interaction between the two domains requires assignment of the NMR of the IgC domain, which is ongoing, but these differences bring us full-circle to the possibility that the hinge region may control the binding ability of PD-L1. The IgC domain may not be the spectator it appears to be.

## 3.3 Evaluation of BMS-X cellular activity

### 3.3.1 Effect of BMS compounds on functional immune response

Despite the high potency of the BMS compounds *in vitro*, it was unclear whether the induced dimerization mechanism of action would translate to cellular efficacy. While not especially sterically demanding, the induced dimer nevertheless requires close contact between two molecules of PD-L1. This in turn requires proximity of the transmembrane and intracellular domains, which may introduce their own steric clashes. Moreover, it requires a high local concentration of PD-L1 at a given patch of the cell membrane, which may be precluded by the composition of the lipid membrane or binding by other transmembrane proteins.

In order to probe the question of whether these compounds can enhance immune function, they were tested in a mixed lymphocyte response assay at Inception Sciences. In this experimental setup, effector T-cells were stimulated with antigen-presenting cells in the presence or absence of PD-L1 inhibitors. The degree of immune induction was then determined indirectly by measuring interferon-gamma production from the T cells. DCs were stimulated with bacterial lipopolysaccharide as a positive control, and the approved anti-PD-L1 antibody Keytruda (pembrolizumab) was included to show immune activation due to PD1/PD-L1 inhibition.

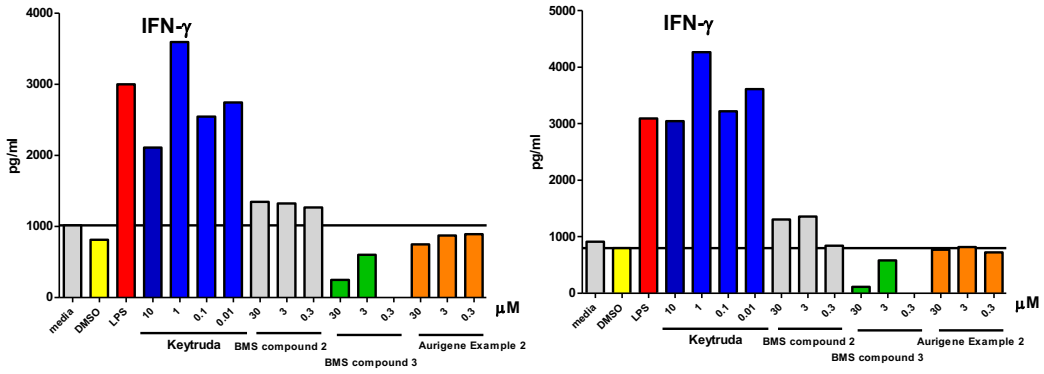


**Figure 48: IFN-γ release by T cells in mixed-lymphocyte response assay with BMS PD-L1 inhibitors. IFN-γ was quantified by ELISA of cell culture supernatants. Left: initial results after 5 days of co-culture. Right: fresh immature DCs were added to the co-cultures and incubated a further 24 hours.**

As seen in Figure 48, while the results for compound 3 are uninterpretable due to toxicity, the complete failure of BMS-2 to induce IFN-gamma production strongly suggests that the compounds are ineffective at inhibiting the PD-L1/PD1 interaction on live cells. Whether this is due to promiscuous binding of the compounds elsewhere, compound degradation, or some other reason has important implications for the further development of these compounds as drug candidates. Metabolic or stability issues can be addressed with medicinal chemistry of the core structure, or different formulations and drug conjugates. However, if the compounds are unable to bind PD-L1 on a cell membrane, the further development of this class of compounds, as well as any other compounds that function through a similar mechanism, is limited to the inhibition of soluble PD-L1 whose clinical significance is still controversial. These compounds would therefore be much more limited and less competitive compared to antibodies.

### 3.3.2 Effect of BMS compounds on oligomerization state and binding ability of cellular PD-L1

While the question of whether the BMS compounds worked in a cellular context seemed resolved in the negative, the answer to why this should be the case remained elusive. Our work and that of the Holak and BMS groups has shown that the induced dimerization mechanism is operational for both single-domain and double-domain fusion protein constructs, can operate in the presence of BSA and detergents, is not affected by glycosylation, and does not seem to require any particular preincubation period. In short, the basic molecular features of the PD-L1 protein and of the cellular culture medium do not seem to affect compound-induced dimerization.

Moreover, while the oligomerization state of soluble PD-L1 depends upon both the presence of compound and the construct, the ability of full length PD-L1 to dimerize in a cell membrane, with or without compound, was also unknown. PD-L1 has been proposed to be monomeric in the cell membrane, and its binding to PD1 expressed on T-cells has been proposed to obey a 1:1 stoichiometry[98, 103, 248], but most of the evidence for these affirmations has been either indirect or based on soluble constructs/systems.

While other variables related to the switch from an in vitro to cellular system cannot be discounted as possible reasons for the lack of activity (serum binding, enzymatic degradation, intracellular sequestration, subtle changes in protein folding), the ability of PD-L1 to dimerize in the membrane seemed the most crucial unknown, and therefore the most likely cause for the lack of activity. The Holak group has noted that, in studying this

series of compounds, they were unable to find any examples of compounds that inhibited the PD1/PD-L1 interaction without also inducing dimerization[314]. Moreover, neither we nor the Holak group have detected the 1:1 complex of the BMS series with PD-L1. While the channel that forms between two molecules of PD-L1 is very hydrophobic and eager to accept the biphenyl benzyl ether moiety, there exists no groove on either monomer that could protect that hydrophobic group on its own. Taken together, these results suggest that dimerization is required for activity.

a)

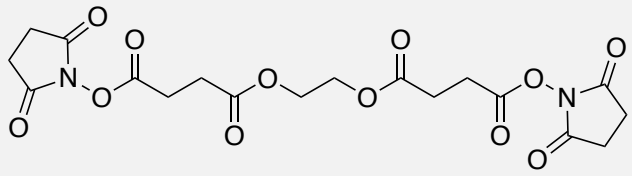

**EGS**

b)

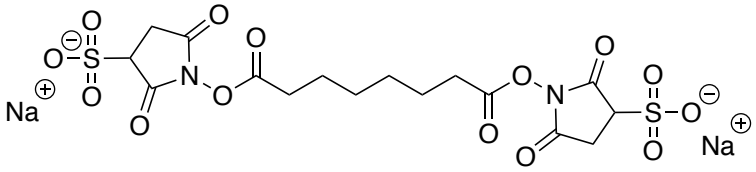

**BS$^3$**

c)

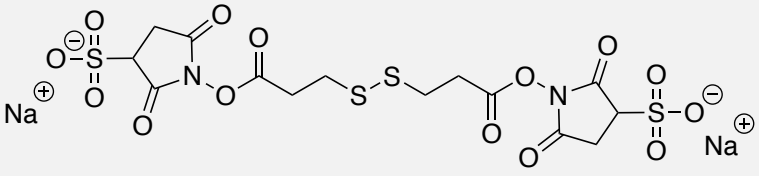

**DTSSP**

**Figure 49: Amine-reactive crosslinking agents used for PD-L1 crosslinking. a) Water-soluble, membrane-permeable crosslinker used for soluble PD-L1 crosslinking[102]. b) Water-soluble, membrane-impermeable, non-cleavable crosslinker used for cell surface crosslinking. c) Water-soluble, membrane-impermeable, cleavable crosslinker used for cell surface crosslinking.**

Cell-surface crosslinking experiments were performed to probe the oligomerization state of native PD-L1, and were unable to detect any oligomer formation. MDA-MB-231 cells naturally and constitutively express full-length PD-L1 on their cell surfaces[315-316]. PD-L1 does not contain any free solvent-exposed cysteines for labelling, but it does have free lysines at the distal IgV domain, and the protein had previously been crosslinked with an amine-reactive reagent[102], suggesting that this would be the ideal reactive handle for a crosslinker to use. We therefore applied the various BMS compounds to adherent cultures of MDA-MB-231 cells, with and without the addition of an amine-specific, membrane-impermeable crosslinking agent (the cleavable DTSSP or non-cleavable $BS^3$). Even under conditions of very high compound concentration, no PD-L1 dimers were detected by Western blot following cell lysis (see Figure 51). The presence of PD-L1 at the cell surface was validated by antibody staining of non-permeabilized cells, and the activity of the crosslinker was confirmed by the detection of PD1 dimers from what was supposed to be an assay for PD1/PD-L1 binding (the PD1 construct used was an Ig-fusion, and Ig domains homodimerize).

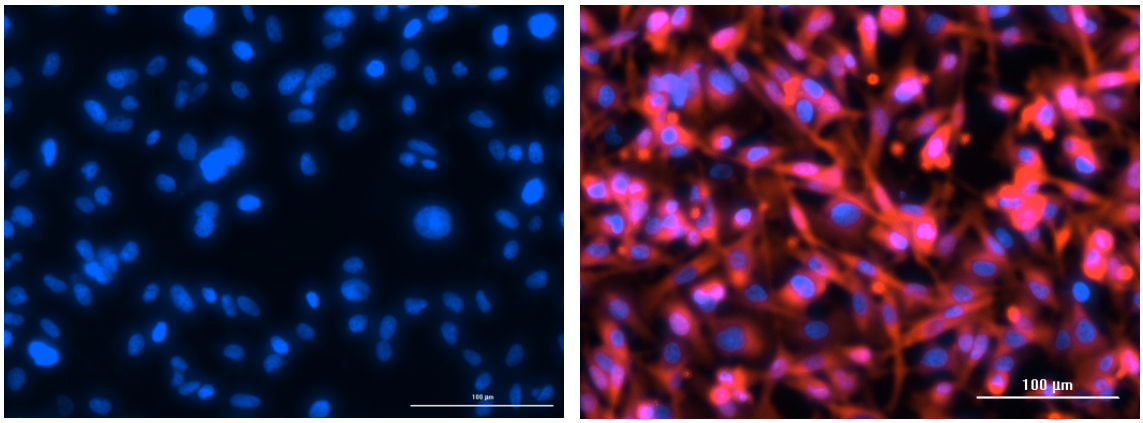


**Figure 50: Staining of fixed, unpermeabilized MDA-MB-231 cells with anti-PD-L1 antibody. Left: no antibody. Right: with antibody. Blue: DAPI. Red: anti-PD-L1-AlexaFluor-568.**

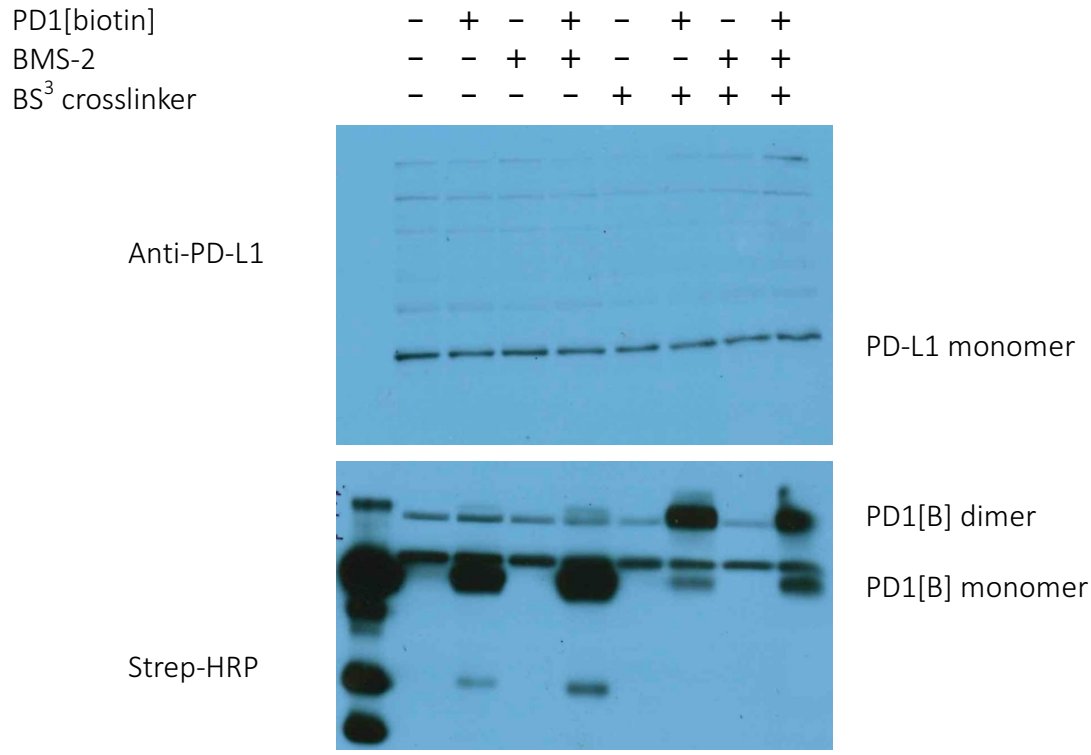


**Figure 51: Western blot after surface crosslinking on live MDA-MB-231 cells.**

Intriguingly, while no PD-L1 dimers were detected in the presence of BMS compounds, no dimers were formed in the absence in compound, either. Both the single- and double-domain constructs of extracellular PD-L1 form apo-dimers in the absence of compound. The absence of any apo-dimers in a cellular context suggests that there is some additional barrier to dimerization in the cell membrane for PD-L1 that is not present in solution, and that the solution phase behaviour of PD-L1 is not necessarily predictive of its behaviour in the cell membrane. These differences between solution phase and membrane bound behaviour could be due to structural differences in the protein itself (due to the addition of the transmembrane & intracellular domains), the constraints of being membrane-bound versus freely moving and rotating in solution, the effective local concentration of protein,

or exogenous factors involved in membrane trafficking (sequestration by other membrane proteins, lipid composition, etc). Our experimental results can offer no clarity on this issue.

While the lack of any dimer formation in the crosslinking experiments is suggestive, the absence of dimer bands is not conclusive proof that dimerization does not occur. Furthermore, while the compounds act on soluble PD-L1 by forming dimers incapable of PD1 binding, a non dimer-dependent mechanism of PD-L1 inhibition cannot be ruled out for membrane-bound protein. It was therefore imperative that we establish conclusively whether or not the compounds are capable of inhibiting cellular PD-L1 from binding to PD1.

In order to obtain conclusive evidence that the membrane-bound nature of PD-L1 is responsible for the compounds' lack of cellular activity, we employed a live cell-based binding assay in which one protein partner is soluble and one is membrane-bound. Using HEK293 cells, which express neither PD1 nor PD-L1, we first transfected the cells with a constitutive expression plasmid coding for either PD1 or PD-L1 fused at the C-terminus to a monomeric green fluorescent protein (GFP) construct. The GFP at the C-terminus is intracellular and is not expected to interfere with extracellular ligand binding, and it allows for confirmation of successful transfection. The cells were then allowed to express protein and then incubated with the complementary binding protein (PD1 for PD-L1-transfected cells, PD-L1 for PD1-transfected cells) fused to phycoerythrin, a red fluorescent protein. Binding was then detected by imaging the cell culture and identifying cells fluorescing red.

The expression of the fusion protein was confirmed by the green fluorescence observed from the transfected cells—this fluorescence is localized to intact cells and does not appear in untransfected cells. Oddly, although both PD-L1 and PD1 are membrane proteins, the majority of the fluorescence was localized to the interior of the cells. This could indicate either protein misfolding or that these proteins are held in reserve intracellularly. Nevertheless, labeling of live cells with an AlexaFluor 568-conjugated anti-PD-L1 antibody confirmed the presence of sufficient quantities of PD-L1 at the cell membrane (see Figure 52). Untransfected cells did not stain with this antibody, confirming that HEK293 cells do not express native PD-L1 to an appreciable degree.

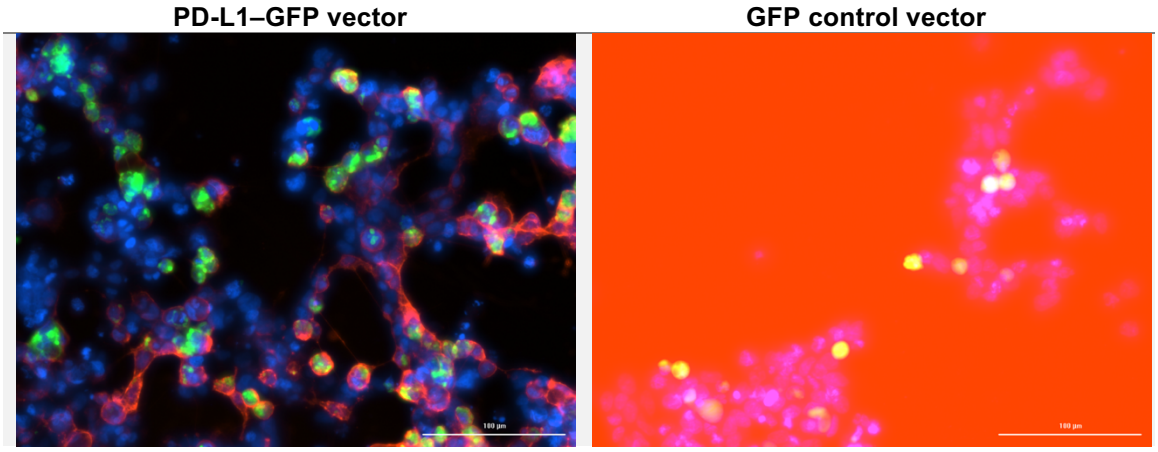


**Figure 52: Validation of PD-L1–GFP expression following transfection. Images taken at 20X magnification following 24 hours of transfection and staining with Hoescht 33342 (blue, nuclear stain) and anti-PD-L1–AlexaFluor 568 antibody (red). Left: HEK293 cells transfected with PD-L1–GFP vector. Right: HEK293 cells transfected with GFP control vector (gain and integration time set to maximum on red channel; no specific staining observed at any camera settings).**

Preliminary experiments revealed that we would not be able to use our best-characterized compound, BMS-2, for fluorescence studies. The purification of BMS-2 (**RH3.09** – see Scheme 10) had always been problematic, because the compound is zwitterionic and can only by purified by reverse-phase HPLC. This had previously limited the quantities of BMS-2 available for study, but it introduced a new problem for imaging applications. Later batches of BMS-2 (**RH3.09**) formed large insoluble aggregates in test wells, far too large to be cells (see Figure 53). Moreover, these aggregates are particularly adept at adsorbing PE-tagged proteins. We doubted that these aggregates were particles of the compound itself, as it has good solubility in DMSO/buffer mixtures. We also doubted that they were particles of the lactam (**RH3.08**), as the cyclization reaction is relatively slow in DMSO stock solutions, and the lactam itself possesses fairly good solubility. We therefore believe these particles to be contaminants from the HPLC column used to "purify" the material; they must be either inorganic or polymeric, as the $^{1}H$ and $^{13}C$ NMR for these compounds are clean. We could have filtered the compounds to remove the debris prior to use, but the concentration of compound in that solution would still be unknown. We therefore chose BMS-3 to use for fluorescence studies. BMS-3 is toxic to cells (based on observations from Inception and from our group), but stable and soluble enough for short-term use. We also note that the washes required to remove cellular media and Hoescht stain tend to delaminate the cellular monolayer. Longer incubation/adhesion times post-transfection result in cellular overgrowth, while seeding fewer cells pre-transfection leads to cell death. The cells shown in these images are therefore not a healthy monolayer; use of a more adherent culture surface (such as poly-D-lysine) or subculturing after transfection would probably improve cellular health and image quality.

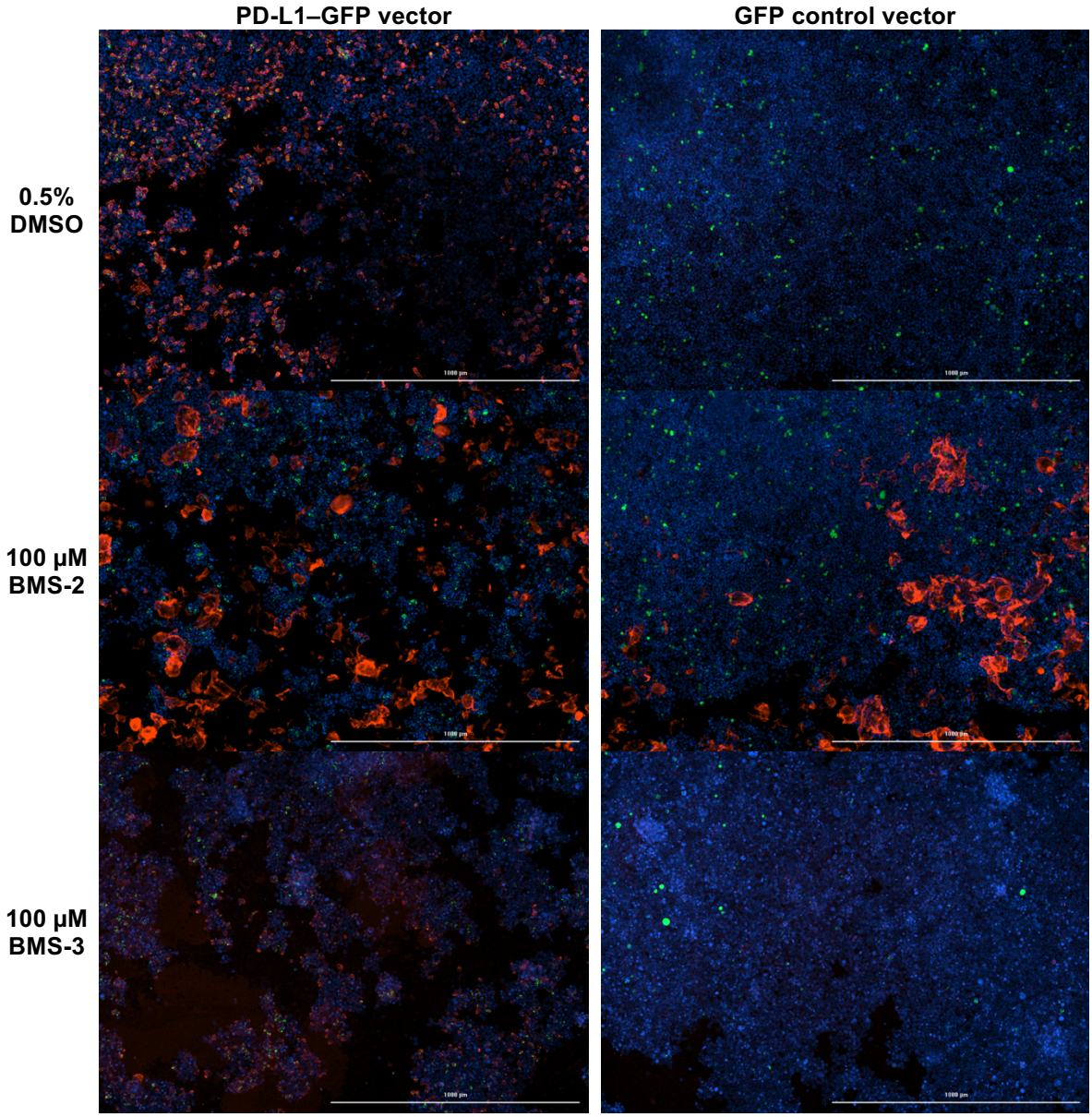


**Figure 53: Insoluble debris in fluorescent imaging of BMS-2. Images taken at 4X magnification following 24 hours of transfection and staining with Hoescht 33342 (blue, nuclear stain) and incubation with PD1–PE (red) plus compound. Aggregates occur in both the BMS-2/PD-L1 and BMS-2/control wells, are larger (~10 µm) than HEK cells (~1 µm), and are unique to BMS-2 (BMS-3 does not form aggregates). Gain and integration time settings identical for all conditions.**

In the event, BMS-3 (**RH3.06**) was only moderately able to inhibit binding of PD1–PE to PD-L1–GFP-expressing cells (see Figure 54). The phycoerythrin-labeled PD1 showed robust staining of PD-L1-transfected cell membranes, with no detectable binding to either untransfected cells or cells transfected with a GFP control vector. As expected, a validated anti-PD-L1 blocking antibody completely abolished PD1/PD-L1 binding at a concentration of 500 nM. As the antibody is bivalent, the total amount of PD-L1 expressed on the cell surface can be expected to be a maximum of 1 μM relative to the total solution volume in the well. Some inhibition of PD1–PE binding was observed with BMS-3, but at concentrations well above those required for inhibition of soluble PD-L1. Even at these high concentrations, the inhibition was only partial, suggesting that they bind to membrane-bound PD-L1 with only moderate affinity.

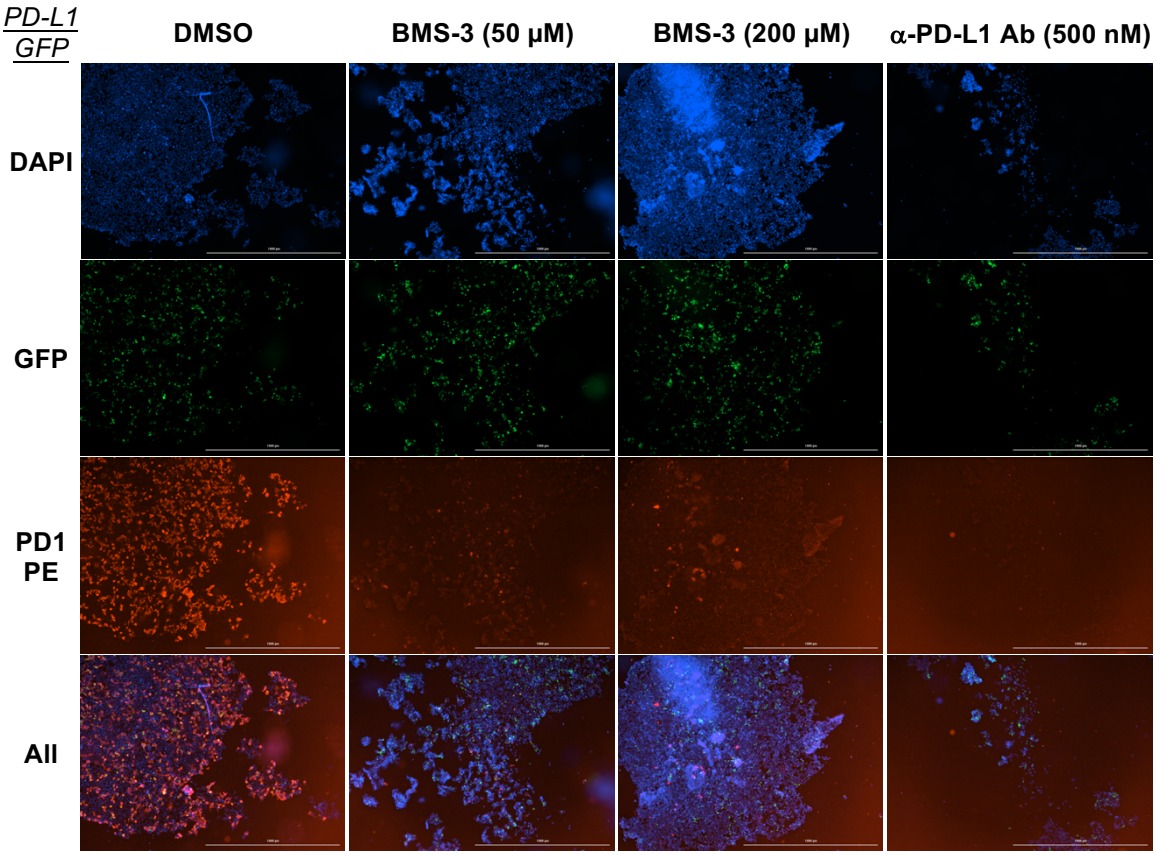


**Figure 54: Inhibition of PD1–PE binding to PD-L1–GFP transfected cells. Images taken at 4X magnification following 24 hours of transfection and staining with Hoescht 33342 (blue, nuclear stain) and incubation with PD1–PE (red) plus compound. BMS compounds partially abolish PD1–PE staining, while an anti-PD-L1 antibody inhibits it completely. Gain and integration time settings identical for all conditions.**

The reverse experiment, in which cells were transfected with PD1–GFP and probed with PD-L1–PE (see Figure 55), yielded predictable results. BMS-3 was able to inhibit most of the PD-L1–PE binding, consistent with its ability to form PD-L1 dimers in solution. Again, though, the inhibition was not complete, in contrast to the anti-PD-L1 antibody. These results indicate that while PD-L1 dimerization (or at least PD-L1 binding and inhibition)

is possible on the cell surface, these compounds are probably not potent enough to be useful therapeutically. One wonders whether the residual binding at high compound concentrations would be fully inhibited by a more potent compound, or whether the dimerization-dependent mechanism of these compounds will always leave some "isolated" monomeric PD-L1 free to bind PD1.

The concentrations of BMS-3 used here are still too high to estimate an effective concentration. A full titration down to 1 μM would have to be done in order to fully quantify the effects of the BMS compounds on cells. Moreover, these results are only qualitative. In order to obtain quantitative binding data, the degree of PD(L)1–PE binding to each cell could be determined by demarcating cell outlines and quantifying the fluorescence intensity within those shapes. Flow cytometry could also be used. Those experiments are hampered by the inconsistency of PD(L)1–GFP expression following transfection, which makes automated gating of transfected cells difficult. Further optimization of the transfection protocol could open the door to more quantitative data analysis.

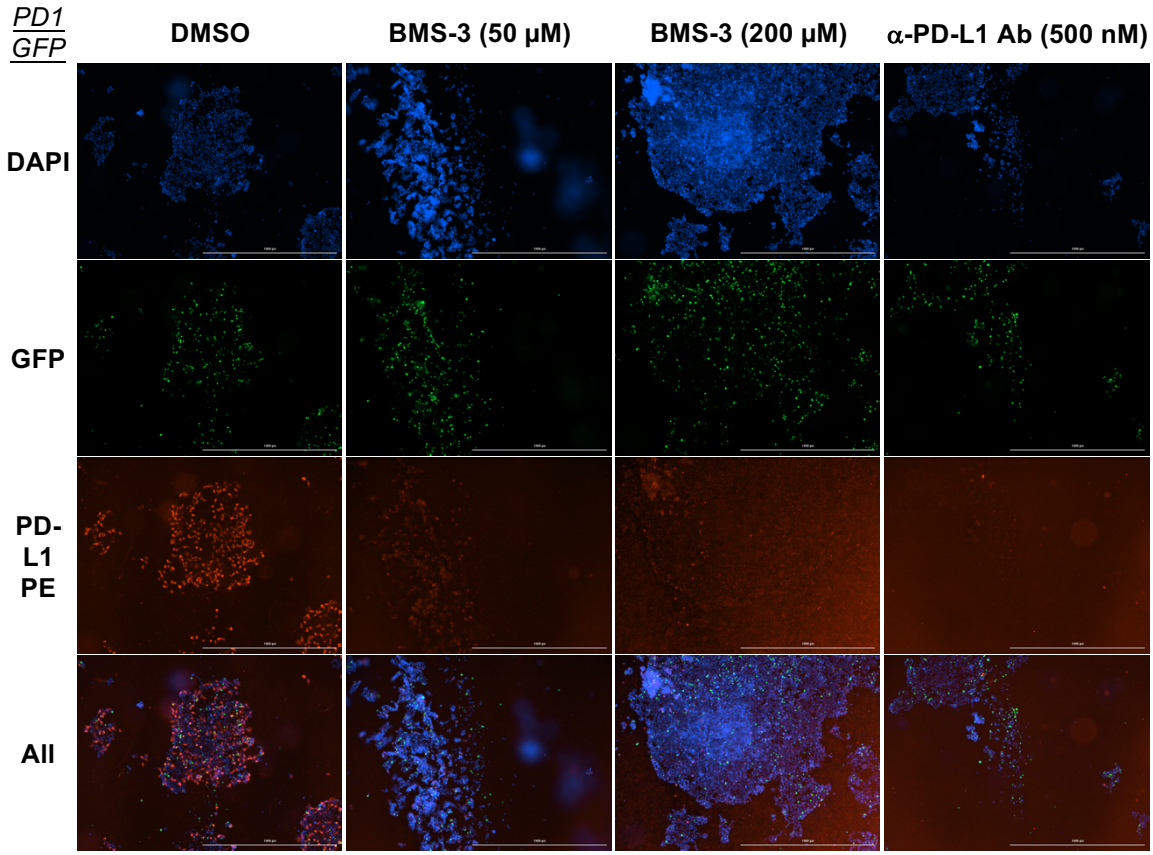


**Figure 55: Inhibition of PD-L1–PE binding to PD1–GFP transfected cells. Images taken at 4X magnification following 24 hours of transfection and staining with Hoescht 33342 (blue, nuclear stain) and incubation with PD-L1–PE (red) plus compound. BMS compounds mostly abolish PD-L1–PE staining, while an anti-PD-L1 antibody inhibits it completely. Gain and integration time settings identical for all conditions.**

## 3.4 Conclusions about the long-term prospects of the BMS series

The molecules patented by Bristol-Myers Squibb in 2015 were claimed to inhibit the PD1/PD-L1 interaction and to be useful as immunomodulators. We synthesized example compounds and analogues thereof, and tested their ability to bind and inhibit PD-L1 in vitro as well as in cell culture. Our results have confirmed those of the Holak group, showing that the BMS series effect PD1/PD-L1 inhibition by inducing dimerization of the

PD-L1 IgV domain. This dimerization sequesters the PD1-binding face of both PD-L1 units, preventing PD1-binding.

The ability of the compounds to induce PD-L1 dimerization on the cell surface remains ambiguous. Our crosslinking studies using MDA-MB-231 cells seemed to indicate that the compounds did not induce dimerization at all. However, our live cell imaging experiments did show that BMS-3 was able to inhibit the binding of membrane-bound PD-L1 to soluble PD1. Given that we have never been able to detect a 1:1 complex of BMS compound to PD-L1, we assume that inhibition of binding must imply the existence of some dimers on the cell surface. The apparent discrepancy between these two experiments may come down to the expression level of PD-L1. The expression vector for PD-L1–GFP is probably transcribed and translated at a far higher level than the natural expression of PD-L1 on MDA-MB-231 cells. This higher concentration of PD-L1–GFP would then result in facile dimerization, in keeping with our observations of higher compound efficiency at higher PD-L1 concentrations in SPR experiments.

While the BMS series of compounds can inhibit the *in vitro* and *in cellulo* interaction of PD1/PD-L1 as described in the experimental section, their billing as "compounds useful as immunomodulators" is debatable. Even at very high concentrations, the BMS compounds were never able to fully abolish the PD1/PD-L1 interaction on the cell surface. Moreover, functional assays showed that these compounds were ineffective at inducing IFN-γ production. It seems unlikely that these first-generation BMS compounds are potent enough to be useful immunomodulators compared to their antibody competitors (Kd =

0.667 nM, 1.75 nM, 0.83 nM, and 46.7 pM for durvalumab, atezolizumab, BMS-936559, and avelumab, respectively[317]).

### 3.4.1 Literature update

During the redaction of this dissertation, the Holak group published a paper on the functional inhibition of the PD1/PD-L1 interaction by first and second-generation BMS[318]. While the first-generation compounds are unable to induce T cell activation in a cellular assay (consistent with our own experimental results), the second-generation compounds *are* able to do so. The activity of these compounds is presumably due to their increased affinity for PD-L1 imparted by the added ring systems (see Figure 56), although the BMS patents[242-243] are not very specific in reporting $IC_{50}$ values (the best first generation compounds have $IC_{50}$ values of 6-100 nM, while the best second generation compounds have $IC_{50}$ values of 0.6-10 nM), and the Holak group has not independently quantified or ranked their inhibition. It could also be that the newer compounds induce dimerization in a manner that is less encumbered on a cell surface, although the apparent binding site and dimer structures are very similar to the first-generation compounds.

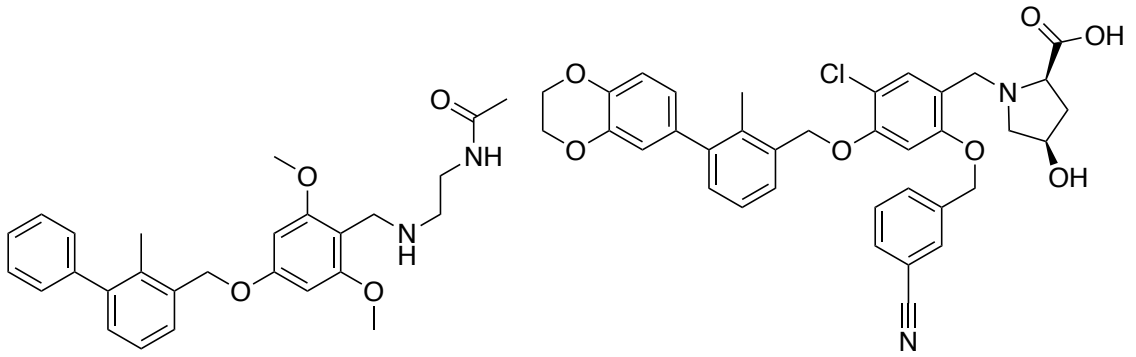


**BMS-3**
**Example 37 from first BMS patent**

**BMS-1166**
**Example 1166 from second BMS patent**

**Figure 56: Example compounds from first and second BMS patents.**

In a reporter gene assay, Jurkat cells were engineered to carry a TCR-dependent luciferase gene as well as to constitutively express PD1. These cells were stimulated with PD-L1-expressing antigen-presenting cells, and the extent of TCR activation monitored by luciferase activity. This setup should capture the nuances of the interaction between membrane-bound PD1 and membrane-bound PD-L1. Thus, the ability of the second-generation BMS compounds to enhance Jurkat cell activation demonstrates that they are able to inhibit membrane-bound PD-L1, while the first generation compounds are inactive up to 1 μM. It is noteworthy that the extent of activation by the second-generation BMS compounds does not reach the same levels as antibody controls, which could again be due to incomplete blockade of PD-L1 by the dimerization mechanism.

Moreover, the Holak group has demonstrated that these compounds can disrupt the binding of soluble PD-L1 to PD1-expressing cells, as measured by staining with dye-labeled PD-L1 followed by flow cytometry. These results again match our own, showing that the dimerization mechanism is operative for unencumbered, soluble proteins.

# Chapter 4

This chapter describes the contributions this work made to the field, the relevant advances that happened elsewhere concurrently with this work, and future directions based on this work.

## 4.1 Contributions

### 4.1.1 Discovery of salicylates as interference compounds in TR-FRET assays

In the past 7 years, there has been a growing recognition in the academic literature that not all compound classes are created equal when it comes to assay performance[319]. Some motifs are innocuous and well-behaved in all assays; some compound classes are even privileged scaffolds for bioactivity. Other idiosyncratic compounds interfere with assay readouts, or bind biomolecules promiscuously. However, there are also general structural motifs that interfere with various assay formats. There is now a concerted effort to predict, flag, and sometimes remove PAINs compounds from screening libraries[305]. Most of these efforts have focused on "filters" based on known interferants, and rely on shared functional group motifs and physicochemical properties[281, 300, 302].

Some mechanisms of assay interference are known, others are not. It is therefore important not only to flag PAINs compounds, but also to identify what types of assays they may

interfere with, so that biologically active compounds are not discarded just because they happen to show up on a list of bad actors.

In screening assays, TR-FRET and SPR are often used as the gold standards for biophysical compound validation. Indeed, many PAINs-focused papers use TR-FRET as the counter-screen to validate PAINs in the first place[301]! To our knowledge, other than general fluorescence quenchers (which should be easy to identify), there is only one known frequent-hitter in TR-FRET assays–chloranil–reported prior to our work[301].

Our discovery that salicylates can interfere with TR-FRET assays in an apparently dose-dependent manner should hopefully underline that even the most robust assay has flaws. While TR-FRET can correct for many mechanisms of assay interference, chelation by hard oxygen-based ligands should always be considered a possibility. Moreover, with salicylic acids being so well-represented among approved drugs (4-aminosalicylic acid for tuberculosis[320]; mesalazine, sulfasalazine, balsalazide, and olsalazine for ulcerative colitis[321]; diflunisal as an NSAID[322]), as well as their well-characterized bioisosterism for phosphotyrosine[323-324], one might imagine this family of compounds being treated with less scrutiny than others. It is important to recognize that interferants often cannot be confirmed or discounted by their appearance or by their use in other indications – only by empirical evidence.

While the effects of salicylate interference on TR-FRET ratios was most apparent above 500 μM, the interference was still observable at relevant concentrations for fragment

screening[325]. Low molecular weight compounds of low complexity are expected to be weak binders, and high concentrations are often needed to detect inhibition. The salicylate interference was observable down to 100 μM, a common concentration in fragment screening, and even higher concentrations are often used[326-328]. Moreover, there was considerable variability in the magnitude of TR-FRET amplification observed between compounds, with more conjugation generally resulting in more activity. It is quite possible that compound libraries contain "super-enhancers" that would show FRET enhancement at even lower concentrations than those at which we tested.

### 4.1.2 Characterization of BMS compounds as PD1/PD-L1 inhibitors

Prior to our work, there had been few reports of small molecule inhibitors of PD1/PD-L1; of these, most were patents and none described the biophysical interaction of the inhibitor with the target protein. Our work has validated that the compounds disclosed by BMS are in fact capable of inhibiting the direct interaction of PD1 with PD-L1; that they bind to PD-L1 and induce dimerization of the terminal IgV domain; that the interaction with the full-length protein is far more complex than with the IgV domain alone; and that they are only very weak inhibitors of the PD1/PD-L1 interaction on the cell surface. These structural and functional insights will help guide the design of PD1/PD-L1 inhibitors from different scaffolds, and may lead to the development of a non-dimer-inducing PD-L1 inhibitors. These insights will also guide the use of BMS inhibitors as tool compounds, since there are applications in which they would be useful positive controls (*in vitro* binding assays) and others where an antibody or antibody fragment would be a far more appropriate tool

compound (functional and cellular assays, multivalent polymers or nanoparticles, targeting agents for imaging modalities).

### 4.1.3 Absence of direct PD1/PD-L1 inhibition by sulfamethizole

Our work has also shown in two orthogonal assays (ELISA, TR-FRET) that sulfamethizole is *not* a direct agonist or antagonist of the PD1/PD-L1 interaction, despite what the Sharpe group has reported[244]. We cannot comment on sulfamethizole or its derivatives' ability to regulate PD1 signaling by binding to some other biological target, only that it does not bind to either PD1 or PD-L1. This clarifies its mode of action somewhat, and again guides its use as a tool compound – it should not be used as a positive control for any kind of biophysical PD1/PD-L1 inhibition assay.

## 4.2 Relevant advances and the state of the field

Concurrently with our work, the Holak and Dömling groups at the Jagellonian Institute and the University of Groningen, respectively, have published frequently on the mode of action of the many PD1/PD-L1 inhibitors discovered by BMS[247, 311, 314, 318]. Many of these studies overlap significantly with our own, and in some cases our discoveries followed or were inspired by their work. While we have focused on the small molecules disclosed in the earlier BMS patent, the Holak and Dömling groups have explored the initial small molecule series, the updated patent with more potent compounds, as well as the peptidic compounds

disclosed much earlier. However, these groups have mostly approached the field from a medicinal chemistry point of view: how do these compounds work, where do they bind, do they work on cells, etc. While they were the first group to report the induced dimerization mechanism of the BMS small molecule, as well as the first group to show their efficacy in a cellular model, they have paid relatively little attention to the oligomerization state and interactions of the proteins themselves.

The development of CA-170 by Curis/Aurigene continues apace, with preliminary results from their phase I trial indicating that the molecule has a good safety profile at high dosages and that it can increase activation of peripheral $T_c$ cells in patients with advanced solid tumours and lymphomas[329]. On the basis of these results, the company has initiated a phase II clinical trial[330].

Other than the continued development of CA-170 and the preclinical development of CA-327 (mixed PD1/TIM3 inhibitor), however, there have been no new small molecule inhibitors of either PD1 or PD-L1 reported, either in the academic literature or in patents. The field is clearly in its infancy, and creative new solutions will be required to discover new and better small molecule inhibitors.

## 4.3 Future work

### 4.3.1 Origin of apparent tryptophan agonism in ELISA assay

While the tryptophan compounds described in Chapter 2 ultimately did not have any activity in either TR-FRET or SPR assays, we still cannot rationalize why they exhibited such apparently strong agonism in the ELISA assay. Due to assay instability, we were never able to test the re-synthesized NCI 280784 in the ELISA format. It is thus impossible to know whether the aberrant activity was due to the reported structure or some impurity.

If the reported structure were actually active, its apparent ability to increase PD1/PD-L1 binding in an ELISA assay, but not TR-FRET or SPR, presents an interesting conundrum. The compound was only active when PD-L1 was deposited on the plate, as the compound did nothing when added alongside biotinylated PD1 to a blank well, although we never tested the inverse setup (blank plate with biotinylated PD-L1). The activity was therefore dependent on the presence of a specific binding event between PD1 and PD-L1. Moreover, the compound did not seem to increase HRP enzyme activity in our admittedly crude experiments. How then does the compound act?

The key difference, as far as we can see, is that while both the TR-FRET and SPR assays are carried out in buffer with no blocking protein, the ELISA plate surface is coated with inert protein – we assume it to be bovine or human serum albumin, although the kit does not specify. However, bovine and human serum albumin are *not* always inert. In fact, BSA and HSA have a well-characterized binding partner of moderate affinity: L-tryptophan$^{331-}$

[332]. If the tryptophan analogues were to bind to the blocking protein, they might act through one of two ways. One, the BSA-tryptophan complex might enhance PD1/PD-L1 binding where compound alone does not, leading to the increased signal observed. Two, the tryptophan compound might be retained by the BSA through all the wash steps, and then be present to increase the catalytic activity of the PD1-HRP complex[333]. This BSA-dependent compound retention would explain the apparently higher activity of L- over D-tryptophan (the same selectivity is seen in tryptophan binding by BSA), and justify why we were never able to reproduce the ELISA results in any other assay.

In order to probe this hypothesis, the ELISA would have to be repeated in the presence of stock NCI 280784 as well as the resynthesized compound. If the new batch were also active (regardless how noisy the assay may be), then we could validate the first hypothesis (BSA-tryptophan can enhance PD1/PD-L1) by conducting PD1/PD-L1 SPR experiments as before, except with the addition of BSA to the analyte solution. The second hypothesis (BSA retains tryptophan, which then enhances HRP activity) could be validated by performing careful enzyme kinetics studied on HRP in the presence and absence of the tryptophan derivatives (with or without BSA). In both cases, compound binding to BSA could be tested by saturation transfer difference (STD) NMR[334-335].

### 4.3.2 Oligomerization of PD-L1 on the cell surface

The state of PD-L1 oligomerization on the cell surface remains an open question. We have been able to show that PD-L1 does not form apo dimers on the cell surface, and that the

first-generation BMS compounds are very weak inhibitors of the PD1/PD-L1 interaction on the cell surface and that they also do not induce detectable dimer formation. Both we and the Holak group have shown that first-generation BMS compounds are ineffective at promoting cellular immune enhancement. The Holak group has also shown that the second-generation compounds *are* able to promote cellular immune enhancement, and that they are able to inhibit the binding of *soluble* PD-L1 to PD1-expressing cells[318]. The fundamental hole in the literature is proof that these compounds are able to inhibit the binding of cellular PD-L1 to PD1, and that they do so by induction of dimer formation.

We have tried to study this phenomenon by covalent crosslinking, but were thwarted by two issues. First, the compounds we were using (the first generation BMS compounds) were clearly not potent enough to induce any kind of PD1/PD-L1 inhibition in cellular contexts. We would therefore need to synthesize and study second generation compounds, like those in the latest Holak papers[243, 318]. Second, we did not have a rigorous assay for oligomerization, with clear negative and positive outcomes. The more systematic and unambiguous method to determine protein homooligomerization (though also the most technically challenging) is cellular FRET. Cells expressing PD-L1 bearing two different fluorophores that form a FRET pair would show no FRET response when the proteins are monomeric. In the presence of a ligand that induces dimerization or proximity (a bivalent antibody or a BMS compound), at least some of the complexes should contain one each of the two fluorophore-labelled PD-L1 molecules. The FRET signal can then be detected.

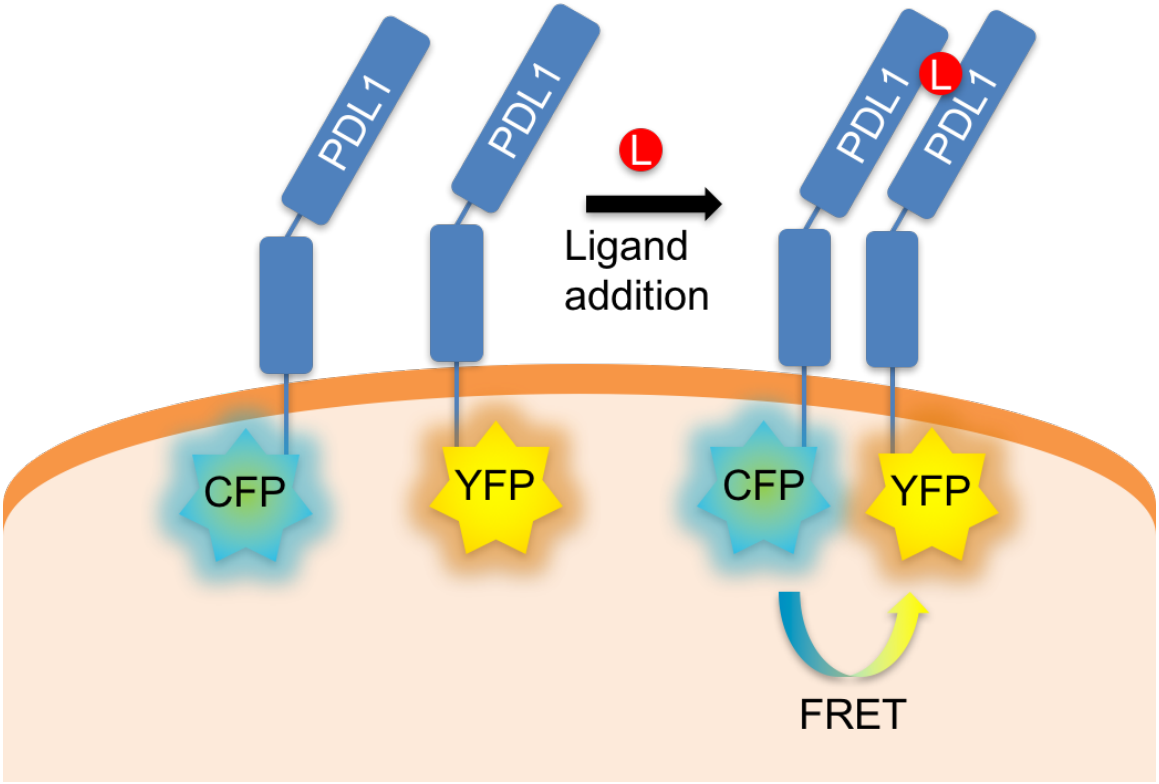


**Figure 57: FRET signal between mixed populations of PD-L1-CFP and PD-L1-YFP fusion proteins.**

Since we have already shown that it is possible to express GFP-labelled PD-L1 in HEK293 cells, and that these cells have no detectable endogenous PD-L1 expression, we could create a PD-L1–CFP HEK293 cell line by stable transfection. Some small number of cells will incorporate transfected DNA into their genomes; culturing transfected cells with a selective antibiotic over several weeks will eventually select for the stably transfected cells (non-incorporated plasmids eventually stop propagating). With a stable PD-L1–CFP-expressing cell line in hand, transient transfection with YFP-tagged PD-L1 would provide the mixed-fluorophore system needed to carry out FRET measurements[336-338].

### 4.3.3 Investigation of the mechanism of action of the Aurigene compounds

While both the Holak group and our own group have studied the BMS compounds in depth, there have been no reports of any kind on the mechanism of action of the Aurigene small molecule compounds. These molecules are in many ways more interesting than the BMS compounds. For one, they have shown efficacy in various preclinical animal models, and are apparently showing efficacy in actual humans[329]. Moreover, these compounds are reported to inhibit both PD-L1 and VISTA, despite the fact that VISTA has not been reported to bind PD1. Most importantly, according to our current knowledge of PD1 and PD-L1 and their interactions and structures, these compounds *should not work.* The sequences of PD1 from which they are derived do not form any part of the PD-L1-binding surface. The pared-down structures of their heterocyclic compounds contain the sidechains of only three amino acids – a tiny motif compared to the large peptides and molecules previously shown to inhibit the PD-L1 binding surface. Most importantly, preliminary work from our group has shown that these compounds do not actually inhibit the direct interaction of PD1 with PD-L1 (unpublished data). Nevertheless, these compounds show impressive PD1-dependent activation of immune cells and tumour clearance. Clearly, they must work. And given that their activity is PD1/PD-L1-dependent, and that they are derived from peptides based on the PD1 sequence, the most plausible mechanism of action is that they bind some other protein involved in PD1/PD-L1 signaling, either alone or as a ternary complex with PD1 or PD-L1. In addition, these compounds were derived from long, linear, cell-impermeable peptides, making it unlikely that they hit some intracellular target.

Since there is no way to know which protein these compounds bind to, or even what third partner (if one exists) is necessary, protein NMR would be of limited value. It would be impossible to isotopically label all possible binding partners, and even the spectra of PD-L1 could become complex in a mixture of proteins. However, ligand-observed NMR would provide a good method of determining the protein binding partner. Synthesis of a fluorinated Aurigene compound would provide an NMR handle, and changes in fluorine chemical shift and line width would indicate binding by exogenous unlabelled protein[339-341]. This would allow for rapid screening of protein mixtures and simple spectral changes to interpret.

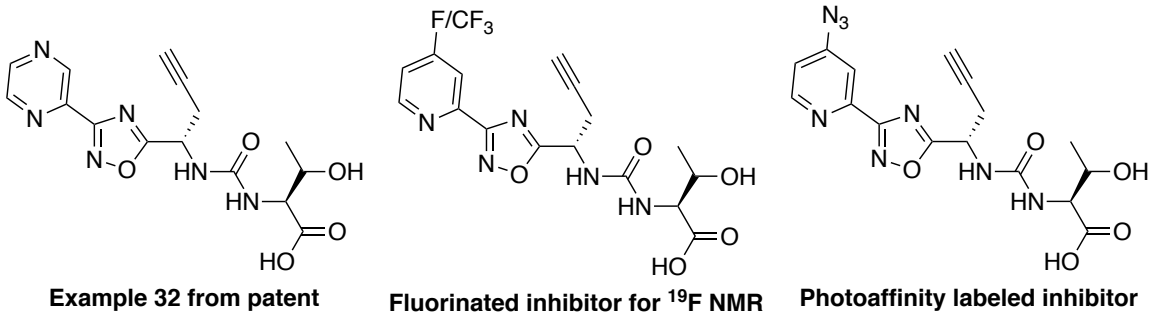


**Figure 58: Example of heterocyclic Aurigene compound containing an alkyne, with proposed fluorinated and photoaffinity tool compounds.**

In addition to ligand-observed NMR, photocrosslinking could provide an additional way of determining the binding partner of these compounds. The latest patent already includes small heterocyclic compounds containing alkynes and electron-deficient pyridine rings[342]. If the pyridine were modified to an electron-deficient azidopyridine, this molecule would contain both a photoaffinity label that would permit covalent bond formation to nearby proteins on irradiation, as well as an alkyne for click chemistry to biotin-azide and streptavidin pulldown. Irradiation of this molecule in a cell lysate (or even on a cell surface)

would link the molecule to the protein binding partner, and the pulldown would allow identification of that protein through mass spectrometry-based sequencing. These studies would be complemented by protein crosslinking in the presence of compound, followed by pulldown of the complex.

### 4.3.4 Tethering for the discovery of new PD1/PD-L1 inhibitor fragments

One of the issues we faced in our screening campaign was the necessity of testing our compounds at high concentrations. We did not expect to find potent binders in our initial screen, so inhibitory fragments with low potency would only be detected at high concentrations. However, these high concentrations amplified the problems of assay interference mechanisms and insolubility. Indeed, many of the compounds we tested formed suspensions in our assay wells.

One method of reducing compound concentration in screening campaigns is to artificially increase the affinity of the compound for the protein through covalent tethering[326, 343]. A free cysteine is introduced into the protein near the intended binding site. Next, a library of thiol-containing fragments is incubated with the protein under conditions which favour disulfide exchange. Fragments that possess an intrinsic affinity for the protein will form disulfides preferentially because the thermodynamic stability of protein binding plus disulfide formation combined is greater than the thermodynamic stability gained by disulfide formation alone. The reaction is then quenched, and the protein subjected to mass spectrometry (either as a whole or after proteolysis) to determine the molecular weight (and

thus the identity) of the bound fragment. The strength and specificity of apparent hits could be determined by incubation of a single thiol conjugate with PD1 under increasing concentrations of a reductant or disulfide competitor, such as ß-mercaptoethanol. Maintenance of labelling in the presence of the ß-mercaptoethanol would indicate that complex (and disulfide) formation is energetically favourable compared to reduction.

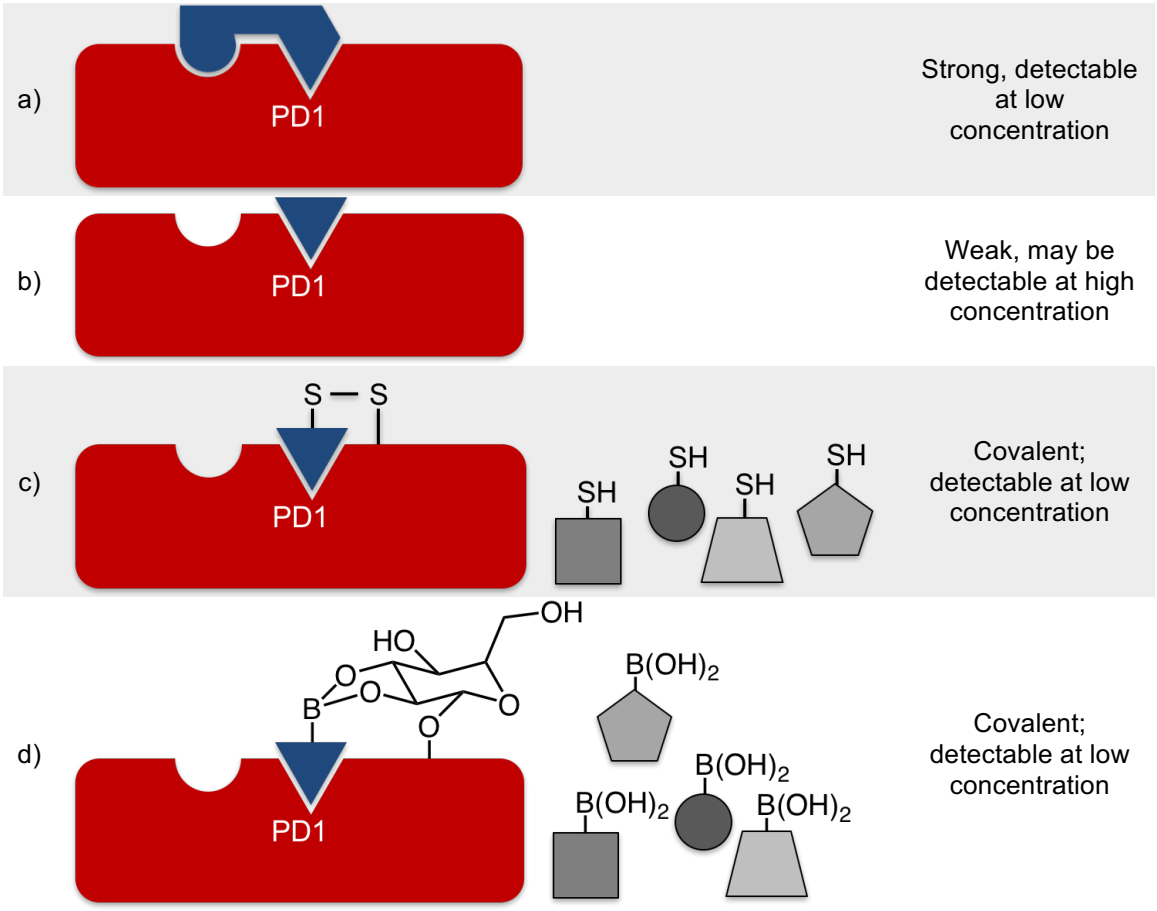


**Figure 59: Protein tethering to enable dynamic covalent chemistry for fragment screening. a) Screening for high-affinity binders. b) Screening for fragment binders. c) Disulfide-tethered fragment screening. d) Boronate-tethered fragment screening.**

This technology could be used to find fragments that bind to either PD1 or PD-L1. For PD1, Asn74 provides a convenient handle for cysteine mutation. It is positioned proximal

to both the PD-L1 binding surface as well as the computationally discovered allosteric site for C`C`` loop inhibition. Moreover, Asn74 is N-glycosylated in the native protein, so the sidechain itself is unlikely to be important for intra- or inter-molecular interactions in folding or PD-L1 binding. For PD-L1, Ala132 is positioned at the floor of the hinge groove; mutation to a cysteine would then place the thiol tether right at the terminus of the groove. Meanwhile, Gly33 is position just above the other end of the hinge groove, providing a convenient handle on the other half of the hinge.

a)

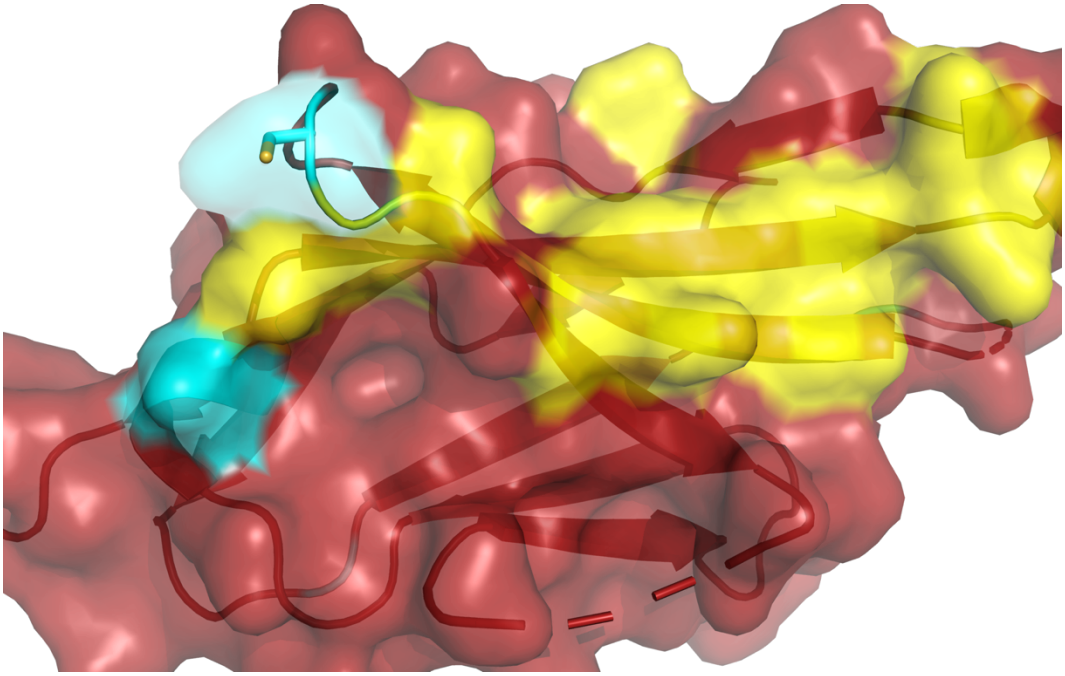

b)

c)

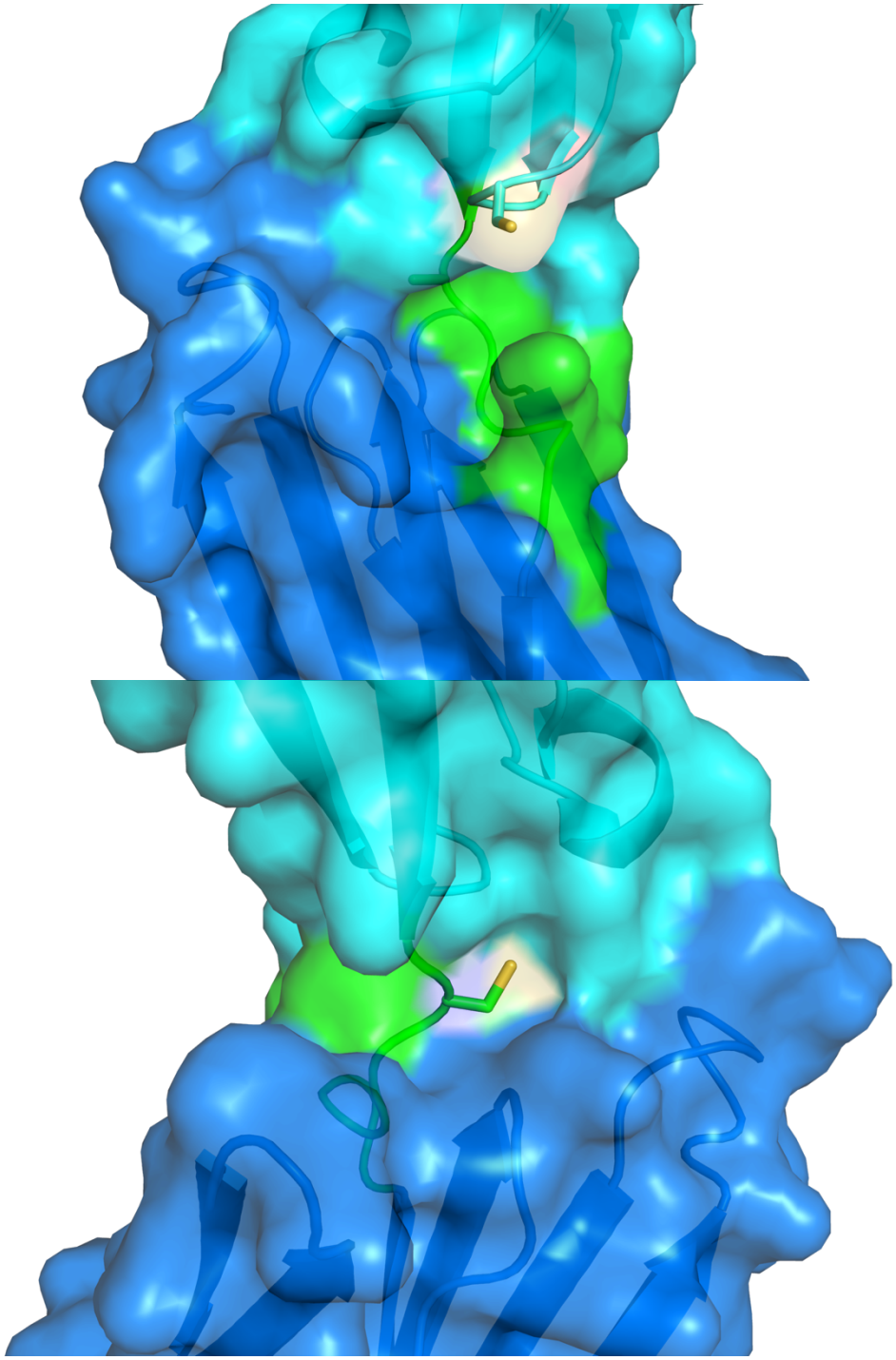

**Figure 60: Cysteine mutations for disulfide-tethered compound screening. a) Asn74 to Cys on PD1 places a cysteine proximal to the PD-L1 binding face (yellow) and the C`C`` pocket. b) Gly32 to Cys places a cysteine at one end of the hinge groove (green). c) Ala132 to Cys places a cysteine at the other end of the hinge groove (green). PD1 in red (PDB: 3RRQ); PD-L1 IgV in cyan, IgC in dark blue (PDB: 3BIS).**

The central positioning of Asn74 in PD1 also presents an opportunity to expand the scope of fragment tethering in drug discovery. As mentioned, Asn74 is one of the main sites of N-linked glycosylation on PD1. While disulfides are the most commonly used exchangeable covalent bond used for ligand tethering, the reversible covalent bond between boronic acids and diols has also been used in the context of glucose sensing and glycan affinity chromatography[344-346]. If a PD1 construct where all other glycosylation sites other than Asn74 have been mutated were expressed in mammalian cells, only Asn74 would contain glycans available for boronic acid binding. Exposure of this protein to a library of substituted boronic acids would function the same way as the disulfide tethering, where fragments with some affinity for PD1 would preferentially form glycan boronates. Mass spectrometry of the complex would then provide the molecular weight of the bound fragment. The advantage of boronic acid tethering is threefold. First, boronic acids tend to be water-soluble, decreasing the likelihood of fragment precipitation. Second, the glycan is part of the native protein as expressed on the cell surface; fragments from this boronic acid screen are therefore far more likely to bind the native protein than fragments tested on purified, deglycosylated protein. Third, while the boronic acid is merely a tether, it could conceivably be retained in a final inhibitor structure. PD1 is expressed on the cell surface, so membrane permeability is not a limiting factor, and glycan binding may compensate for otherwise weak binding.

### 4.3.6 Prospects for small molecule screening and studies of known inhibitors

Ultimately, our own efforts to find new inhibitors of the PD1/PD-L1 interaction were not successful. Moreover, our screening did not even uncover fragments that possessed binding affinity to PD1 or PD-L1 (as far as we know). Any renewed efforts to discover novel small molecule inhibitors of this interaction would receive no advantage from our previous screening work, and would be starting from scratch.

Our understanding of PD1/PD-L1 inhibition by small molecules has advanced remarkably in the past 4 years; we have gone from no reported small molecules, to a few known small molecules with no target or mechanism of action, to a full mechanistic understanding and *in vitro* validation of the BMS compounds (albeit without proof of cell-surface dimerization). However, the BMS compounds and the Aurigene compounds are the only small molecule inhibitors of PD1/PD-L1 known to date. Thus, both our efforts, and the efforts of every other research group interested in PD1/PD-L1 have been focused on the same small group of molecules with unusual mechanisms of action. If any general conclusions are to be drawn about the design of PD1/PD-L1 inhibitors, or immunoreceptor inhibitors in general, new inhibitor scaffolds must be discovered.

# Chapter 5

This chapter comprises the experimental procedures used, as well as the characterization data for new compounds.

## 5.1 General experimental remarks

### 5.1.1 Synthetic chemistry

All reactions were performed in oven- or flame-dried glassware fitted with a rubber septum, under a positive pressure of argon, unless otherwise indicated. All solvents and reagents were used as received unless otherwise indicated. Reagents or solvents denoted as "dry" were purified as follows: dichloromethane and acetonitrile were stored over activated 4 Å molecular sieves; tetrahydrofuran was distilled over sodium and benzophenone; benzene and triethylamine were distilled over calcium hydride; methanol and ethanol were distilled over magnesium ribbon; diethyl ether and toluene were passed over a column of alumina in a commercial solvent purification system (SPS). Liquid reagents and solvents were transferred using either glass or rubber-free plastic syringes fitted with stainless steel needles. Organic solutions were concentrated between 35–40 ˚C by rotary evaporation under vacuum. Analytical thin-layer chromatography (TLC) was performed using aluminum plates pre-coated with silica gel (0.20mm, 60 Å pore-size, 230-400 mesh, Macherey-Nagel) impregnated with a fluorescent indicator (254 nm). TLC plates were visualized by exposure to ultraviolet light followed by staining with potassium. Flash-column chromatography was performed over either silica gel 60 (SiliCycle, 40-63 μM) or Florisil (standard grade, 100-200 mesh, Caledon).

All reagents were reagent grade or better, and purchased from Sigma Aldrich, Alfa Aesar, ChemImpex, or Caledon Labs.

Nuclear magnetic resonance (NMR) spectra were recorded on either a Bruker AV300 (300 MHz) or Bruker Avance 500 (500 MHz) spectrometer as indicated. Proton ($^{1}H$) chemical shifts are reported in parts per million (ppm, δ scale) downfield from tetramethylsilane, and are referenced to residual protium in the NMR solvent ($CDCl_3$, δ 7.26; $CD_3C(O)CD_3$, δ 2.05; $CD_3OD$, 3.31; $CD_3S(O)CD_3$, 2.50; $D_2O$, 4.79). Data are represented as follows: chemical shift, multiplicity (s = singlet, d = doublet, t = triplet, q = quartet, m = multiplet and/or multiple resonances, br = broad, app = apparent), coupling constant in Hertz (Hz), and integration. Likewise, carbon ($^{13}C$) chemical shifts are reported in parts per million downfield from tetramethylsilane and are referenced to the carbon resonances of the solvent ($CDCl_3$, δ 77.22; $CD_3C(O)CD_3$, δ 29.85; $CD_3OD$, 49.00; $CD_3S(O)CD_3$, 39.52). Infrared (IR) spectra were obtained using a Perkin Elmer Spectrum Two spectrometer fitter with an attenuated total internal reflectance (ATR) attachment, referenced to a polystyrene standard with an air background. Diagnostic peaks are represented as follows: frequency of absorption (cm–1). HR-ESI-MS data was obtained using a Thermo Scientific Exactive system. Microwave reactions were performed using a Biotage Initiator.

The following buffer compositions were used:

Phosphate-buffered saline ("PBS"): 10 mM sodium/potassium phosphate pH 7.4, 137.5 mM NaCl, 2.75 mM KCl

Whole cell lysis buffer ("lysis buffer"): 50 mM Tris pH 8.0, 150 mM NaCl, 1.0% Triton-X100, 0.5% sodium deoxycholate, 0.1% SDS, 5 mM EDTA. Supplemented with protease inhibitors immediately prior to use.

Tris-buffered saline ("TBS"): 50 mM Tris pH 8.0, 150 mM NaCl

Tris-buffered saline + Tween-20 ("TBS-T"): TBS with 0.05% Tween-20

Live cell imaging solution: 20 mM HEPES pH 7.4, 140 mM NaCl, 2.5 mM KCl, 1.8 mM $CaCl_2$, 1.0 mM $MgCl_2$

### 5.1.2 Materials and instrumentation for *in vitro* biological assays

Test chemicals were either sourced from the National Cancer Institute's Developmental Therapeutics Program (any compound with the "NCI" prefix) or purchased from eMolecules. Tryptophan methyl ester hydrochloride, salicylic acid, and p-aminosalicylic acid was purchased from Sigma Aldrich, while tryptophan ethyl ester hydrochloride and tryptophan benzyl ester hydrochloride were purchased from ChemImpex.

SYPRO Orange was purchased from ThermoFisher. ELISA assay kits were purchased from BPS Bioscience: PD-1[Biotinylated]:PD-L1 Inhibitor Screening Assay Kit (catalog #72005) and PD-1:PD-L1[Biotinylated] Inhibitor Screening Assay Kit (catalog #72003). TR-FRET kits were purchased from BPS Bioscience: PD-1:PD-L2 TR-FRET Assay Kit (catalog #72012).

For thermal shift assays, full-length PD-L1 was produced in insect cell lines and was a generous gift from Dr. Martin Boulanger. For SPR assays, initial experiments were conducted with PD-L1-FLAG from BPS Bioscience (catalog #71183). Later experiments were performed using the IgV domain of PD-L1 produced in *E. coli* and refolded by slow dilution (courtesy of Kayleigh Walker and Dr. Mark Carr). In all cases, biotinylated proteins were sourced from BPS Bioscience: PD-1 (CD279), Fc fusion, Biotin-labeled (Human) HiP™ (catalog #71109) and PD-L1 (CD274), Fc fusion, Biotin-labeled (Human) HiP™ (catalog #71105).

The antibody used in ELISA and SPR experiments was purchased from BPS Bioscience: Anti-PD-L1 (CD274) Neutralizing Antibody (catalog #71213).

All plate-based absorbance, fluorescence, and luminescence readings (with the exception of thermal shift experiments) were taken on a Spectra Max M5 plate reader. Thermal shift assays were performed in a StepOnePlus Real-Time PCR system. Surface plasmon resonance measurements were taken on a Biacore X100 from GE Healthcare. All associated Biacore components (chips, buffers, etc) were also purchased from GE.

### 5.1.3 Materials and instrumentation for cell-based experiments

Media and reagents were purchased from ThermoFisher, Sigma Aldrich, or QIAGEN. $BS^3$ and DTSSP were purchased from ThermoFisher. The rabbit polyclonal anti-PD-L1

antibody (PA5-20343) and goat anti-rabbit HRP-conjugated secondary antibody (A16110) were also purchased from ThermoFisher. Protease inhibitor cocktail was purchased from Roche.

Live Cell Imaging solution was purchased from ThermoFisher (catalog # A14291DJ). Hoescht 33342 was purchased from Sigma Aldrich.

Cell cultures were generated from low passage number seed stocks stored in vapour-phase nitrogen between -140 and -180 ˚C. Stocks were generated by suspending $1x10^6$ cells in 1 mL of media supplemented with 10% DMSO as cryoprotectant, aliquoting into cryovials, and cooling to -80 ˚C in a Mr. Frosty freezing container filled with isopropanol before transferring to nitrogen vapour phase storage.

The MDA-MB-231 cell line was a generous gift from Dr. Matt Moffitt, while the HEK293 cell line was a generous gift from Dr. Chris Nelson.

Cells were cultured in DMEM/F12 Ham media supplemented with 10% fetal bovine serum, and incubated at 37˚C and 5% $CO_2$. T25 and T75 vented culture flasks from Sarstedt were used for routine culture maintenance. Cells were passaged at ~80% confluence by aspiration of spent media, dissociation with Trypsin-EDTA (0.05%), quenching of trypsin with fresh media and seeding fresh media at a 1:6 to 1:10 split ratio. Cells seeded for experiments were spun down at 1000 x *g* after trypsin quenching, the supernatant aspirated,

and cell pellet suspended in fresh media, in order to prevent trypsin or EDTA contamination of the experimental culture.

Confluence was estimated by bright-field microscope; cell counting was done by dilution of fully dissociated cultures into buffered Trypan Blue and counting on a hemocytometer. Cellular imaging was performed using a Cytation 5 instrument.

## 5.2 Procedures and characterization for Chapter 2

### 5.2.1 Guanidinium chloride denaturation assay

A 2X stock solution of 8 μM PD-L1 was made up in PBS with 0.5% DMSO. A separate 2X stock solution consisting of 1 mM test compound, SYPRO Orange (diluted 1/100 from the received solution), and 0, 1 mM, or 1.5 mM guanidinium chloride in PBS at a DMSO concentration of 0.5%. To each well of a 384-well plate was added 10 μL of the PD-L1 stock solution and 10 μL of the guanidinium chloride/compound/SYPRO Orange solution. The plate was spun down at 3750 rpm for 5 minutes, then sealed and incubated at room temperature for 30 minutes. Fluorescence readings at 570 nm were then taken (excitation at 480 nm, cutoff at 515 nm).

### 5.2.2 Thermal shift assay

To a qPCR low-volume 96-well plate was added PD-L1, SYPRO Orange, and test compound in PBS + 1% DMSO to the following final concentrations: 0.1 mg / mL PD-L1 and 1/1000 dilution of SYPRO Orange. The plate was sealed and placed in the RT-PCR system. The temperature was ramped from 25˚C to 99˚C at a rate of either 0.5˚ / minute or 1˚ / minute while monitoring the fluorescence in the "ROX" channel.

### 5.2.3 ELISA assays

Assays were performed per the manufacturer protocol[287, 297].

### 5.2.4 TR-FRET assays

Assays were performed per the manufacturer protocol[298].

### 5.2.5 Biacore assays

All assays were performed on a Biacore X100 instrument. 1X HBS-EP+ was used as the running buffer (10 mM HEPES pH 7.4, 150 mM NaCl, 3 mM EDTA, 0.05% P20), and was passed through a 0.45 μm filter prior to use. The running buffer was not adjusted to maintain a constant DMSO concentration, however all test samples were. All samples were centrifuged or filtered through a 0.45 μm filter prior to use. All measurements were taken within a week of chip immobilization; when not in use, the chip was stored in a dry 50 mL conical tube at 4˚C.

*Immobilization*

A stock solution of 110 nM PD1-biotin was made up in running buffer without concern for buffer exchange. A streptavidin (SA) chip was docked into the instrument, and the standard biotin–SA immobilization protocol followed. The ligand was injected in pulses until an immobilization value of 2000 ± 50 RU was reached on flow cell 2, while flow cell 1 was no conjugated at all and served as a reference cell.

*Sample run*

A 2X stock solution of PD-L1 was made by dilution into running buffer. A 2X stock of each compound was also made up by dilution, keeping the concentration of DMSO constant for each sample. The compound solutions were then added to the PD-L1 stock solution, and diluted serially to maintain a constant concentration of PD-L1. 105 μL of each mixture was run over the chip at a flow rate of 30 μL/min for 2 minutes, followed by a dissociation time of 10 minutes in running buffer (no regeneration steps were taken). Equilibrium binding was calculated by substracting the baseline reading before injection as well as the binding value from flow cell 1.

### 5.2.6 Synthetic chemistry

**General procedure A for the Claisen condensation of acetophenones with dimethyl oxalate**: to a flask was added the acetophenone (1 equivalent), dimethyl oxalate (1.3 equivalents), and dry toluene (5 mL per equivalent). This was set to stir vigorously, and potassium *tert*-butoxide (1 M in THF, 1.25 equivalents) was added dropwise. The colour changed several times, from deep green to bright yellow, and a thick precipitate formed,

necessitating vigorous stirring. After stirring for 24 hours at room temperature, the mixture was acidified with aqueous HCl (1 M, 1.5 equivalents) and stirred for 1 hour. The mixture was extracted thrice with toluene, and the combined organic layers were washed once with distilled water, once with brine, dried over $Na_2SO_4$, filtered, and concentrated to a beige or yellow solid. Recrystallization from boiling hexanes provided the aryl diketoester as a green, yellow, or beige solid (predominantly in the enol form).

**General procedure B for pyrazole formation from aryl diketoesters**: a solution of the diketoester (1 equivalent) was added to a flask with isopropyl alcohol (5 mL per equivalent) and glacial acetic acid (1 mL per equivalent). Then hydrazine hydrate (8.8 equivalents) was added dropwise, accompanied by evolution of gas or mist. The reaction was then heated to 60˚C over 24 hours. The solution was cooled, and the solvents removed by rotary evaporation. Distilled water was added, and the mixture stirred vigorously at room temperature for 2 to 3 hours. The fine white/tan precipitate was filtered off and dried to provide the aryl pyrazole methyl ester as a white or off-white powder.

**General procedure C for methyl ester hydrolysis**: to a flask was added aryl pyrazole methyl ester (1 equivalent) and aqueous potassium hydroxide (0.45 M, 3.3 equivalents). The reaction was heated to reflux for 1 hour, then cooled to room temperature and adjusted to pH 1 with 15% hydrochloric acid. The solid that precipitated upon acidification was filtered off and dried to provide the aryl pyrazole carboxylate as a white powder.

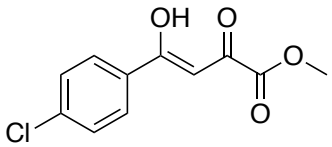


**RH2.1**

Prepared according to general procedure A. Faint green powder (3.54 g, 75%).

$^1$H NMR (300 MHz, $d_6$-DMSO) – mixture of keto and enol tautomers ∂ 7.85 (d, *J* = 8.4 Hz, 2H), 7.47 (d, *J* = 8.4 Hz, 2H), 3.66 (s, 3H)

7.78 (br d, *J* = 7.6 Hz, 2H), 7.43 (br d, *J* = 7.6 Hz, 2H), 6.29 (br s, 1H)

IR (neat, $cm^{-1}$) 2961, 1731, 1614, 1590, 1571, 1516, 1477, 1434, 1248, 1091, 1010, 760

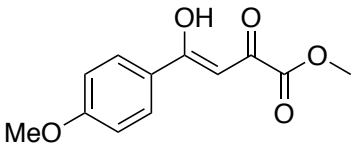


**RH2.2**

Prepared according to general procedure A. Beige powder (2.69 g, 75%).

$^1$H NMR (300 MHz, $CDCl_3$) ∂ 7.96 (d, *J* = 8.8 Hz, 2H), 7.00 (br s, 1H), 6.95 (d, *J* = 8.8 Hz, 2H), 3.90 (s, 3H), 3.86 (s, 3H)

IR (neat, $cm^{-1}$) 1753, 1743, 1595, 1430, 1249, 1170, 1131, 1117, 1017, 967, 776

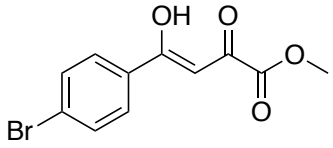


**RH2.3**

Prepared according to general procedure A. Yellow powder (2.7 g, 75%).

$^1$H NMR (300 MHz, $d_6$-acetone) ∂ 8.05 (d, *J* = 8.6 Hz, 2H), 7.79 (d, *J* = 8.6 Hz, 2H), 7.14 (s, 1H), 3.92 (s, 3H)

$^{13}$C NMR (77 MHz, $CDCl_3$) ∂ 190.8, 170.8, 162.9, 134.9, 133.2, 130.6, 129.3, 98.7, 53.4

IR (neat, $cm^{-1}$) 2957, 1729, 1583 br, 1434, 1273 br, 768, 464

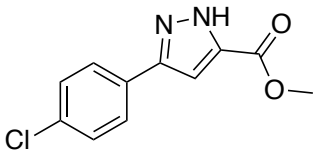

**RH2.4**

Prepared according to general procedure B. White solid (405 mg, 34%).

$^1$H NMR (300 MHz, $d_6$-DMSO) ∂ 7.89 (d, *J* = 8.7 Hz, 2H), 7.50 (d, *J* = 8.7 Hz, 2H), 7.31 (s, 1H), 3.84 (s, 3H)

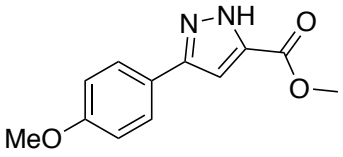

**RH2.5**

Prepared according to general procedure B. White solid (910 mg, 79%).

$^1$H NMR (300 MHz, $d_6$-acetone) ∂ 12.95 (br s, 1H), 7.82 (d, *J* = 8.8 Hz, 2H), 7.12 (s, 1H), 7.03 (d, *J* = 8.8 Hz, 2H), 3.88 (s, 3H), 3.85 (s, 3H)

$^{13}$C NMR (77 MHz, $d_6$-acetone) ∂ 160.9, 127.7, 115.1, 105.3, 55.6, 52.0

IR (neat, cm$^{-1}$) 3228, 1695, 1495, 1268, 1251, 1186, 1027, 1002, 838, 814, 774

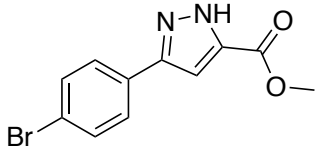

**RH2.6**

Prepared according to general procedure B. Yellow powder (1.32 g, 94%).

$^1$H NMR (300 MHz, $CDCl_3$) ∂ 7.65 (d, *J* = 8.5 Hz, 2H), 7.56 (d, *J* = 8.5 Hz, 2H), 7.11 (s, 1H), 3.96 (s, 3H)

IR (neat, cm$^{-1}$) 3135, 1729, 1484, 1240, 1008, 822, 779, 712, 501

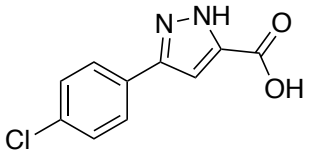

**RH2.7**

Prepared according to general procedure C. White powder (291 mg, quantitative).

$^{1}$H NMR (300 MHz, $d_6$-acetone) $\partial$ 7.94 (d, $J$ = 8.5 Hz, 2H), 7.49 (d, $J$ = 8.5Hz, 2H), 7.27 (s, 1H)

$^{13}$C NMR (77 MHz, $d_6$-acetone) $\partial$ 161.2, 150.0, 138.9, 134.2, 132.0, 129.7, 128.0, 106.5

IR (neat, cm$^{-1}$) 3270, 1684, 1491, 1271, 1256, 1099, 1007, 816, 771, 733, 499

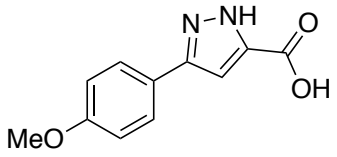

**RH2.8**

Prepared according to general procedure C. White powder (740 mg, 84%).

$^{1}$H NMR (300 MHz, $d_6$-DMSO) $\partial$ 7.75 (d, $J$ = 8.8 Hz, 2H), 7.07 (s, 1H), 6.98 (d, $J$ = 8.8 Hz, 2H), 3.77 (s, 3H)

$^{13}$C NMR (77 MHz, $CDCl_3$) $\partial$ 162.0, 159.2, 126.6, 114.2, 104.3, 55.1

IR (neat, cm$^{-1}$) 3251, 1679, 1501, 1248, 1184, 1028, 1006, 955, 816, 768

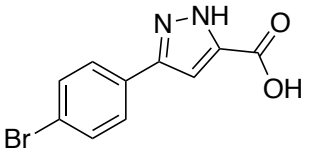

**RH2.9**

Prepared according to general procedure C. White powder (222 mg, quantitative).

$^{1}$H NMR (300 MHz, $d_6$-acetone) $\partial$ 7.88 (d, $J$ = 8.6 Hz, 2H), 7.63 (d, $J$ = 8.6 Hz, 2H), 7.28 (s, 1H)

$^{13}$C NMR (77 MHz, $d_6$-acetone) $\partial$ 161.2, 150.1, 138.9, 132.7, 132.4, 128.2, 122.3, 106.5

IR (neat, $cm^{-1}$) 3270, 1684, 1487, 1269, 1254, 1077, 1007, 961, 812, 771, 715, 496

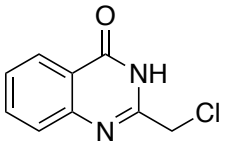


**RH2.10**

An HCl generator was set up, whereby concentrated $H_2SO_4$ is slowly added from a stoppered pressure-equalizing addition funnel to a two-necked flask containing sodium chloride. The side arm of the two-necked flask is connected to a rubber hose packed with $CaCl_2$ and connected to a pipette. To an oven-dried Schlenk tube was added 26 mL of dry 1,4-dioxane. The pipette from the gas generator was inserted below the surface of the dioxane, and HCl gas was bubbled through at room temperature with vigorous stirring for 1 hour. The gas generator was then disconnected, and the dioxane solution of HCl cooled in an ice/water bath. Chloroacetonitrile (3.2 mL, 50 mmol) and methyl anthranilate (3.2 mL, 25 mmol) were added consecutively, and a slight white precipitate was formed. The solution was brought back to room temperature, whereupon the solid dissolved to yield a pale straw-coloured solution, and stirred overnight. The reaction mixture was poured into 200 mL of ice water, then neutralized to pH 7 with aqueous ammonium hydroxide (2 M). The white precipitate that was formed was filtered and dried to yield the product as a white powder (4.67 g, 97%).

$^1$H NMR (300 MHz, $d_6$-DMSO) $\partial$ 12.52 (br s, 1H), 8.11 (ddd, $J$ = 8.0, 1.5, 0.5 Hz, 1H), 7.82 (ddd, $J$ = 8.0, 7.2, 1.5 Hz, H), 7.66 (d, $J$ = 8.0 Hz, 1H), 7.53 (ddd, $J$ = 8.0, 7.2, 1.3 Hz, 1H), 4.54 (s, 2H)

$^{13}$C NMR (77 MHz, $d_6$-DMSO) $\partial$ 161.5, 152.3, 148.2, 134.6, 127.2 (2), 125.8, 121.2, 43.2

HRMS (ESI) calc'd for $C_9H_7ClN_2O$ (M+H) 195.03199, found 195.03227.

IR (neat, $cm^{-1}$) 2888, 2811, 1683, 1609, 1468, 777, 756

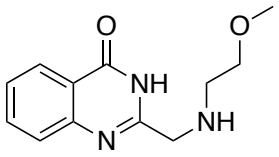

**RH2.11**

To an oven-dried microwave vial was added **RH2.10** (584 mg, 3 mmol), 2-methoxyethylamine (2.6 mL, 30 mmol), $K_2CO_3$ (842 mg, 6 mmol), a crystal of KI, and 6 mL of dry acetonitrile. The reaction was heated to 90˚C for 6 hours in a microwave reactor. The reaction was cooled and diluted with 25 mL of distilled water, and the aqueous layer adjusted to pH 7 with 15% aqueous HCl. The reaction mixture was then extracted with three 50 mL portions of ethyl acetate, and the combined organic layers were washed with 25 mL water, 25 mL saturated ammonium chloride, and 25 mL of brine, then dried over $Na_2SO_4$, filtered, and concentrated to a yellow oil. Silica gel chromatography (69:30:1 ether/acetonitrile/triethylamine) provided the product as an off-white solid (340 mg, 48%).

$^1$H NMR (300 MHz, $CDCl_3$) $\partial$ 8.27 (dd, $J$ = 8, 1.5 Hz, 1H), 7.74 (ddd, $J$ = 8.2, 7.1, 1.5 Hz, 1H), 7.64 (dd, $J$ = 8.2, 0.8 Hz, 1H), 7.45 (ddd, $J$ = 8.2, 7.1, 1.3 Hz, 1H), 3.89 (s, 2H), 3.51 (dd, $J$ = 5.3, 4.4 Hz, 1H), 3.38 (s, 3H), 2.85 (dd, $J$ = 5.3, 4.4 Hz, 2H)

$^{13}$C NMR (77 MHz, $CDCl_3$) $\partial$ 161.8, 155.2, 149.1, 134.6, 126.9, 126.6, 126.4, 121.6, 71.5, 58.9, 51.1, 49.2

IR (neat, $cm^{-1}$) 3342, 2879, 1669, 1616, 1452, 1115, 773

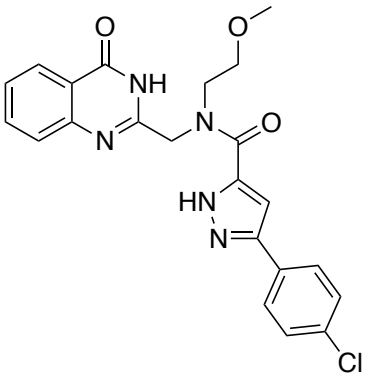

**RH2.12**

To a flask was added **RH2.7** (35 mg, 0.15 mmol), **RH2.11** (34 mg, 0.15 mmol), EDC•HCl (43 mg, 0.23 mmol), triethylamine (52 µL, 0.38 mmol), HOBt hydrate (37 mg, 0.23 mmol), and 1.5 mL of dry DMF. The reaction was stirred at room temperature for 2 days, then the DMF was removed under reduced pressure. The residue was triturated with 10 mL water (aided by sonication), and the precipitate was filtered off and recrystallized from minimal ethanol to yield the product as white crystals (41 mg, 62%).

$^{1}$H NMR (300 MHz, $d_6$-DMSO) ∂ 8.08 (d, $J$ = 8.0 Hz, 1H), 7.80-7.91 (m, 1H), 7.69-7.80 (m, 2H), 7.40-7.61 (m, 4H), 7.13 (s, 1H), 5.05 (br s, 1H), 4.64 (s, 1H), 3.65-3.81 (m, 2H), 3.60 (t, $J$ = 4.9 Hz, 1H), 3.11-3.27 (m, 3H)

$^{13}$C NMR (77 MHz, $d_6$-DMSO) ∂ 161.5, 148.5, 134.3, 129.0, 126.9, 126.2, 125.7, 121.1, 69.8, 58.1, 56.0, 49.2

IR (neat, cm$^{-1}$) 3210, 2918, 1666, 1596, 1489, 1085, 965, 776, 761, 501

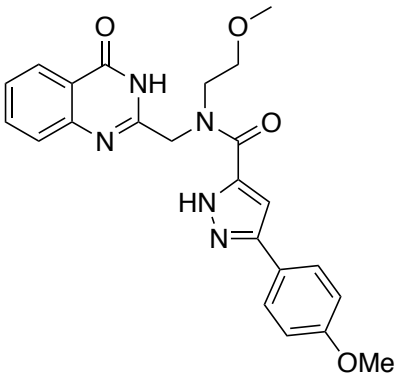


**RH2.13**

To a flask was added **RH2.8** (109 mg, 0.5 mmol), **RH2.11** (117 mg, 0.5 mmol), EDC•HCl (115 mg, 0.6 mmol), triethylamine (175 µL, 1.25 mmol), HOBt (81 mg, 0.6 mmol), and 5 mL of dry DMF. The reaction was stirred at room temperature for 2 days, then the DMF was removed under reduced pressure. The residue was diluted with water and extracted exhaustively with mixtures of DCM and methanol, dried over $Na_2SO_4$, filtered, and concentrated to a residue. Silica gel chromatography (methanol in DCM) yielded the product as a yellow solid (151 mg, 70%).

$^1$H NMR (300 MHz, $CDCl_3$ + $d_4$-MeOD) $\partial$ 8.24 (d, $J$ = 8.0 Hz, 1H), 7.67-7.80 (m, 2H), 7.55 (d, $J$ = 8.7 Hz, 2H), 7.48 (ddd, $J$ = 8.1, 6.8, 1.4 Hz, 1H), 6.94 (d, $J$ = 8.7 Hz, 2H), 6.91 (s, 1H), 4.78 (s, 2H), 3.80 (s, 3H), 3.72 (br s, 2H), 3.64 (t, $J$ = 5.0 Hz, 2H), 3.22 (s, 3H)

$^{13}$C NMR (77 MHz, $CDCl_3$ + $d_4$-MeOD) $\partial$ 160.2, 152.5, 148.6, 134.8, 127.4, 127.2, 127.0, 126.3, 121.4, 114.5, 104.5, 77.2, 70.1, 58.7, 55.3, 53.9

IR (neat, $cm^{-1}$) 3200, 3152, 2933, 1674, 1606, 1500, 1467, 1253, 1110, 1026, 808, 766, 759

HRMS (ESI) calc'd for $C_{23}H_{23}N_5O_4$ (M+H) 434.18230, found 434.18203.

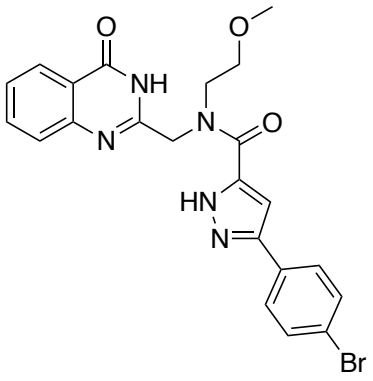

**RH2.14**

To a flask was added **RH2.9** (40 mg, 0.15 mmol), **RH2.11** (34 mg, 0.15 mmol), EDC•HCl (43 mg, 0.23 mmol), triethylamine (52 µL, 0.38 mmol), HOBt hydrate (37 mg, 0.23 mmol), and 1.5 mL of dry DMF. The reaction was stirred at room temperature for 2 days, then the DMF was removed under reduced pressure. The residue was triturated with 10 mL water (aided by sonication), and the precipitate was filtered off and recrystallized from minimal ethanol to yield the product as white crystals (46 mg, 64%).

$^{1}$H NMR (300 MHz, $d_6$-DMSO) $\partial$ 8.09 (d, $J$ = 8.0 Hz, 1H), 7.75 (t, $J$ = 7.6 Hz, 1H), 7.53-7.74 (m, 5H), 7.46 (t, $J$ = 7.6 Hz, 1H), 7.13 (s, 1H), 5.05 (br s, 1H), 4.64 (br s, 1H), 3.65-3.81 (m, 2H), 3.59 (t, $J$ = 4.7 Hz, 1H), 3.17-3.27 (m, 3H)

$^{13}$C NMR (77 MHz, $d_6$-DMSO) $\partial$ 161.5, 148.5, 134.3, 131.9, 127.2, 127.0, 126.2, 125.7, 121.1, 69.8, 58.1, 51.5, 49.2

IR (neat, cm$^{-1}$) 3526, 3136, 2893, 1641, 1620, 1468, 1233, 1115, 970, 826, 773, 586, 500

**General procedure D for Boc deprotection of (di)amines**: to a vial containing the Boc-protected diamine (1 equivalent) was added HCl (1.25 M in methanol, 3 mL per equivalent, 3.75 equivalents) and stirred at room temperature overnight. The solvent was removed *in*

*vacuo*, and the crude solid triturated with ether to yield the product as a white to brown solid.

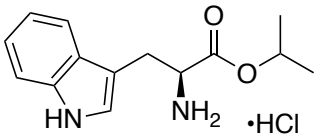


**RH2.15**

To a flask was added L-tryptophan (510 mg, 2.5 mmol) and 5 mL of isopropyl alcohol. Thionyl chloride (440 µL, 6 mmol) was then added dropwise with stirring. The reaction was then heated to reflux overnight. The reaction was cooled, and the solvents removed *in vacuo* to yield the product as a beige powder (151 mg, 20% – product lost during drying). $^1$H NMR (300 MHz, $d_6$-DMSO) ∂ 11.1 (br s, 1H), 8.44 (br s, 3H), 7.52 (d, $J$ = 7.5 Hz, 1H), 7.36 (d, $J$ = 7.9 Hz, 1H), 7.22 (d, $J$ = 2.3 Hz, 1H), 7.09 (dd, $J$ = 7.9, 7.5 Hz, 1H), 7.00 (dd, $J$ = 7.9, 7.5 Hz, 1H), 4.84 (p, $J$ = 6.4 Hz, 1H), 4.14 (t, $J$ = 6.6 Hz, 1H), 3.28 (dd, $J$ = 15.0, 6.3 Hz, 1H), 3.20 (dd, $J$ = 15.0, 7.4 Hz, 1H), 1.13 (d, $J$ = 6.2 Hz, 3H), 0.97 (d, $J$ = 6.2 Hz, 3H)

IR (neat, cm$^{-1}$) 3391, 3296, 2936, 1740, 1500, 1232, 1101, 735

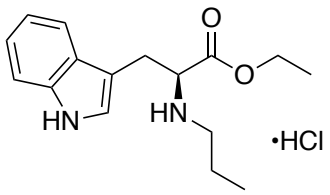


**RH2.16**

To a flask was added tryptophan ethyl ester hydrochloride (537 mg, 2 mmol) and 3 mL of methanol. Sodium hydroxide (1 M in methanol, 2 mL, 2 mmol) was then added, and the reaction stirred until clear. Propionaldehyde (72 µL, 1 mmol) was then added and stirred

for 5 minutes, followed by addition of $NaBH_3CN$ (125 mg, 2 mmol). The reaction was stirred overnight. The next day, the reaction was quenched by addition of ammonium chloride and stirred for 30 minutes, then basified with aqueous sodium bicarbonate. The aqueous phase was extracted thrice with ethyl acetate, and the combined organic layers washed once with water and once with brine, dried over $Na_2SO_4$, filtered, and concentrated to an oil. Silica gel chromatography (3:1 hexanes/ethyl acetate) provided the product as a pink oil. This oil was diluted in ~100 mL of ether, and hydrogen chloride (1.25 M in methanol, ~3 mL, ~3.75 mmol) was added dropwise. The flask was put in the freezer overnight, whereupon fine pink crystals formed. The crystals were filtered off and washed with ether, although they became a gummy residue on filtration. Isolation of the solid and evaporation from ether provided a light pink solid (82 mg, 27%).

$^1$H NMR (300 MHz, $D_2O$) ∂ 7.49 (dt, *J* = 8.0, 1 Hz, 1H), 7.43 (dt, *J* = 8.0, 1 Hz, 1H), 7.20 (s, 1H), 7.18 (ddd, *J* = 8, 7.2, 1Hz, 1H), 7.09 (ddd, *J* = 8.0, 7.2, 1.0 Hz, 1H), 4.24 (dd, *J* = 7.4, 5.7 Hz, 1H), 4.04 (q, *J* = 7.2 Hz, 2H), 3.44 (dd, *J* = 15.1, 5.7 Hz, 1H), 3.33 (dd, *J* = 15.1, 7.4 Hz, 1H), 2.86-3.03 (m, 2H), 1.57 (sextet, *J* = 7.6 Hz, 2H), 0.99 (t, *J* = 7.2 Hz, 3H), 0.83 (t, *J* = 7.4 Hz, 3H)

$^{13}$C NMR (77 MHz, $D_2O$) ∂ 169.4, 136.2, 126.4, 125.2, 122.2, 119.6, 118.0, 112.0, 105.8, 63.7, 60.1, 48.3, 25.1, 19.1, 12.8, 10.1

IR (neat, $cm^{-1}$) 3245, 2965, 2659, 1734, 1459, 1437, 1250, 1215, 1034, 735

HRMS (ESI) calc'd for $C_{16}H_{22}N_2O_2$ (M+H) 275.17543, found 275.17542.

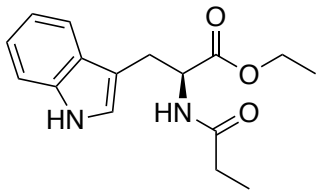


**RH2.17**

To a vial was added tryptophan ethyl ester (267 mg, 1 mmol), pyridine (250 µL, 3 mmol), and 2 mL of dichloromethane. The mixture was cooled in an ice/water bath, and propionic anhydride (140 µL, 1.1 mmol) was added dropwise. The reaction was left to come to room temperature overnight. The reaction was then diluted with water and the aqueous phase extracted twice with dichloromethane. The combined organic layers were washed once with 1 M HCl, once with saturated sodium bicarbonate, and once with brine, then dried over $Na_2SO_4$, filtered, and concentrated to a brown oil. Silica gel chromatography (2:1 ethyl acetate/hexanes) provided the product as an orange solid (231 mg, 81%).

$^1$H NMR (300 MHz, $CDCl_3$) $\partial$ 8.32 (br s, 1H), 7.54 (dd, $J$ = 8.0, 1.0 Hz, H), 7.36 (dt, $J$ = 8.0, 1.0 Hz, 1H), 7.19 (ddd, $J$ = 8.0, 7.1, 1.0 Hz, 1H), 7.12 (ddd, $J$ = 8.0, 7.1, 1.0 Hz, 1H), 6.97 (d, $J$ = 2.4 Hz, 1H), 6.01 (br s, $J$ = 7.8 Hz, 1H), 4.96 (dt, $J$ = 7.9, 5.4 Hz, 1H), 4.06-4.23 ($ABX_3$ m, 2H), 3.26-3.41 (ABX m, $J_{AX} = J_{BX}$ = 5.0, 2H), 2.18 (q, $J$ = 7.6 Hz, 2H), 1.23 (t, $J$ = 7.2 Hz, 3H), 1.11 (t, $J$ = 7.6 Hz, 3H)

$^{13}$C NMR (77 MHz, $CDCl_3$) $\partial$ 173.4, 172.1, 136.1, 127.8, 122.7, 122.2, 119.6, 118.6, 111.3, 110.1, 61.5, 53.0, 29.6, 27.6, 14.1, 9.6

IR (neat, $cm^{-1}$) 3396, 3309 br, 2981, 1732, 1666, 1520, 1208, 1184, 746

HRMS (ESI) calc'd for $C_{16}H_{20}N_2O_3$ (M+H) 289.15469, found 289.15460.

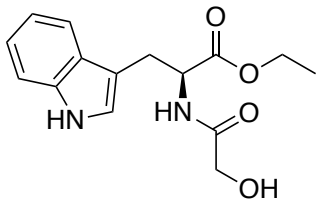


**RH2.18**

To a vial was added tryptophan ethyl ester hydrochloride (270 mg, 1 mmol), Hünig's base (300 µL, 1.75 mmol), and 1 mL acetonitrile. Stirred for 5 minutes until clear to neutralize the hydrochloride. To a separate vial was added EDC•HCl (288 mg, 1.5 mmol),

HOBt•x$H_2O$ (243 mg, 1.5 mmol), Hünig's base (300 µL, 1.75 mmol), glycolic acid (70% in water, 87 µL, 1 mmol), and 4 mL acetonitrile. This second mixture was stirred for 30 minutes until clear. The tryptophan solution was then added, and the reaction stirred at room temperature for 2 days. The reaction was diluted with water and extracted thrice with ethyl acetate. The combined organic layers were washed once with 1M HCl, once with saturated sodium bicarbonate, and once with brine, then dried over $Na_2SO_4$, filtered, and concentrated to a brown oil. Silica gel chromatography (ethyl acetate) provided the product as a yellowish oil (101 mg, 35%). NMR indicates an approximately 3:1 mixture of rotamers.

$^1$H NMR – major rotamer only (300 MHz, $CDCl_3$) ∂ 8.52 (br s, 1H), 7.51 (d, *J* = 7.5 Hz, 1H), 7.28 (d, *J* = 8.0 Hz, 1H), 7.15 (t, *J* = 7.2 Hz, 1H), 7.08 (t, *J* = 7.2 Hz, 1H), 6.93 (d, *J* = 2.3 Hz, 1H), 4.9 (dt, *J* = 8.0, 5.7 Hz, 1H), 4.04-4.21 ($ABX_3$ m, 2H), 3.89 (s, 2H), 3.31 (d, *J* = 5.6 Hz, 2H), 1.22 (t, *J* = 7.2 Hz, 3H)

$^{13}$C NMR – major rotamer only (77 MHz, $CDCl_3$) ∂ 172.0, 166.5, 136.1, 127.5, 123.0, 122.2, 119.5, 118.4, 111.4, 109.6, 62.0, 61.8, 52.4, 27.6, 14.0

HRMS (ESI) calc'd for $C_{15}H_{18}N_2O_4$ (M+H) 291.13396, found 291.13399.

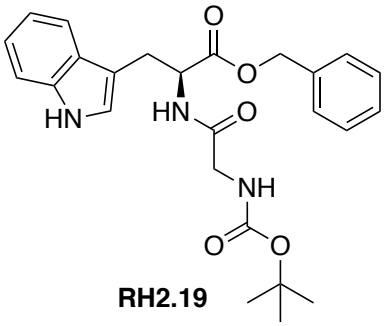


**RH2.19**

To a flask was added N-Boc glycine (88 mg, 0.5 mmol), EDC•HCl (144 mg, 0.75 mmol), 6-chloro-hydroxybenzotriazole (127 mg, 0.75 mmol), and 2 mL of dichloromethane. The

reaction was stirred for 10 minutes at room temperature, then Hünig's base (261 μL, 1.5 mmol) and tryptophan benzyl ester hydrochloride (147 mg, 0.5 mmol) were added. The reaction was stirred overnight, then quenched with saturated sodium bicarbonate. The aqueous phase was extracted thrice with ethyl acetate, and the combined organic layers washed once with sat $NH_4Cl$ , once with water, once with saturated sodium bicarbonate, and once with brine, then dried over $Na_2SO_4$, filtered, and concentrated to a brown residue. Silica gel chromatography (2:1 hexanes/ethyl acetate) provided the compound as a yellow solid (181 mg, 80%).

$^1$H NMR (300 MHz, $CDCl_3$) ∂ 8.10 (br s, 1H), 7.50 (d, *J* = 7.8 Hz, 1H), 7.31-7.40 (m, 4H), 7.22-7.29 (m, 2H), 7.19 (td, *J* = 8.0, 1.0 Hz, 1H), 7.10 (td, *J* = 7.4, 1.0 Hz, 1H), 6.79 (d, *J* = 2.5 Hz, 1H), 6.55 (br d, *J* = 8 Hz, 1H), 5.09 (s, 2H), 4.98 (dt, *J* = 7.8, 5.4 Hz, 1H), 3.66-3.82 (m, 2H), 3.33 (d, *J* = 5.4 Hz, 2H), 1.42 (s, 9H)

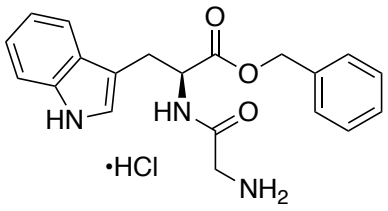


**RH2.20**

Prepared according to general procedure D. Brown solid (52 mg, quantitative).

$^1$H NMR (300 MHz, $d_6$-DMSO) ∂ 10.97 (br s, 1H), 8.96 (dd, *J* = 18.7, 7.4 Hz, 1H), 8.12 (br s, 3H), 7.48 (d, *J* = 7.6 Hz, 1H), 7.13-7.40 (m, 5H), 7.07 (t, *J* = 7.4 Hz, 1H), 6.98 (t, *J* = 7.4 Hz, 1H), 5.05 (dd, *J* = 23.7, 12.6 Hz, 1H),

HRMS (ESI) calc'd for $C_{20}H_{21}N_3O_3$ (M+H) 352.16559, found 352.16546.

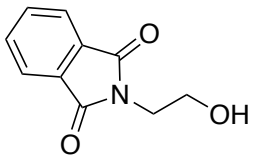


**RH2.21**

To a flask was added phthalic anhydride (14.85 g, 100 mmol). Ethanolamine (6.7 mL, 111 mmol) was added dropwise, though there is no noticeable exotherm or gas evolution. The flask was heated to 175 ˚C for 6 hours, and the melt then cooled to room temperature, and the yellow syrup solidified on standing. Recrystallization from 100 mL of boiling water yielded the product as pearly white flaky crystals (12.1 g, 63%).

$^{1}$H NMR (300 MHz, $CDCl_3$) ∂ 7.79-7.87 (AA`XX` m, 2H), 7.67-7.75 (AA`XX` m, 2H), 3.87 ($A_2B_2$ m, 4H)

$^{13}$C NMR (77 MHz, $CDCl_3$) ∂ 168.8, 134.1, 131.9, 123.4, 61.0, 40.8

IR (neat, $cm^{-1}$) 3468, 2954, 1765, 1692, 1427, 1391, 1055, 722

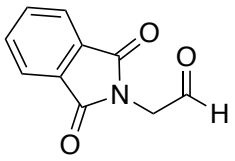


**RH2.22**

To a flame-dried flask was added 40 mL of dry dichloromethane. The flask was cooled to -78 ˚C in a dry ice/acetone bath, and anhydrous DMSO (1.7 mL, 24 mmol) was added. Oxalyl chloride (1.0 mL, 12 mmol) was then added dropwise, accompanied by gas evolution. The reaction was stirred at this temperature for 30 minutes, then T!8 (1.15 g, 6 mmol) in 1 mL of dry DMSO and 5 mL of dry dichloromethane was added. The reaction was stirred another 30 minutes at -78 ˚C, then trimethylamine (3.4 mL, 24 mmol) was added. The reaction was allowed to come to -10 ˚C over 4 hours, then quenched by addition of water. The reaction was extracted with 4x30 mL portions of dichloromethane, and the

combined organic layers were washed with sat $NH_4Cl$ , saturated sodium bicarbonate, and brine, then dried over $Na_2SO_4$, filtered, and concentrated to a brown residue. Used crude, as column chromatography resulted in decomposition without noticeable improvements in purity.

$^1$H NMR (300 MHz, $CDCl_3$) ∂ 7.87-7.94 (AA`XX` m, 2H), 7.73-7.81 (AA`XX` m, 2H), 4.57 (s, 2H)

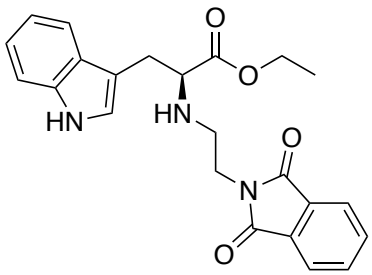


**RH2.23**

To a solution of tryptophan ethyl ester hydrochloride (537 mg, 2 mmol) in 10 mL of methanol was added glacial acetic acid (500 µL, 8.6 mmol) and T!9 (416 mg, 2.2 mmol). Next, $NaBH_3CN$ (1 M in methanol, 4 mL, 4 mmol) was added, and the reaction stirred overnight. The reaction was quenched with saturated sodium bicarbonate, and the aqueous phase extracted thrice with ethyl acetate. The combined organic layers were washed with brine, dried over $Na_2SO_4$, filtered, and concentrated to a brown residue. Silica gel chromatography (methanol in ethyl acetate) provided the compound as a beige residue (202 mg, 25%).

$^1$H NMR (300 MHz, $CDCl_3$) ∂ 8.45 (br s, 1H), 7.71-7.81 (AA`XX` m, 2H), 7.61-7.69 (AA`XX` m, 2H), 7.50 (d, $J$ = 7.8 Hz, 1H), 7.23 (d, $J$ = 8.2 Hz, 1H), 7.06 (ddd, $J$ = 8.2, 7.2, 1 Hz, 1H), 6.99 (ddd, $J$ = 8.2, 7.2, 1.0 Hz, 1H), 6.97 (d, $J$ = 2.3 Hz, 1H), 4.00 (q, $J$ =

7.2 Hz, 2H), 3.65-3.77 ($ABX_2$ m, 2H), 3.60 (t, $J$ = 6.4 Hz, 1H), 3.05 (d, $J$ = 6.4 Hz, 2H), 2.93 (dt, $J$ = 12.1, 6.2 Hz, 1H), 2.73 (dt, $J$ = 6.2 Hz, 1H), 1.06 (t, $J$ = 7.2 Hz, 3H)

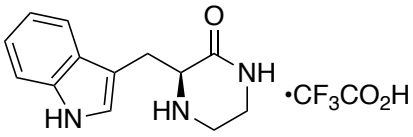


**RH2.24**

To a solution of **RH2.23** (202 mg, 0.5 mmol) in 1 mL of ethanol was added hydrazine hydrate (253 μL, 5.2 mmol). The solution was heated to 70 ˚C overnight, then cooled and filtered. The residue was dissolved in ether and trifluoroacetic acid was added dropwise. The precipitate was filtered to yield the product as a brown solid (39 mg, 22%).

$^1$H NMR (300 MHz, $d_6$-DMSO) ∂ 11.07 (br s, 1H), 9.12 (br s, 2H), 8.38 (br s, 1H), 7.56 (d, $J$ = 7.8 Hz, 1H), 7.39 (d, $J$ = 7.8 Hz, 1H), 7.25 (d, $J$ = 2.1 Hz, 1H), 7.11 (t, $J$ = 7.5 Hz, 1H), 7.01 (t, $J$ = 7.5 Hz, 1H), 4.13 (d, $J$ = 7.0 Hz, 1H), 3.52 (dd, $J$ = 15.4, 3.8 Hz, 1H), 3.20-3.42 (m, 4H), 3.15 (dd, $J$ = 15.4, 9.8 Hz, 1H)

$^{13}$C NMR (77 MHz, $d_6$-DMSO) ∂ 165.2, 136.4, 126.9, 124.9, 121.2, 118.6, 118.2, 111.5, 107.2, 56.3, 37.4, 24.8, 15.1

HRMS (ESI) calc'd for $C_{13}H_{15}N_3O$ (M+H) 230.12824, found 230.12865.

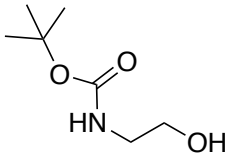


**RH2.25**

To a flask was added ethanolamine (6.1 g, 100 mmol) and triethylamine (2.79 mL, 20 mmol) in 150 mL of dichloromethane. $Boc_2O$ (21.8 g, 100 mmol) was added portionwise with rapid stirring, and the reaction warmed slightly and evolved gas. The reaction was stirred at room temperature overnight, then quenched with water and the organic layer

washed thrice with 1 M HCl and once with brine, then dried over $Na_2SO_4$, filtered, and concentrated to a viscous clear oil (11.56 g, 72%).

$^1$H NMR (300 MHz, $CDCl_3$) $\partial$ 5.14 (br s, 1H), 3.66 (q, $J$ = 4.8 Hz, 2H), 3.25 (q, $J$ = 5.2 Hz, 2H), 3.16 (br s, 1H), 1.42 (s, 9H)

$^{13}$C NMR (77 MHz, $CDCl_3$) $\partial$ 156.8, 79.6, 62.3, 43.1, 28.3

IR (neat, $cm^{-1}$) 3346, 2977, 2933, 1683, 1519, 1168

HRMS (ESI) calc'd for $C_7H_{15}NO_3$ (M+Na) 184.09440, found 184.09439.

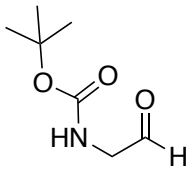


**RH2.26**

To a flask was added **RH2.25** (1.13 g, 7 mmol), IBX (2.94 g, 10.5 mmol), and 35 mL of ethyl acetate. The reaction was heated to reflux for 3.5 hours, then cooled and filtered through Celite with ample ethyl acetate washes. The organic layer was concentrated to a pale yellow oil and used immediately, using crude NMR to determine the concentration of aldehyde (-C*H*O) compared to ethyl acetate.

$^1$H NMR (300 MHz, $CDCl_3$) $\partial$ 9.66 (s, 1H), 4.07 (s, 2H), 1.46 (s, 9H)

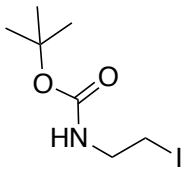


**RH2.27**

To a flame-dried flask was added imidazole (833 mg, 12 mmol), triphenylphosphine (2.52 g, 9.6 mmol), and 30 mL of dry dichloromethane. Next, iodine (2.44 g, 9.6 mmol) was added, and the reaction turned green, then bright yellow in quick succession. The reaction was cooled in an ice/water bath, and **RH2.25** (1.31 g, 8.1 mmol) was added dropwise. The

reaction was then allowed to come to room temperature overnight. The dark red solution was quenched by addition of 0.5 M sodium thiosulphate, and the organic phase extracted twice with dichloromethane. The combined organic layers were washed with water, then brine, dried over $MgSO_4$, filtered, and concentrated to a yellow paste. The paste was suspended in ether and kept at -20 ˚C overnight. The precipitate (triphenylphosphine oxide) was filtered off and rinsed with pentane, and ether. The filtrate was concentrated to a yellow oil, which was then purified by silica gel chromatography to yield a yellow oil that solidified in the freezer (1.47 g, 68%).

$^1$H NMR (300 MHz, $CDCl_3$) $\partial$ 4.93 (br s, 1H), 3.47 (q, $J$ = 6.3 Hz, 2H), 3.23 (t, $J$ = 6.3 Hz, 2H), 1.44 (s, 9H)

$^{13}$C NMR (77 MHz, $CDCl_3$) $\partial$ 155.4, 79.8, 43.0, 28.3, 5.97

IR (neat, cm$^{-1}$) 3336, 2973, 2929, 2900, 1711, 1683, 1529, 1161

HRMS (ESI) not detected – too labile.

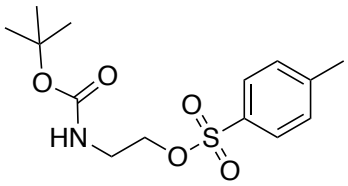


**RH2.28**

To a flask was added **RH2.25** (1.29 g, 8 mmol), triethylamine (1.67 mL, 12 mmol), and 27 mL of dichloromethane. The solution was cooled in an ice/water bath, and tosyl chloride (1.72 g, 9 mmol) was added portionwise. The reaction was allowed to come to room temperature overnight. The solution was filtered to remove triethylammonium chloride, and the filtrate was diluted with dichloromethane, washed once with saturated sodium bicarbonate and once with brine, dried over $Na_2SO_4$, filtered, and concentrated to a

colourless oil. Silica gel chromatography (4:1 to 2:1 hexanes/ethyl acetate) yielded the product as a white crystalline solid (1.49 g, 59%).

$^{1}$H NMR (300 MHz, $CDCl_3$) $\partial$ 7.78 (d, $J$ = 8.3 Hz, 2H), 7.34 (d, $J$ = 8.2 Hz, 2H), 4.87 (br s, 1H), 4.06 (t, $J$ = 5.1 Hz, 2H), 3.37 (q, $J$ = 5.2 Hz, 2H), 2.44 (s, 3H), 1.40 (s, 9H)

$^{13}$C NMR (77 MHz, $CDCl_3$) $\partial$ 155.6, 145.0, 132.6, 130.0, 127.9, 79.8, 69.5, 39.7, 28.3, 21.6

IR (neat, $cm^{-1}$) 3409, 3001, 2931, 1713, 1516, 1346, 1175, 971, 829

HRMS (ESI) calc'd for $C_{14}H_{21}NO_5S$ (M+Na) 338.10325, found 338.10327.

**General procedure E for the installation of Boc-protected ethylenediamines and TBS-protected ethanolamines by reductive amination**: to a solution of the tryptophan ester hydrochloride (1 equivalent) in methanol (5 mL per equivalent) was added freshly made aldehyde **RH2.26** or **RH2.35** (1 equivalent, as determined by NMR) and $NaBH_3CN$ (2 equivalents). The reaction was stirred at room temperature overnight, then quenched by addition of saturated sodium bicarbonate. The aqueous phase was extracted thrice with ethyl acetate, washed once with saturated sodium bicarbonate and once with brine, dried over $Na_2SO_4$, filtered, and concentrated to a brown residue. Silica gel chromatography (hexanes/ethyl acetate with 1% triethylamine) yielded the product as a gummy residue, which solidified somewhat upon trituration with pentane.

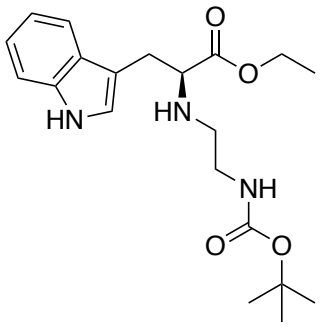

**RH2.29**

Prepared according to general procedure E. Yellow residue (20 mg, 20%).

$^{1}$H NMR (300 MHz, $CDCl_3$) ∂ 8.11 (br s, 1H), 7.61 (d, *J* = 7.8 Hz, 1H), 7.35 (d, *J* = 7.8 Hz, 1H), 7.19 (t, *J* = 7.5 Hz, 1H), 7.11 (t, *J* = 7.4 Hz, 1H), 7.05 (br s, 1H), 4.92 (br s, 1H), 4.09 (q, *J* = 7.2 Hz, 2H), 3.57 (t, *J* = 6.5 Hz, 1H), 3.00-3.23 (ABCD m, 4H), 2.73 (dt, *J* = 11.8, 5.6 Hz, 1H), 2.59 (dt, *J* = 11.8, 5.3 Hz, 1H), 1.42 (s, 9H), 1.15 (t, *J* = 7.2 Hz, 3H)

$^{13}$C NMR (77 MHz, $CDCl_3$) ∂ 174.9, 156.0, 136.2, 127.5, 122.8, 122.1, 119.5, 118.8, 111.4, 111.2, 61.7, 60.8, 47.4, 40.3, 29.3, 28.4, 14.1

IR (neat, $cm^{-1}$) 3324 br, 2977, 2931, 1688 br, 1510, 1457, 1365, 1164 br, 739

HRMS (ESI) calc'd for $C_{20}H_{29}N_3O_4$ (M+H) 376.22311, found 376.22313.

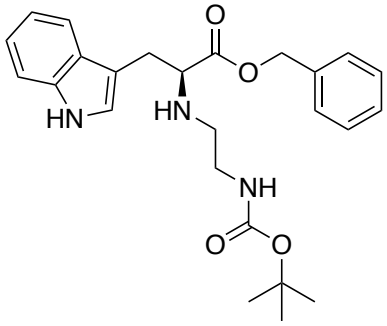

**RH2.30**

Prepared according to general procedure E. Yellow residue (40 mg, 37%).

$^1$H NMR (300 MHz, $CDCl_3$) ∂ 8.21 (br s, 1H), 7.60 (d, *J* = 7.8 Hz, 1H), 7.27-7.37 (m, 4H), 7.07-7.23 (m, 4H), 6.92 (d, *J* = 2.3 Hz, 1H), 5.05 (s, 2H), 3.65 (t, *J* = 6.6 Hz, 1H), 3.00-3.24 (m, 4H), 2.68-2.79 (m, 1H), 2.59 (dt, *J* = 11.6, 5.8 Hz, 1H), 1.44 (s, 9H)

$^{13}$C NMR (77 MHz, $CDCl_3$) ∂ 174.8, 156.1, 136.2, 135.6, 128.5, 128.2, 127.5, 122.9, 122.1, 119.5, 118.7, 111.2, 111.1, 79.1, 66.5, 62.6, 61.9, 47.4, 29.4, 28.4

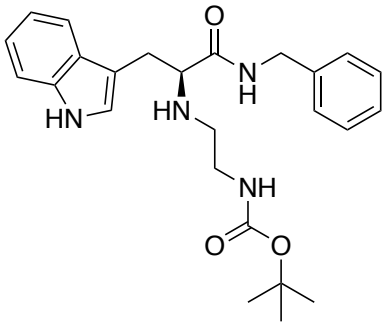


**RH2.31**

Prepared according to general procedure E. Yellow residue (35 mg, 16%).

$^1$H NMR (300 MHz, $CDCl_3$) ∂ 8.22 (br s, 1H), 7.60 (d, *J* = 7.8 Hz, 1H), 7.39 (br t, *J* = 5.2 Hz, 1H), 7.29 (d, *J* = 8 Hz, 1H), 7.00-7.26 (m, 7H), 6.94 (d, *J* = 2.2 Hz, 1H), 4.25-4.48 (ABX m, 2H), 3.39 (dd, *J* = 8.7, 4.5 Hz, 1H), 3.28 (dd, *J* = 14.4, 4.2 Hz, 1H), 2.77-3.04 (m, *3*H), 2.50 (m, 2H), 1.31 (s, 9H)

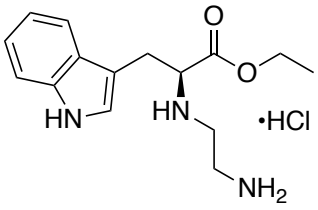


**RH2.32**

Prepared according to general procedure D. Brown solid (14 mg, quantitative).

$^1$H NMR (300 MHz, $d_4$-MeOD) ∂ 7.57 (d, *J* = 7.8 Hz, H), 7.40 (d, *J* = 8.1 Hz, 1H), 7.33 (s, 1H), 7.15 (t, *J* = 7.2 Hz, 1H), 7.07 (t, *J* = 7.4 Hz, 1H), 4.44 (br t, *J* = 5.1 Hz, 1H), 4.07-4.27

(ABX$_3$ m, 2H), 3.62 (dd, *J* = 15.2, 5.1 Hz, 1H), 3.52 (dd, *J* = 15.2, 6.6 Hz, 1H), 3.27-3.44 (br s, 4H), 1.15 (t, *J* = 7.2 Hz, 3H)

$^{13}$C NMR (77 MHz, d$_4$-MeOD) ∂ 169.8, 138.2, 128.3, 125.9, 123.0, 120.3, 119.0, 112.7, 107.0, 64.1, 62.4, 45.0, 36.8, 27.0, 14.0

HRMS (ESI) calc'd for $C_{15}H_{21}N_3O_2$ (M+H) 276.17068, found 276.17069.

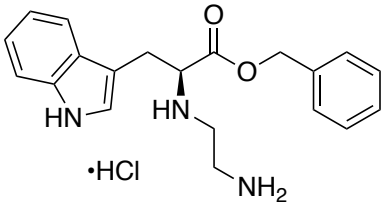


**RH2.33**

Prepared according to general procedure D. Brown solid (20 mg, quantitative).

$^1$H NMR (300 MHz, d$_4$-MeOD) ∂ 7.52 (d, *J* = 8.0 Hz, 1H), 7.41 (d, *J* = 8.0 Hz, 1H), 7.25-7.34 (m, 3H), 7.11-7.19 (m, 2H), 7.01-7.11 (m, 3H), 5.11 (d, *J* = 12.0 Hz, 1H), 5.02 (d, *J* = 12.0 Hz, 1H), 4.37 (dd, *J* = 7.3, 5.4 Hz, 1H), 3.55 (dd, *J* = 15.0, 5.4 Hz, 1H), 3.45 (dd, *J* = 15.0, 7.3 Hz, 1H), 3.25-3.40 (m, 4H)

$^{13}$C NMR (77 MHz, d$_4$-MeOD) ∂ 171.0, 138.1, 135.8, 129.8, 129.7, 128.3, 125.7, 123.0, 120.4, 119.0, 112.8, 107.5, 69.5, 62.7, 45.0, 37.4, 27.6

HRMS (ESI) calc'd for $C_{20}H_{23}N_3O_2$ (M+H) 338.18633, found 338.18634.

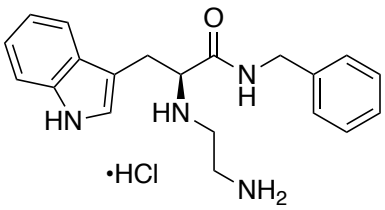


**RH2.34**

Prepared according to general procedure D. Brown solid (36 mg, quantitative).

$^1$H NMR (300 MHz, d$_4$-MeOD) ∂ 8.62 (br t, *J* = 5.4 Hz, < 1H), 7.64 (dd, *J* = 7.8, 1.0 Hz, 1H), 7.40 (dd, *J* = 8.2, 1.0 Hz, 1H), 7.11-7.24 (m, 5H), 7.06 (ddd, *J* = 8.2, 7.2, 1.0 Hz, 1H),

6.87-6.95 (m, 2H), 4.30 (d, *J* = 15.0 Hz, 1H), 4.21 (dd, *J* = 8.6, 5.6 Hz, 1H),4.18 (d, *J* = 15.0 Hz, 1H), 3.50 (dd, *J* = 14.2, 5.6 Hz, 1H), 3.41 (dd, *J* = 14.2, 8.6 Hz, 1H), 3.28-3.40 (m, 4H)

$^{13}$C NMR (77 MHz, $d_4$-MeOD) ∂ 168.3, 138.4, 138.1, 129.7, 129.6, 128.8, 128.5, 125.8, 122.9, 120.3, 119.3, 112.6, 107.4, 63.3, 44.7, 37.8, 36.9, 28.0

HRMS (ESI) calc'd for $C_{20}H_{24}N_4O$ (M+H) 337.20231, found 337.20226.

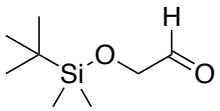


**RH2.35**

To a flask was added O-tertbutyldimethylsilyl ethyleneglycol (360 mg, 2 mmol), IBX (1.13 g, 4 mmol), and 10 mL of ethyl acetate. The reaction was heated to reflux for 3 hours, then cooled and filtered through Celite, rinsing with ethyl acetate. The filtrate was concentrated to a clear oil, whose aldehyde content was estimated from crude NMR (C*H*O vs ethyl acetate). Used crude.

$^1$H NMR (300 MHz, $CDCl_3$) ∂ (, *J* = Hz, H) 9.70 (s, 1H), 4.21 (s, 2H), 0.93 (s, 9H), 0.10 (s, 6H)

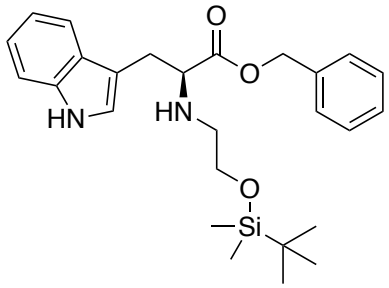


**RH2.36**

To a vial was added tryptophan benzyl ester hydrochloride (121 mg, 0.41 mmol), $NaBH_3CN$ (51 mg, 0.82 mmol), **RH2.35** (1 aldehyde to 0.8 ethyl acetate, effective molecular weight = 244 g/mol, 200 mg, 0.82 mmol), and 1 mL of methanol. Stirred at room

temperature overnight. The reaction was quenched by addition of 1 M HCl and stirred for 30 minutes. The reaction was then basified to pH 9 with saturated sodium bicarbonate, extracted thrice with dichloromethane, and the combined organic layers washed once with brine and dried over $Na_2SO_4$, filtered, and concentrated to a brown oil. Silica gel chromatography (99:0:1 to 0:99:1 hexanes/ethyl acetate/triethylamine) yielded the product as a brown residue (51 mg, 27%).

$^1$H NMR (300 MHz, $CDCl_3$) ∂ 8.04 (br s, 1H), 7.63 (d, *J* = 7.8 Hz, 1H), 7.32 (ddd, *J* = 8.3, 7.6, 0.9 Hz, H), 7.26-7.31 (m, 3H), 7.19 (td, *J* = 7.4, 6.9, 1.0 Hz, 1H), 7.10-7.16 (m, 2H), 7.11 (td, *J* = 8.3, 7.0, 1.0 Hz, 1H), 6.95 (d, *J* = 2.3 Hz, 1H), 5.05 (s, 2H), 3.74 (t, *J* = 6.8 Hz, 1H), 3.68 (t, *J* = 5.4 Hz, 2H), 3.18 (dd, *J* = 6.8, 1.2 Hz, 2H), 2.77 (dt, *J* = 11.6, 5.5 Hz, 1H), 2.61 (dt, *J* = 11.6, 5.2 Hz, 1H), 0.83 (s, 9H), 0.00 (s, 3H), -0.01 (s, 3H)

HRMS (ESI) calc'd for $C_{20}H_{22}N_2O_3$ (M+H) 339.17034, found 339.17013.

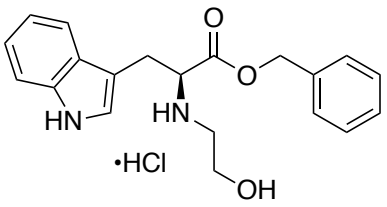


**RH2.37**

Prepared according to general procedure D. Brown solid (35 mg, 84%).

$^1$H NMR (300 MHz, $d_6$-DMSO) ∂ 11.05 (br s, 1H), 7.52 (d, *J* = 8.1 Hz, 1H), 7.38 (d, *J* = 8.1 Hz, 1H), 7.17-7.32 (m, 4H), 6.95-7.14 (m, 4H), 5.05 (d, *J* = 12.5 Hz, 1H), 4.91 (d, *J* = 12.5 Hz, 1H), 4.37 (br s, 1H), 3.71 (t, *J* = 5.2 Hz, 2H), 3.22-3.56 (m, 4H)

$^{13}$C NMR (77 MHz, $d_4$-MeOD) ∂ 170.9, 139.2, 136.8, 130.6, 130.5, 129.2, 126.4, 123.9, 121.3, 119.9, 113.7, 108.3, 70.3, 62.6, 58.9, 28.00

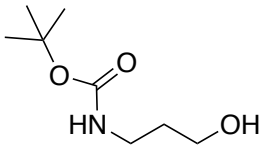

**RH2.38**

To a flask was added 3-amino-1-propanol (1.15 mL, 15 mmol) and triethylamine (4.2 mL, 30 mmol) in 21 mL of dry THF. The reaction was cooled in an ice/water bath, and $Boc_2O$ (3.6 g, 16.5 mmol) was added portionwise with rapid stirring, and the reaction warmed slightly and evolved gas. The reaction was stirred at room temperature for 3 hours, then quenched with water and extracted thrice with dichloromethane. The combined organic layers were washed thrice with 1 M HCl and once with brine, then dried over $Na_2SO_4$, filtered, and concentrated to a viscous clear oil (11.56 g, 72%).

$^1$H NMR (300 MHz, $CDCl_3$) $\partial$ 4.79 (br s, 1H), 3.66 (q, $J$ = 5.8 Hz, 2H), 3.29 (q, $J$ = 6.2 Hz, 2H), 2.99 (br t, $J$ = 5.8, 1H), 1.66 (p, $J$ = 6.0 Hz, H), 1.44 (s, 9H)

IR (neat, cm$^{-1}$) 3348 br, 2977, 1683, 1520, 1366, 1275, 1251, 1165, 1044

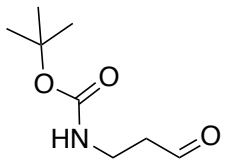

**RH2.39** T!26 RH-04-063

To a flask was added **RH2.38** (710 mg, 4 mmol), tetrabutylammonium chloride hydrate (111 mg, 0.4 mmol), TEMPO (63 mg, 0.4 mmol), N-chlorosuccinimide (961 mg, 7.2 mmol), a solution of sodium bicarbonate (588 mg, 7 mmol) and potassium carbonate (97 mg, 0.7 mmol) in 14 mL of distilled water, and 14 mL of chloroform. The reaction was stirred at room temperature for 2 hours. The precipitate was filtered off, the layers were separated, and the organic layer dried over $MgSO_4$, filtered, and concentrated to a yellow oil.

$^1$H NMR (300 MHz, $CDCl_3$) ∂ 9.82 (s, 1H), 4.92 (br s, 1H), 3.39-3.50 (m, 2H), 2.72 (t, *J* = 5.5 Hz, 2H), 1.44 (s, 9H)

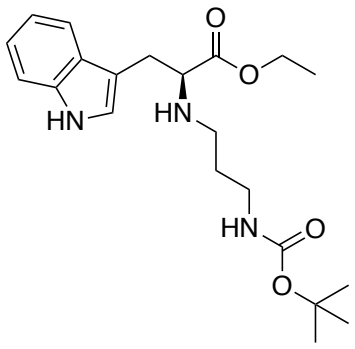

**RH2.40**

To a vial was added tryptophan ethyl ester hydrochloride (350 mg, 1.3 mmol), **RH2.39** (225 mg, 1.3 mmol), and 3 mL of methanol. $NaBH_3CN$ (122 mg, 1.95 mmol) was added, and the reaction stirred at room temperature overnight. The reaction was quenched with 1 M HCl, stirred for 30 minutes, then basified with saturated sodium bicarbonate and extracted thrice with dichloromethane. The combined organic layers were washed with brine, dried over $Na_2SO_4$, filtered, and concentrated to an oil. Silica gel chromatography (99:0:1 to 0:99:1 hexanes/ethyl acetate/triethylamine) provided the product as a yellow residue (149 mg, 30%).

$^1$H NMR (300 MHz, $CDCl_3$) ∂ 8.60 (br s, 1H), 7.60 (d, *J* = 7.8 Hz, 1H), 7.32 (d, *J* = 8.1 Hz, 1H), 7.16 (td, *J* = 7.5, 1.1 Hz, 1H), 7.10 (td, *J* = 7.2, 0.9 Hz, 1H), 7.01 (s, 1H), 5.20 (br s, 1H), 4.09 (q, *J* = 7.2 Hz, 2H), 3.58 (t, *J* = 6.5 Hz, 1H), 2.97-3.22 (m, 4H), 2.67 (dt, *J* = 11.5, 6.6 Hz, H), 2.49 (dt, *J* = 11.5, 6.3 Hz, 1H), 1.55 (p, *J* = 6.5 Hz, 2H), 1.44 (s, 9H), 1.14 (t, *J* = 7.2 Hz, 3H)

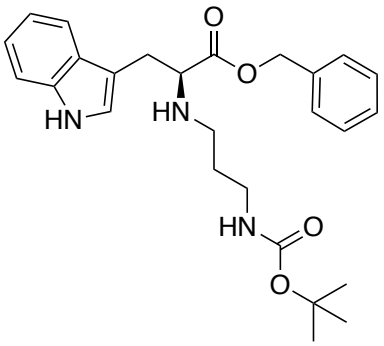

**RH2.41**

To a vial was added tryptophan benzyl ester hydrochloride (3383 mg, 1.3 mmol), **RH2.39** (225 mg, 1.3 mmol), and 3 mL of methanol. $NaBH_3CN$ (122 mg, 1.95 mmol) was added, and the reaction stirred at room temperature overnight. The reaction was quenched with 1 M HCl, stirred for 30 minutes, then basified with saturated sodium bicarbonate and extracted thrice with dichloromethane. The combined organic layers were washed with brine, dried over $Na_2SO_4$, filtered, and concentrated to an oil. Silica gel chromatography (99:0:1 to 0:99:1 hexanes/ethyl acetate/triethylamine) provided the product as a yellow residue (265 mg, 45%).

$^1$H NMR (300 MHz, $CDCl_3$) $\partial$ 8.59 (br s, 1H), 7.61 (d, $J$ = 7.8 Hz, 1H), 7.24-7.39 (m, 4H), 7.19 (t, $J$ = 7.4 Hz, 1H), 7.12-7.18 (m, 2H), 7.11 (t, $J$ = 7.2 Hz, 1H), 6.91 (s, 1H), 5.20 (br s, 1H), 5.06 (s, 2H), 3.68 (t, $J$ = 6.6 Hz, 1H), 3.00-3.23 (m, 4H), 2.69 (dt, $J$ = 11.5, 6.6 Hz, 1H), 2.50 (dt, $J$ = 11.5, 6.6 Hz, 1H), 1.55 (p, $J$ = 6.5 Hz, 2H), 1.47 (s, 9H)

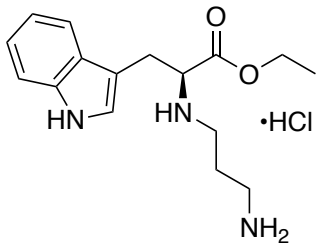

**RH2.42**

Prepared according to general procedure D. Brown solid (128 mg, quantitative).

$^1$H NMR (300 MHz, $d_6$-MeOD) ∂ 7.58 (d, *J* = 7.7 Hz, 1H), 7.41 (d, *J* = 8.0 Hz, H), 7.30 (s, 1H), 7.15 (ddd, *J* = 8.0, 7.1, 0.9 Hz, 1H), 7.07 (ddd, *J* = 7.8, 7.0, 1.0 Hz, 1H), 4.37 (dd, *J* = 7.7, 5.5 Hz, H), 4.02-4.21 ($ABX_3$ m, 2H), 3.62 (dd, *J* = 14.9, 5.3 Hz, 1H), 3.48 (dd, *J* = 14.9, 7.8 Hz, 1H), 3.13-3.30 (m, 2H), 3.07 (t, *J* = 7.6 Hz, 2H), 2.06-2.29 (m, 2H), 1.06 (t, *J* = 7.2 Hz, 3H)

$^{13}$C NMR (77 MHz, $d_6$-MeOD) ∂ 172.4, 140.6, 130.9, 128.2, 125.4, 122.8, 121.5, 115.2, 109.8, 66.4, 64.7, 48.6, 47.7, 40.5, 29.5, 27.9, 16.5

HRMS (ESI) calc'd for $C_{16}H_{23}N_3O_2$ (M+H) 290.18633, found 290.18642.

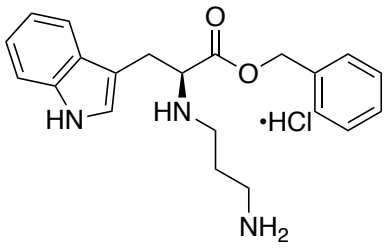


**RH2.43**

Prepared according to general procedure D. Brown solid (222 mg, 97%).

$^1$H NMR (300 MHz, $CDCl_3$) ∂ 11.10 (br s, 1H), 8.24 (br s, 2H), 7.56 (d, *J* = 7.5 Hz, 1H), 7.38 (d, *J* = 8.1 Hz, 1H), 7.22-7.31 (m, 3H), 7.15-7.22 (m, 1H), 7.09 (t, *J* = 7.6 Hz, 1H), 6.92-7.05 (m, 3H), 5.06 (d, *J* = 12.4 Hz, 1H), 4.94 (d, *J* = 12.4 Hz, 1H), 4.27 (br s, 1H), 3.55 (m, 1H), 2.81-3.24 (m, 4H), 2.07 (p, *J* = 7.3 Hz, 2H),

HRMS (ESI) calc'd for $C_{21}H_{25}N_3O_2$ (M+H) 352.20198, found 352.20180.

**General procedure F for the N-acylation of aminobenzoic acids**: to a vial was added the aminobenzoic acid (1 equivalent) and acetone (1.3 mL per equivalent). The vial was cooled in an ice/water bath, and the appropriate acid anhydride (1.1 equivalents) was added with stirring. The reaction was stirred at room temperature overnight, and the solvent was removed *in vacuo*. Distilled water was added and the reaction stirred for an hour, then the

precipitate was filtered. Trituration with ether was sufficient to remove traces of N,O-diacylated products.

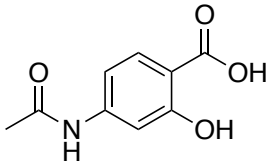

**RH2.44**

Prepared according to general procedure F. White solid (126 mg, 65%).

$^1$H NMR (300 MHz, $d_6$-DMSO) $\partial$ 10.18 (s, 1H), 7.69 (d, $J$ = 8.6 Hz, 1H), 7.33 (s, 1H), 7.02 (d, $J$ = 8.6 Hz, 1H), 2.05 (s, 3H)

$^{13}$C NMR (77 MHz, $d_6$-DMSO) $\partial$ 171.6, 169.0, 162.1, 145.6, 130.9, 110.0, 107.4, 105.6, 24.2

IR (neat, cm$^{-1}$) 3351, 2870 br, 1759, 1674, 1601, 1538, 1411, 1280, 1215, 1162, 792, 681

HRMS (ESI) calc'd for $C_9H_9NO_4$ (M-H) 194.04586, found 194.04561.

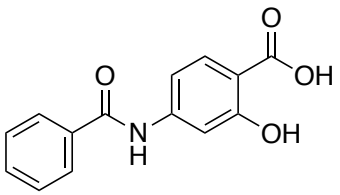

**RH2.45**

Prepared according to general procedure F. White solid (97 mg, 38%).

$^1$H NMR (300 MHz, $d_6$-DMSO) $\partial$ 10.46 (s, 1H), 7.94 (d, $J$ = 7.7 Hz, 2H), 7.76 (d, $J$ = 8.6 Hz, 1H), 7.45-7.66 (m, 4H), 7.34 (dd, $J$ = 8.6, 1.8 Hz, 1H)

$^{13}$C NMR (77 MHz, $d_6$-DMSO) $\partial$ 171.6, 166.1, 161.2, 145.6, 134.5, 131.9, 130.8, 128.4, 127.8, 111.1, 107.9, 106.9

IR (neat, cm$^{-1}$) 3402, 3005, 1671, 1636, 1600, 1524, 1455, 1383, 1308, 1240, 1164, 685

HRMS (ESI) calc'd for $C_{14}H_{11}NO_4$ (M-H) 256.06151, found 256.06121.

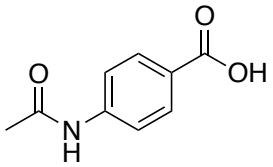

**RH2.46**

Prepared according to general procedure F. White solid (142 mg, 79%).

$^{1}$H NMR (300 MHz, $d_6$-DMSO) $\partial$ 10.23 (s, 1H), 7.86 (d, $J$ = 8.6 Hz, 2H), 7.67 (d, $J$ = 8.6 Hz, 2H), 2.07 (s, 3H)

$^{13}$C NMR (77 MHz, $d_6$-DMSO) $\partial$ 168.8, 166.9, 143.3, 130.3, 124.9, 118.1, 24.1

IR (neat, cm$^{-1}$) 3302, 2820, 1668, 1608, 1590, 1519, 1424, 1290, 1262, 1178, 767

HRMS (ESI) calc'd for $C_9H_9NO_3$ (M-H) 178.05094, found 178.05072.

## 5.3 Procedures and characterization for Chapter 3

### 5.3.1 Biacore assays

Biacore assays for this chapter were performed as described above for Chapter 2.

### 5.3.2 Cell staining for PD-L1 expression

MDA-MD-231 cells were seeded at a density of 20,000 cells in 100 µL of media per well in a 96-well plate, and allowed to grow overnight. The next day, the media were aspirated, and the cells were rinsed three times with 100 µL of ice-cold PBS. The cells were then fixed in 4% formaldehyde in PBS for 10 minutes at room temperature. The formaldehyde solution was aspirated, and the cells washed 3x5 minutes with 100 µL PBS. The wells were then blocked with 100 µL of 1% BSA and 0.3 M glycine in PBS at room temperature for

1 hour. This solution was aspirated, and a solution of AlexaFluor568-conjugated anti-PD-L1 antibody (Abcam; ab213359) diluted 1/100 in 1% BSA/PBS (or just BSA/PBS) was added. The plate was sealed, covered with aluminum foil and incubated at 4˚C overnight. The next day, the solutions were aspirated, and the plate washed once with 0.02 mg / mL Hoescht 33342 in PBS for 5 minutes at room temperature, then twice with PBS for 5 minutes at room temperature. To each well was added Citifluor AF3 imaging solution, and images taken using the DAPI, Texas Red, and bright field channels.

### 5.3.3 Crosslinking experiments

MDA-MD-231 cells were seeded at a density of 200,000 cells in 2 mL of media per well in a 6-well plate, and allowed to grow overnight. The next day, the media were aspirated, and the cells were rinsed three times with 0.5 mL of ice-cold PBS. To each well was added 250 μL of the test compound or an equivalent amount of DMSO diluted in PBS, plus 250 μL of 100 nM PD1-biotin in PBS or an equivalent amount of PBS. The plate was incubated with gentle rocking at 4˚C for 1 hour. To each well was then added either 100 μL of a fresh 6 mM solution of $BS^3$ in PBS (1 mM final concentration) or 100 μL of PBS. The plate was then incubated with gentle rocking at 4˚C for 30 minutes. 100 μL of 0.5 M glycine was then added to each well to quench the reaction, and the plate was shaken for 5 minutes. The supernatant was aspirated, and 300 μL lysis buffer was added to each well. The cells were scraped off into the lysis buffer, transferred to an microfuge tube, and agitated on a rotary shaker for 2 hours at 4˚C. The tubes were spun down at 13,000 rpm for 20 minutes at 4˚C,

and the supernatants pipetted into fresh microfuge tubes. The protein concentration of each lysate was determined by Pierce BCA assay.

The protein lysates were then separated by SDS-PAGE (10 μg total protein per lane) and transferred to a nitrocellulose membrane. The membrane was blocked with 3% BSA in TBS-T for 2 hours, then a 1/5000 dilution of the rabbit anti-PD-L1 antibody in 1% BSA/TBS-T was added and incubated at room temperature for 1 hour. The solution was decanted, and the membrane was washed with TBS-T 3 times for 5 minutes each. An anti-rabbit antibody conjugated to HRP was then diluted 1/10000 in 1% BSA/TBS-T, added to the membrane, and incubated for 1 hour at 4˚C. The membrane was then washed 3 times for 5 minutes each with TBS-T, and membrane was dipped in ECL reagent and exposed to film for between 5 seconds and 10 minutes, depending on signal saturation.

### 5.3.4 Plasmid propagation

Plasmids were propagated in DH5α cells using kanamycin at the selective antibiotic. Plasmids were isolated from overnight cultures in LB medium supplemented with 50 μg/mL kanamycin, using QIAGEN MiniPrep Spin kits according to the manufacturer instructions.

### 5.3.5 Live cell imaging experiments

HEK293T cells were seeded in a 96-well plate at a density of 20,000 cells in 100 μL of medium per well, and allowed to grow undisturbed for 24 to 36 hours.

Plasmid DNA (100 ng per well) was added to a solution of serum-free DMEM (5 μL per well) and P3000 reagent (2 per μg of DNA, 0.2 μL per well). Lipofectamine 3000 (1.5 μL per μg of DNA, 0.15 μL per well) was added to a separate tube with serum-free DMEM (5 μL per well). The DNA solution was added into the Lipofectamine solution, mixed by pipetting 20 times, and incubated at room temperature for 15 minutes.

The media were gently aspirated from the cells, and replaced with serum-free DMEM media. The DNA–lipid complex (10 μL per well) was then added to each well and gently mixed by pipetting up and down three times. The cells were then incubated undisturbed at 37˚C for 6 to 8 hours. After that time had elapsed, the medium was aspirated and replaced with complete F12/DMEM medium supplemented with FBS, and the cells were allowed to grow overnight.

After 24 hours had elapsed from the time of medium replacement, the media were aspirated and the cells incubated with live cell imaging solution containing 0.02 mg/mL Hoescht 33342 for 10 minutes at 37˚C. This solution was then aspirated, the cells were rinsed once more with live cell imaging solution.

A solution of PD1 phycoerythrin conjugate or PD-L1 phycoerythrin conjugate (10 μg/mL) in live cell imaging solution was mixed 1:1 with a solution of the test compound (400 or

100 μM in live cell imaging solution, 1% DMSO), antibody (1 μM in live cell imaging solution) or DMSO (1% in live cell imaging solution) and incubated at room temperature for 15 minutes. 50 μL of these solutions were then added to the rinsed, stained cells and incubated at 37˚C for 15 minutes. The plates were then imaged at 4X magnification using the bright field, DAPI (Hoescht 33342), GFP (GFP-PD1, GFP-PD-L1, or GFP), and Texas Red (PD1-PE or PD-L1-PE) channels, maintaining constant exposure and gain settings across all wells.

### 5.3.6 Synthetic chemistry

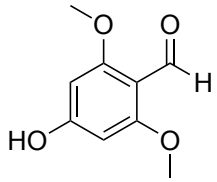


**RH3.01**

To a flame-dried flask was added 3,5-dimethoxyphenol (3.1 g, 20 mmol), imidazole (2.8 g, 41 mmol), and 50 mL of dry DMF. Triisopropylsilyl chloride (6.4 mL, 30 mmol) was then added dropwise, and the reaction was allowed to proceed at room temperature overnight. The reaction was quenched with 75 mL of 10% aqueous sodium bicarbonate and extracted with three 40 mL portions of hexanes. The combined organics were washed with 50 mL 0.5 M HCl, then 50 mL distilled water, dried over $MgSO_4$, filtered, and concentrated to a limpid oil ($^1$H NMR matches the literature).

To a solution of this crude product was added 100 mL of dry THF, then *n*-butylllithium (2.5 M in hexanes, 10.3 mL, 25.9 mmol) was added dropwise. The reaction was stirred at room temperature for 1 hour, yielding a pale straw-coloured solution. To a separate flask

was added 40 mL of dry THF and dry DMF (16 mL, 212 mmol), and the solution was cooled in an ice/water bath. The aryllithium solution was added dropwise to the DMF solution by cannula, and stirred for an additional 2 hours. A solution of 2% HCl in 95% ethanol was made by diluting 3 mL of HCl into 50 mL of absolute ethanol; this solution was added to the DMF solution above at 0 ˚C. The solution turned cloudy and bright yellow, and was stirred overnight. The solution was then cooled to 0 ˚C, 5.5 g of sodium bicarbonate were added, and the reaction was poured into 300 mL of distilled water. The aqueous layer was extracted with three 100 mL portions of 1:1 ether/hexanes, which were then discarded. The aqueous layer was then brought to pH 1 by addition of 10% aqueous HCl, and extracted with 7x100 mL portions of dichloromethane. The combined organics were dried over $Na_2SO_4$, filtered, and concentrated to a bright orange solid (2.47 g, 68%).

$^1$H NMR (300 MHz, $d_6$-DMSO) ∂ 10.62 (br s, 1H), 10.15 (s, 1H), 6.08 (s, 2H), 3.75 (s, 6H)

$^{13}$C NMR (77 MHz, $d_6$-DMSO) ∂ 185.2, 165.0, 163.6, 106.8, 91.7, 55.7

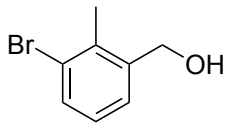


**RH3.02**

To an oven-dried flask under argon was added 3-bromo-2-methylbenzoic acid (7.17 g, 33.3 mmol) and 48 mL of dry THF. The solution was cooled in an ice/water bath, and borane dimethylsulfide complex (5M in THF, 10 mL, 50 mmol) was added dropwise with effervescence. The reaction was left to come to room temperature overnight, then poured into 10% aqueous HCl in an ice/water bath and stirred for 1 hour. The aqueous layer was extracted thrice with ether, and the combined organics washed with water then dried over $MgSO_4$, filtered, and concentrated to a thick oil that solidified in the freezer. The product

was recrystallized from ethyl acetate and hexanes to provide the compound as white crystals (5.65 g, 84%).

$^{1}$H NMR (300 MHz, $CDCl_3$) ∂ 7.51 (d, *J* = 8.0 Hz, 1H), 7.30(d, *J* = 8.0 Hz, 1H), 7.05 (t, *J* = 7.9 Hz, 1H), 4.68 (s, 2H), 2.41 (s, 3H), 1.97 (br s, 1H)

$^{13}$C NMR (77 MHz, $CDCl_3$) ∂

IR (neat, $cm^{-1}$) 3193, 2965, 2884, 1439, 1169, 1012, 775, 716, 631

HRMS (ESI) not found .

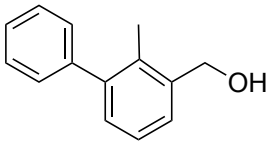


**RH3.03**

To an oven-dried flask was added **RH3.04** (3.12 g, 14.7 mmol) and 30 mL of dry THF. The solution was cooled in an ice/water bath, and borane dimethylsulfide complex (5 M in THF, 4.41 mL, 22.1 mmol) was added dropwise with effervescence and the production of a small amount of black precipitate, assumed to be palladium black. The reaction was left to come to room temperature overnight, then poured into 10% aqueous HCl in an ice/water bath and stirred for 1 hour. The aqueous layer was extracted thrice with ether, and the combined organics washed with twice with saturated sodium bicarbonate and once with water. The solution was then filtered through coarse cottom to remove the black impurity, dried over $MgSO_4$, then filtered again and concentrated to a pale yellow oil that solidified on standing. The product was recrystallized from 10 mL of hexanes to provide the compound as tan crystals (2.52 g, 86%).

$^{1}$H NMR (300 MHz, $CDCl_3$) ∂ 7.19-7.46 (m, 8H), 4.79 (br d, *J* = 5.3 Hz, 2H), 2.25 (s, 3H)

$^{13}$C NMR (77 MHz, $CDCl_3$) ∂ 142.9, 142.0, 139.2, 133.6, 129.6, 129.4, 128.1, 126.8, 126.7, 125.6, 60.1, 15.9

IR (neat, $cm^{-1}$) 3356, 1462, 1423, 1363, 1047, 756, 706

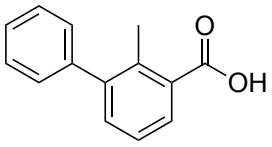


**RH3.04**

To a microwave vial was added 3-bromo-2-methylbenzoic acid (1.6 g, 7.5 mmol), phenylboronic acid (960 mg, 7.9 mmol), sodium carbonate (2.4 g, 22.5 mmol), palladium acetate (7 mg, 0.03 mmol), and 15 mL of distilled water. The vial was sealed and heated in a microwave reactor for 10 minutes at 150 ˚C. The solution was cooled, and the mixture acidified to pH 2 with 15% aqueous HCl. The precipitated product was collected by filtration to yield an off-white solid (1.48 g, 93%).

$^{1}$H NMR (300 MHz, $CDCl_3$) ∂ 8.04 (dd, *J* = 7.8, 1.5 Hz, 1H), 7.28-7.49 (m, 7H), 2.52 (s, 3H)

$^{13}$C NMR (77 MHz, $CDCl_3$) ∂ 173.7, 144.0, 141.4, 138.0, 134.3, 130.3, 129.8, 129.4, 128.2, 127.2, 125.3, 18.8

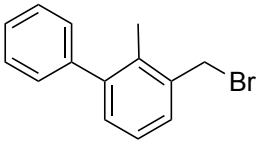


**RH3.05**

To a flask was added **RH3.03** (2.5 g, 12.7 mmol) and 30 mL of dry dichloromethane. The flask was cooled to 0˚C in an ice/water bath, and phosphorus tribromide (1.4 mL, 15 mmol) was added dropwise. The reaction was left to come to room temperature overnight. The next day, the reaction was quenched with distilled water, and extracted thrice with dichloromethane. The combined organic extracts were washed twice with saturated sodium bicarbonate to remove phosphite salts, then once with brine and dried over $Na_2SO_4$, filtered, and concentrated to a clear oil that solidified to a wax on standing. Used without further purification (2.58 g, 78%).

$^1$H NMR (300 MHz, $CDCl_3$) ∂ 7.19-7.47 (m, 8H), 4.61 (s, 2H), 2.31 (s, 3H)

$^{13}$C NMR (77 MHz, $CDCl_3$) ∂

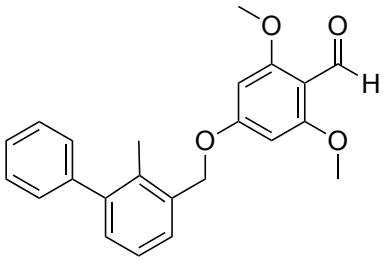


**RH3.06**

To a flask containing the benzyl bromide **RH3.06** (2.58 g, 9.87 mmol) was added **RH3.01** (1.8 g, 9.9 mmol), $Cs_2CO_3$ (7.8 g, 24 mmol), and 50 mL of dry DMF. The reaction was heated to 70 ˚C and stirred at that temperature overnight. The next day, the brown solution was poured into 200 mL of distilled water and the aqueous layer extracted with 3x150 mL portions of ethyl acetate (the product is poorly soluble). The combined organics were washed with 10x200 mL portions of distilled water, then 2x100 mL portions of brine, dried over $Na_2SO_4$, filtered and concentrated to an orange solid. This solid was recrystallized from 1:1 ethyl acetate/hexanes to provide the product as golden needles (3.15 g, 88%).

$^{1}$H NMR (300 MHz, $CDCl_3$) ∂ 10.38 (s, 1H), 7.25-7.48 (m, 8H), 6.22 (s, 2H), 5.17 (s, 2H), 3.90 (s, 6H), 2.28 (s, 3H)

$^{13}$C NMR (77 MHz, $CDCl_3$) ∂ 187.7, 165.5, 164.1, 143.2, 141.7, 134.6, 134.1, 130.1, 129.3, 128.4, 128.1, 127.0, 125.8, 109.0, 91.0, 69.5, 56.1, 16.3

IR (neat, $cm^{-1}$) 2935, 2772, 1668, 1575, 1464, 1443, 1409, 1231, 1204, 1164, 1120, 1022, 798, 768, 708

HRMS (ESI) calc'd for $C_{23}H_{22}O_4$ (M+H) 363.15930, found 363.15928.

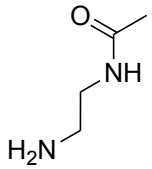


**RH.3.07**

To a flask was added anhydrous ethylenediamine (8 mL, 120 mmol), 30 mL of methanol, and ethyl acetate (2 mL, 20 mmol). The flask was capped and stirred at room temperature for 4 days. The methanol and ethylenediamine were then removed *in vacuo*, leaving an oil that solidified in the freezer. Beige solid, contaminated with ~5% N,N'-diacetylethylenediamine.

$^{1}$H NMR (300 MHz, $CDCl_3$) ∂ 6.51 (br s, 1 H), 3.22 (q, $J$ = 5.9Hz, 2H), 2.77 (t, $J$ = 5.9Hz, 2H), 1.94 (s, 3H), 1.36 (br s, 2H)

$^{13}$C NMR (77 MHz, $CDCl_3$) ∂ 170.6, 42.2, 41.3, 23.2

IR (neat, $cm^{-1}$) 3324, 3288, 3207, 2950, 1634, 1563, 1435, 1368, 1293, 1046, 938, 615, 516

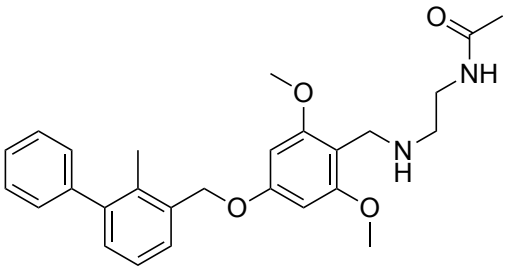

**RH3.08**

To a vial was added **RH3.06** (102 mg, 0.28 mmol), N-acetylethylenediamine (50.8 mg, 0.49 mmol), and 1.5 mL of methanol. The reaction was stirred for 1 hour to ensure complete imine formation. The clear, golden-yellow solution was then cooled in an ice/water bath, and NaBH4 (24 mg, 0.63 mmol) was added. Bubbling was observed. The reaction was stirred at 0 ˚C for 2 hours, then quenched with saturated sodium bicarbonate. The aqueous solution was extracted thrice with ethyl acetate, and the combined organic layers were dried over $Na_2SO_4$, filtered, and concentrated to a clear oil that solidified on standing. Recrystallization from hexanes/ethyl acetate provided the compound as a white crystalline solid (98 mg, 78%).

$^1$H NMR (300 MHz, $CDCl_3$) ∂ 7.23-7.48 (m, 8H), 6.26 (s, 2H), 6.24 (br s, 1H), 5.09 (s, 2H), 3.82 (s, 6H), 3.77 (s, 2H), 3.34 (q, *J* = 5.8Hz, 2H), 2.69 (t, *J* = 5.8Hz, 2H), 2.28 (s, 3H), 1.98 (s, 3H)

$^{13}$C NMR (77 MHz, $CDCl_3$) ∂ 170.1, 159.8, 159.3, 143.0, 141.9, 135.1, 134.5, 130.3, 129.4, 128.3, 128.1, 126.9, 125.6, 109.0, 91.3, 69.3, 55.7, 47.0, 40.3, 38.9, 23.3, 16.2

IR (neat, $cm^{-1}$) 3317, 2934, 1645, 1615, 1596, 1456, 1199, 1145, 1031, 798, 701

HRMS (ESI) calc'd for $C_{27}H_{32}N_2O_4$ (M+H) 449.24351, found 449.24350.

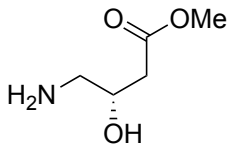

**RH3.09**

Methanolic hydrogen chloride was prepared by cooling 7 mL of methanol in an ice-water bath, followed by addition of acetyl chloride (1.4 mL, 20 mmol) with rapid stirring. The solution was stirred at 0 ˚C for 30 minutes, then at room temperature for 15 minutes. (S)-(+)-4-amino-3-hydroxybutyric acid (200 mg, 1.68 mmol) was then added, and the solution heated to reflux overnight. The solvent was removed in vacuo and the crude product used without purification.

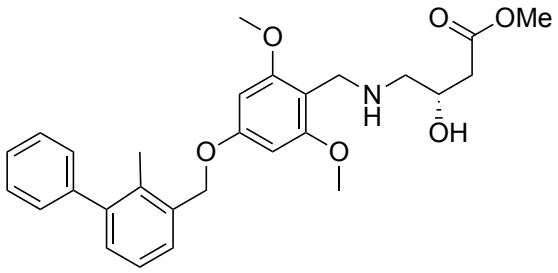

**RH3.10**

To a solution of the amino ester hydrochloride **RH3.09** (107 mg, 0.6 mmol) in 2.5 mL of methanol was added **RH3.06** (217 mg, 0.6 mmol)—the solution turned pink—and stirred at room temperature for 3 hours until all solids had dissolved. $NaBH_3CN$ (60 mg, 0.95 mmol) was added in one portion—the pink colour reverted to pale yellow—and the reaction was stirred at room temperature overnight. The reaction was diluted with distilled water, and extracted thrice with ethyl acetate. The combined organic layers were washed with saturated sodium bicarbonate, then with brine, dried over $Na_2SO_4$, filtered, and concentrated to an oil. Purification by chromatography over silica gel (66:33:1 to 0:99:1

dichloromethane/ethyl acetate/trimethylamine) yielded an oil that was then triturated with pentane to yield a solid (130 mg, 45%).

$^1$H NMR (300 MHz, $CDCl_3$) ∂ 7.13-7.38 (m, 8H), 6.16 (s, 2H), 5.00 (s, 2H), 4.04 (m, 1H), 3.72 (s, 8H), 3.60 (s, 3H), 2.95 (br s, 2H), 2.60 (dd, *J* = 12.2, 3.7 Hz, 1H), 2.28-2.47 (m, *3*H), 2.19 (s, 3H)

$^{13}$C NMR (77 MHz, $CDCl_3$) ∂ 172.5, 159.8, 159.4, 143.0, 141.9, 135.1, 134.5, 130.3, 129.4, 128.3, 128.1, 126.9, 125.6, 108.8, 91.3, 69.3, 66.1, 55.7, 53.2, 51.7, 40.7, 39.7, 16.2

IR (neat, $cm^{-1}$) 2940, 2839, 1733, 1593, 1195, 1135, 762, 728, 702

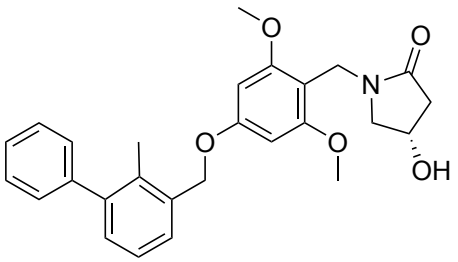


**RH3.11**

To a flask was added **RH3.10** (127 mg, 0.27 mmol), then sodium hydroxide (1 M, 6 mL, 6 mmol) and 6 mL of methanol, heated to 60 ˚C and stirred overnight. The solvent was evaporated, and the residue purified by silica gel chromatography (2% to 4% methanol in dichloromethane) to yield a tan solid (88 mg, 73%).

$^1$H NMR (300 MHz, $CDCl_3$) ∂ 7.23-7.48 (m, 8H), 6.24 (s, 2H), 5.09 (s, 2H), 4.57 (d, *J* = 13.6 Hz, 1H), 4.50 (d, *J* = 13.6 Hz, 1H), 4.38 (ddt, *J* = 6.6, 5.8, 2.4 Hz, H), 3.80 (s, 6H), 3.41 (dd, *J* = 11.2, 5.8 Hz, 1H), 3.12 (dd, *J* = 11.2, 2.3 Hz, 1H), 2.68 (dd, *J* = 17.2, 6.7 Hz, 1H), 2.38 (dd, *J* = 17.2, 2.6 Hz, 1H), 2.28 (s, 3H)

$^{13}$C NMR (77 MHz, $CDCl_3$) ∂ 171.9, 160.5, 159.9, 143.1, 141.9, 134.9, 134.5, 130.4, 129.4, 128.3, 128.1, 127.9, 125.6, 104.4, 91.2, 69.3, 64.6, 55.8, 55.2, 41.6, 34.5, 16.2

IR (neat, $cm^{-1}$) 3324, 2921, 1657, 1611, 1450, 1226, 1148, 1127, 758, 701

HRMS (ESI) calc'd for $C_{27}H_{29}NO_5$ (M+Na) 470.19434, found 470.19363.

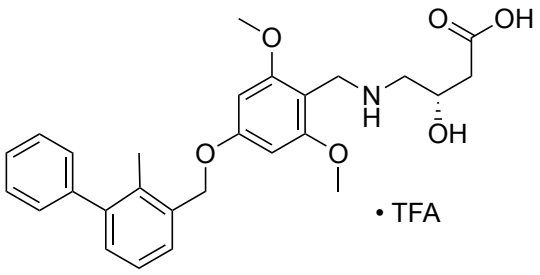


**RH3.12**

To a vial was added (S)-(+)-4-amino-3-hydroxybutyric acid (30 mg, 0.25 mmol), lithium hydroxide monohydrate (12 mg, 0.26 mmol), and 1.25 mL of methanol. Stirred until all the solid was dissolved, about 5 minutes. To the vial was then added **RH3.06** (101 mg, 0.28 mmol), and stirred for 1 hour. The vial was cooled in an ice/water bath, and solid $NaBH_4$ (19 mg, 0.5 mmol) was then added in one portion. The reaction was stirred for 2 hours, then quenched by addition of saturated aqueous ammonium chloride. The reaction was diluted with isopropanol to precipitate the borate and ammonium salts, filtered through cotton, and concentrated to a residue. This residue was purified by HPLC-MS. White solid (23 mg, 16%).

$^1$H NMR (300 MHz, $CDCl_3$) $\partial$ 7.06-7.37 (m, 8H), 6.31 (s, 2H), 5.10 (s, 2H), 4.17 (dtd, $J$ = 9.5, 6.6, 3.4 Hz, 1H), 4.13 (d, $J$ = 1.3 Hz, 2H), 3.79 (s, 6H), 3.00 (dd, $J$ = 12.9, 3.4 Hz, 1H), 2.81 (dd, $J$ = 12.9, 9.5 Hz, 1H), 2.39 (d, $J$ = 6.6 Hz, 2H), 2.14 (s, 3H)

$^{13}$C NMR (77 MHz, $CDCl_3$) $\partial$ 175.1, 163.8, 161.3, 144.4, 143.4, 136.6, 135.7, 131.1, 130.4, 129.4, 129.2, 128.0, 126.6, 100.5, 92.5, 70.6, 64.5, 56.5, 52.3, 41.5, 40.9, 16.4

IR (neat, $cm^{-1}$) 2500-3400, 2943, 1669, 1608, 1594, 1454, 1421, 1195, 1134, 1024

HRMS (ESI) calc'd for $C_{27}H_{31}NO_6$ (M+H) 466.22230, found 466.22244.

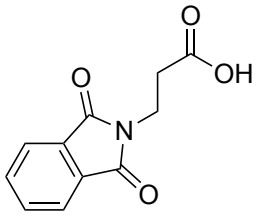

**RH3.13**

Phthalic anhydride (7.43 g, 50 mmol) and ß-alanine (4.47 g, 50 mmol) were melted together in a flask heated to 170 ˚C. The reaction was accompanied by copious evolution of steam. The melt was held at this temperature for 2 hours, then cooled to room temperature. The reaction mass formed a solid. This was recrystallized from 75 mL of distilled water to yield white flaky crystals (9.97 g, 91%).

$^{1}$H NMR (300 MHz, $CDCl_3$) $\partial$ 7.81-7.90 (AA`XX` m, 2H), 7.68-7.77 (AA`XX` m, 2H), 4.00 (t, $J$ = 7.4 Hz, 2H), 2.80 (t, $J$ = 7.4 Hz, 2H)

$^{13}$C NMR (77 MHz, $CDCl_3$) $\partial$ 176.4, 168.0, 134.1, 131.9, 123.4, 33.4, 32.6

IR (neat, $cm^{-1}$) 3196, 1769, 1685, 1466, 1439, 1376, 1191, 1000

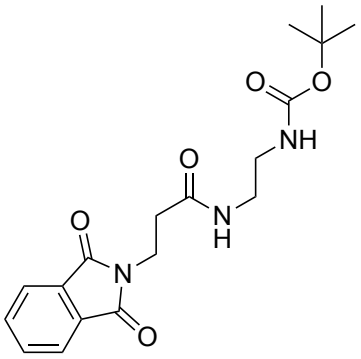

**RH3.14**

To a flask was added N-phthaloyl ß-alanine (5.48 g, 25 mmol), EDC•HCl (7.2 g, 37.5 mmol), and 125 mL dichloromethane and stirred at room temperature for 10 minutes. A solution of N-Boc ethylenediamine (4 g, 25 mmol), DMAP (311 mg, 2.54 mmol), and

triethylamine (7 mL, 50 mmol) in 25 mL of dichloromethane was then added to the reaction flask, and the reaction allowed to proceed overnight. The next day, the milky-white solution was diluted with water, and the aqueous layer extracted thrice with dichloromethane. The combined organic layers were washed twice with 1M HCl, twice with saturated sodium bicarbonate, and once with brine, then dried over $Na_2SO_4$, filtered, and concentrated to a fluffy white solid (7.06 g, 78%).

$^1$H NMR (300 MHz, $CDCl_3$) ∂ 7.79-7.88 (AA`XX` m, 2H), 7.67-7.75 (AA`XX` m, 2H), 6.45, (br s, 1H), 5.05 (br s, 1H), 4.00 (t, $J$ = 7.2 Hz, 2H), 3.17-3.38 ($A_2B_2$, $J$ ~ 5.7 Hz, 4H), 2.60 (t, $J$ = 7.2Hz, 2H), 1.42 (s, 9H)

$^{13}$C NMR (77 MHz, $CDCl_3$) ∂ 170.4, 168.2, 134.0, 132.0, 123.3, 40.6, 40.1, 34.9, 34.4, 29.3

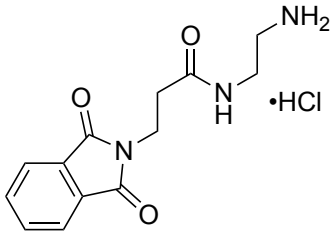


**RH3.15**

A methanolic solution of hydrogen chloride was made by cooling 14 mL of methanol in an ice/water bath. Acetyl chloride (2 mL, 28 mmol) was then added dropwise with rapid stirring, and left to react at 0 ˚C for 30 minutes and a further 15 minutes at room temperature. **RH3.14** (1.02 g, 2.8 mmol) was then added in one portion, and allowed to react overnight. The next day, the solution was poured into an excess of ether, and the precipitate was collected by filtration to yield a white solid contaminated with a small amount of ethylenediamine dihydrochloride (708 mg, 85%).

$^1$H NMR (300 MHz, $D_2O$) ∂ 7.70 (s, 4H), 3.83 (t, *J* = 6.6 Hz, 2H), 3.34 (t, *J* = 6.0 Hz, 2H), 3.00 (t, *J* = 6.0 Hz, 2H), 2.51 (t, *J* = 6.6 Hz, 2H)

$^{13}$C NMR (77 MHz, $D_2O$) ∂ 174.6, 170.0, 134.8, 131.0, 123.4, 39.0, 36.8, 34.5, 34.5

IR (neat, $cm^{-1}$) 3369, 2912, 1769, 1708, 1646, 1380, 872, 723

HRMS (ESI) calc'd for $C_{15}H_{25}N_3O_4$ (M+H) 312.19230, found 312.19202.

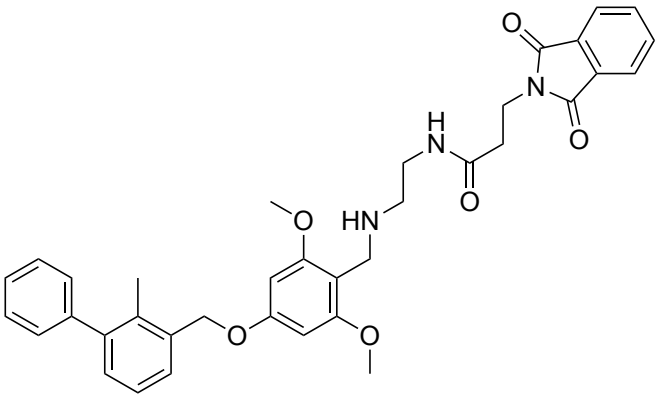


**RH3.16**

To a vial was added **RH3.06** (362 mg, 1 mmol), **RH3.15** (300 mg, 1 mmol), and 20 mL of methanol. The reaction was stirred overnight to ensure iminium formation, resulting in a peach-coloured solution. To the vial was added $NaBH_3CN$ (180 mg, 2.86 mmol), and the solution turned pale yellow. The reaction was stirred at room temperature for 3 hours, then quenched by addition of saturated sodium bicarbonate. The aqueous solution was extracted thrice with dichloromethane, and the combined organic layers were dried over $Na_2SO_4$, filtered, and concentrated to a sticky pale yellow oil. Purification by silica gel chromatography (1.5 to 10% methanol in dichloromethane) yielded the product as a yellow glass (232.3 mg, 38%).

$^1$H NMR (300 MHz, $CDCl_3$) ∂ 7.68-7.76 (AA`XX` m, 2H), 7.56-7.64 (AA`XX` m, 2H), 7.15-7.39 (m, 8H), 7.03 (br s, 1H), 6.17 (s, 2H), 5.00 (s, 2H), 3.93 (t, *J* = 7.2 Hz, 2H), 3.81

(s, 2H), 3.75 (s, 6H), 3.31 (br q, $J$ = 5 Hz, 2H), 2.68 (br t, $J$ = 5 Hz, 2H), 2.54 (, $J$ = 7.2 Hz, 2H), 2.18 (s, 3H)

$^{13}$C NMR (77 MHz, $CDCl_3$) $\partial$ 170.1, 168.1, 160.6, 159.5, 143.0, 141.9, 134.9, 134.5, 133.9, 132.1, 130.3, 129.4, 128.3, 128.1, 126.9, 125.6, 123.2, 105.4, 91.2, 69.3, 55.8, 46.8, 40.2, 37.6, 34.7, 34.5, 16.2

IR (neat, $cm^{-1}$) 3228, 2937, 1772, 1710, 1665, 1593, 1139, 762, 717, 703, 530

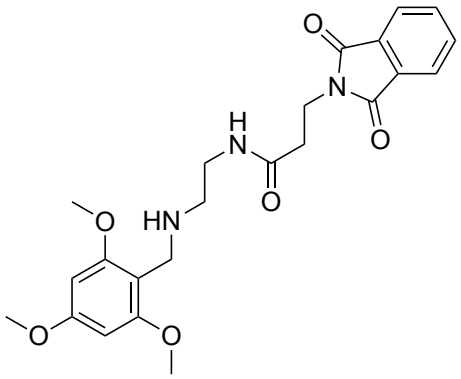


**RH3.17**

To a vial was added 2,4,6-trimethoxybenzaldehyde (196 mg, 1 mmol), **RH3.15** (300 mg, 1 mmol), and 5 mL of methanol. The reaction was stirred overnight to ensure iminium formation – the solution turned pink. Solid $NaBH_3CN$ (150 mg, 2.4 mmol) was added in one portion—the solution turned yellow—and the reaction stirred at room temperature for 3 hours. The reaction was quenched with saturated aqueous sodium bicarbonate, and extracted thrice with dichloromethane. The combined organic layers were dried over $Na_2SO_4$, filtered, and concentrated to a pale yellow oil that crystallized on standing. Purification by silica gel chromatography (3 to 15% methanol in dichloromethane) provided the product as an off-white solid (95 mg, 22%).

$^1$H NMR (300 MHz, $CDCl_3$) ∂ 7.77-7.86 (AA`XX` m, 2H), 7.64-7.73 (AA`XX` m, 2H), 6.44 (br s, 1H), 6.10 (s, 2H), 4.00 (t, *J* = 7.4 Hz, 2H), 3.79 (s, 3H), 3.78 (s, 6H), 3.71 (br s, 2H), 3.30 (q, *J* = 5.5 Hz, 2H), 2.63 (t, *J* = 5.6 Hz, 2H), 2.60 (q, *J* = 7.4 Hz, H)

$^{13}$C NMR (77 MHz, $CDCl_3$) ∂ 169.7, 168.1, 160.5, 159.3, 133.9, 132.1, 123.2, 108.1, 90.4, 55.6, 55.3, 46.8, 40.2, 38.6, 34.7, 34.5

IR (neat, $cm^{-1}$) 3305, 3186, 2933, 2839, 1773, 1719, 1661, 1596, 1143, 823, 718

HRMS (ESI) calc'd for $C_{23}H_{27}N_3O_6$ (M+H) 442.19730, found 442.19686.

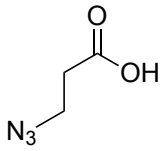


**RH3.18**

To a microwave vial was added 3-bromopropionic acid (1.53 g, 10 mmol). A solution of sodium azide (845 mg, 13 mmol) and sodium bicarbonate (840 mg, 10 mmol) in 20 mL of distilled water was then added dropwise (caution: vigorous evolution of gas) at room temperature. After the bubbling had subsided, the vial was capped and heated in a microwave reactor at 120 ˚C for 30 minutes. The reaction was cooled, acidified to pH 2, and extracted thrice with ether. The combined organic fractions were dried over $MgSO_4$, filtered, and concentrated to an oil (1.64 g, 71%).

$^1$H NMR (300 MHz, $CDCl_3$) ∂ 3.60 (t, *J* = 6.4 Hz, 2H), 2.65 (t, *J* = 6.4 Hz, 2H)

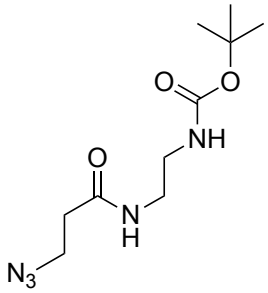


**RH3.19**

To a flask was added 3-azidopropionic acid **RH3.18** (1.96 g, 17 mmol), EDC•HCl (4.89 g, 25.5 mmol), and 80 mL of dichloromethane. Dissolved N-Boc ethylenediamine (3.27 g, 20.4 mmol) and Hünig's base (6 mL, 34.4 mmol) in 10 mL of dichloromethane and added to the reaction with stirring. DMAP (208 mg, 1.7 mmol) was then added. The reaction was stirred at room temperature overnight, then diluted with another 90 mL of dichloromethane, washed twice with 1 M HCl and twice with saturated sodium bicarbonate. The organic layer was dried over $Na_2SO_4$, filtered, and concentrated to a white solid. Purified by silica gel column chromatography (ethyl acetate; poor solubility in this solvent) to yield a white powder (2.05 g, 47%).

$^1$H NMR (300 MHz, $CDCl_3$) $\partial$ 6.58 (br s, 1H), 5.03 (br s, 1H), 3.60 (t, $J$ = 6.5 Hz, 2H), 3.37 (q, $J$ = 6.0 Hz, 2H), 3.27 (, $J$ = 6.0 Hz, 2H), 2.42 (t, $J$ = 6.5Hz, 2H)

$^{13}$C NMR (77 MHz, $CDCl_3$) $\partial$ 170.5, 157.1, 79.8, 47.3, 40.95, 40.0, 35.8, 28.3

IR (neat, cm$^{-1}$) 3341, 3304, 2981, 2944, 2103, 1706, 1656, 1557, 1535, 1283, 1239, 1170, 1151, 976, 656

HRMS (ESI) calc'd for $C_{10}H_{19}N_5O_3$ (M+Na) 280.13800, found 280.13779.

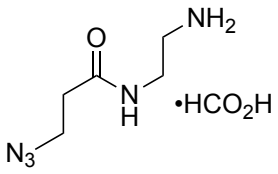


**RH3.20**

To a vial containing **RH3.19** (514 mg, 2 mmol) was added 1 mL of formic acid. The reaction was stirred overnight, then the formic acid removed by azeotropic distillation with toluene. The residue was triturated with ether to yield a yellow oily residue (quantitiative yield).

$^1$H NMR (300 MHz, $D_2O$) ∂ 8.24 (s, 1H), 3.50 (t, *J* = 6.4 Hz, 2H), 3.42 (t, *J* = 6.0 Hz, 2H), 3.05 (t, *J* = 6.0 Hz, 2H), 2.46 (t, *J* = 6.3 Hz, 2H)

$^{13}$C NMR (77 MHz, $D_2O$) ∂ 174.6, 168.5, 46.9, 39.0, 36.8, 34.8

IR (neat, $cm^{-1}$) 2500-3400, 2929, 2101, 1652, 1539, 1179

HRMS (ESI) calc'd for $C_5H_{11}N_5O$ (M+H) 158.10370, found 158.10367.

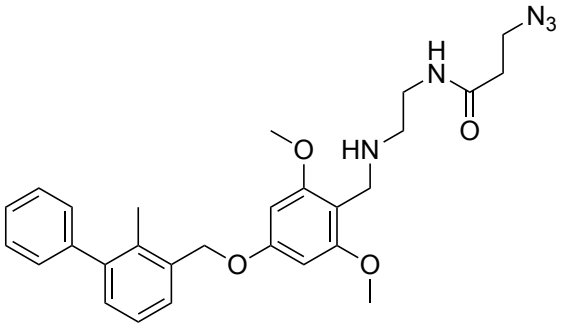


**RH3.21**

To a flask was added **RH3.20** (1 M in methanol, 1 mL, 1 mmol), **RH3.06** (362 mg, 1 mmol), and 4 mL of methanol. The reaction was stirred overnight at room temperature to ensure iminium formation. $NaBH_3CN$ (125 mg, 2 mmol) was then added, and the reaction stirred at room temperature for 3 hours. The reaction was quenched with aqueous sodium bicarbonate, extracted thrice with dichloromethane, washed once with saturated sodium bicarbonate, dried over $Na_2SO_4$, filtered, and concentrated to a yellow oil. Silica gel chromatography (2 to 8% methanol in dichloromethane) provided the product as a sticky residue (321 mg, 64%).

$^1$H NMR (300 MHz, $CDCl_3$) ∂ 7.23-7.47 (m, 8H), 6.91 (br t, *J* ~ 4 Hz, 1H), 6.25 (s, 2H), 5.09 (s, 2H), 3.82 (s, 6H), 3.80 (dd, *J* = 9.7, 3.3 Hz, 2H), 3.60 (t, *J* = 6.5 Hz, 2H), 3.39 (q, *J* = 5.5 Hz, 2H), 3.19 (br s, 2H), 2.73 (t, *J* = 5.5 Hz, 2H), 2.44 (t, *J* = 6.5, Hz, 2H), 2.27 (s, 3H)

$^{13}$C NMR (77 MHz, $CDCl_3$) ∂ 170.0, 160.2, 159.4, 143.1, 141.9, 135.0, 134.5, 130.4, 129.4, 128.3, 128.1, 126.9, 125.7, 107.1, 91.2, 69.4, 55.7, 47.4, 46.9, 40.3, 38.3, 35.7, 16.2

IR (neat, $cm^{-1}$) 3300, 2933, 2098, 1654, 1593, 1454, 1138, 1027, 761, 702

HRMS (ESI) calc'd for $C_{28}H_{33}N_5O_4$ (M+H) 504.26060, found 504.26091.

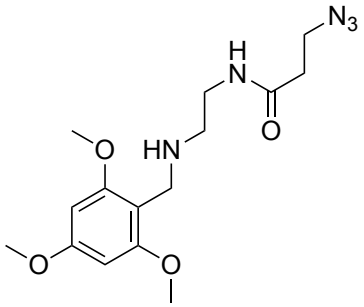


**RH3.22**

To a flask was added **RH3.20** (1 M in methanol, 1 mL, 1 mmol), 2,4,6-trimethoxybenzaldehyde (196 mg, 1 mmol), and 4 mL of methanol. The reaction was stirred overnight at room temperature to ensure iminium formation. $NaBH_3CN$ (125 mg, 2 mmol) was then added, and the reaction stirred at room temperature for 3 hours. The reaction was quenched with aqueous sodium bicarbonate, extracted thrice with dichloromethane, washed once with saturated sodium bicarbonate, dried over $Na_2SO_4$, filtered, and concentrated to a yellow oil. Silica gel chromatography (2 to 8% methanol in dichloromethane) provided the product as a sticky residue (142 mg, 42%).

$^1$H NMR (300 MHz, $CDCl_3$) ∂ 7.42 (br s, 1H), 6.10 (s, 2H), 3.91 (s, 2H), 3.82 (s, 6H), 3.79 (s, 3H), 3.58 (t, $J$ = 6.5 Hz, 2H), 3.41 (q, $J$ = 5.2 Hz, 2H), 2.77 (t, $J$ = 5.2 Hz, 2H), 2.45 (t, $J$ = 6.5 Hz, 2H)

$^{13}$C NMR (77 MHz, $CDCl_3$) ∂ 170.3, 161.6, 159.5, 103.7, 90.4, 55.7, 55.4, 47.3, 46.8, 40.2, 37.3, 35.6

IR (neat, $cm^{-1}$) 3288, 2939, 2839, 2098, 1652, 1593, 1455, 1418, 1203, 1137, 949, 813

HRMS (ESI) calc'd for $C_{15}H_{23}N_5O_4$ (M+H) 338.18230, found 338.18162.

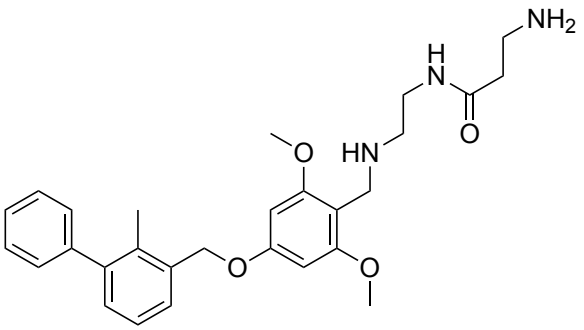


**RH3.23**

To a vial containing **RH3.16** (147 mg, 0.24 mmol) was added 1.5 mL anhydrous ethanol. Hydrazine hydrate (50 µL, 0.96 mmol) was then added, and the vial was capped and stirred overnight at room temperature. The next day, the white slurry was centrifuged at 13,000 rpm for 5 minutes in a microfuge tube, and the solid rinsed with ethanol two more times. The combined supernatants were concentrated to a white paste, and this paste was mixed with 1.5 mL of ethanol and filtered through a very thin pad of Celite. The filtrate was concentrated to a sticky residue (64 mg, 64%)

$^1$H NMR (300 MHz, $d_4$-MeOD) ∂ 7.14-7.47 (m, 8H), 6.34 (s, 2H), 5.15 (s, 2H), 3.83 (s, 6H), 3.82 (d, *J* = 7.8 Hz, 2H), 3.34 (t, *J* = 6.3 Hz, 2H), 2.98 (t, *J* = 6.6 Hz, 2H), 2.69 (t, *J* = 6.3 Hz, 2H), 2.37 (t, *J* = 6.6 Hz, 2H), 2.24 (s, 3H)

$^{13}$C NMR (77 MHz, $d_4$-MeOD) ∂ 174.5, 161.8, 160.8, 144.3, 143.5, 137.0, 135.6, 131.0, 130.4, 129.4, 129.2, 128.0, 126.6, 107.9, 92.4, 70.4, 61.6, 58.3, 56.3, 41.4, 39.6, 38.8, 16.4

HRMS (ESI) calc'd for $C_{28}H_{35}N_3O_4$ (M+H) 478.27030, found 478.27002.

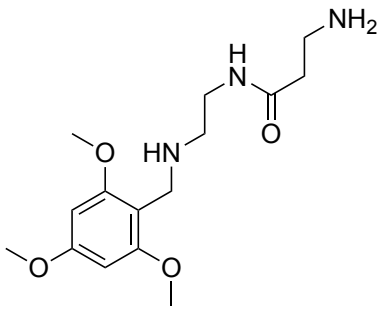

**RH3.24**

To a vial containing **RH3.17** (104 mg, 0.24 mmol) was added 1.5 mL anhydrous ethanol. Hydrazine hydrate (50 µL, 0.96 mmol) was then added, and the vial was capped and stirred overnight at room temperature. The next day, the white slurry was centrifuged at 13,000 rpm for 5 minutes in a microfuge tube, and the solid rinsed with ethanol two more times. The combined supernatants were concentrated to a white paste, and this paste was mixed with 1.5 mL of ethanol and filtered through a very thin pad of Celite. The filtrate was concentrated to a sticky residue (52 mg, 70%)

$^{1}$H NMR (300 MHz, $d_4$-MeOD) $\partial$ 6.25 (s, 2H), 3.85 (buried $CH_2$), 3.85 (s, 6H), 3.84 (s, 3H), 3.36 (t, $J$ = 6.6 Hz, 2H), 2.95 (t, $J$ = 6.6 Hz, 2H), 2.72 (t, $J$ = 6.2 Hz, 2H), 2.40 (t, $J$ = 6.6 Hz, 2H)

$^{13}$C NMR (77 MHz, $d_4$-MeOD) $\partial$ 174.5, 162.8, 160.8, 107.3, 91.7, 91.5, 58.3, 56.2, 55.8, 41.4, 39.5, 38.8, 38.7

# Bibliography


1. Cooper, G., The Cell: A Molecular Approach, 2nd edn. The Cell: A Molecular Approach. Sunderland, MA. USA: Sinauer Associates: 2000.
2. Defining Cancer. https://www.cancer.gov/about-cancer/understanding/what-is-cancer (accessed November 20, 2017).
3. Croce , C. M., Oncogenes and Cancer. *New England Journal of Medicine* **2008,** *358* (5), 502-511.
4. Hansford, S.; Huntsman, D. G., Boveri at 100: Theodor Boveri and genetic predisposition to cancer. *Journal of Pathology* **2014,** *234* (2), 142-145.
5. Knudson, A. G., Two genetic hits (more or less) to cancer. *Nature Reviews Cancer* **2001,** *1*, 157.
6. Warburg, O., On the Origin of Cancer Cells. *Science* **1956,** *123* (3191), 309-314.
7. Hanahan, D.; Weinberg, R. A., The Hallmarks of Cancer. *Cell* **2000,** *100* (1), 57-70.
8. Eriksson, D.; Stigbrand, T., Radiation-induced cell death mechanisms. *Tumor Biology* **2010,** *31* (4), 363-372.
9. Housman, G.; Byler, S.; Heerboth, S.; Lapinska, K.; Longacre, M.; Snyder, N.; Sarkar, S., Drug Resistance in Cancer: An Overview. *Cancers* **2014,** *6* (3), 1769-1792.
10. Luqmani, Y. A., Mechanisms of drug resistance in cancer chemotherapy. *Medical Principles and Practice* **2005,** *14 Suppl 1*, 35-48.
11. Zahreddine, H.; Borden, K. L. B., Mechanisms and insights into drug resistance in cancer. *Frontiers in Pharmacology* **2013,** *4*, 28.
12. McAllister, S. S.; Weinberg, R. A., Tumor-Host Interactions: A Far-Reaching Relationship. *Journal of Clinical Oncology* **2010,** *28* (26), 4022-4028.
13. Li, H.; Fan, X.; Houghton, J., Tumor microenvironment: The role of the tumor stroma in cancer. *Journal of Cellular Biochemistry* **2007,** *101* (4), 805-815.
14. Wang, M.; Zhao, J.; Zhang, L.; Wei, F.; Lian, Y.; Wu, Y.; Gong, Z.; Zhang, S.; Zhou, J.; Cao, K.; Li, X.; Xiong, W.; Li, G.; Zeng, Z.; Guo, C., Role of tumor microenvironment in tumorigenesis. *Journal of Cancer* **2017,** *8* (5), 761-773.
15. Balkwill, F. R.; Capasso, M.; Hagemann, T., The tumor microenvironment at a glance. *Journal of Cell Science* **2012,** *125* (23), 5591-5596.
16. Whiteside, T. L., The tumor microenvironment and its role in promoting tumor growth. *Oncogene* **2008,** *27*, 5904.
17. Hanahan, D.; Weinberg, Robert A., Hallmarks of Cancer: The Next Generation. *Cell* **2011,** *144* (5), 646-674.
18. Woo, S.-R.; Corrales, L.; Gajewski, T. F., Innate Immune Recognition of Cancer. *Annual Review of Immunology* **2015,** *33* (1), 445-474.
19. Shurin, M. R., Cancer as an immune-mediated disease. *ImmunoTargets and Therapy* **2012,** *1*, 1-6.
20. Liu, Y.; Zeng, G., Cancer and Innate Immune System Interactions: Translational Potentials for Cancer Immunotherapy. *Journal of Immunotherapy* **2012,** *35* (4), 299-308.
21. Hagerling, C.; Casbon, A.-J.; Werb, Z., Balancing the innate immune system in tumor development. *Trends in Cell Biology* **2015,** *25* (4), 214-220.

22. Warrington, R.; Watson, W.; Kim, H. L.; Antonetti, F. R., An introduction to immunology and immunopathology. *Allergy, Asthma & Clinical Immunology* **2011,** *7* (1), S1.
23. Marcus, A.; Gowen, B. G.; Thompson, T. W.; Iannello, A.; Ardolino, M.; Deng, W.; Wang, L.; Shifrin, N.; Raulet, D. H., Recognition of tumors by the innate immune system and natural killer cells. *Advances in Immunology* **2014,** *122*, 91-128.
24. Rao, C. V.; Yamada, H. Y., Genomic Instability and Colon Carcinogenesis: From the Perspective of Genes. *Frontiers in Oncology* **2013,** *3*, 130.
25. Hubbard, G. K.; Mutton, L. N.; Khalili, M.; McMullin, R. P.; Hicks, J. L.; Bianchi-Frias, D.; Horn, L. A.; Kulac, I.; Moubarek, M. S.; Nelson, P. S.; Yegnasubramanian, S.; De Marzo, A. M.; Bieberich, C. J., Combined MYC activation and Pten loss are sufficient to create genomic instability and lethal metastatic prostate cancer. *Cancer Research* **2016,** *76* (2), 283-292.
26. Taylor, R. A.; Fraser, M.; Livingstone, J.; Espiritu, S. M. G.; Thorne, H.; Huang, V.; Lo, W.; Shiah, Y.-J.; Yamaguchi, T. N.; Sliwinski, A.; Horsburgh, S.; Meng, A.; Heisler, L. E.; Yu, N.; Yousif, F.; Papargiris, M.; Lawrence, M. G.; Timms, L.; Murphy, D. G.; Frydenberg, M.; Hopkins, J. F.; Bolton, D.; Clouston, D.; McPherson, J. D.; van der Kwast, T.; Boutros, P. C.; Risbridger, G. P.; Bristow, R. G., Germline BRCA2 mutations drive prostate cancers with distinct evolutionary trajectories. *Nature Communications* **2017,** *8*, 13671.
27. Bayani, J.; Marrano, P.; Graham, C.; Zheng, Y.; Li, L.; Katsaros, D.; Lassus, H.; Butzow, R.; Squire, J. A.; Diamandis, E. P., Genomic instability and copy-number heterogeneity of chromosome 19q, including the kallikrein locus, in ovarian carcinomas. *Molecular Oncology* **2011,** *5* (1), 48-60.
28. Mold, J. E.; McCune, J. M., Chapter 3 - Immunological Tolerance During Fetal Development: From Mouse to Man. In *Advances in Immunology*, Alt, F. W., Ed. Academic Press: 2012; Vol. 115, pp 73-111.
29. Xing, Y.; Hogquist, K. A., T-Cell Tolerance: Central and Peripheral. *Cold Spring Harbor Perspectives in Biology* **2012,** *4* (6).
30. Schreiber, R. D.; Old, L. J.; Smyth, M. J., Cancer Immunoediting: Integrating Immunity's Roles in Cancer Suppression and Promotion. *Science* **2011,** *331* (6024), 1565-1570.
31. Kim, R.; Emi, M.; Tanabe, K., Cancer immunoediting from immune surveillance to immune escape. *Immunology* **2007,** *121* (1), 1-14.
32. Vesely, M. D.; Schreiber, R. D., Cancer immunoediting: antigens, mechanisms, and implications to cancer immunotherapy. *Annals of the New York Academy of Sciences* **2013,** *1284* (1), 1-5.
33. Mittal, D.; Gubin, M. M.; Schreiber, R. D.; Smyth, M. J., New insights into cancer immunoediting and its three component phases—elimination, equilibrium and escape. *Current Opinion in Immunology* **2014,** *27* (Supplement C), 16-25.
34. Rudd, C. E., Cell cycle 'check points' T cell anergy. *Nature Immunology* **2006,** *7*, 1130.
35. Bardhan, K.; Anagnostou, T.; Boussiotis, V. A., The PD1:PD-L1/2 Pathway from Discovery to Clinical Implementation. *Frontiers in Immunology* **2016,** *7* (550).
36. Waldmann, T. A., Effective Cancer Therapy Through Immunomodulation. *Annual Review of Medicine* **2006,** *57* (1), 65-81.

37. Weichselbaum, R. R.; Liang, H.; Deng, L.; Fu, Y.-X., Radiotherapy and immunotherapy: a beneficial liaison? *Nature Reviews Clinical Oncology* **2017,** *14*, 365.
38. Tang, C.; Wang, X.; Soh, H.; Seyedin, S.; Cortez, M. A.; Krishnan, S.; Massarelli, E.; Hong, D.; Naing, A.; Diab, A.; Gomez, D.; Ye, H.; Heymach, J.; Komaki, R.; Allison, J. P.; Sharma, P.; Welsh, J. W., Combining Radiation and Immunotherapy: A New Systemic Therapy for Solid Tumors? *Cancer Immunology Research* **2014,** *2* (9), 831-838.
39. Emens, L. A.; Middleton, G., The Interplay of Immunotherapy and Chemotherapy: Harnessing Potential Synergies. *Cancer Immunology Research* **2015,** *3* (5), 436-443.
40. Drake, C. G., Combination immunotherapy approaches. *Annals of Oncology* **2012,** *23* (suppl_8), viii41-viii46.
41. Janeway Jr, C. A.; Travers, P.; Walport, M.; Shlomchik, M. J., T-cell receptor gene rearrangement. In *Immunobiology: The Immune System in Health and Disease*, 5th ed.; Janeway Jr, C. A., Ed. Garland Science: New York, 2001.
42. Francisco, L. M.; Sage, P. T.; Sharpe, A. H., The PD-1 pathway in tolerance and autoimmunity. *Immunological Reviews* **2010,** *236* (1), 219-242.
43. Janeway Jr, C. A.; Travers, P.; Walport, M.; Shlomchik, M. J., The production of armed effector T cells. In *Immunobiology: The Immune System in Health and Disease.*, Garland Science: New York, 2001.
44. Arasanz, H.; Gato-Cañas, M.; Zuazo, M.; Ibañez-Vea, M.; Breckpot, K.; Kochan, G.; Escors, D., PD1 signal transduction pathways in T cells. *Oncotarget* **2017,** *8* (31), 51936-51945.
45. Pennock, N. D.; White, J. T.; Cross, E. W.; Cheney, E. E.; Tamburini, B. A.; Kedl, R. M., T cell responses: naïve to memory and everything in between. *Advances in Physiology Education* **2013,** *37* (4), 273-283.
46. Borowski, A. B.; Boesteanu, A. C.; Mueller, Y. M.; Carafides, C.; Topham, D. J.; Altman, J. D.; Jennings, S. R.; Katsikis, P. D., Memory CD8+ T Cells Require CD28 Costimulation. *The Journal of Immunology* **2007,** *179* (10), 6494-6503.
47. Boesteanu, A. C.; Katsikis, P. D., Memory T cells need CD28 costimulation to remember. *Seminars in Immunology* **2009,** *21* (2), 69-77.
48. Cantrell, D. A., T-cell antigen receptor signal transduction. *Immunology* **2002,** *105* (4), 369-374.
49. Parry, R. V.; Chemnitz, J. M.; Frauwirth, K. A.; Lanfranco, A. R.; Braunstein, I.; Kobayashi, S. V.; Linsley, P. S.; Thompson, C. B.; Riley, J. L., CTLA-4 and PD-1 Receptors Inhibit T-Cell Activation by Distinct Mechanisms. *Molecular and Cellular Biology* **2005,** *25* (21), 9543-9553.
50. Sharpe, A. H.; Pauken, K. E., The diverse functions of the PD1 inhibitory pathway. *Nature Reviews Immunology* **2017**.
51. Tsai, H.-F.; Hsu, P.-N., Cancer immunotherapy by targeting immune checkpoints: mechanism of T cell dysfunction in cancer immunity and new therapeutic targets. *Journal of Biomedical Science* **2017,** *24* (1), 35.
52. Sharpe, A. H., Introduction to checkpoint inhibitors and cancer immunotherapy. *Immunological Reviews* **2017,** *276* (1), 5-8.
53. Wykes, M. N.; Lewin, S. R., Immune checkpoint blockade in infectious diseases. *Nature Reviews Immunology* **2017**.

54. Anderson, A. C., Tim-3: An Emerging Target in the Cancer Immunotherapy Landscape. *Cancer Immunology Research* **2014,** *2* (5), 393-398.
55. Wang, L.; Rubinstein, R.; Lines, J. L.; Wasiuk, A.; Ahonen, C.; Guo, Y.; Lu, L.-F.; Gondek, D.; Wang, Y.; Fava, R. A.; Fiser, A.; Almo, S.; Noelle, R. J., VISTA, a novel mouse Ig superfamily ligand that negatively regulates T cell responses. *Journal of Experimental Medicine* **2011,** *208* (3), 577-592.
56. Linsley, P. S.; Brady, B.; Urnes, M.; Grosmaire, L. S.; Damle, N. K.; Ledbetter, J. A., CTLA-4 is a second receptor for the B cell activation antigen B7. *Journal of Experimental Medicine* **1991,** *174*, 561-569.
57. Linsley, P. S.; Bradshaw, J.; Greene, J.; Peach, R.; Bennett, K. L.; Mittler, R. S., Intracellular Trafficking of CTLA-4 and Focal Localization Towards Sites of TCR Engagement. *Immunity* **1996,** *4* (6), 535-543.
58. Merwe, P. A.; Bodian, D. L.; Daenke, S.; Linsley, P.; Davis, S. J., CD80 (B7-1) binds both CD28 and CTLA-4 with a low affinity and very fast kinetics. *Journal of Experimental Medicine* **1997,** *185*, 393-403.
59. Qureshi, O. S.; Zheng, Y.; Nakamura, K.; Attridge, K.; Manzotti, C.; Schmidt, E. M.; Baker, J.; Jeffery, L. E.; Kaur, S.; Briggs, Z.; Hou, T. Z.; Futter, C. E.; Anderson, G.; Walker, L. S. K.; Sansom, D. M., Trans-Endocytosis of CD80 and CD86: A Molecular Basis for the Cell-Extrinsic Function of CTLA-4. *Science* **2011,** *332* (6029), 600-603.
60. Lee, K.-M.; Chuang, E.; Griffin, M.; Khattri, R.; Hong, D. K.; Zhang, W.; Straus, D.; Samelson, L. E.; Thompson, C. B.; Bluestone, J. A., Molecular Basis of T Cell Inactivation by CTLA-4. *Science* **1998,** *282* (5397), 2263-2266.
61. Blair, P. J.; Riley, J. L.; Levine, B. L.; Lee, K. P.; Craighead, N.; Francomano, T.; Perfetto, S. J.; Gray, G. S.; Carreno, B. M.; June, C. H., Cutting Edge: CTLA-4 Ligation Delivers a Unique Signal to Resting Human CD4 T Cells That Inhibits Interleukin-2 Secretion but Allows Bcl-XL Induction. *The Journal of Immunology* **1998,** *160* (1), 12-15.
62. Jago, C. B.; Yates, J.; Olsen Saraiva Câmara, N.; Lechler, R. I.; Lombardi, G., Differential expression of CTLA-4 among T cell subsets. *Clinical & Experimental Immunology* **2004,** *136* (3), 463-471.
63. McCoy, K. D.; Le Gros, G., The role of CTLA-4 in the regulation of T cell immune responses. *Immunology and cell biology* **1999,** *77* (1), 1-10.
64. Bradshaw, J. D.; Lu, P.; Leytze, G.; Rodgers, J.; Schieven, G. L.; Bennett, K. L.; Linsley, P. S.; Kurtz, S. E., Interaction of the Cytoplasmic Tail of CTLA-4 (CD152) with a Clathrin-Associated Protein Is Negatively Regulated by Tyrosine Phosphorylation. *Biochemistry* **1997,** *36* (50), 15975-15982.
65. Wekerle, T.; Grinyó, J. M., Belatacept: from rational design to clinical application. *Transplant International* **2012,** *25* (2), 139-150.
66. Horvat, T. Z.; Adel, N. G.; Dang, T. O.; Momtaz, P.; Postow, M. A.; Callahan, M. K.; Carvajal, R. D.; Dickson, M. A.; D'Angelo, S. P.; Woo, K. M., Immune-related adverse events, need for systemic immunosuppression, and effects on survival and time to treatment failure in patients with melanoma treated with ipilimumab at memorial Sloan Kettering cancer center. *Journal of Clinical Oncology* **2015,** *33*, 3193-3198.
67. Weber, J. S.; Dummer, R.; Pril, V.; Lebbe, C.; Hodi, F. S.; Investigators, M. D. X., Patterns of onset and resolution of immune-related adverse events of special interest

with ipilimumab: detailed safety analysis from a phase 3 trial in patients with advanced melanoma. *Cancer* **2013,** *119*, 1675-1682.
68. Collin, M., Immune checkpoint inhibitors: a patent review (2010-2015). *Expert Opinion on Therapeutic Patents* **2016,** *26* (5), 555-564.
69. Wikenheiser, D. J.; Stumhofer, J. S., ICOS Co-Stimulation: Friend or Foe? *Frontiers in Immunology* **2016,** *7*, 304.
70. Aspeslagh, S.; Postel-Vinay, S.; Rusakiewicz, S.; Soria, J.-C.; Zitvogel, L.; Marabelle, A., Rationale for anti-OX40 cancer immunotherapy. *European Journal of Cancer* **2016,** *52* (Supplement C), 50-66.
71. Linch, S. N.; McNamara, M. J.; Redmond, W. L., OX40 Agonists and Combination Immunotherapy: Putting the Pedal to the Metal. *Frontiers in Oncology* **2015,** *5*, 34.
72. Burris, H. A.; Infante, J. R.; Ansell, S. M.; Nemunaitis, J. J.; Weiss, G. R.; Villalobos, V. M.; Sikic, B. I.; Taylor, M. H.; Northfelt, D. W.; III, W. E. C.; Hawthorne, T. R.; Davis, T. A.; Yellin, M. J.; Keler, T.; Bullock, T., Safety and Activity of Varlilumab, a Novel and First-in-Class Agonist Anti-CD27 Antibody, in Patients With Advanced Solid Tumors. *Journal of Clinical Oncology* **2017,** *35* (18), 2028-2036.
73. Elgueta, R.; Benson, M. J.; de Vries, V. C.; Wasiuk, A.; Guo, Y.; Noelle, R. J., Molecular mechanism and function of CD40/CD40L engagement in the immune system. *Immunological Reviews* **2009,** *229* (1), 10.1111/j.1600-065X.2009.00782.x.
74. Yonezawa, A.; Dutt, S.; Chester, C.; Kim, J.; Kohrt, H. E., Boosting Cancer Immunotherapy with Anti-CD137 Antibody Therapy. *Clinical Cancer Research* **2015,** *21* (14), 3113-3120.
75. Bartkowiak, T.; Curran, M. A., 4-1BB Agonists: Multi-Potent Potentiators of Tumor Immunity. *Frontiers in Oncology* **2015,** *5*, 117.
76. Knee, D. A.; Hewes, B.; Brogdon, J. L., Rationale for anti-GITR cancer immunotherapy. *European Journal of Cancer* **2016,** *67* (Supplement C), 1-10.
77. Schaer, D. A.; Murphy, J. T.; Wolchok, J. D., Modulation of GITR for cancer immunotherapy. *Current Opinion in Immunology* **2012,** *24* (2), 217-224.
78. Pardoll, D. M., The blockade of immune checkpoints in cancer immunotherapy. *Nature Reviews Cancer* **2012,** *12*, 252-264.
79. Butte, M. J.; Keir, M. E.; Phamduy, T. B.; Sharpe, A. H.; Freeman, G. J., Programmed Death-1 Ligand 1 Interacts Specifically with the B7-1 Costimulatory Molecule to Inhibit T Cell Responses. *Immunity* **2007,** *27* (1), 111-122.
80. Butte, M. J.; Peña-Cruz, V.; Kim, M.-J.; Freeman, G. J.; Sharpe, A. H., Interaction of human PD-L1 and B7-1. *Molecular Immunology* **2008,** *45* (13), 3567-3572.
81. Dong, C.; Juedes, A. E.; Temann, U.-A.; Shresta, S.; Allison, J. P.; Ruddle, N. H.; Flavell, R. A., ICOS co-stimulatory receptor is essential for T-cell activation and function. *Nature* **2001,** *409*, 97-101.
82. Song, J.; Salek-Ardakani, S.; Rogers, P. R.; Cheng, M.; Van Parijs, L.; Croft, M., The costimulation-regulated duration of PKB activation controls T cell longevity. *Nature Immunology* **2004,** *5*, 150-158.
83. Song, J.; So, T.; Cheng, M.; Tang, X.; Croft, M., Sustained Survivin Expression from OX40 Costimulatory Signals Drives T Cell Clonal Expansion. *Immunity* **2005,** *22* (5), 621-631.

84. Rogers, P. R.; Song, J.; Gramaglia, I.; Killeen, N.; Croft, M., OX40 Promotes Bcl-xL and Bcl-2 Expression and Is Essential for Long-Term Survival of CD4 T Cells. *Immunity* **2001,** *15* (3), 445-455.
85. Bally, A. P. R.; Austin, J. W.; Boss, J. M., Genetic and Epigenetic Regulation of PD-1 Expression. *The Journal of Immunology* **2016,** *196* (6), 2431-2437.
86. Chemnitz, J. M.; Parry, R. V.; Nichols, K. E.; June, C. H.; Riley, J. L., SHP-1 and SHP-2 associate with immunoreceptor tyrosine-based switch motif of programmed death 1 upon primary human T cell stimulation, but only receptor ligation prevents T cell activation. *The Journal of Immunology* **2004,** *173*, 945-954.
87. Yamazaki, T.; Akiba, H.; Iwai, H.; Matsuda, H.; Aoki, M.; Tanno, Y.; Shin, T.; Tsuchiya, H.; Pardoll, D. M.; Okumura, K.; Azuma, M.; Yagita, H., Expression of Programmed Death 1 Ligands by Murine T Cells and APC. *The Journal of Immunology* **2002,** *169* (10), 5538-5545.
88. Liang, S. C.; Latchman, Y. E.; Buhlmann, J. E.; Tomczak, M. F.; Horwitz, B. H.; Freeman, G. J.; Sharpe, A. H., Regulation of PD-1, PD-L1, and PD-L2 expression during normal and autoimmune responses. *European Journal of Immunology* **2003,** *33* (10), 2706-2716.
89. Shi, L.; Chen, S.; Yang, L.; Li, Y., The role of PD-1 and PD-L1 in T-cell immune suppression in patients with hematological malignancies. *Journal of Hematology & Oncology* **2013,** *6*, 74-74.
90. Keir, M. E.; Liang, S. C.; Guleria, I.; Latchman, Y. E.; Qipo, A.; Albacker, L. A.; Koulmanda, M.; Freeman, G. J.; Sayegh, M. H.; Sharpe, A. H., Tissue expression of PD-L1 mediates peripheral T cell tolerance. *The Journal of Experimental Medicine* **2006,** *203* (4), 883-895.
91. Keir, M. E.; Freeman, G. J.; Sharpe, A. H., PD-1 Regulates Self-Reactive CD8+ T Cell Responses to Antigen in Lymph Nodes and Tissues. *The Journal of Immunology* **2007,** *179* (8), 5064-5070.
92. Freeman, G. J.; Wherry, E. J.; Ahmed, R.; Sharpe, A. H., Reinvigorating exhausted HIV-specific T cells via PD-1–PD-1 ligand blockade. *The Journal of Experimental Medicine* **2006,** *203* (10), 2223-2227.
93. Francisco, L. M.; Salinas, V. H.; Brown, K. E.; Vanguri, V. K.; Freeman, G. J.; Kuchroo, V. K.; Sharpe, A. H., PD-L1 regulates the development, maintenance, and function of induced regulatory T cells. *The Journal of Experimental Medicine* **2009,** *206* (13), 3015-3029.
94. James, E. S.; Harney, S.; Wordsworth, B. P.; Cookson, W. O. C. M.; Davis, S. J.; Moffatt, M. F., PDCD1: a tissue-specific susceptibility locus for inherited inflammatory disorders. *Genes & Immunology* **2005,** *6* (5), 430-437.
95. Riley, J. L., PD-1 signaling in primary T cells. *Immunological Reviews* **2009,** *229* (1), 114-125.
96. Zhang, X.; Schwartz, J.-C. D.; Guo, X.; Bhatia, S.; Cao, E.; Chen, L.; Zhang, Z.-Y.; Edidin, M. A.; Nathenson, S. G.; Almo, S. C., Structural and Functional Analysis of the Costimulatory Receptor Programmed Death-1. *Immunity* **2004,** *20* (3), 337-347.
97. Zak, K. M.; Kitel, R.; Przetocka, S.; Golik, P.; Guzik, K.; Musielak, B.; Dömling, A.; Dubin, G.; Holak, T. A., Structure of the complex of human programmed death 1, PD-1, and its ligand PD-L1. *Structure* **2015,** *23* (12), 2341-2348.

98. Cheng, X.; Veverka, V.; Radhakrishnan, A.; Waters, L. C.; Muskett, F. W.; Morgan, S. H.; Huo, J.; Yu, C.; Evans, E. J.; Leslie, A. J.; Griffiths, M.; Stubberfield, C.; Griffin, R.; Henry, A. J.; Jansson, A.; Ladbury, J. E.; Ikemizu, S.; Carr, M. D.; Davis, S. J., Structure and interactions of the human programmed cell death 1 receptor. *Journal of Biological Chemistry* **2013,** *288* (17), 11771-85.
99. Lázár-Molnár, E.; Yan, Q.; Cao, E.; Ramagopal, U.; Nathenson, S. G.; Almo, S. C., Crystal structure of the complex between programmed death-1 (PD-1) and its ligand PD-L2. *Proceedings of the National Academy of Sciences* **2008,** *105* (30), 10483-10488.
100. Tan, S.; Zhang, H.; Chai, Y.; Song, H.; Tong, Z.; Wang, Q.; Qi, J.; Wong, G.; Zhu, X.; Liu, W. J.; Gao, S.; Wang, Z.; Shi, Y.; Yang, F.; Gao, G. F.; Yan, J., An unexpected N-terminal loop in PD-1 dominates binding by nivolumab. *Nature Communications* **2017,** *8*, 14369.
101. Okada, M.; Chikuma, S.; Kondo, T.; Hibino, S.; Machiyama, H.; Yokosuka, T.; Nakano, M.; Yoshimura, A., Blockage of Core Fucosylation Reduces Cell-Surface Expression of PD-1 and Promotes Anti-tumor Immune Responses of T Cells. *Cell Reports* **2017,** *20* (5), 1017-1028.
102. Chen, Y.; Liu, P.; Gao, F.; Cheng, H.; Qi, J.; Gao, G. F., A dimeric structure of PD-L1: functional units or evolutionary relics? *Protein & Cell* **2010,** *1* (2), 153-160.
103. Lin, D. Y.-w.; Tanaka, Y.; Iwasaki, M.; Gittis, A. G.; Su, H.-P.; Mikami, B.; Okazaki, T.; Honjo, T.; Minato, N.; Garboczi, D. N., The PD-1/PD-L1 complex resembles the antigen-binding Fv domains of antibodies and T cell receptors. *Proceedings of the National Academy of Sciences* **2008,** *105* (8), 3011-3016.
104. Li, C.-W.; Lim, S.-O.; Xia, W.; Lee, H.-H.; Chan, L.-C.; Kuo, C.-W.; Khoo, K.-H.; Chang, S.-S.; Cha, J.-H.; Kim, T.; Hsu, J. L.; Wu, Y.; Hsu, J.-M.; Yamaguchi, H.; Ding, Q.; Wang, Y.; Yao, J.; Lee, C.-C.; Wu, H.-J.; Sahin, A. A.; Allison, J. P.; Yu, D.; Hortobagyi, G. N.; Hung, M.-C., Glycosylation and stabilization of programmed death ligand-1 suppresses T-cell activity. *Nature Communications* **2016,** *7*, 12632.
105. Pascolutti, R.; Sun, X.; Kao, J.; Maute, Roy L.; Ring, Aaron M.; Bowman, Gregory R.; Kruse, Andrew C., Structure and Dynamics of PD-L1 and an Ultra-High-Affinity PD-1 Receptor Mutant. *Structure* **2016,** *24* (10), 1719-1728.
106. Lázár-Molnár, E.; Scandiuzzi, L.; Basu, I.; Quinn, T.; Sylvestre, E.; Palmieri, E.; Ramagopal, U. A.; Nathenson, S. G.; Guha, C.; Almo, S. C., Structure-guided development of a high-affinity human Programmed Cell Death-1: Implications for tumor immunotherapy. *EBioMedicine* **2017,** *17* (Supplement C), 30-44.
107. Zhu, X.; Lang, J., Soluble PD-1 and PD-L1: predictive and prognostic significance in cancer. *Oncotarget* **2017,** *5* (57), 97671-97682.
108. Wu, H.; Miao, M.; Zhang, G.; Hu, Y.; Ming, Z.; Zhang, X., Soluble PD-1 is associated with aberrant regulation of T cells activation in aplastic anemia. *Immunological investigations* **2009,** *38* (5), 408-21.
109. Sorensen, S. F.; Demuth, C.; Weber, B.; Sorensen, B. S.; Meldgaard, P., Increase in soluble PD-1 is associated with prolonged survival in patients with advanced EGFR-mutated non-small cell lung cancer treated with erlotinib. *Lung Cancer* **2016,** *100* (Supplement C), 77-84.
110. Liu, C.; Jiang, J.; Gao, L.; Wang, X.; Hu, X.; Wu, M.; Wu, J.; Xu, T.; Shi, Q.; Zhang, X., Soluble PD-1 aggravates progression of collagen-induced arthritis through Th1 and Th17 pathways. *Arthritis Research & Therapy* **2015,** *17* (1), 340.

111. Wan, B.; Nie, H.; Liu, A.; Feng, G.; He, D.; Xu, R., Aberrant regulation of synovial T cell activation by soluble costimulatory molecules in rheumatoid arthritis. *The Journal of Immunology* **2006,** *177*, 8844-8850.
112. Nielsen, C.; Ohm-Laursen, L.; Barington, T.; Husby, S.; Lillevang, S. T., Alternative splice variants of the human PD-1 gene. *Cellular Immunology* **2005,** *235*, 109-116.
113. Wang, D.; Zhou, D.; Du, Q.; Liang, Q.; Wang, Q.; Fang, L.; Wang, G.; Fan, Q.; Liu, B.; Zhou, J.; Tang, Z.; Wu, H.; Guo, X.; Jiao, Y.; Zhang, G., Aberrant production of soluble inducible T-cell co-stimulator (sICOS) and soluble programmed cell death protein 1 (sPD-1) in patients with chronic hepatitis C. *Molecular medicine reports* **2013,** *7* (4), 1197-202.
114. Kruger, S.; Legenstein, M. L.; Rosgen, V.; Haas, M.; Modest, D. P.; Westphalen, C. B.; Ormanns, S.; Kirchner, T.; Heinemann, V.; Holdenrieder, S.; Boeck, S., Serum levels of soluble programmed death protein 1 (sPD-1) and soluble programmed death ligand 1 (sPD-L1) in advanced pancreatic cancer. *Oncoimmunology* **2017,** *6* (5), e1310358.
115. Hassan, W. A.; Baraka, E. A.; Fouad, N. A., Clinical significance of soluble programmed death-1(sPD-1) in rheumatoid arthritis patients: Relation to disease activity and functional status. *The Egyptian Rheumatologist* **2015,** *37* (4), 165-169.
116. Bartee, M. Y.; Dunlap, K. M.; Bartee, E., Tumor-Localized Secretion of Soluble PD1 Enhances Oncolytic Virotherapy. *Cancer Research* **2017,** *77* (11), 2952-2963.
117. Shin, S. P.; Seo, H. H.; Shin, J. H.; Park, H. B.; Lim, D. P.; Eom, H. S., Adenovirus expressing both thymidine kinase and soluble PD1 enhances antitumor immunity by strengthening CD8 T-cell response. *Molecular Therapy* **2013,** *21*, 688-695.
118. Atesoglu, E. B.; Tarkun, P.; Demirsoy, E. T.; Geduk, A.; Mehtap, O.; Batman, A.; Kaya, F.; Cekmen, M. B.; Gulbas, Z.; Hacıhanefioglu, A., Soluble Programmed Death 1 (PD-1) Is Decreased in Patients With Immune Thrombocytopenia (ITP):Potential Involvement of PD-1 Pathway in ITP Immunopathogenesis. *Clinical and Applied Thrombosis/Hemostasis* **2016,** *22* (3), 248-251.
119. Cheng, H. Y.; Kang, P. J.; Chuang, Y. H.; Wang, Y. H.; Jan, M. C.; Wu, C. F.; Lin, C. L.; Liu, C. J.; Liaw, Y. F.; Lin, S. M.; Chen, P. J.; Lee, S. D.; Yu, M. W., Circulating programmed death-1 as a marker for sustained high hepatitis B viral load and risk of hepatocellular carcinoma. *PLoS One* **2014,** *9* (11), e95870.
120. Dezutter-Dambuyant, C.; Durand, I.; Alberti, L.; Bendriss-Vermare, N.; Valladeau-Guilemond, J.; Duc, A.; Magron, A.; Morel, A.-P.; Sisirak, V.; Rodriguez, C.; Cox, D.; Olive, D.; Caux, C., A novel regulation of PD-1 ligands on mesenchymal stromal cells through MMP-mediated proteolytic cleavage. *OncoImmunology* **2016,** *5* (3), e1091146.
121. Chen, Y.; Wang, Q.; Shi, B.; Xu, P.; Hu, Z.; Bai, L.; Zhang, X., Development of a sandwich ELISA for evaluating soluble PD-L1 (CD274) in human sera of different ages as well as supernatants of PD-L1+ cell lines. *Cytokine* **2011,** *56* (2), 231-8.
122. Frigola, X.; Inman, B. A.; Lohse, C. M.; Krco, C. J.; Cheville, J. C.; Thompson, R. H.; Leibovich, B.; Blute, M. L.; Dong, H.; Kwon, E. D., Identification of a soluble form of B7-H1 that retains immunosuppressive activity and is associated with aggressive renal cell carcinoma. *Clinical Cancer Research* **2011,** *17* (7), 1915-23.

123. Frigola, X.; Inman, B. A.; Krco, C. J.; Liu, X.; Harrington, S. M.; Bulur, P. A.; Dietz, A. B.; Dong, H.; Kwon, E. D., Soluble B7-H1: differences in production between dendritic cells and T cells. *Immunology letters* **2012,** *142* (1-2), 78-82.
124. Finkelmeier, F.; Canli, O.; Tal, A.; Pleli, T.; Trojan, J.; Schmidt, M.; Kronenberger, B.; Zeuzem, S.; Piiper, A.; Greten, F. R.; Waidmann, O., High levels of the soluble programmed death-ligand (sPD-L1) identify hepatocellular carcinoma patients with a poor prognosis. *European Journal of Cancer* **2016,** *59*, 152-159.
125. Dronca, R. S.; Mansfield, A. S.; Liu, X.; Harrington, S.; Enninga, E. A.; Kottschade, L. A.; Koo, C. W.; McWilliams, R. R.; Block, M. S.; Nevala, W. K.; Markovic, S.; Dong, H., Bim and soluble PD-L1 (sPD-L1) as predictive biomarkers of response to anti-PD-1 therapy in patients with melanoma and lung carcinoma. *Journal of Clinical Oncology* **2017,** *35* (15_suppl), 11534-11534.
126. Ha, H.; Nam, A. R.; Bang, J. H.; Park, J. E.; Kim, T. Y.; Lee, K. H.; Han, S. W.; Im, S. A.; Kim, T. Y.; Bang, Y. J.; Oh, D. Y., Soluble programmed death-ligand 1 (sPDL1) and neutrophil-to-lymphocyte ratio (NLR) predicts survival in advanced biliary tract cancer patients treated with palliative chemotherapy. *Oncotarget* **2016,** *7* (47), 76604-76612.
127. Nagato, T.; Ohkuri, T.; Ohara, K.; Hirata, Y.; Kishibe, K.; Komabayashi, Y.; Ueda, S.; Takahara, M.; Kumai, T.; Ishibashi, K.; Kosaka, A.; Aoki, N.; Oikawa, K.; Uno, Y.; Akiyama, N.; Sado, M.; Takei, H.; Celis, E.; Harabuchi, Y.; Kobayashi, H., Programmed death-ligand 1 and its soluble form are highly expressed in nasal natural killer/T-cell lymphoma: a potential rationale for immunotherapy. *Cancer Immunology, Immunotherapy* **2017,** *66* (7), 877-890.
128. Okuma, Y.; Hosomi, Y.; Nakahara, Y.; Watanabe, K.; Sagawa, Y.; Homma, S., High plasma levels of soluble programmed cell death ligand 1 are prognostic for reduced survival in advanced lung cancer. *Lung Cancer* **2017,** *104*, 1-6.
129. Bi, X. W.; Wang, H.; Zhang, W. W.; Wang, J. H.; Liu, W. J.; Xia, Z. J.; Huang, H. Q.; Jiang, W. Q.; Zhang, Y. J.; Wang, L., PD-L1 is upregulated by EBV-driven LMP1 through NF-kappaB pathway and correlates with poor prognosis in natural killer/T-cell lymphoma. *Journal of Hematology & Oncology* **2016,** *9* (1), 109.
130. Takahashi, N.; Iwasa, S.; Sasaki, Y.; Shoji, H.; Honma, Y.; Takashima, A.; Okita, N. T.; Kato, K.; Hamaguchi, T.; Yamada, Y., Serum levels of soluble programmed cell death ligand 1 as a prognostic factor on the first-line treatment of metastatic or recurrent gastric cancer. *Journal of cancer research and clinical oncology* **2016,** *142* (8), 1727-38.
131. Rossille, D.; Gressier, M.; Damotte, D.; Maucort-Boulch, D.; Pangault, C.; Semana, G.; Le Gouill, S.; Haioun, C.; Tarte, K.; Lamy, T.; Milpied, N.; Fest, T., High level of soluble programmed cell death ligand 1 in blood impacts overall survival in aggressive diffuse large B-Cell lymphoma: results from a French multicenter clinical trial. *Leukemia* **2014,** *28* (12), 2367-75.
132. Petrovas, C.; Price, D. A.; Mattapallil, J.; Ambrozak, D. R.; Geldmacher, C.; Cecchinato, V.; Vaccari, M.; Tryniszewska, E.; Gostick, E.; Roederer, M.; Douek, D. C.; Morgan, S. H.; Davis, S. J.; Franchini, G.; Koup, R. A., SIV-specific CD8+ T cells express high levels of PD1 and cytokines but have impaired proliferative capacity in acute and chronic SIVmac251 infection. *Blood* **2007,** *110* (3), 928-36.
133. Trautmann, L.; Janbazian, L.; Chomont, N.; Said, E. A.; Gimmig, S.; Bessette, B.; Boulassel, M.-R.; Delwart, E.; Sepulveda, H.; Balderas, R. S.; Routy, J.-P.; Haddad, E.

K.; Sekaly, R.-P., Upregulation of PD-1 expression on HIV-specific CD8+ T cells leads to reversible immune dysfunction. *Nature Medicine* **2006,** *12*, 1198-1202.
134. Urbani, S.; Amadei, B.; Tola, D.; Massari, M.; Schivazappa, S.; Missale, G.; Ferrari, C., PD-1 expression in acute hepatitis C virus (HCV) infection is associated with HCV-specific CD8 exhaustion. *Journal of virology* **2006,** *80* (22), 11398-403.
135. Sharpe, A. H.; Wherry, E. J.; Ahmed, R.; Freeman, G. J., The function of programmed cell death 1 and its ligands in regulating autoimmunity and infection. *Nature Immunology* **2007,** *8*, 239-245.
136. Foldi, J.; Kozhaya, L.; McCarty, B.; Mwamzuka, M.; Marshed, F.; Ilmet, T.; Kilberg, M.; Kravietz, A.; Ahmed, A.; Borkowsky, W.; Unutmaz, D.; Khaitan, A., HIV-Infected Children Have Elevated Levels of PD-1+ Memory CD4 T Cells With Low Proliferative Capacity and High Inflammatory Cytokine Effector Functions. *Journal of Infectious Diseases* **2017,** *216* (6), 641-650.
137. Day, C. L.; Kaufmann, D. E.; Kiepiela, P.; Brown, J. A.; Moodley, E. S.; Reddy, S.; Mackey, E. W.; Miller, J. D.; Leslie, A. J.; DePierres, C.; Mncube, Z.; Duraiswamy, J.; Zhu, B.; Eichbaum, Q.; Altfeld, M.; Wherry, E. J.; Coovadia, H. M.; Goulder, P. J. R.; Klenerman, P.; Ahmed, R.; Freeman, G. J.; Walker, B. D., PD-1 expression on HIV-specific T cells is associated with T-cell exhaustion and disease progression. *Nature* **2006,** *443*, 350-354.
138. Petrovas, C.; Casazza, J. P.; Brenchley, J. M.; Price, D. A.; Gostick, E.; Adams, W. C.; Precopio, M. L.; Schacker, T.; Roederer, M.; Douek, D. C.; Koup, R. A., PD-1 is a regulator of virus-specific CD8+ T cell survival in HIV infection. *Journal of Experimental Medicine* **2006,** *203* (10), 2281-92.
139. Bonnet, F.; Lewden, C.; May, T.; Heripret, L.; Jougla, E.; Bevilacqua, S.; Costagliola, D.; Salmon, D.; Chene, G.; Morlat, P., Opportunistic infections as causes of death in HIV-infected patients in the HAART era in France. *Scandinavian journal of infectious diseases* **2005,** *37* (6-7), 482-7.
140. Lewden, C.; Salmon, D.; Morlat, P.; Bévilacqua, S.; Jougla, E.; Bonnet, F.; Héripret, L.; Costagliola, D.; May, T.; Chêne, G., Causes of death among human immunodeficiency virus (HIV)-infected adults in the era of potent antiretroviral therapy: emerging role of hepatitis and cancers, persistent role of AIDS. *International Journal of Epidemiology* **2005,** *34* (1), 121-130.
141. Barber, D. L.; Mayer-Barber, K. D.; Feng, C. G.; Sharpe, A. H.; Sher, A., CD4 T Cells Promote Rather than Control Tuberculosis in the Absence of PD-1–Mediated Inhibition. *The Journal of Immunology* **2011,** *186* (3), 1598-1607.
142. Lázár-Molnár, E.; Chen, B.; Sweeney, K. A.; Wang, E. J.; Liu, W.; Lin, J.; Porcelli, S. A.; Almo, S. C.; Nathenson, S. G.; Jacobs, W. R., Programmed death-1 (PD-1)–deficient mice are extraordinarily sensitive to tuberculosis. *Proceedings of the National Academy of Sciences* **2010,** *107* (30), 13402-13407.
143. Velu, V.; Shetty, R. D.; Larsson, M.; Shankar, E. M., Role of PD-1 co-inhibitory pathway in HIV infection and potential therapeutic options. *Retrovirology* **2015,** *12* (1), 14.
144. Riley, J. L.; June, C. H., The road to recovery: translating PD-1 biology into clinical benefit. *Trends in Immunology* **2007,** *28* (2), 48-50.
145. Thompson, R. H.; Gillett, M. D.; Cheville, J. C.; Lohse, C. M.; Dong, H.; Webster, W. S.; Krejci, K. G.; Lobo, J. R.; Shomik Sengupta, L. C.; Zincke, H.; Blute, M.

L.; Strome, S. E.; Leibovich, B. C.; Kwon, E. D., Costimulatory B7-H1 in renal cell carcinoma patients: Indicator of tumor aggressiveness and potential therapeutic target. *Proceedings of the National Academy of Sciences* **2004,** *101*, 17174-17179.
146. Thompson, R. H.; Kuntz, S. M.; Leibovich, B. C.; Dong, H.; Lohse, C. M.; Webster, W. S.; Sengupta, S.; Frank, I.; Parker, A. S.; Zincke, H.; Blute, M. L.; Sebo, T. J.; Cheville, J. C.; Kwon, E. D., Tumor B7-H1 is associated with poor prognosis in renal cell carcinoma patients with long-term follow-up. *Cancer Research* **2006,** *66* (7), 3381-3385.
147. Wu, C.; Zhu, Y.; Jiang, J.; Zhao, J.; Zhang, X.-G.; Xu, N., Immunohistochemical localization of programmed death-1 ligand-1 (PD-L1) in gastric carcinoma and its clinical significance. *Acta Histochemica* **2006,** *108*, 19-24.
148. Ghebeh, H.; Mohammed, S.; Al-Omair, A.; Qattan, A.; Lehe, C.; Al-Qudaihi, G.; Elkum, N.; Alshabanah, M.; Bin Amer, S.; Tulbah, A.; Ajarim, D.; Al-Tweigeri, T.; Dermime, S., The B7-H1 (PD-L1) T lymphocyte-inhibitory molecule is expressed in breast cancer patients with infiltrating ductal carcinoma: correlation with important high-risk prognostic factors. *Neoplasia* **2006,** *8* (3), 190-198.
149. Ohigashi, Y.; Sho, M.; Yamada, Y.; Tsurui, Y.; Hamada, K.; Ikeda, N.; Mizuno, T.; Yoriki, R.; Kashizuka, H.; Yane, K.; Tsushima, F.; Otsuki, N.; Yagita, H.; Azuma, M.; Nakajima, Y., Clinical significance of programmed death-1 ligand-1 and programmed death-1 ligand-2 expression in human esophageal cancer. *Clinical Cancer Research* **2005,** *11* (8), 2947-53.
150. Kim, J. R.; Moon, Y. J.; Kwon, K. S.; Bae, J. S.; Wagle, S.; Kim, K. M.; Park, H. S.; Lee, H.; Moon, W. S.; Chung, M. J.; Kang, M. J.; Jang, K. Y., Tumor infiltrating PD1-positive lymphocytes and the expression of PD-L1 predict poor prognosis of soft tissue sarcomas. *PLoS One* **2013,** *8* (12), e82870.
151. Nakanishi, J.; Wada, Y.; Matsumoto, K.; Azuma, M.; Kikuchi, K.; Ueda, S., Overexpression of B7-H1 (PD-L1) significantly associates with tumor grade and postoperative prognosis in human urothelial cancers. *Cancer Immunology, Immunotherapy* **2007,** *56* (8), 1173-1182.
152. Inman, B. A.; Sebo, T. J.; Frigola, X.; Dong, H.; Bergstralh, E. J.; Frank, I.; Fradet, Y.; Lacombe, L.; Kwon, E. D., PD-L1 (B7-H1) expression by urothelial carcinoma of the bladder and BCG-induced granulomata: associations with localized stage progression. *Cancer* **2007,** *109* (8), 1499-505.
153. Gao, Q.; Wang, X. Y.; Qiu, S. J.; Yamato, I.; Sho, M.; Nakajima, Y.; Zhou, J.; Li, B. Z.; Shi, Y. H.; Xiao, Y. S.; Xu, Y.; Fan, J., Overexpression of PD-L1 significantly associates with tumor aggressiveness and postoperative recurrence in human hepatocellular carcinoma. *Clinical Cancer Research* **2009,** *15* (3), 971-979.
154. Nomi, T.; Sho, M.; Akahori, T.; Hamada, K.; Kubo, A.; Kanehiro, H.; Nakamura, S.; Enomoto, K.; Yagita, H.; Azuma, M.; Nakajima, Y., Clinical significance and therapeutic potential of the programmed death-1 ligand/programmed death-1 pathway in human pancreatic cancer. *Clinical Cancer Research* **2007,** *13* (7), 2151-2157.
155. Shi, F.; Shi, M.; Zeng, Z.; Qi, R. Z.; Liu, Z. W.; Zhang, J. Y.; Yang, Y. P.; Tien, P.; Wang, F. S., PD-1 and PD-L1 upregulation promotes CD8(+) T-cell apoptosis and postoperative recurrence in hepatocellular carcinoma patients. *International Journal of Cancer* **2011,** *128* (4), 887-96.

156. Konishi, J.; Yamazaki, K.; Azuma, M.; Kinoshita, I.; Dosaka-Akita, H.; Nishimura, M., B7-H1 expression on non-small cell lung cancer cells and its relationship with tumor-infiltrating lymphocytes and their PD-1 expression. *Clinical Cancer Research* **2004,** *10* (15), 5094-100.
157. Mu, C. Y.; Huang, J. A.; Chen, Y.; Chen, C.; Zhang, X. G., High expression of PD-L1 in lung cancer may contribute to poor prognosis and tumor cells immune escape through suppressing tumor infiltrating dendritic cells maturation. *Medical Oncology* **2011,** *28* (3), 682-8.
158. Chen, Y. B.; Mu, C. Y.; Huang, J. A., Clinical significance of programmed death-1 ligand-1 expression in patients with non-small cell lung cancer: a 5-year-follow-up study. *Tumori* **2012,** *98* (6), 751-5.
159. Velcheti, V.; Rimm, D. L.; Schalper, K. A., Sarcomatoid lung carcinomas show high levels of programmed death ligand-1 (PD-L1). *Journal of thoracic oncology : official publication of the International Association for the Study of Lung Cancer* **2013,** *8* (6), 803-5.
160. Velcheti, V.; Schalper, K. A.; Carvajal, D. E.; Anagnostou, V. K.; Syrigos, K. N.; Sznol, M.; Herbst, R. S.; Gettinger, S. N.; Chen, L.; Rimm, D. L., Programmed death ligand-1 expression in non-small cell lung cancer. *Laboratory investigation; a journal of technical methods and pathology* **2014,** *94* (1), 107-116.
161. Chen, Y. Y.; Wang, L. B.; Zhu, H. L.; Li, X. Y.; Zhu, Y. P.; Yin, Y. L.; Lu, F. Z.; Wang, Z. L.; Qu, J. M., Relationship between programmed death-ligand 1 and clinicopathological characteristics in non-small cell lung cancer patients. *Chinese Medical Sciences Journal* **2013,** *28* (3), 147-51.
162. Zhang, Y.; Huang, S.; Gong, D.; Qin, Y.; Shen, Q., Programmed death-1 upregulation is correlated with dysfunction of tumor-infiltrating CD8+ T lymphocytes in human non-small cell lung cancer. *Cellular & molecular immunology* **2010,** *7* (5), 389-95.
163. Hamanishi, J.; Mandai, M.; Iwasaki, M.; Okazaki, T.; Tanaka, Y.; Yamaguchi, K.; Higuchi, T.; Yagi, H.; Takakura, K.; Minato, N.; Honjo, T.; Fujii, S., Programmed cell death 1 ligand 1 and tumor-infiltrating CD8+ T lymphocytes are prognostic factors of human ovarian cancer. *Proceedings of the National Academy of Sciences* **2007,** *104* (9), 3360-3365.
164. Abiko, K.; Mandai, M.; Hamanishi, J.; Yoshioka, Y.; Matsumura, N.; Baba, T.; Yamaguchi, K.; Murakami, R.; Yamamoto, A.; Kharma, B.; Kosaka, K.; Konishi, I., PD-L1 on tumor cells is induced in ascites and promotes peritoneal dissemination of ovarian cancer through CTL dysfunction. *Clinical Cancer Research* **2013,** *19* (6), 1363-74.
165. Maine, C. J.; Aziz, N. H.; Chatterjee, J.; Hayford, C.; Brewig, N.; Whilding, L.; George, A. J.; Ghaem-Maghami, S., Programmed death ligand-1 over-expression correlates with malignancy and contributes to immune regulation in ovarian cancer. *Cancer Immunology, Immunotherapy* **2014,** *63* (3), 215-24.
166. Sun, J.; Xu, K.; Wu, C.; Wang, Y.; Hu, Y.; Zhu, Y.; Chen, Y.; Shi, Q.; Yu, G.; Zhang, X., PD-L1 expression analysis in gastric carcinoma tissue and blocking of tumor-associated PD-L1 signaling by two functional monoclonal antibodies. *Tissue antigens* **2007,** *69* (1), 19-27.

167. Salih, H. R.; Wintterle, S.; Krusch, M.; Kroner, A.; Huang, Y. H.; Chen, L.; Wiendl, H., The role of leukemia-derived B7-H1 (PD-L1) in tumor-T-cell interactions in humans. *Experimental hematology* **2006,** *34* (7), 888-94.
168. Chen, X.; Liu, S.; Wang, L.; Zhang, W.; Ji, Y.; Ma, X., Clinical significance of B7-H1 (PD-L1) expression in human acute leukemia. *Cancer biology & therapy* **2008,** *7* (5), 622-7.
169. Kozako, T.; Yoshimitsu, M.; Fujiwara, H.; Masamoto, I.; Horai, S.; White, Y.; Akimoto, M.; Suzuki, S.; Matsushita, K.; Uozumi, K.; Tei, C.; Arima, N., PD-1/PD-L1 expression in human T-cell leukemia virus type 1 carriers and adult T-cell leukemia/lymphoma patients. *Leukemia* **2009,** *23* (2), 375-82.
170. Shimauchi, T.; Kabashima, K.; Nakashima, D.; Sugita, K.; Yamada, Y.; Hino, R.; Tokura, Y., Augmented expression of programmed death-1 in both neoplastic and non-neoplastic CD4+ T-cells in adult T-cell leukemia/lymphoma. *International Journal of Cancer* **2007,** *121* (12), 2585-90.
171. Andorsky, D. J.; Yamada, R. E.; Said, J.; Pinkus, G. S.; Betting, D. J.; Timmerman, J. M., Programmed death ligand 1 is expressed by non-hodgkin lymphomas and inhibits the activity of tumor-associated T cells. *Clinical Cancer Research* **2011,** *17* (13), 4232-44.
172. Grzywnowicz, M.; Zaleska, J.; Mertens, D.; Tomczak, W.; Wlasiuk, P.; Kosior, K.; Piechnik, A.; Bojarska-Junak, A.; Dmoszynska, A.; Giannopoulos, K., Programmed death-1 and its ligand are novel immunotolerant molecules expressed on leukemic B cells in chronic lymphocytic leukemia. *PLoS One* **2012,** *7* (4), e35178.
173. Brusa, D.; Serra, S.; Coscia, M.; Rossi, D.; D'Arena, G.; Laurenti, L.; Jaksic, O.; Fedele, G.; Inghirami, G.; Gaidano, G.; Malavasi, F.; Deaglio, S., The PD-1/PD-L1 axis contributes to T-cell dysfunction in chronic lymphocytic leukemia. *Haematologica* **2013,** *98* (6), 953-63.
174. Chen, B. J.; Chapuy, B.; Ouyang, J.; Sun, H. H.; Roemer, M. G.; Xu, M. L.; Yu, H.; Fletcher, C. D.; Freeman, G. J.; Shipp, M. A.; Rodig, S. J., PD-L1 expression is characteristic of a subset of aggressive B-cell lymphomas and virus-associated malignancies. *Clinical Cancer Research* **2013,** *19* (13), 3462-73.
175. Wilcox, R. A.; Feldman, A. L.; Wada, D. A.; Yang, Z. Z.; Comfere, N. I.; Dong, H.; Kwon, E. D.; Novak, A. J.; Markovic, S. N.; Pittelkow, M. R.; Witzig, T. E.; Ansell, S. M., B7-H1 (PD-L1, CD274) suppresses host immunity in T-cell lymphoproliferative disorders. *Blood* **2009,** *114* (10), 2149-58.
176. Paydas, S.; Bagir, E.; Seydaoglu, G.; Ercolak, V.; Ergin, M., Programmed death-1 (PD-1), programmed death-ligand 1 (PD-L1), and EBV-encoded RNA (EBER) expression in Hodgkin lymphoma. *Annals of hematology* **2015,** *94* (9), 1545-52.
177. Soliman, H.; Khalil, F.; Antonia, S., PD-L1 expression is increased in a subset of basal type breast cancer cells. *PLoS One* **2014,** *9* (2), e88557.
178. Muenst, S.; Schaerli, A. R.; Gao, F.; Däster, S.; Trella, E.; Droeser, R. A.; Muraro, M. G.; Zajac, P.; Zanetti, R.; Gillanders, W. E.; Weber, W. P.; Soysal, S. D., Expression of programmed death ligand 1 (PD-L1) is associated with poor prognosis in human breast cancer. *Breast Cancer Research and Treatment* **2014,** *146* (1), 15-24.
179. Malaspina, T. S.; Gasparoto, T. H.; Costa, M. R.; de Melo, E. F., Jr.; Ikoma, M. R.; Damante, J. H.; Cavassani, K. A.; Garlet, G. P.; da Silva, J. S.; Campanelli, A. P., Enhanced programmed death 1 (PD-1) and PD-1 ligand (PD-L1) expression in patients

with actinic cheilitis and oral squamous cell carcinoma. *Cancer Immunology, Immunotherapy* **2011,** *60* (7), 965-74.
180. Loos, M.; Langer, R.; Schuster, T.; Gertler, R.; Walch, A.; Rauser, S.; Friess, H.; Feith, M., Clinical significance of the costimulatory molecule B7-H1 in Barrett carcinoma. *The Annals of thoracic surgery* **2011,** *91* (4), 1025-31.
181. Cho, Y. A.; Yoon, H. J.; Lee, J. I.; Hong, S. P.; Hong, S. D., Relationship between the expressions of PD-L1 and tumor-infiltrating lymphocytes in oral squamous cell carcinoma. *Oral oncology* **2011,** *47* (12), 1148-53.
182. Hino, R.; Kabashima, K.; Kato, Y.; Yagi, H.; Nakamura, M.; Honjo, T.; Okazaki, T.; Tokura, Y., Tumor cell expression of programmed cell death-1 ligand 1 is a prognostic factor for malignant melanoma. *Cancer* **2010,** *116* (7), 1757-66.
183. Gadiot, J.; Hooijkaas, A. I.; Kaiser, A. D.; van Tinteren, H.; van Boven, H.; Blank, C., Overall survival and PD-L1 expression in metastasized malignant melanoma. *Cancer* **2011,** *117* (10), 2192-201.
184. Jilaveanu, L. B.; Shuch, B.; Zito, C. R.; Parisi, F.; Barr, M.; Kluger, Y.; Chen, L.; Kluger, H. M., PD-L1 Expression in Clear Cell Renal Cell Carcinoma: An Analysis of Nephrectomy and Sites of Metastases. *Journal of Cancer* **2014,** *5* (3), 166-72.
185. Choueiri, T. K.; Fay, A. P.; Gray, K. P.; Callea, M.; Ho, T. H.; Albiges, L.; Bellmunt, J.; Song, J.; Carvo, I.; Lampron, M.; Stanton, M. L.; Hodi, F. S.; McDermott, D. F.; Atkins, M. B.; Freeman, G. J.; Hirsch, M. S.; Signoretti, S., PD-L1 expression in nonclear-cell renal cell carcinoma. *Annals of Oncology* **2014,** *25* (11), 2178-84.
186. Callea, M.; Albiges, L.; Gupta, M.; Cheng, S. C.; Genega, E. M.; Fay, A. P.; Song, J.; Carvo, I.; Bhatt, R. S.; Atkins, M. B.; Hodi, F. S.; Choueiri, T. K.; McDermott, D. F.; Freeman, G. J.; Signoretti, S., Differential Expression of PD-L1 between Primary and Metastatic Sites in Clear-Cell Renal Cell Carcinoma. *Cancer Immunology Research* **2015,** *3* (10), 1158-64.
187. Blank, C.; Kuball, J.; Voelkl, S.; Wiendl, H.; Becker, B.; Walter, B.; Majdic, O.; Gajewski, T. F.; Theobald, M.; Andreesen, R.; Mackensen, A., Blockade of PD-L1 (B7-H1) augments human tumor-specific T cell responses in vitro. *International Journal of Cancer* **2006,** *119* (2), 317-27.
188. Iwai, Y., Involvement of PD-L1 on tumor cells in the escape from host immune system and tumor immunotherapy by PD-L1 blockade. *Proceedings of the National Academy of Sciences* **2002,** *99*, 12293-12297.
189. Iwai, Y.; Terawaki, S.; Honjo, T., PD-1 blockade inhibits hematogenous spread of poorly immunogenic tumor cells by enhanced recruitment of effector T cells. *International Immunology* **2005,** *17*, 133-144.
190. Iwai, Y.; Hamanishi, J.; Chamoto, K.; Honjo, T., Cancer immunotherapies targeting the PD-1 signaling pathway. *Journal of Biomedical Science* **2017,** *24* (1), 26.
191. Zhang, L.; Gajewski, T. F.; Kline, J., PD-1/PD-L1 interactions inhibit antitumor immune responses in a murine acute myeloid leukemia model. *Blood* **2009,** *114* (8), 1545-1552.
192. Naidoo, J.; Page, D. B.; Wolchok, J. D., Immune modulation for cancer therapy. *British Journal Of Cancer* **2014,** *111*, 2214.
193. Zarganes-Tzitzikas, T.; Konstantinidou, M.; Gao, Y.; Krzemien, D.; Zak, K.; Dubin, G.; Holak, T. A.; Dömling, A., Inhibitors of programmed cell death 1 (PD-1): a

patent review (2010-2015). *Expert Opinion on Therapeutic Patents* **2016,** *26* (9), 973-977.
194. Li, Y.; Li, F.; Jiang, F.; Lv, X.; Zhang, R.; Lu, A.; Zhang, G., A Mini-Review for Cancer Immunotherapy: Molecular Understanding of PD-1/PD-L1 Pathway & Translational Blockade of Immune Checkpoints. *International Journal of Molecular Sciences* **2016,** *17* (7), 1151.
195. Balar, A. V.; Weber, J. S., PD-1 and PD-L1 antibodies in cancer: current status and future directions. *Cancer Immunology, Immunotherapy* **2017,** *66* (5), 551-564.
196. FDA approves first cancer treatment for any solid tumor with a specific genetic feature. U.S. Food and Drug Administration: 2017.
197. Horita, S.; Nomura, Y.; Sato, Y.; Shimamura, T.; Iwata, S.; Nomura, N., High-resolution crystal structure of the therapeutic antibody pembrolizumab bound to the human PD-1. *Scientific Reports* **2016,** *6*, 35297.
198. Na, Z.; Yeo, S. P.; Bharath, S. R.; Bowler, M. W.; Balıkçı, E.; Wang, C.-I.; Song, H., Structural basis for blocking PD-1-mediated immune suppression by therapeutic antibody pembrolizumab. *Cell Research* **2016,** *27*, 147.
199. Zhan, M.-M.; Hu, X.-Q.; Liu, X.-X.; Ruan, B.-F.; Xu, J.; Liao, C., From monoclonal antibodies to small molecules: the development of inhibitors targeting the PD-1/PD-L1 pathway. *Drug Discovery Today* **2016,** *21* (6), 1027-1036.
200. Dempke, W. C. M.; Fenchel, K.; Uciechowski, P.; Dale, S. P., Second- and third-generation drugs for immuno-oncology treatment—The more the better? *European Journal of Cancer* **2017,** *74* (Supplement C), 55-72.
201. Remon, J.; Besse, B.; Soria, J.-C., Successes and failures: what did we learn from recent first-line treatment immunotherapy trials in non-small cell lung cancer? *BMC Medicine* **2017,** *15* (1), 55.
202. Meng, X.; Liu, Y.; Zhang, J.; Teng, F.; Xing, L.; Yu, J., PD-1/PD-L1 checkpoint blockades in non-small cell lung cancer: New development and challenges. *Cancer Letters* **2017,** *405* (Supplement C), 29-37.
203. Clark, D. P., Biomarkers for immune checkpoint inhibitors: The importance of tumor topography and the challenges to cytopathology. *Cancer Cytopathology* **2017**.
204. Bommareddy, P. K.; Kaufman, H. L., Avelumab and other recent advances in Merkel-cell carcinoma. *Future Oncology* **2017,** *13*, 2771-2783.
205. Powles, T.; O'Donnell, P. H.; Massard, C.; Arkenau, H. T.; Friedlander, T. W.; Hoimes, C. J.; Lee, J. L.; Ong, M.; Sridhar, S. S.; Vogelzang, N. J.; Fishman, M. N.; Zhang, J.; Srinivas, S.; Parikh, J.; Antal, J.; Jin, X.; Gupta, A. K.; Ben, Y.; Hahn, N. M., Efficacy and Safety of Durvalumab in Locally Advanced or Metastatic Urothelial Carcinoma: Updated Results From a Phase 1/2 Open-label Study. *JAMA oncology* **2017,** *3* (9), e172411.
206. Guan, J.; Lim, K. S.; Mekhail, T.; Chang, C. C., Programmed Death Ligand-1 (PD-L1) Expression in the Programmed Death Receptor-1 (PD-1)/PD-L1 Blockade: A Key Player Against Various Cancers. *Archives of Pathology & Laboratory Ledicine* **2017,** *141* (6), 851-861.
207. Dal Bello, M. G.; Alama, A.; Coco, S.; Vanni, I.; Grossi, F., Understanding the checkpoint blockade in lung cancer immunotherapy. *Drug Discovery Today* **2017,** *22* (8), 1266-1273.

208. Sukari, A.; Nagasaka, M.; Al-Hadidi, A.; Lum, L. G., Cancer Immunology and Immunotherapy. *Anticancer Research* **2016,** *36* (11), 5593-5606.
209. Sharma, P.; Hu-Lieskovan, S.; Wargo, J. A.; Ribas, A., Primary, Adaptive, and Acquired Resistance to Cancer Immunotherapy. *Cell* **2017,** *168* (4), 707-723.
210. Bu, X.; Mahoney, K. M.; Freeman, G. J., Learning from PD-1 Resistance: New Combination Strategies. *Trends in Molecular Medicine* **2016,** *22* (6), 448-451.
211. Feng, M.; Xiong, G.; Cao, Z.; Yang, G.; Zheng, S.; Song, X.; You, L.; Zheng, L.; Zhang, T.; Zhao, Y., PD-1/PD-L1 and immunotherapy for pancreatic cancer. *Cancer Letters* **2017,** *407* (Supplement C), 57-65.
212. Guo, S.; Contratto, M.; Miller, G.; Leichman, L.; Wu, J., Immunotherapy in pancreatic cancer: Unleash its potential through novel combinations. *World Journal of Clinical Oncology* **2017,** *8* (3), 230-240.
213. Maleki Vareki, S.; Garrigós, C.; Duran, I., Biomarkers of response to PD-1/PD-L1 inhibition. *Critical Reviews in Oncology/Hematology* **2017,** *116* (Supplement C), 116-124.
214. Meng, X.; Huang, Z.; Teng, F.; Xing, L.; Yu, J., Predictive biomarkers in PD-1/PD-L1 checkpoint blockade immunotherapy. *Cancer Treatment Reviews* **2015,** *41* (10), 868-876.
215. Taube, J. M.; Anders, R. A.; Young, G. D.; Xu, H.; Sharma, R.; McMiller, T. L.; Chen, S.; Klein, A. P.; Pardoll, D. M.; Topalian, S. L., Colocalization of inflammatory response with B7-h1 expression in human melanocytic lesions supports an adaptive resistance mechanism of immune escape. *Science Translational Medicine* **2012,** *4*, 127ra37.
216. Patel, S. P.; Kurzrock, R., PD-L1 Expression as a Predictive Biomarker in Cancer Immunotherapy. *Molecular Cancer Therapeutics* **2015,** *14* (4), 847-856.
217. Grigg, C.; Rizvi, N. A., PD-L1 biomarker testing for non-small cell lung cancer: truth or fiction? *Journal for ImmunoTherapy of Cancer* **2016,** *4* (1), 48.
218. Fusi, A.; Festino, L.; Botti, G.; Masucci, G.; Melero, I.; Lorigan, P.; Ascierto, P. A., PD-L1 expression as a potential predictive biomarker. *The Lancet Oncology* **2015,** *16* (13), 1285-1287.
219. Wolchok, J. D., Nivolumab plus ipilimumab in advanced melanoma. *New England Journal of Medicine* **2013,** *369*, 122-133.
220. Spigel, D. R.; Gettinger, S. N.; Horn, L.; Herbst, R. S.; Gandhi, L.; Gordon, M. S.; Cruz, C.; Conkling, P.; Cassier, P. A.; Antonia, S. J.; Burris, H. A.; Fine, G. D.; Mokatrin, A.; Kowanetz, M.; Shen, X.; Chen, D. S.; Soria, J.-C., Clinical activity, safety, and biomarkers of MPDL3280A, an engineered PD-L1 antibody in patients with locally advanced or metastatic non-small cell lung cancer (NSCLC). *Journal of Clinical Oncology* **2013,** *31* (15_suppl), 8008-8008.
221. Yaghmour, G.; Pandey, M.; Ireland, C.; Patel, K.; Nunnery, S.; Powell, D.; Baum, S.; Wiedower, E.; Schwartzberg, L. S.; Martin, M. G., Role of Genomic Instability in Immunotherapy with Checkpoint Inhibitors. *Anticancer Research* **2016,** *36* (8), 4033-4038.
222. Costa, R.; Carneiro, B. A.; Agulnik, M.; Rademaker, A. W.; Pai, S. G.; Villaflor, V. M.; Cristofanilli, M.; Sosman, J. A.; Giles, F. J., Toxicity profile of approved anti-PD-1 monoclonal antibodies in solid tumors: a systematic review and meta-analysis of randomized clinical trials. *Oncotarget* **2017,** *8* (5), 8910-8920.

223. Naidoo, J., Toxicities of the anti-PD-1 and anti-PD-L1 immune checkpoint antibodies. *Annals of Oncology* **2015,** *26*, 2375-2391.
224. Michot, J. M.; Bigenwald, C.; Champiat, S.; Collins, M.; Carbonnel, F.; Postel-Vinay, S.; Berdelou, A.; Varga, A.; Bahleda, R.; Hollebecque, A.; Massard, C.; Fuerea, A.; Ribrag, V.; Gazzah, A.; Armand, J. P.; Amellal, N.; Angevin, E.; Noel, N.; Boutros, C.; Mateus, C.; Robert, C.; Soria, J. C.; Marabelle, A.; Lambotte, O., Immune-related adverse events with immune checkpoint blockade: a comprehensive review. *European Journal of Cancer* **2016,** *54* (Supplement C), 139-148.
225. Shimizu, T.; Seto, T.; Hirai, F.; Takenoyama, M.; Nosaki, K.; Tsurutani, J.; Kaneda, H.; Iwasa, T.; Kawakami, H.; Noguchi, K.; Shimamoto, T.; Nakagawa, K., Phase 1 study of pembrolizumab (MK-3475; anti-PD-1 monoclonal antibody) in Japanese patients with advanced solid tumors. *Investigational New Drugs* **2016,** *34* (3), 347-354.
226. Ahamadi, M.; Freshwater, T.; Prohn, M.; Li, C. H.; Alwis, D. P. d.; Greef, R. d.; Elassaiss-Schaap, J.; Kondic, A.; Stone, J. A., Model-Based Characterization of the Pharmacokinetics of Pembrolizumab: A Humanized Anti–PD-1 Monoclonal Antibody in Advanced Solid Tumors. *CPT: Pharmacometrics & Systems Pharmacology* **2017,** *6* (1), 49-57.
227. Glassman, P. M.; Balthasar, J. P., Mechanistic considerations for the use of monoclonal antibodies for cancer therapy. *Cancer Biology & Medicine* **2014,** *11* (1), 20-33.
228. Gaillard, S. L.; Secord, A. A.; Monk, B., The role of immune checkpoint inhibition in the treatment of ovarian cancer. *Gynecologic Oncology Research and Practice* **2016,** *3* (1), 11.
229. Tan, S.; Zhang, C. W. H.; Gao, G. F., Seeing is believing: anti-PD-1/PD-L1 monoclonal antibodies in action for checkpoint blockade tumor immunotherapy. *Signal Transduction And Targeted Therapy* **2016,** *1*, 16029.
230. Lee, C. M.; Tannock, I. F., The distribution of the therapeutic monoclonal antibodies cetuximab and trastuzumab within solid tumors. *BMC Cancer* **2010,** *10*, 255.
231. Maute, R. L.; Gordon, S. R.; Mayer, A. T.; McCracken, M. N.; Natarajan, A.; Ring, N. G.; Kimura, R.; Tsai, J. M.; Manglik, A.; Kruse, A. C.; Gambhir, S. S.; Weissman, I. L.; Ring, A. M., Engineering high-affinity PD-1 variants for optimized immunotherapy and immuno-PET imaging. *Proceedings of the National Academy of Sciences* **2015,** *112* (47), E6506-E6514.
232. Shaughnessy, A. F., Monoclonal antibodies: magic bullets with a hefty price tag. *BMJ : British Medical Journal* **2012,** *345*, e8346.
233. Li, Q.; Quan, L.; Lyu, J.; He, Z.; Wang, X.; Meng, J.; Zhao, Z.; Zhu, L.; Liu, X.; Li, H., Discovery of peptide inhibitors targeting human programmed death 1 (PD-1) receptor. *Oncotarget* **2016,** *7* (40), 64967-64976.
234. Wang, F.; Ma, J.; Liu, J.; Jin, H.; Huang, D., Synthetic small peptides acting on B7H1 enhance apoptosis in pancreatic cancer cells. *Molecular medicine reports* **2012,** *6* (3), 553-7.
235. Miller, M. M.; Mapelli, C.; Allen, M. P.; Bowsher, M. S.; Boy, K. M.; Gillis, E. P.; Langley, D. R.; Mull, E.; Poirier, M. A.; Sanghvi, N. Macrocyclic inhibitors of the PD-1/PD-L1 and CD80(B7-1)/PD-L1 protein/protein interactions. US 20140294898 A1, 2014.

236. Chang, H. N.; Liu, B. Y.; Qi, Y. K.; Zhou, Y.; Chen, Y. P.; Pan, K. M.; Li, W. W.; Zhou, X. M.; Ma, W. W.; Fu, C. Y.; Qi, Y. M.; Liu, L.; Gao, Y. F., Blocking of the PD-1/PD-L1 Interaction by a D-Peptide Antagonist for Cancer Immunotherapy. *Angewandte Chemie International Edition* **2015,** *54* (40), 11760-11764.
237. Sasikumar, P. G. N.; Ramachandra, M.; Vadlamani, S. K.; Vemula, K. R.; Satyam, L. K.; Subbarao, K.; Shrimali, K. R.; Kandepu, S. Immunosuppression modulating compounds. US 20110318373 A1, 2011.
238. Sasikumar, P. G. N.; Ramachandra, M.; Vadlamani, S. K.; Shrimali, K. R.; Subbarao, K. Therapeutic compounds for immunomodulation. WO 2012168944 A1, 2012.
239. Sasikumar, P. G. N.; Ramachandra, M. Immunomodulating cyclic compounds from the bc loop of human pd1. WO 2013144704 A1, 2013.
240. Sasikumar, P. G. N.; Ramachandra, M.; Naremaddepalli, S. S. S. Peptidomimetic compounds as immunomodulators. US 20130237580 A1, 2013.
241. Sasikumar, P. G. N.; Ramachandra, M.; Naremaddepalli, S. S. S. 1,3,4-oxadiazole and 1,3,4-thiadiazole derivatives as immunomodulators. WO 2015033301 A1, 2015.
242. Chupak, L. S.; Zheng, X. Compounds useful as immunomodulators. WO 2015034820 A1, 2014.
243. Chupak, L. S.; Ding, M.; Martin, S. W.; Zheng, X.; Hewawasam, P.; Connolly, T. P.; Xu, N.; Yeung, K.-S.; Zhu, J.; Langley, D. R. Compounds useful as immunomodulators. US 20150291549 A1, 2015.
244. Sharpe, A. H.; Butte, M. J.; Oyama, S. Modulators of immunoinhibitory receptor pd-1, and methods of use thereof. WO 2011082400 A2, 2011.
245. Liu, A.; Dong, L.; Wei, X.-L.; Yang, X.-H.; Xiao, J.-H.; Liu, Z.-Q., Development of amino- and dimethylcarbamate-substituted resorcinol as programmed cell death-1 (PD-1) inhibitor. *European Journal of Pharmaceutical Sciences* **2016,** *88* (Supplement C), 50-58.
246. DeLano, W. L., Unraveling hot spots in binding interfaces: progress and challenges. *Current Opinion in Structural Biology* **2002,** *12* (1), 14-20.
247. Magiera-Mularz, K.; Skalniak, L.; Zak, K. M.; Musielak, B.; Rudzinska-Szostak, E.; Berlicki, Ł.; Kocik, J.; Grudnik, P.; Sala, D.; Zarganes-Tzitzikas, T.; Shaabani, S.; Dömling, A.; Dubin, G.; Holak, T. A., Bioactive Macrocyclic Inhibitors of the PD-1/PD-L1 Immune Checkpoint. *Angewandte Chemie International Edition* **2017,** *56* (44), 13732-13735.
248. Freeman, G. J., Structures of PD-1 with its ligands: Sideways and dancing cheek to cheek. *Proceedings of the National Academy of Sciences* **2008,** *105* (30), 10275-10276.
249. Vauquelin, G.; Charlton, S. J., Exploring avidity: understanding the potential gains in functional affinity and target residence time of bivalent and heterobivalent ligands. *British Journal of Pharmacology* **2013,** *168* (8), 1771-1785.
250. Pentcheva-Hoang, T.; Chen, L.; Pardoll, D. M.; Allison, J. P., Programmed death-1 concentration at the immunological synapse is determined by ligand affinity and availability. *Proceedings of the National Academy of Sciences* **2007,** *104* (45), 17765-17770.
251. Yokosuka, T.; Takamatsu, M.; Kobayashi-Imanishi, W.; Hashimoto-Tane, A.; Azuma, M.; Saito, T., Programmed cell death 1 forms negative costimulatory

microclusters that directly inhibit T cell receptor signaling by recruiting phosphatase SHP2. *The Journal of Experimental Medicine* **2012,** *209* (6), 1201-1217.
252. Li, B.; Fouts, A. E.; Stengel, K.; Luan, P.; Dillon, M.; Liang, W.-C.; Feierbach, B.; Kelley, R. F.; Hötzel, I., In vitro affinity maturation of a natural human antibody overcomes a barrier to in vivo affinity maturation. *mAbs* **2014,** *6* (2), 437-445.
253. Bishop, G. J.; Price, B. J.; Sutherland, I. O., Torsional barriers in N,N`-diacylhydrazines. *Chemical Communications (London)* **1967,** (14), 672-674.
254. A Study of CA-170 (Oral PD-L1, PD-L2 and VISTA Checkpoint Antagonist) in Patients With Advanced Tumors and Lymphomas.
255. Khanfar, M. A.; AbuKhader, M. M.; Alqtaishat, S.; Taha, M. O., Pharmacophore modeling, homology modeling, and in silico screening reveal mammalian target of rapamycin inhibitory activities for sotalol, glyburide, metipranolol, sulfamethizole, glipizide, and pioglitazone. *Journal of Molecular Graphics and Modelling* **2013,** *42* (Supplement C), 39-49.
256. Rodrigues, T.; Roudnicky, F.; Koch, C. P.; Kudoh, T.; Reker, D.; Detmar, M.; Schneider, G., De novo design and optimization of Aurora A kinase inhibitors. *Chemical Science* **2013,** *4* (3), 1229-1233.
257. Meuillet, E. J.; Zuohe, S.; Lemos, R.; Ihle, N.; Kingston, J.; Watkins, R.; Moses, S. A.; Zhang, S.; Du-Cuny, L.; Herbst, R.; Jacoby, J. J.; Zhou, L. L.; Ahad, A. M.; Mash, E. A.; Kirkpatrick, D. L.; Powis, G., Molecular Pharmacology and Antitumor Activity of PHT-427, a Novel Akt/Phosphatidylinositide-Dependent Protein Kinase 1 Pleckstrin Homology Domain Inhibitor. *Molecular Cancer Therapeutics* **2010,** *9* (3), 706-717.
258. Moses, S. A.; Ali, M. A.; Zuohe, S.; Du-Cuny, L.; Zhou, L. L.; Lemos, R.; Ihle, N.; Skillman, A. G.; Zhang, S.; Mash, E. A.; Powis, G.; Meuillet, E. J., In vitro and In vivo Activity of Novel Small-Molecule Inhibitors Targeting the Pleckstrin Homology Domain of Protein Kinase B/AKT. *Cancer Research* **2009,** *69* (12), 5073-5081.
259. Mahadevan, D.; Powis, G.; Mash, E. A.; George, B.; Gokhale, V. M.; Zhang, S.; Shakalya, K.; Du-Cuny, L.; Berggren, M.; Ali, M. A.; Jana, U.; Ihle, N.; Moses, S.; Franklin, C.; Narayan, S.; Shirahatti, N.; Meuillet, E. J., Discovery of a novel class of AKT pleckstrin homology domain inhibitors. *Molecular Cancer Therapeutics* **2008,** *7* (9), 2621-2632.
260. Ahad, A. M.; Zuohe, S.; Du-Cuny, L.; Moses, S. A.; Zhou, L. L.; Zhang, S.; Powis, G.; Meuillet, E. J.; Mash, E. A., Development of sulfonamide AKT PH domain inhibitors. *Bioorganic & Medicinal Chemistry* **2011,** *19* (6), 2046-2054.
261. Meyer, B.; Peters, T., NMR Spectroscopy Techniques for Screening and Identifying Ligand Binding to Protein Receptors. *Angewandte Chemie International Edition* **2003,** *42* (8), 864-890.
262. Villoutreix, B. O.; Kuenemann, M. A.; Poyet, J. L.; Bruzzoni-Giovanelli, H.; Labbé, C.; Lagorce, D.; Sperandio, O.; Miteva, M. A., Drug-Like Protein-Protein Interaction Modulators: Challenges and Opportunities for Drug Discovery and Chemical Biology. *Molecular Informatics* **2014,** *33* (6-7), 414-437.
263. Varma, H.; Lo, D. C.; Stockwell, B. R., High-throughput and high-content screening for Huntington's disease therapeutics. *Neurobiology of Huntington's Disease: Applications to Drug Discovery. DC Lo, RE Hughes (eds.)* **2011**, 121-1461.

264. Voter, A. F.; Manthei, K. A.; Keck, J. L., A High-Throughput Screening Strategy to Identify Protein-Protein Interaction Inhibitors That Block the Fanconi Anemia DNA Repair Pathway. *Journal of Biomolecular Screening* **2016,** *21* (6), 626-633.
265. Milhas, S.; Raux, B.; Betzi, S.; Derviaux, C.; Roche, P.; Restouin, A.; Basse, M.-J.; Rebuffet, E.; Lugari, A.; Badol, M.; Kashyap, R.; Lissitzky, J.-C.; Eydoux, C.; Hamon, V.; Gourdel, M.-E.; Combes, S.; Zimmermann, P.; Aurrand-Lions, M.; Roux, T.; Rogers, C.; Müller, S.; Knapp, S.; Trinquet, E.; Collette, Y.; Guillemot, J.-C.; Morelli, X., Protein–Protein Interaction Inhibition (2P2I)-Oriented Chemical Library Accelerates Hit Discovery. *ACS Chemical Biology* **2016,** *11* (8), 2140-2148.
266. Nero, T. L.; Morton, C. J.; Holien, J. K.; Wielens, J.; Parker, M. W., Oncogenic protein interfaces: small molecules, big challenges. *Nature Reviews Cancer* **2014,** *14*, 248.
267. Jubb, H.; Higueruelo, A. P.; Winter, A.; Blundell, T. L., Structural biology and drug discovery for protein–protein interactions. *Trends in Pharmacological Sciences* **2012,** *33* (5), 241-248.
268. Scior, T.; Bender, A.; Tresadern, G.; Medina-Franco, J. L.; Martínez-Mayorga, K.; Langer, T.; Cuanalo-Contreras, K.; Agrafiotis, D. K., Recognizing Pitfalls in Virtual Screening: A Critical Review. *Journal of Chemical Information and Modeling* **2012,** *52* (4), 867-881.
269. Cheng, T.; Li, Q.; Zhou, Z.; Wang, Y.; Bryant, S. H., Structure-Based Virtual Screening for Drug Discovery: a Problem-Centric Review. *The AAPS Journal* **2012,** *14* (1), 133-141.
270. Waszkowycz, B.; Clark, D. E.; Gancia, E., Outstanding challenges in protein–ligand docking and structure-based virtual screening. *Wiley Interdisciplinary Reviews: Computational Molecular Science* **2011,** *1* (2), 229-259.
271. Zhang, F.; Wei, H.; Wang, X.; Bai, Y.; Wang, P.; Wu, J.; Jiang, X.; Wang, Y.; Cai, H.; Xu, T.; Zhou, A., Structural basis of a novel PD-L1 nanobody for immune checkpoint blockade. *Cell Discovery* **2017,** *3*, 17004.
272. Wang, S.; Bajorath, J.; Flies, D. B.; Dong, H.; Honjo, T.; Chen, L., Molecular Modeling and Functional Mapping of B7-H1 and B7-DC Uncouple Costimulatory Function from PD-1 Interaction. *The Journal of Experimental Medicine* **2003,** *197* (9), 1083-1091.
273. An, J.; Totrov, M.; Abagyan, R., Pocketome via Comprehensive Identification and Classification of Ligand Binding Envelopes. *Molecular & Cellular Proteomics* **2005,** *4* (6), 752-761.
274. Abagyan, R.; Totrov, M.; Kuznetsov, D., ICM—A new method for protein modeling and design: Applications to docking and structure prediction from the distorted native conformation. *Journal of Computational Chemistry* **1994,** *15* (5), 488-506.
275. Irwin, J. J.; Shoichet, B. K., ZINC − A Free Database of Commercially Available Compounds for Virtual Screening. *Journal of Chemical Information and Modeling* **2005,** *45* (1), 177-182.
276. Vieth, M.; Siegel, M. G.; Higgs, R. E.; Watson, I. A.; Robertson, D. H.; Savin, K. A.; Durst, G. L.; Hipskind, P. A., Characteristic Physical Properties and Structural Fragments of Marketed Oral Drugs. *Journal of Medicinal Chemistry* **2004,** *47* (1), 224-232.

277. Xu, L.; Liu, Y.; He, X., Expression and purification of soluble human programmed death-1 in Escherichia coli. *Cellular & molecular immunology* **2006,** *3* (2), 139-43.
278. Terawaki, S.; Tanaka, Y.; Nagakura, T.; Hayashi, T.; Shibayama, S.; Muroi, K.; Okazaki, T.; Mikami, B.; Garboczi, D. N.; Honjo, T.; Minato, N., Specific and high-affinity binding of tetramerized PD-L1 extracellular domain to PD-1-expressing cells: possible application to enhance T cell function. *International Immunology* **2007,** *19* (7), 881-890.
279. Schormann, N.; Sommers, C. I.; Prichard, M. N.; Keith, K. A.; Noah, J. W.; Nuth, M.; Ricciardi, R. P.; Chattopadhyay, D., Identification of Protein-Protein Interaction Inhibitors Targeting Vaccinia Virus Processivity Factor for Development of Antiviral Agents. *Antimicrobial Agents and Chemotherapy* **2011,** *55* (11), 5054-5062.
280. Joseph-McCarthy, D.; Campbell, A. J.; Kern, G.; Moustakas, D., Fragment-Based Lead Discovery and Design. *Journal of Chemical Information and Modeling* **2014,** *54* (3), 693-704.
281. Baell, J. B.; Holloway, G. A., New Substructure Filters for Removal of Pan Assay Interference Compounds (PAINS) from Screening Libraries and for Their Exclusion in Bioassays. *Journal of Medicinal Chemistry* **2010,** *53* (7), 2719-2740.
282. Irwin, J. J.; Duan, D.; Torosyan, H.; Doak, A. K.; Ziebart, K. T.; Sterling, T.; Tumanian, G.; Shoichet, B. K., An Aggregation Advisor for Ligand Discovery. *Journal of Medicinal Chemistry* **2015,** *58* (17), 7076-7087.
283. Morreale, F. E.; Testa, A.; Chaugule, V. K.; Bortoluzzi, A.; Ciulli, A.; Walden, H., Mind the Metal: A Fragment Library-Derived Zinc Impurity Binds the E2 Ubiquitin-Conjugating Enzyme Ube2T and Induces Structural Rearrangements. *Journal of Medicinal Chemistry* **2017,** *60* (19), 8183-8191.
284. Pantoliano, M. W.; Petrella, E. C.; Kwasnoski, J. D.; Lobanov, V. S.; Myslik, J.; Graf, E.; Carver, T.; Asel, E.; Springer, B. A.; Lane, P.; Salemme, F. R., High-Density Miniaturized Thermal Shift Assays as a General Strategy for Drug Discovery. *Journal of Biomolecular Screening* **2001,** *6* (6), 429-440.
285. Krishna, S. N.; Luan, C.-H.; Mishra, R. K.; Xu, L.; Scheidt, K. A.; Anderson, W. F.; Bergan, R. C., A Fluorescence-Based Thermal Shift Assay Identifies Inhibitors of Mitogen Activated Protein Kinase Kinase 4. *PLOS ONE* **2013,** *8* (12), e81504.
286. Lo, M.-C.; Aulabaugh, A.; Jin, G.; Cowling, R.; Bard, J.; Malamas, M.; Ellestad, G., Evaluation of fluorescence-based thermal shift assays for hit identification in drug discovery. *Analytical Biochemistry* **2004,** *332* (1), 153-159.
287. PD-1[Biotinylated]:PD-L1 Inhibitor Screening Assay Kit. BPS Bioscience, catalog number 72005. http://bpsbioscience.com/pd-l1-inhibitor-screening-assay-kit-72005.
288. Ferreiros-Vidal, I.; Gomez-Reino, J. J.; Barros, F.; Carracedo, A.; Carreira, P.; Gonzalez-Escribano, F.; Liz, M.; Martin, J.; Ordi, J.; Vicario, J. L.; Gonzalez, A., Association of PDCD1 with susceptibility to systemic lupus erythematosus. *Arthritis & Rheumatism* **2004,** *50* (8), 2590-2597.
289. Bertsias, G. K.; Nakou, M.; Choulaki, C.; Raptopoulou, A.; Papadimitraki, E.; Goulielmos, G., Genetic, immunologic, and immunohistochemical analysis of the programmed death 1/programmed death ligand 1 pathway in human systemic lupus erythematosus. *Arthritis & Rheumatism* **2009,** *60*, 207-218.

290. Onodera, K.; Hirano, S.; Kashimura, N., Oxidation of Carbohydrates with Dimethyl Sulfoxide Containing Phosphorus Pentoxide. *Journal of the American Chemical Society* **1965,** *87* (20), 4651-4652.
291. Taber, D. F.; Amedio, J. C.; Jung, K. Y., Phosphorus pentoxide/dimethyl sulfoxide/triethylamine (PDT): a convenient procedure for oxidation of alcohols to ketones and aldehydes. *The Journal of Organic Chemistry* **1987,** *52* (25), 5621-5622.
292. Lucio Anelli, P.; Biffi, C.; Montanari, F.; Quici, S., Fast and selective oxidation of primary alcohols to aldehydes or to carboxylic acids and of secondary alcohols to ketones mediated by oxoammonium salts under two-phase conditions. *The Journal of Organic Chemistry* **1987,** *52* (12), 2559-2562.
293. Bolm, C.; Magnus, A. S.; Hildebrand, J. P., Catalytic Synthesis of Aldehydes and Ketones under Mild Conditions Using TEMPO/Oxone. *Organic Letters* **2000,** *2* (8), 1173-1175.
294. Miller, R. A.; Hoerrner, R. S., Iodine as a Chemoselective Reoxidant of TEMPO: Application to the Oxidation of Alcohols to Aldehydes and Ketones. *Organic Letters* **2003,** *5* (3), 285-287.
295. Dueholm, K. L.; Egholm, M.; Buchardt, O., An efficient synthesis of Boc-aminoacetaldehyde and its application to the synthesis of N-(2-Boc-aminoethyl)glycine esters. *Organic Preparations and Procedures International* **1993,** *25* (4), 457-461.
296. Horvath, S. W. Small Molecule Modulation of the PD1–PDL1 Interaction. University of Victoria, Victoria, British Columbia, Canada, 2015.
297. PD-1:PD-L1[Biotinylated] Inhibitor Screening Assay Kit. BPS Bioscience, catalog number 72003. http://bpsbioscience.com/pd-1-pd-l1-biotinylated-inhibitor-screening-assay-kit-72003.
298. PD-1:PD-L2 TR-FRET Assay Kit. BPS Bioscience, catalog number 72012. http://bpsbioscience.com/pd-1-pd-l2-tr-fret-assay-kit.
299. Degorce, F.; Card, A.; Soh, S.; Trinquet, E.; Knapik, G. P.; Xie, B., HTRF: A Technology Tailored for Drug Discovery –A Review of Theoretical Aspects and Recent Applications. *Current Chemical Genomics* **2009,** *3*, 22-32.
300. Dahlin, J. L.; Nissink, J. W. M.; Strasser, J. M.; Francis, S.; Higgins, L.; Zhou, H.; Zhang, Z.; Walters, M. A., PAINS in the Assay: Chemical Mechanisms of Assay Interference and Promiscuous Enzymatic Inhibition Observed during a Sulfhydryl-Scavenging HTS. *Journal of Medicinal Chemistry* **2015,** *58* (5), 2091-2113.
301. Schorpp, K.; Rothenaigner, I.; Salmina, E.; Reinshagen, J.; Low, T.; Brenke, J. K.; Gopalakrishnan, J.; Tetko, I. V.; Gul, S.; Hadian, K., Identification of Small-Molecule Frequent Hitters from AlphaScreen High-Throughput Screens. *Journal of Biomolecular Screening* **2014,** *19* (5), 715-726.
302. Tomasic, T.; Peterlin Masic, L., Rhodanine as a scaffold in drug discovery: a critical review of its biological activities and mechanisms of target modulation. *Expert opinion on drug discovery* **2012,** *7* (7), 549-60.
303. Kuke, S.; Marmodée, B.; Eidner, S.; Schilde, U.; Kumke, M. U., Intramolecular deactivation processes in complexes of salicylic acid or glycolic acid with Eu(III). *Spectrochimica Acta Part A: Molecular and Biomolecular Spectroscopy* **2010,** *75* (4), 1333-1340.

304. Barkleit, A.; Acker, M.; Bernhard, G., Europium(III) complexation with salicylic acid at elevated temperatures. *Inorganica Chimica Acta* **2013,** *394* (Supplement C), 535-541.
305. Baell, J.; Walters, M. A., Chemistry: Chemical con artists foil drug discovery. *Nature* **2014,** *513* (7519), 481-3.
306. Dahlin, J. L.; Walters, M. A., The essential roles of chemistry in high-throughput screening triage. *Future Medicinal Chemistry* **2014,** *6* (11), 1265-90.
307. Gaulton, A.; Hersey, A.; Nowotka, M.; Bento, A. P.; Chambers, J.; Mendez, D.; Mutowo, P.; Atkinson, F.; Bellis, L. J.; Cibrián-Uhalte, E.; Davies, M.; Dedman, N.; Karlsson, A.; Magariños, M. P.; Overington, J. P.; Papadatos, G.; Smit, I.; Leach, A. R., The ChEMBL database in 2017. *Nucleic Acids Research* **2017,** *45* (Database issue), D945-D954.
308. Tang, Y.; Zeng, X.; Liang, J., Surface Plasmon Resonance: An Introduction to a Surface Spectroscopy Technique. *Journal of Chemical Education* **2010,** *87* (7), 742-746.
309. Schasfoort, R. B.; Tudos, A., Introduction to surface plasmon resonance. In *Handbook of surface Plasmon resonance*, Royal Society of Chemistry: 2017; pp 1-26.
310. Leadbeater, N. E.; Marco, M., Ligand-Free Palladium Catalysis of the Suzuki Reaction in Water Using Microwave Heating. *Organic Letters* **2002,** *4* (17), 2973-2976.
311. Zak, K. M.; Grudnik, P.; Guzik, K.; Zieba, B. J.; Musielak, B.; Dömling, A.; Dubin, G.; Holak, T. A., Structural basis for small molecule targeting of the programmed death ligand 1 (PD-L1). *Oncotarget* **2016,** *7* (21), 30323.
312. Zak, K. M.; Grudnik, P.; Magiera, K.; Dömling, A.; Dubin, G.; Holak, T. A., Structural Biology of the Immune Checkpoint Receptor PD-1 and Its Ligands PD-L1/PD-L2. *Structure* **2017,** *25* (8), 1163-1174.
313. Pintacuda, G.; Otting, G., Identification of Protein Surfaces by NMR Measurements with a Paramagnetic Gd(III) Chelate. *Journal of the American Chemical Society* **2002,** *124* (3), 372-373.
314. Guzik, K.; Zak, K. M.; Grudnik, P.; Magiera, K.; Musielak, B.; Törner, R.; Skalniak, L.; Dömling, A.; Dubin, G.; Holak, T. A., Small-Molecule Inhibitors of the Programmed Cell Death-1/Programmed Death-Ligand 1 (PD-1/PD-L1) Interaction via Transiently Induced Protein States and Dimerization of PD-L1. *Journal of Medicinal Chemistry* **2017,** *60* (13), 5857-5867.
315. Mittendorf, E. A.; Philips, A. V.; Meric-Bernstam, F.; Qiao, N.; Wu, Y.; Harrington, S.; Su, X.; Wang, Y.; Gonzalez-Angulo, A. M.; Akcakanat, A.; Chawla, A.; Curran, M.; Hwu, P.; Sharma, P.; Litton, J. K.; Molldrem, J. J.; Alatrash, G., PD-L1 Expression in Triple-Negative Breast Cancer. *Cancer Immunology Research* **2014,** *2* (4), 361-370.
316. Mazel, M.; Jacot, W.; Pantel, K.; Bartkowiak, K.; Topart, D.; Cayrefourcq, L.; Rossille, D.; Maudelonde, T.; Fest, T.; Alix-Panabières, C., Frequent expression of PD-L1 on circulating breast cancer cells. *Molecular Oncology* **2015,** *9* (9), 1773-1782.
317. Tan, S.; Liu, K.; Chai, Y.; Zhang, C. W.-H.; Gao, S.; Gao, G. F.; Qi, J., Distinct PD-L1 binding characteristics of therapeutic monoclonal antibody durvalumab. *Protein & Cell* **2018,** *9* (1), 135-139.
318. Skalniak, L.; Zak, K. M.; Guzik, K.; Magiera, K.; Musielak, B.; Pachota, M.; Szelazek, B.; Kocik, J.; Grudnik, P.; Tomala, M.; Krzanik, S.; Pyrc, K.; Dömling, A.; Dubin, G.; Holak, T. A., Small-molecule inhibitors of PD-1/PD-L1 immune checkpoint

alleviate the PD-L1-induced exhaustion of T-cells. *Oncotarget* **2017,** *8* (42), 72167-72181.
319. Baell, J. B.; Nissink, J. W. M., Seven Year Itch: Pan-Assay Interference Compounds (PAINS) in 2017—Utility and Limitations. *ACS Chemical Biology* **2018,** *13* (1), 36-44.
320. Donald, P. R.; Diacon, A. H., Para-aminosalicylic acid: the return of an old friend. *The Lancet Infectious Diseases* **2015,** *15* (9), 1091-1099.
321. Sandborn, W. J., Treatment of ulcerative colitis with oral mesalamine: advances in drug formulation, efficacy expectations and dose response, compliance, and chemoprevention. *Reviews in gastroenterological disorders* **2006,** *6* (2), 97-105.
322. Brogden, R. N.; Heel, R. C.; Pakes, G. E.; Speight, T. M.; Avery, G. S., Diflunisal: A Review of its Pharmacological Properties and Therapeutic Use in Pain and Musculoskeletal Strains and Sprains and Pain in Osteoarthritis. *Drugs* **1980,** *19* (2), 84-106.
323. Huang, Z.; He, Y.; Zhang, X.; Gunawan, A.; Wu, L.; Zhang, Z.-Y.; Wong, C. F., Derivatives of Salicylic Acid as Inhibitors of YopH in Yersinia pestis. *Chemical biology & drug design* **2010,** *76* (2), 85-99.
324. Fletcher, S.; Page, B. D.; Zhang, X.; Yue, P.; Li, Z. H.; Sharmeen, S.; Singh, J.; Zhao, W.; Schimmer, A. D.; Trudel, S.; Turkson, J.; Gunning, P. T., Antagonism of the Stat3-Stat3 protein dimer with salicylic acid based small molecules. *ChemMedChem* **2011,** *6* (8), 1459-70.
325. Amano, Y.; Yamaguchi, T.; Tanabe, E., Structural insights into binding of inhibitors to soluble epoxide hydrolase gained by fragment screening and X-ray crystallography. *Bioorganic & Medicinal Chemistry* **2014,** *22* (8), 2427-2434.
326. Erlanson, D. A.; Wells, J. A.; Braisted, A. C., Tethering: fragment-based drug discovery. *Annual review of biophysics and biomolecular structure* **2004,** *33*, 199-223.
327. Ruepp, M.-D.; Brozik, J. A.; de Esch, I. J. P.; Farndale, R. W.; Murrell-Lagnado, R. D.; Thompson, A. J., A fluorescent approach for identifying P2X1 ligands. *Neuropharmacology* **2015,** *98* (Supplement C), 13-21.
328. Silvestre, H. L.; Blundell, T. L.; Abell, C.; Ciulli, A., Integrated biophysical approach to fragment screening and validation for fragment-based lead discovery. *Proceedings of the National Academy of Sciences* **2013,** *110* (32), 12984-12989.
329. Powderly, J.; Patel, M. R.; Lee, J. J.; Brody, J.; Meric-Bernstam, F.; Hamilton, E.; Ponce Aix, S.; Garcia-Corbacho, J.; Bang, Y. J.; Ahn, M. J.; Rha, S. Y.; Kim, K. P.; Gil Martin, M.; Wang, H.; Lazorchak, A.; Wyant, T.; Ma, A.; Agarwal, S.; Tuck, D.; Daud, A., CA-170, a first in class oral small molecule dual inhibitor of immune checkpoints PD-L1 and VISTA, demonstrates tumor growth inhibition in pre-clinical models and promotes T cell activation in Phase 1 study. *Annals of Oncology* **2017,** *28* (suppl_5), mdx376.007-mdx376.007.
330. Curis and Aurigene Announce CA-170 Program Update Following Data Presented at ESMO 2017. Schull, D., Ed. 2017.
331. McMenamy, R. H.; Oncley, J. L., The Specific Binding of l-Tryptophan to Serum Albumin. *Journal of Biological Chemistry* **1958,** *233* (6), 1436-1447.
332. Okabe, N.; Adachi, K., Binding Characteristics of Tryptophan Metabolites to Bovine Serum Albumin. *Chemical & Pharmaceutical Bulletin* **1992,** *40* (2), 499-500.

333. Silva, E.; Cilento, G., Dual effects of tryptophan in the horseradish peroxidase system that generates triplet acetone. *Photochemistry and Photobiology* **1989,** *50* (2), 259-262.
334. Fielding, L.; Rutherford, S.; Fletcher, D., Determination of protein–ligand binding affinity by NMR: observations from serum albumin model systems. *Magnetic Resonance in Chemistry* **2005,** *43* (6), 463-470.
335. Viegas, A.; Manso, J.; Nobrega, F. L.; Cabrita, E. J., Saturation-Transfer Difference (STD) NMR: A Simple and Fast Method for Ligand Screening and Characterization of Protein Binding. *Journal of Chemical Education* **2011,** *88* (7), 990-994.
336. Dinant, C.; van Royen, M. E.; Vermeulen, W.; Houtsmuller, A. B., Fluorescence resonance energy transfer of GFP and YFP by spectral imaging and quantitative acceptor photobleaching. *Journal of microscopy* **2008,** *231* (Pt 1), 97-104.
337. Sekar, R. B.; Periasamy, A., Fluorescence resonance energy transfer (FRET) microscopy imaging of live cell protein localizations. *The Journal of Cell Biology* **2003,** *160* (5), 629-633.
338. Sohn, H. W.; Tolar, P.; Jin, T.; Pierce, S. K., Fluorescence resonance energy transfer in living cells reveals dynamic membrane changes in the initiation of B cell signaling. *Proceedings of the National Academy of Sciences of the United States of America* **2006,** *103* (21), 8143-8148.
339. Vulpetti, A.; Dalvit, C., Fluorine local environment: from screening to drug design. *Drug Discovery Today* **2012,** *17* (15-16), 890-7.
340. Norton, R. S.; Leung, E. W.; Chandrashekaran, I. R.; MacRaild, C. A., Applications of (19)F-NMR in Fragment-Based Drug Discovery. *Molecules (Basel, Switzerland)* **2016,** *21* (7).
341. Jordan, J. B.; Poppe, L.; Xia, X.; Cheng, A. C.; Sun, Y.; Michelsen, K.; Eastwood, H.; Schnier, P. D.; Nixey, T.; Zhong, W., Fragment Based Drug Discovery: Practical Implementation Based on 19F NMR Spectroscopy. *Journal of Medicinal Chemistry* **2012,** *55* (2), 678-687.
342. Sasikumar, P. G. N. R., Muralidhara ; Prasad, Appukkuttan ; Naremaddepalli, Seetharamaiah Setty Sudarshan 3-substituted-1,2,4-oxadiazole and thiadiazole compounds as immunomodulators. WO2016142886 A2, 2016.
343. Kathman, S. G.; Statsyuk, A. V., Covalent tethering of fragments for covalent probe discovery. *MedChemComm* **2016,** *7* (4), 576-585.
344. Egawa, Y.; Miki, R.; Seki, T., Colorimetric Sugar Sensing Using Boronic Acid-Substituted Azobenzenes. *Materials* **2014,** *7* (2), 1201-1220.
345. Shinkai, S.; Takeuchi, M., Molecular design of synthetic receptors with dynamic, imprinting, and allosteric functions. *Biosensors and Bioelectronics* **2004,** *20* (6), 1250-1259.
346. Bull, S. D.; Davidson, M. G.; van den Elsen, J. M. H.; Fossey, J. S.; Jenkins, A. T. A.; Jiang, Y.-B.; Kubo, Y.; Marken, F.; Sakurai, K.; Zhao, J.; James, T. D., Exploiting the Reversible Covalent Bonding of Boronic Acids: Recognition, Sensing, and Assembly. *Accounts of Chemical Research* **2013,** *46* (2), 312-326.